# Identification of emotions through EEG: Elicitation protocols, mapping methods, signal processing and classification strategies, applications

Edited by
Giuseppe Placidi and Daniela Iacoviello

About Frontiers

Frontiers is more than just an open access publisher of scholarly articles: it is a pioneering approach to the world of academia, radically improving the way scholarly research is managed. The grand vision of Frontiers is a world where all people have an equal opportunity to seek, share and generate knowledge. Frontiers provides immediate and permanent online open access to all its publications, but this alone is not enough to realize our grand goals.

Frontiers journal series

The Frontiers journal series is a multi-tier and interdisciplinary set of open-access, online journals, promising a paradigm shift from the current review, selection and dissemination processes in academic publishing. All Frontiers journals are driven by researchers for researchers; therefore, they constitute a service to the scholarly community. At the same time, the *Frontiers journal series* operates on a revolutionary invention, the tiered publishing system, initially addressing specific communities of scholars, and gradually climbing up to broader public understanding, thus serving the interests of the lay society, too.

Dedication to quality

Each Frontiers article is a landmark of the highest quality, thanks to genuinely collaborative interactions between authors and review editors, who include some of the world's best academicians. Research must be certified by peers before entering a stream of knowledge that may eventually reach the public – and shape society; therefore, Frontiers only applies the most rigorous and unbiased reviews. Frontiers revolutionizes research publishing by freely delivering the most outstanding research, evaluated with no bias from both the academic and social point of view. By applying the most advanced information technologies, Frontiers is catapulting scholarly publishing into a new generation.

What are Frontiers Research Topics?

Frontiers Research Topics are very popular trademarks of the *Frontiers journals series*: they are collections of at least ten articles, all centered on a particular subject. With their unique mix of varied contributions from Original Research to Review Articles, Frontiers Research Topics unify the most influential researchers, the latest key findings and historical advances in a hot research area.

Find out more on how to host your own Frontiers Research Topic or contribute to one as an author by contacting the Frontiers editorial office: frontiersin.org/about/contact

Identification of emotions through EEG: Elicitation protocols, mapping methods, signal processing and classification strategies, applications

Topic editors

Giuseppe Placidi — University of L'Aquila, Italy
Daniela Iacoviello — Sapienza University of Rome, Italy

Table of
contents

Classification of Emotional Expressions Is Affected by Inversion: Behavioral and Electrophysiological Evidence

Jian Song[1†], Min Liu[2†], Shun Yao[1], Yan Yan[1], Huichao Ding[1], Tianyi Yan[3], Lun Zhao[3] and Guozheng Xu[1*]

[1]Department of Neurosurgery, Wuhan General Hospital of PLA, Wuhan, China, [2]No 457 Hospital of PLA, Wuhan, China, [3]Brain Research Institute, Beijing Yiran Sunny Technology Co. Ltd., Beijing, China

It has been shown that emotionally positive facial expressions are recognized substantially faster than emotionally negative facial expressions, the positive classification advantage (PCA). In this experiment we explored the involvement of configural computations while processing positive and negative faces in an expression categorization task using artificial faces. Analyzing the reaction times (RTs), we found that happy faces were categorized more quickly than sad faces (PCA) and this effect disappeared for inverted faces. Event-related potentials (ERPs) data showed that the face-sensitive N170 component was larger for sad than for happy faces only at upright condition and that face inversion significantly enhanced N170 amplitudes only for happy faces. Moreover, the happy faces elicited shorter N170 latency than did the sad faces, whereas for inverted condition the N170 latency did not differ between happy and sad faces. Finally, the significant positive correlation between the RTs and the latency of the N170 was not found for N170 amplitudes. Because the configural computation was task-irrelevant in the present study, these behavioral and ERP data indicated that one of the sources of PCA is the configural analysis applied by default while categorizing facial emotions.

Keywords: face classification, expression, face inversion, N170

INTRODUCTION

Facial expressions reflect a person's emotional state, current motives and intentions. It is therefore important for adaptive purposes that the cognitive system can rapidly extract accurate information from the observed expressions. It has been shown that emotionally positive facial expressions are recognized substantially faster than negative facial expressions, the positive classification advantage (PCA). This effect was conspicuous for happiness recognition faster than sadness (e.g., Crews and Harrison, 1994; Leppänen and Hietanen, 2004; Liu et al., 2013), anger (e.g., Billings et al., 1993), disgust (e.g., Stalans and Wedding, 1985) and emotional neutrality (e.g., Hugdahl et al., 1993; Liu et al., 2013).

Several perceptual strategies are used by humans while processing faces: local and configural processing (e.g., Maurer et al., 2002). Local information mostly refers to distinct circumscribed characteristics of the face, such as the mouth or the nose. General spatial relations of the face (e.g., the eyes are above the nose) are usually described as configural information or first-order relations,

whereas second-order relations refer to specific spatial relations (e.g., distance between eyes and nose) and possess a higher discriminative value (Leder and Carbon, 2006). Evidence has accumulated that the configural analysis underlying face recognition also applies to facial-emotion recognition, being dependent upon facial features and spatial arrays (e.g., McKelvie, 1995; Calder et al., 2000). For example, McKelvie (1995) assessed the effect of face inversion on the recognition of facial expressions of emotion and found that inversion impaired the recognition of sad, fearful, angry and disgusted, but not of happy expressions.

Face classification is based on visual information that is similar to all "facial action patterns" irrespective of the faces that are making them and the expression classification processes of faces include the extraction of attributes of expressions (Ganel and Goshen-Gottstein, 2002). Although the PCA has been proposed in previous studies, it is less clear whether configural processing is also required in the classification of facial expressions of emotion. The present research was designed to address this issue by recording the N170 of event-related potentials (ERPs) while the participants categorized the upright and inverted face stimuli according to their expressions.

The N170 component at occipito-temporal electrodes, a negative ERP occurring between 140 ms and 180 ms after stimulus onset, is the earliest component associated with face perceptual processing and is reliably larger to faces than other stimulus categories (Bentin et al., 1996). Based on data showing that the N170 is not sensitive to the face identity (Bentin and Deouell, 2000; Eimer, 2000; Anaki et al., 2007), larger (and delayed) for face components (particularly eyes) than full faces (Bentin et al., 1996; Itier et al., 2006), larger (and delayed) for inverted faces (Bentin et al., 1996; Rossion and Gauthier, 2002) and equally large for scrambled and normally configured faces (Zion-Golumbic and Bentin, 2007), it was suggested that the N170 is closely relevant to the detection of global face structures as well as other information of faces. Importantly, several studies found that the N170 component was entirely unaffected by any of the basic emotional expressions (e.g., Eimer and Holmes, 2002; Ashley et al., 2003; Eimer et al., 2003), implicating that expression processing of faces occurs at post-perceptual stage. Recently, however, growing evidence suggests that the N170 can be modulated by facial emotion, e.g., happy faces elicit smaller amplitude than other emotions (e.g., Caharel et al., 2005). One recent study investigated the time course of the PCA by recording ERPs and found that, compared with sad faces, happy faces elicited a smaller N170 (Liu et al., 2013). However, in Liu et al. (2013) study the face inversion effect was not investigated.

The goal of the current study was to map the effect of face inversion on the early stage of face classification by expression. In the present study, we adopted schematic face stimuli like previous studies (e.g., Leppänen and Hietanen, 2004; Liu et al., 2013). Several studies using schematic facial expressions, emoticons or smileys have shown the comparable emotional effect elicited by photographic facial expressions (Boucsein et al., 2001; Eger et al., 2003; Babiloni et al., 2010). Schematic faces may be ideal experimental stimuli because they allowed us to fully control the low-level physical features,

to exclude additional information related to facial identity, such as gender, race, etc., and to minimize the confounding effects of general arousal rather than valence *per se*. As the specific index of configural processing, face inversion disrupts the global configural information, resulting in the decrease of recognition accuracy, the increase of reaction time (RT) and the enlargement or delay of N170 component. If the PCA phenomenon relies more on high-level configural information, it is expected attenuated PCA in face inversion condition.

MATERIALS AND METHODS
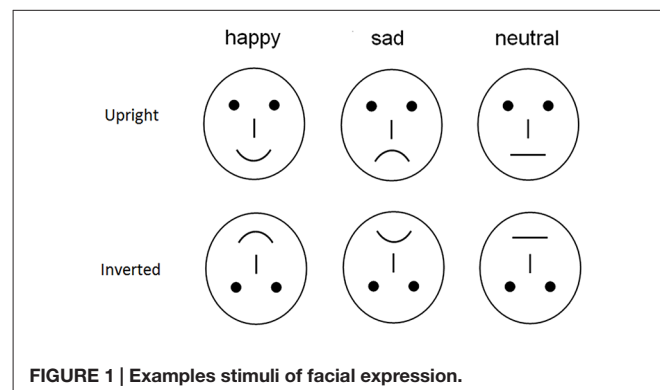
Participants

Thirty-six young healthy individuals participated in our study (16 female, aged 20–25 years, mean age: 22.6 years). All participants were right-handed and had normal or corrected-to-normal visual acuity and were free of a neurological or psychiatric history. They received payments for their participation and gave their written informed consent before the experiment. This study was approved by the Ethical Committee of Wuhan General Hospital in accordance with the ethical principles of Declaration of Helsinki.

Stimuli

To avoid the low-level processing of facial features as well as boredom by the excessive repetition of one single model, each emotional category consisted of 20 different schematic face models by manipulating the distance among facial features and by manipulating the shape of the facial features (**Figure 1**; Liu et al., 2013). All stimuli were presented at the center of a video monitor and viewed from a distance of 100 cm at a visual angle of approximately 7.27 × 6.06°. The experiment consisted of four blocks of 120 trials each (480 trials in total with 80 trials × 3 expressions × 2 orientations).

Procedure

Following the electrode application, the participants were seated in a dimly lit and sound-attenuated cabin. They were instructed to classify each face by the expression it represented and to respond to sad or happy faces (ignoring neutral faces) by pressing correspondingly labeled buttons on the keyboard with the left index finger ("Z" key) or right index


FIGURE 1 | Examples stimuli of facial expression.

finger ("/" key), respectively. Speed and accuracy were equally emphasized. All 480 stimuli were randomly presented in a mixed design, with four blocks of 120 stimuli each, with a short break in between, and the labels of the response buttons (happy–sad/sad–happy) were counterbalanced across the participants. Each face was presented for 300 ms with an intertrial interval ranging randomly between 600 ms and 800 ms, starting after response. The participants completed one practice sequence of 30 stimuli (five from each type, equally representing the three facial expressions). These stimuli were not used in the main experiment.

EEG Recording

EEG was recorded continuously by Neuro-Cap with a set of 32 Ag/AgCl electrodes placed according to the 10/20 system. In order to monitor eye movements and blinks, EOG was recorded via electrodes placed on the bilateral external canthi and the left infraorbital and supraorbital areas. Both EEG and EOG signals were sampled at 500 Hz, with a 0.1–100 Hz band pass using a NeuroLab® digital amplifiers system. During recording, we used the tip of the nose as reference and a common average reference was calculated off-line. Electrode impedances were kept below 5 kΩ.

We corrected EOG artifacts off-line using a correlation method proposed by Semlitsch et al. (1986) and supplied as part of the EEGLab software. The EEG was segmented in epochs of 1000 ms beginning 200 ms prior to stimulus onset and averaged separately for each condition (happy and sad faces for upright and inverted conditions, respectively). Segments with an incorrect response or contaminated with peak-to-peak deflection exceeding ±100 μV were excluded from averaging. After this procedure, averaged ERPs included at least 65 trials for each of face conditions. The averaged ERP waveforms were low-pass filtered at 30 Hz (24 dB/octave).

Data Analysis

RTs (from the stimulus onset) and accuracy rates were recorded and analyzed using a two-way analysis of variance (ANOVA) with *Expression* (happy, sad) and *Orientation* (upright, inverted) as within-subject factors.

Based on previous studies (e.g., Bentin et al., 1996) and limited by the 32-sites montage (see montage in **Figure 2**), the peak amplitudes and latencies of the N170 were measured automatically between 120 ms and 200 ms at P7, P8, TP7, TP8, O1 and O2 sites. These measures were analyzed using a four-way ANOVA with *Expression* (happy, sad), *Orientation* (upright, inverted), *Hemisphere* (left, right) and *Site* (P7/8, TP7/8, O1/2) as within-subject factors. Degrees of freedom were corrected whenever necessary using the Greenhouse–Geisser epsilon correction factor.

RESULTS

Performance

A 2 (*Expression*) × 2 (*Orientation*) repeated-measures ANOVA was conducted for the percentage of correct responses. Neither

the main effect of *Expression* (93.5% and 93.0% for happy and sad faces, respectively; $F < 1$) nor the main effect of *Orientation* (93.3% and 93.2% for upright and inverted faces, respectively; $F < 1$) was significant. The two-way interaction was not significant ($F < 1$).

For each participant, incorrect responses or responses with RTs more than ± 2 *SD*s from the mean in each condition were excluded for RT analysis. On average, 8.7% of responses were removed (**Table 1**). The RTs were analyzed using the same statistical model as that for percentages of correct responses. There was a significant main effect of *Expression*, $F_{(1,35)} = 7.49$, $p < 0.01$, partial $\eta^2 = 0.176$, showing that happy face categorization was faster (598 ms) than classifying sad faces (615 ms). The main effect of *Orientation* was also significant, $F_{(1,35)} = 146.6$, $p < 0.001$, partial $\eta^2 = 0.807$, showing that upright faces was classified more quickly (584 ms) than classifying inverted faces (629 ms). Importantly, we found the significant two-way interaction of *Expression* * *Orientation*, $F_{(1,35)} = 9.45$, $p < 0.01$, partial $\eta^2 = 0.414$. Further analysis for the interaction reflected that, although the inversion effects were similar ($p = 0.259$) between sad and happy conditions (573 ms and 623 ms for upright and inverted happy faces, respectively; $p < 0.001$; 594 ms and 635 ms for upright and inverted sad faces, respectively; $p < 0.001$), quickly happy face classification vs. sad faces was exhibited for upright (21 ms, $p < 0.005$) not for inverted condition (12 ms, $p = 0.135$). In addition, we conducted a Pearson correlation analysis between PCA and the RTs and found that there was an overall significant positive correlation between the RT to negative face stimuli and the size of the PCA, $r = 0.52$, $p < 0.01$ (two tailed), but not between the RT to positive face stimuli and the PCA, $r = 0.10$, $p > 0.05$.
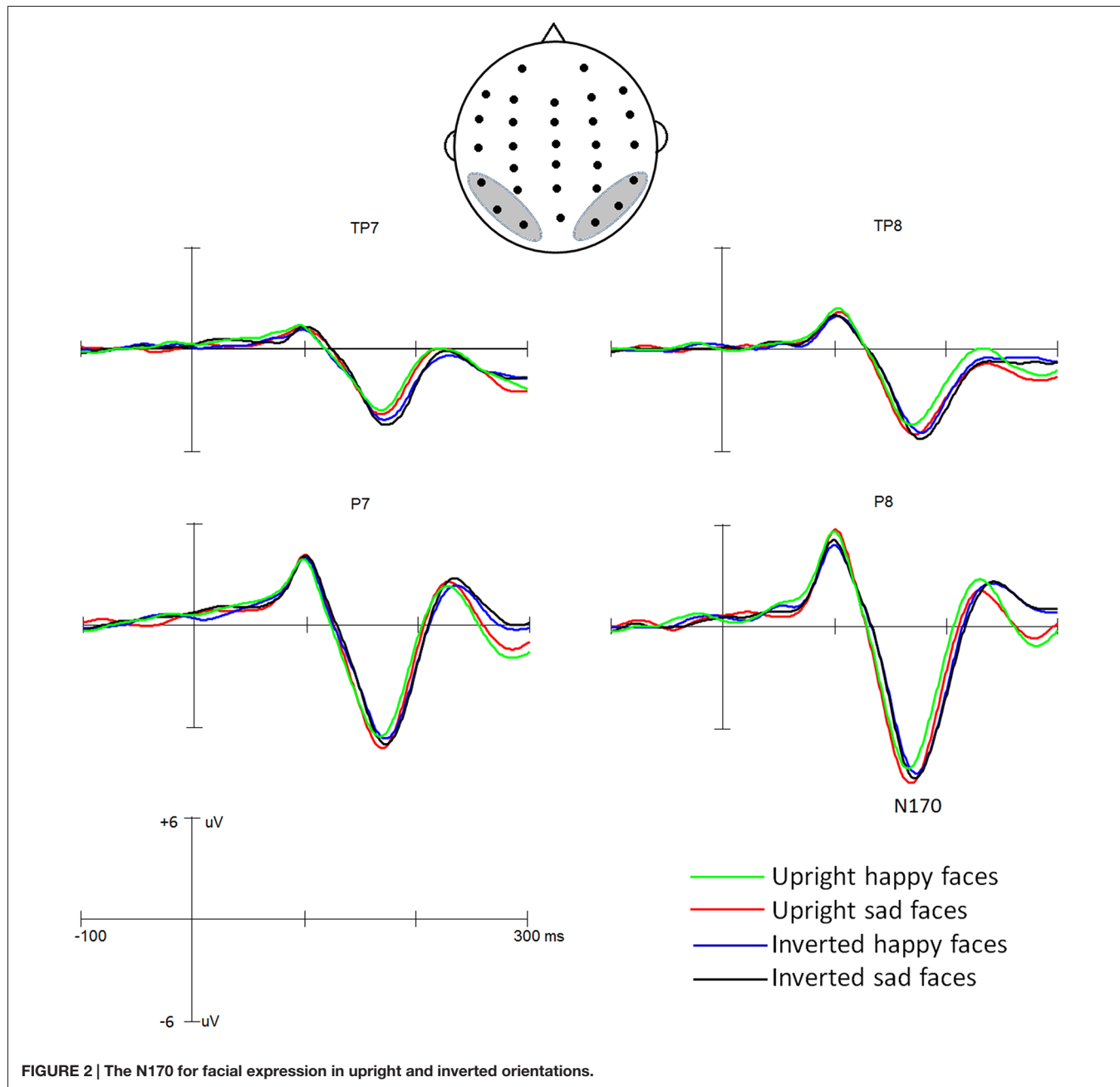
N170 Component

Grand average ERP waveforms are presented in **Figure 2**. The effects of the *Expression*, *Orientation*, *Hemisphere* and *Site* were analyzed by ANOVA using a mixed model design as described in the "Materials and Methods" Section.

ANOVA of N170 latencies revealed a significant main effect of *Orientation*, $F_{(1,35)} = 38.0$, $p < 0.001$, partial $\eta^2 = 0.521$, with a delayed N170 latency for inverted (172 ms) than upright (166 ms) conditions. The main effects of *Expression* was not significant, $F_{(1,35)} = 1.41$, $p = 0.24$, partial $\eta^2 = 0.039$, but qualified by the two-way interaction of *Expression* * *Orientation*, $F_{(1,35)} = 9.65$, $p < 0.01$; partial $\eta^2 = 0.216$. Further analysis for this two-way interaction showed that for upright condition the happy face elicited shorter N170 latency (164 ms) than did the sad faces (168 ms; $p < 0.02$), whereas for inverted condition the N170 latency did not differ between happy (173 ms) and sad

TABLE 1 | The reaction times (RTs) and the amplitudes and latencies of N170 component (across occipital-temporal electrode sites) for upright and inverted face conditions, respectively.

	Upright faces		Inverted faces	
	Happy	Sad	Happy	Sad
RTs	565 ms	605 ms	615 ms	638 ms
N170 amplitude	−6.4 uV	−7.2 uV	−7.8 uV	−7.8 uV
N170 latency	164 ms	168 ms	173 ms	172 ms

FIGURE 2 | The N170 for facial expression in upright and inverted orientations.

faces (172 ms; $p = 0.20$) and that the inversion effect was more conspicuous for happy (inverted *minus* upright: 8 ms) than sad (4 ms; $p < 0.05$) faces. There were no other significant effects ($Fs < 1$).

For N170 amplitude analysis, the main effect of *Orientation* was significant, $F_{(1,35)} = 13.36$, $p < 0.01$, partial $\eta^2 = 0.330$, showing that overall, face inversion enhanced the N170 amplitudes (-6.8 μV and -7.8 μV for upright and inverted conditions, respectively). The main effect of *Expression* was not significant, $F_{(1,35)} = 3.37$, $p = 0.075$, partial $\eta^2 = 0.088$, but the two-way interaction of *Expression* $\times$ *Orientation* was significant, $F_{(1,35)} = 5.35$, $p < 0.05$, partial $\eta^2 = 0.135$. Further

analysis for this interaction revealed that the effect of *Expression* was evident for upright condition (-6.4 μV and -7.2 μV for happy and sad faces, respectively; $p < 0.02$) not for inverted condition (-7.8 μV and -7.8 μV for happy and sad faces, respectively; $p = 0.91$) and that the effect of *Orientation* was evident for happy ($p < 0.01$) not for sad faces ($p = 0.08$). The main effect of *Hemisphere* was also significant, $F_{(1,35)} = 8.23$, $p < 0.03$, partial $\eta^2 = 0.517$, showing the right hemisphere dominance of the N170 amplitude (-6.5 μV and -8.2 μV for left and right hemisphere, respectively). The main effect of *Site* was also significant, $F_{(2,70)} = 69.23$, $p < 0.001$, partial $\eta^2 = 0.589$, revealing that the N170 was larger at more occipital-temporal

sites (-9.7 μV, -7.8 μV and -5.3 μV for P7/8, O1/2 and TP7/8, respectively). No other effects reached significant level ($ps > 0.1$).

In addition to the ANOVAs, we calculated the Person correlations between the RTs and the amplitude and latency of the N170 for upright face condition (i.e., PCA was evident). While the RTs did not correlate with the amplitude of N170 ($ps > 0.10$), a significant positive correlation between the RTs and the latency of the N170 was found ($r = 0.47$, $p < 0.05$; that is, the longer the RT the longer the N170 latency).

DISCUSSION

In this experiment we explored the involvement of configural computations while processing positive and negative faces in an expression categorization task. The performance data showed that the classification of happy faces was faster than the classification of sad faces (PCA). Importantly, however, the PCA on the classification speed disappeared for inverted faces. The N170 analysis showed that the N170 was larger for sad than for happy faces only at upright condition and that face inversion significantly enhanced N170 amplitudes only for happy faces. Interestingly, the happy face elicited shorter N170 latency than did the sad faces, whereas for inverted condition the N170 latency did not differ between happy and sad faces. The significant positive correlation between the RTs and the latency of the N170 was also found for N170 amplitudes. Because the configural processing was task-irrelevant in this study, these behavioral and ERP data implicated that the configural analysis is one of the sources of PCA, which is applied by default while categorizing facial emotions.

Several studies have shown the RT advantage for the recognition of happy faces, but none have answered the question whether or not this effect is caused by some high-level configural computations making happy faces visually more distinctive. The present study addressed this question by using upright/inverted schematic happy and sad faces, which were physically comparable but still had the intended emotional value. A widely accepted effect of face inversion refers to the fact that the recognition is severely impaired for inverted relative to upright faces. Actually, the inverted faces impair the structural feature of faces and thus influence configural processing (e.g., Searcy and Bartlett, 1996). Along with this view, the possibly existing difference in configural coding of happy and sad faces is one of sources of the faster categorization of happy faces. Supporting this hypothesis, although face inversion significantly slowed down responses and the inversion effect of RTs is similar between happy and sad faces, the absolute inversion effect of RTs is indeed slightly larger for happy (50 ms) than sad (40 ms) faces, in line with the influence of manipulating configurations larger on happy than sad face identification (e.g., Leppänen and Hietanen, 2004). Supporting this view, Bombari et al. (2013) confirmed that configural processing plays a more prominent role in expression recognition than featural processing, but their relative contribution varies depending on the emotion.There was also evidence that positive and neutral emotions differ to a greater extent than negative

and neutral emotions because the configuration of facial features may change more significantly from neutral to happy expression than from neutral to negative emotions (Leppänen and Hietanen, 2004). Moreover, Srinivasan and Gupta (2011) examined the effect of global and local processing on the recognition of sad and happy faces and found that narrowing attention to local processing facilitated the recognition of sad faces, while broad scope of attention facilitated the recognition of happy faces. It should be noteworthy that the above previous study focused on expression recognition, while the present study directly explored the role of configural processing for face classification by expressions.

In the present task, the N170 component was sensitive to emotional expression, as manifested by larger amplitudes to sad than to happy faces. These data support previous findings for early processing of emotional expression (e.g., Caharel et al., 2005; Liu et al., 2013) and suggest that negative emotions engender a more intense emotional reaction than do positive ones. Moreover, converging evidence showed that valence category reflects initial selective attention capture by salient image content (appetitive, threatening) and that unpleasant stimuli can produce stronger emotional effects than can pleasant stimuli—that is, a phenomenon of negativity bias (e.g., Crawford and Cacioppo, 2002). The present findings of enhanced N170 for sad faces is in line with the above view, further indicating that the negativity bias can occur at the early stage of face perception. The present patterns of N170 effects were also consistent with previous findings that valence of affective pictures appeared to influence relatively early (100–250 ms) components of ERPs (for a review, see Olofsson et al., 2008), indicating that affective processing can be described as an automatic feature of perception (e.g., Fox, 1991; Öhman and Soares, 1998). In addition, we found the right-hemisphere dominance of N170 amplitudes, regardless of happy or sad faces. Actually, the well-established right-hemisphere lateralization of the N170 amplitude has been shown in previous studies and this asymmetry is known specifically for faces (e.g., Bentin et al., 1996; Rossion, 2014). Recently, using ERP source-localization techniques Itier et al. (2007) estimated the location of the neural generator of the N170 and found that its neural generators may be located in the fusiform gyrus (FFA), superior temporal sulcus (STS), or both (Itier and Taylor, 2004). However, it should be noted that these techniques are fraught with potential sources of error, and there is disagreement on the validity of inferences drawn from such findings. Therefore, the neutral generators of N170 component await further investigation.

In line with the previous study that the N170 is delayed and enhanced for inverted faces (e.g., Bentin et al., 1996), the present study showed that face inversion enhanced and delayed N170, regardless of facial expressions. However, we found that the inversion effect of N170 was more conspicuous for happy than sad faces. Apparently, this larger N170 inversion effect for happy faces than sad faces further provided electrophysiological evidence for the above hypothesis that the configuration computation was more conspicuous for happy than sad face

classification. However, the N170 amplitudes did not correlate with RTs and consequently, the modulation of facial expression on N170 amplitudes did not account for the PCA. In contrast, the happy face elicited shorter N170 latency than did the sad faces, whereas for inverted condition the N170 latency did not differ between happy and sad faces. Importantly, we found a significant positive correlation between the RTs and the latency of the N170. To this end, the present fact of N170 latency implicated that the PCA could be based on high-level configural processing at the early stage of face processing reflected by the face-sensitive N170.

Before concluding, we should reiterate two procedural decisions that constrain the interpretation of the present findings. First, all the faces used in this study were schematic unfamiliar faces to the participants. Using unfamiliar faces we hoped to isolate initial stages of face categorization reducing putative effects of face individuation and identification, processes that might have been tainted by memory factors. Therefore, whether the facial familiarity can modulate the PCA awaits further investigation. Second, in the present study we used schematic faces instead of real faces. Although schematic faces allow us to fully control the low-level physical features, to exclude additional information related to facial identity and to minimize the confounding effects of general arousal rather than valence *per se*, these schematic face pictures are less complex, in particular with respect to the configural components. However, the happiness advantage with schematic facial expressions was consistent with the findings of real faces (e.g., Leppänen and Hietanen, 2004; Liu et al., 2013). Since the happy and sad expressions in the present study equally deviated from neutral faces, it is difficult to attribute the observed advantage of happy faces over sad faces to low-level physical differences between happy and sad faces. In addition, the schematic-face inversion significantly modulated the RTs as well as the N170 component, in line with the face inversion effect of real faces (e.g., Bentin et al., 1996). Hence, the present data further indicate that schematic emotional faces may be ideal experimental stimuli.

In sum, this experiment explored the configural computations while processing positive and negative faces in an expression categorization task. The PCA on the classification speed was evident for upright condition and disappeared for inverted faces. The N170 was larger and delayed for sad faces than happy faces and did not differ for inverted condition. The significant positive correlation between the RTs and the latency of the N170 was also found not for N170 amplitudes. These behavioral and ERP data implicated that the configural analysis could be one of the sources of PCA, which is applied by default while categorizing facial emotions.

AUTHOR CONTRIBUTIONS

JS finished experiment and GX finished the article. All authors listed, have made substantial, direct and intellectual contribution to the work, and approved it for publication.

ACKNOWLEDGMENTS

REFERENCES

Anaki, D., Zion-Golumbic, E., and Bentin, S. (2007). Electrophysiological neural mechanisms for detection, configural analysis and recognition of faces. *Neuroimage* 37, 1407–1416. doi: 10.1016/j.neuroimage.2007.05.054

Ashley, V., Vuilleumier, P., and Swick, D. (2003). Time course and specificity of event-related potentials to emotional expressions. *Neuroreport* 15, 211–216. doi: 10.1097/00001756-200401190-00041

Babiloni, C., Vecchio, F., Buffo, P., Buttiglione, M., Cibelli, G., Rossini, P. M., et al. (2010). Cortical responses to consciousness of schematic emotional facial expressions: a high-resolution EEG study. *Hum. Brain Mapp.* 31, 1556–1569. doi: 10.1002/hbm.20958

Bentin, S., Allison, T., Puce, A., Perez, E., and McCarthy, G. (1996). Electrophysiological studies of face perception in humans. *J. Cogn. Neurosci.* 8, 551–565. doi: 10.1162/jocn.1996.8.6.551

Bentin, S., and Deouell, L. Y. (2000). Structural encoding and identification in face processing: ERP evidence for separate mechanisms. *Cogn. Neuropsychol.* 17, 35–55. doi: 10.1080/026432900380472

Billings, L. S., Harrison, D. W., and Alden, J. D. (1993). Age differences among women in the functional asymmetry for bias in facial affect perception. *Bull. Psychon. Soc.* 31, 317–320. doi: 10.3758/bf03334940

Bombari, D., Schmid, P. C., Schmid Mast, M., Birri, S., Mast, F. W., and Lobmaier, J. S. (2013). Emotion recognition: the role of featural and configural face information. *Q. J. Exp. Psychol.* 66, 2426–2442. doi: 10.1080/17470218.2013.789065

Boucsein, W., Schaefer, F., Sokolov, E., Schröder, C., and Furedy, J. (2001). The color-vision approach to emotional space: cortical evoked potential data. *Integr. Physiol. Behav. Sci.* 36, 137–153. doi: 10.1007/bf02734047

Caharel, S., Courtay, N., Bernard, C., Lalonde, R., and Rebaï, M. (2005). Familiarity and emotional expression influence an early stage of face processing: an electrophysiological study. *Brain Cogn.* 59, 96–100. doi: 10.1016/j.bandc.2005.05.005

Calder, A. J., Young, A. W., Keane, J., and Dean, M. (2000). Configural information in facial expression perception. *J. Exp. Psychol. Hum. Percept. Perform.* 26, 527–551. doi: 10.1037/0096-1523.26.2.527

Crawford, L. E., and Cacioppo, J. T. (2002). Learning where to look for danger: integrating affective and spatial information. *Psychol. Sci.* 13, 449–453. doi: 10.1111/1467-9280.00479

Crews, W. D., and Harrison, D. W. (1994). Cerebral asymmetry in facial affect perception by women: neuropsychological effects of depressive mood. *Percept. Mot. Skills* 79, 1667–1679. doi: 10.2466/pms.1994.79.3f.1667

Eger, E., Jedynak, A., Iwaki, T., and Skrandies, W. (2003). Rapid extraction of emotional expression: evidence from evoked potential fields during brief presentation of face stimuli. *Neuropsychologia* 41, 808–817. doi: 10.1016/s0028-3932(02)00287-7

Eimer, M. (2000). The face-specific N170 component reflects late stages in the structural encoding of faces. *Neuroreport* 11, 2319–2324. doi: 10.1097/00001756-200007140-00050

Eimer, M., and Holmes, A. (2002). An ERP study on the time course of emotional face processing. *Neuroreport* 13, 427–431. doi: 10.1097/00001756-200203250-00013

Eimer, M., Holmes, A., and McGlone, F. P. (2003). The role of spatial attention in the processing of face expression: an ERP study of rapid brain responses to six basic emotions. *Cogn. Affect. Behav. Neurosci.* 3, 97–110. doi: 10.3758/cabn.3.2.97

Fox, N. A. (1991). If it's not left, it's right: electroencephalograph asymmetry and the development of emotion. *Am. Psychol.* 46, 863–872. doi: 10.1037//0003-066x.46.8.863

Ganel, T., and Goshen-Gottstein, Y. (2002). Perceptual integrality of sex and identity of faces: further evidence for the single-route hypothesis. *J. Exp. Psychol. Hum. Percept. Perform.* 28, 854–867. doi: 10.1037/0096-1523.28.4.854

Hugdahl, K., Iversen, P. M., and Johnsen, B. H. (1993). Laterality for facial expressions: does the sex of the subjects interact with the sex of the stimulus face? *Cortex* 29, 325–331. doi: 10.1016/s0010-9452(13)80185-2

Itier, R. J., Alain, C., Sedore, K., and McIntosh, A. R. (2007). Early face processing specificity: it's in the eyes! *J. Cogn. Neurosci.* 19, 1815–1826. doi: 10.1162/jocn.2007.19.11.1815

Itier, R. J., Latinus, M., and Taylor, M. J. (2006). Face, eye and object early processing: what is the face specificity? *Neuroimage* 29, 667–676. doi: 10.1016/j.neuroimage.2005.07.041

Itier, R. J., and Taylor, M. J. (2004). Source analysis of the N170 to faces and objects. *Neuroreport* 15, 1261–1265. doi: 10.1097/01.wnr.0000127827.73576.d8

Leder, H., and Carbon, C.-C. (2006). Face-specific configural processing of relational information. *Br. J. Psychol.* 97, 19–29. doi: 10.1348/000712605X54794

Leppänen, J. M., and Hietanen, J. K. (2004). Positive facial expressions are recognized faster than negative facial expressions, but why? *Psychol. Res.* 69, 22–29. doi: 10.1007/s00426-003-0157-2

Liu, X. F., Liao, Y., Zhou, L., Sun, G., Li, M., and Zhao, L. (2013). Mapping the time course of the positive classification advantage: an ERP study. *Cogn. Affect. Behav. Neurosci.* 13, 491–500. doi: 10.3758/s13415-013-0158-6

Maurer, D., Le Grand, R., and Mondloch, C. J. (2002). The many faces of configural processing. *Trends Cogn. Sci.* 6, 255–260. doi: 10.1016/s1364-6613(02)01903-4

McKelvie, S. J. (1995). Emotional expression in upside-down faces: evidence for configurational and componental processing. *Br. J. Soc. Psychol.* 34, 325–334. doi: 10.1111/j.2044-8309.1995.tb01067.x

Öhman, A., and Soares, J. J. (1998). Emotional conditioning to masked stimuli: expectancies for aversive outcomes following nonrecognized fear-relevant stimuli. *J. Exp. Psychol. Gen.* 127, 69–82. doi: 10.1037/0096-3445.127.1.69

Olofsson, J. K., Nordin, S., Sequeira, H., and Polich, J. (2008). Affective picture processing: an integrative review of ERP findings. *Biol. Psychol.* 77, 247–265. doi: 10.1016/j.biopsycho.2007.11.006

Rossion, B. (2014). Understanding face perception by means of human electrophysiology. *Trends Cogn. Sci.* 18, 310–318. doi: 10.1016/j.tics.2014.02.013

Rossion, B., and Gauthier, I. (2002). How does the brain process upright and inverted faces? *Behav. Cogn. Neurosci. Rev.* 1, 63–75. doi: 10.1177/1534582302001001004

Searcy, J. H., and Bartlett, J. C. (1996). Inversion and processing of component and spatial-relational information in faces. *J. Exp. Psychol. Hum. Percept. Perform.* 22, 904–915. doi: 10.10.1037/0096-1523.22.4.904

Semlitsch, H. V., Anderer, P., Schuster, P., and Presslich, O. (1986). A solution for reliable and valid reduction of occular artiofacts applied to the P300 ERP. *Psychophysiology* 23, 695–703. doi: 10.1111/j.1469-8986.1986.tb00696.x

Srinivasan, N., and Gupta, R. (2011). Rapid communication: global-local processing affects recognition of distractor emotional faces. *Q. J. Exp. Psychol.* 64, 425–433. doi: 10.1080/17470218.2011.552981

Stalans, L., and Wedding, D. (1985). Superiority of the left hemisphere in the recognition of emotional faces. *Int. J. Neurosci.* 25, 219–233. doi: 10.3109/00207458508985373

Zion-Golumbic, E., and Bentin, S. (2007). Dissociated neural mechanisms for face detection and configural encoding: evidence from N170 and induced gamma-band oscillation effects. *Cereb. Cortex* 17, 1741–1749. doi: 10.1093/cercor/bhl100

frontiers
in Computational Neuroscience

Improving Cross-Day EEG-Based Emotion Classification Using Robust Principal Component Analysis

Yuan-Pin Lin [1, 2]*, Ping-Keng Jao [3, 4] and Yi-Hsuan Yang [4]

[1] Institute of Medical Science and Technology, National Sun Yat-sen University, Kaohsiung, Taiwan, [2] Institute for Neural Computation, University of California, San Diego, La Jolla, CA, United States, [3] Center for Neuroprosthetics, School of Engineering, École Polytechnique Fédérale de Lausanne, Geneva, Switzerland, [4] Research Center for IT Innovation, Academia Sinica, Taipei, Taiwan

Constructing a robust emotion-aware analytical framework using non-invasively recorded electroencephalogram (EEG) signals has gained intensive attentions nowadays. However, as deploying a laboratory-oriented proof-of-concept study toward real-world applications, researchers are now facing an ecological challenge that the EEG patterns recorded in real life substantially change across days (i.e., day-to-day variability), arguably making the pre-defined predictive model vulnerable to the given EEG signals of a separate day. The present work addressed how to mitigate the inter-day EEG variability of emotional responses with an attempt to facilitate cross-day emotion classification, which was less concerned in the literature. This study proposed a robust principal component analysis (RPCA)-based signal filtering strategy and validated its neurophysiological validity and machine-learning practicability on a binary emotion classification task (happiness vs. sadness) using a five-day EEG dataset of 12 subjects when participated in a music-listening task. The empirical results showed that the RPCA-decomposed sparse signals (RPCA-S) enabled filtering off the background EEG activity that contributed more to the inter-day variability, and predominately captured the EEG oscillations of emotional responses that behaved relatively consistent along days. Through applying a realistic add-day-in classification validation scheme, the RPCA-S progressively exploited more informative features (from 12.67 ± 5.99 to 20.83 ± 7.18) and improved the cross-day binary emotion-classification accuracy (from $58.31 \pm 12.33\%$ to $64.03 \pm 8.40\%$) as trained the EEG signals from one to four recording days and tested against one unseen subsequent day. The original EEG features (prior to RPCA processing) neither achieved the cross-day classification (the accuracy was around chance level) nor replicated the encouraging improvement due to the inter-day EEG variability. This result demonstrated the effectiveness of the proposed method and may shed some light on developing a realistic emotion-classification analytical framework alleviating day-to-day variability.

Keywords: inter-day EEG variability, emotion classification, affective brain-computer interface, EEG oscillation, robust principal component analysis

INTRODUCTION

Implicit emotional reactions behave as a non-verbal psychophysiological communication channel alternative to explicit manners of body gestures, written text, and speech, enriching the interaction in people. Through characterizing such emotional information by leveraging multidisciplinary knowledge and the ever-growing affective computing technology, a conventional human-computer interaction (HCI) scenario can then be augmented with an emotion-aware ability, which facilitates a realistic humanoid closed-loop feedback. Emotion recognition has attracted intensive attention nowadays. Two facets may drive its intensive interest. On one hand, it enables a wide spectrum of intriguing emotion-oriented applications such as, machine intelligence (Chen et al., 2017), receptionist robots (Pinheiro et al., 2017), content recommendation devices (Lee and Shin, 2013), tutoring systems (Muñoz et al., 2010), and music therapy (Ian et al., 2016). On the other hand, recent explosive innovations in wearable sensing technology considerably bring laboratory-demonstrated emotion-aware research closer to our daily life, necessitating a robust and accurate emotion-aware analytical framework.

Existing affective computing research has demonstrated the capacity of assessing implicit emotions by internal changes in physiological signals that are originated from autonomic and central nervous systems (Picard et al., 2001; Kim and Andre, 2008; Chanel et al., 2009; Lin et al., 2010). Among them, electroencephalogram (EEG) is a non-invasive-recording of the electrical activity of the brain. The EEG signals presumably encompass the fundamental yet critical information underlying emotion dynamics, since the limbic system located in the brain plays a key role in emotion regulation (Hariri et al., 2000). There has been promising interdisciplinary analytical frameworks proposed to leverage advanced signal processing, machine learning, and data mining techniques with the attempt to exploit the EEG correlates of emotional responses as well as to later develop an emotion-aware model for emotion recognition (Chanel et al., 2009; Frantzidis et al., 2010; Lin et al., 2010; Petrantonakis and Hadjileontiadis, 2010; Koelstra et al., 2012; Soleymani et al., 2012; Jenke et al., 2014; Gupta et al., 2016; Hu et al., 2017). This area has become an emerging track in the affective brain-computer interface (ABCI), namely EEG-based emotion recognition (Mühl et al., 2014). The successful demonstrations would not only demonstrate the feasibility of emotional computing from EEG signals, but also pose new directions for practical ABCI applications in real life.

A practical issue for exploiting the EEG correlates of implicit emotional responses is about how many EEG samples are needed from an individual to reliably model the emotional responses. The issue has also been recognized as a plausible factor affecting the classification accuracy while training a machine-learning classifier upon the given data. The previous study results may support the argument in part. The works that involved a short-duration (around 1–15 s per trial) emotion elicitation scenario, e.g., image viewing and emotion imagery (Chanel et al., 2009; Frantzidis et al., 2010; Petrantonakis and Hadjileontiadis, 2010), typically led to better results than those involved a long-duration

manner (around 30–120 s per trial), e.g., music listening and video watching (Koelstra et al., 2012; Soleymani et al., 2012; Gupta et al., 2016). In practice, an emotion experiment with EEG recordings faces a trade-off between acquiring more data trials and preventing the human subjects from being bored and drowsy to elicitation materials. In most cases, fewer than a few dozen of trials per targeted emotional class can be collected in a 2∼3-h experiment session for an individual, including the time for instruction briefing and EEG headset capping. The collected EEG trials are thus rare and likely pose a challenge for translating the EEG spatio-spectral oscillations into implicit emotional responses and for utilizing the EEG-emotion relationship to train a realistic subject-specific emotion-classification model.

A straightforward remedy for the aforementioned challenge in a single-day session is to perform a multiple-session EEG recording on separate days. Nevertheless, this raises another issue concerning the substantial inter-day variability in the EEG signals, which has been empirically demonstrated in studies (Christensen et al., 2012; Lin et al., 2015; Das et al., 2016; Yin and Zhang, 2017). That is, EEG features recorded on different days were found distinctively distributed. The data clusters of the same classes across days happened to behave more diversely than the clusters of different classes within a single day (Lin et al., 2015). This finding was in line with the outcomes using peripheral bio-signals (Picard et al., 2001). The class clusters were even dramatically changed by reversal among different days (Christensen et al., 2012). As such, the day-to-day variability inevitably hindered a machine-learning classifier from leveraging an effective set of between-class decision boundaries that can work consistently to the data recorded across days. It might happen that naively aggregating the EEG samples from all of the available recording days degrades rather than upgrades the classification accuracy (Christensen et al., 2012; Lin et al., 2015). Few attempts have been made to alleviate the inter-day variability by either using different normalization schemes or seeking a set of relatively day-robust features in other EEG topics, e.g., cognitive load, mental workload, and biometrics (Christensen et al., 2012; Das et al., 2016; Yin and Zhang, 2017). Till now, most of previous analytical works (Chanel et al., 2009; Frantzidis et al., 2010; Lin et al., 2010; Petrantonakis and Hadjileontiadis, 2010; Koelstra et al., 2012; Soleymani et al., 2012; Jenke et al., 2014; Gupta et al., 2016; Hu et al., 2017) endeavored to optimizing a predicative emotion-aware model based on a non-ecological single-day dataset only. However, for an ecological ABCI scenario, the EEG signals may vary over time, leading to the alternation of the emotion-related EEG oscillations, and thereby making a model trained by the EEG signals of a separate day(s) vulnerable. Relatively fewer efforts have been contributed to thoroughly explore and tackle the impact of the inter-day EEG variability associated with emotional responses, which is believed to be one of critical factors hindering the success of real-life applications.
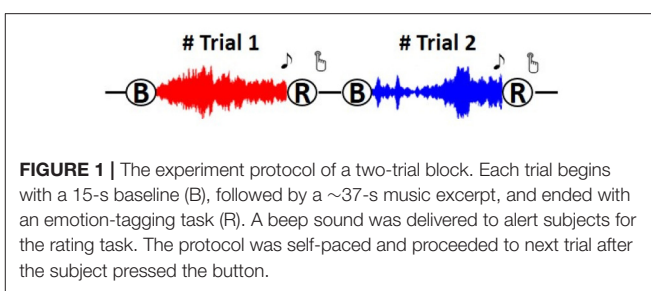
To address the issue mentioned above, this work proposed a signal-filtering strategy based on a core methodology called robust principal component analysis (RPCA) and incorporated it into a machine-learning framework. Its capability was demonstrated in terms of cross-day emotion-classification results

and corresponding neurophysiological meanings through a 5-day EEG dataset of 12 subjects. RPCA behaves as a matrix factorization method and enables parsing the input data matrix into a low-rank matrix and a sparse matrix. The low-rank matrix represents relatively regular activity or patterns in the original input matrix, whereas the sparse matrix accounts for deviant events. RPCA has been applied to improve the tracking of sparse moving targets of interest in video surveillance (Guyon et al., 2012; Bouwmans and Zahzah, 2014) and recently applied to affective computing to better capture the EEG correlates of neurocognitive lapses (Wei et al., 2016) as well as emotional responses (Jao et al., 2015). It is worth noting that this work was an extension from our proof-of-concept study (Jao et al., 2015) with considerable improvement in two aspects. First, this work provided neurophysiological evidence to exclusively elucidate the meanings underlying RPCA decomposition in emotion data. Second, a simulated online BCI validation procedure, i.e., training the data from available days and testing on the data from an unseen day, was employed to assess the cross-day classification performance regarding the accuracy and the number of informative features exploited. The successful demonstration can shed some light on developing a realistic emotion-classification analytical framework accounting for the EEG discrepancy in separate days.

MATERIALS AND METHODS
EEG Dataset
This work assessed the practicability of RPCA framework and its underlying neurophysiological meanings in alleviating the inter-day EEG variability on a 5-day dataset of 12 subjects when they performed a music-listening task (Lin et al., 2015). The details regarding the music excerpts and experiment setup can be found in Lin et al. (2015). Briefly, a 14-channel Emotiv EEG headset, with a default bandwidth of 0.16–43 Hz and a sampling rate of 128 Hz, was employed to measure the EEG signals. The subjects participated in the same music listening experiment on 5 different days within one and half weeks (with an average interval of 7 ± 1.13 days). On each day, they underwent a three-session protocol composed of the same 24~37-s music excerpts to induce two target emotions, happiness and sadness, in which 12 excerpts for each category were selected with a consensus label (Eerola and Vuoskoski, 2011). Each session had four blocks; each of them contained both happy and sad trials in random order. **Figure 1** illustrates the procedures of a two-trial block. Each trial began with a 15-s eye-closed rest period, followed by a music excerpt. A beep sound alerted the subjects to proceed to an emotion-assessment task (assigned either one of target emotions or neutral based on whey they experienced). The experiment was self-paced and allowed the subject to press a button proceeding to the next trial, enabling a moderate rest if necessary. Such an experiment protocol collected 24 pairs of ~37-s EEG trials (plus a 15-s eye-closed baseline) and emotion labels from an individual in each of the 5 recording days. Note that the trials reported as neutral responses were excluded from further analysis.

FIGURE 1 | The experiment protocol of a two-trial block. Each trial begins with a 15-s baseline (B), followed by a ~37-s music excerpt, and ended with an emotion-tagging task (R). A beep sound was delivered to alert subjects for the rating task. The protocol was self-paced and proceeded to next trial after the subject pressed the button.

EEG Feature Extraction
The raw EEG signals were first submitted to a 1-Hz high-pass finite impulse response filter to remove possible DC drifts. The short time Fourier transform was then adopted to estimate the spectral power of the filtered EEG signals using a 1-s Hamming window with a 50% overlap, yielding a number of the samples depended on the time lapse of the given trial (~37-s). The averaged band power over the stereotypical frequency bands of delta (1–3 Hz), theta (4–7 Hz), alpha (8–13 Hz), beta (14–30 Hz), and gamma (31–43 Hz) was calculated prior to feature extraction. Note that Emotiv headset's specification limited the gamma frequency band up to 43 Hz.

Given the five time series of spectral bands, this study adopted a feature-extraction method called MESH (Lin et al., 2014) to correlate EEG spectral oscillations with emotional responses. The MESH method not only includes the spectral oscillation over individual electrodes but also assesses bi-directional power asymmetry over left-right symmetric electrodes (i.e., laterality) and fronto-posterior electrodes (i.e., caudality). As such, the 12 channels (excluding T7 and T8 from the 14-ch Emotiv montage) corresponded to six left-right electrode pairs (i.e., AF3–AF4, F7–F8, F3–F4, FC5–FC6, P7–P8, and O1–O2, the montage refers to **Figure 2B**) and four fronto-posterior pairs (i.e., AF3–O1, F7–P7, AF4–O2, and F8–P8, resulting in a feature dimension of 110 (22 electrode attributes × five frequency bands). Each feature time series was normalized to the range of 0 and 1 using the min-max normalization scheme.

Robust Principal Component Analysis (RPCA)
Unlike classical principal component analysis (PCA) that transforms signals into a set of mutually orthogonal variables for dimensionality reduction, RPCA is a matrix factorization method that decomposes an input matrix $X \epsilon R^{m \times n}$ (m: number of features, n: number of samples) into two superimposed matrices, a low-rank matrix L and a sparse matrix S (Candès et al., 2011). The L accounts for the relatively regular profiles of input signals, whereas the S models its deviant events. The RPCA can be mathematically described as the convex optimization problem (Candès et al., 2011) presented below:

$$\min \text{}_{L,S} \| L \|_* + \lambda \| S \|_1 \qquad s.t. \ X = L + S, \qquad (1)$$

where $\| L \|_*$ denotes the nuclear norm of the matrix L, i.e., the sum of the singular value of L, $\| S \|_1 = \sum_{ij} |S_{ij}|$

represents l-1 norm of S, and λ is a tuning parameter balancing the weights of the two terms; we set λ to $1/\sqrt{\max(m, n)}$ according to Candès et al. (2011). RPCA has been successfully applied to many signal processing and computer vision problems, such as, video processing (Bouwmans and Zahzah, 2014), face recognition (Chen et al., 2012), and music information retrieval (Yang, 2012) as well as a recent demonstration on affective computing using EEG signals (Wei et al., 2016). For example, in the case of video surveillance, RPCA decomposed the still background scene in L and encompassed the sparse moving objects in S. It thus facilitated the detection of moving objects of interest by eliminating the interference from the background. It is worth noting that the robust PCA algorithm proposed by Torre and Black (2003) and the RPCA algorithm (Candès et al., 2011) adopted in this work, though share similar names, are radically different in their mathematical meanings. The former is for data dimension reduction, whereas the latter is for matrix decomposition that enables to parse inputs signals into low-rank and sparse matrices.

In a music-listening study, it is reasonable to assume that EEG oscillations associated with emotional responses are considered as deviant and sparse activity concurrent with intrinsic background EEG activity. Such background EEG activity tends to be relatively regular within days yet more and less diverse across days. The non-stationary background activity may thus submerge the sparse emotion-related EEG oscillations of interest and inevitably hinder the robustness of a cross-day emotion classification framework. With this in mind, this study hypothesized that the more the emotion-irrelevant EEG perturbations can be alleviated in each day, the more the elicited emotion-related EEG oscillations can be revealed. To test the posed hypothesis, this study adopted RPCA to parse the MESH matrix (i.e., 110 features $\times$ n samples, where n depends on the number of samples given a trial) into low-rank L and sparse S matrices. The resultant L presumably described relatively regular background EEG activity, while the resultant S oppositely captured sparse emotion-related dynamics.

EEG Feature Selection and Classification

After applying RPCA framework to the spectral time series, the processed samples were averaged within each trial for feature selection and classification. A straightforward method of F-score feature selection was adopted to elaborate the MESH feature space (either with or without RPCA pre-processing) to exploit an optimal subset of informative features prior to training the classifier. The F-score value refers to the ratio of between-class vs. within-class variance formed by the data distribution of a feature. It has been shown that the features with high F-score values can better discriminate class distributions (Lin et al., 2010; Jenke et al., 2014). Most importantly, as the calculated F-score value was compared to the statistical F-distribution, the corresponding statistical p-value of each feature ($p < 0.05$) can be derived to elucidate the neurophysiological meanings of RPCA-decomposed low-rank and sparse matrices. In this proof-of-concept study, a simple Gaussian Naïve Bayes (GNB) classifier was employed to model the EEG data distributions along two

emotion categories (i.e., happiness vs. sadness). The cross-day classification accuracy referred to how many trials were correctly classified.

Validation of RPCA Framework

This study attempted not only to test the effectiveness of the RPCA framework in alleviating the day-to-day variability in emotion-related EEG dynamics but also endeavored to unveil its underlying neurophysiological evidence. Three cross-day analytical scenarios were conceived and performed accordingly, including emotion classification, emotion-class distribution, and emotion-related spatio-spectral features.

First, a realistic add-day-in (ADI) validation framework was adopted to assess cross-day emotion classification accuracy. The ADI scheme iteratively included the data from one more recording day to train a classifier and test its performance against the data from one unseen recording day. That is, the information of EEG signals to be tested were entirely disjointed from the data used for training the model, which complied with a real-life BCI validation framework. Given a five-day EEG dataset per subject in this study, the cross-day classification accuracy can be obtained for four training day scenarios, including (1) Day 1 vs. Day 2, (2) Days 1–2 vs. Day 3, (3) Days 1–3 vs. Day 4, and (4) Days 1–4 vs. Day 5. The procedures of each ADI framework are detailed as follows.

1) *Train and optimize a GNB classifier*
   This step first concatenated data from D available training day(s) ($D = 1$–4). The concatenated data were then submitted to F-score feature selection to rank MESH features. To prevent the plausible bias caused by class imbalance, the GNB model was trained and optimized given 100 repetitive outcomes with random samples equally selected (according to the minimal class) from binary classes. Each randomization performed a five-fold cross-validation and an add-feature-in scheme, i.e., iteratively adding one more feature with high F-score at a time. The optimal MESH feature subspace leading to a maximal training accuracy could be selected.
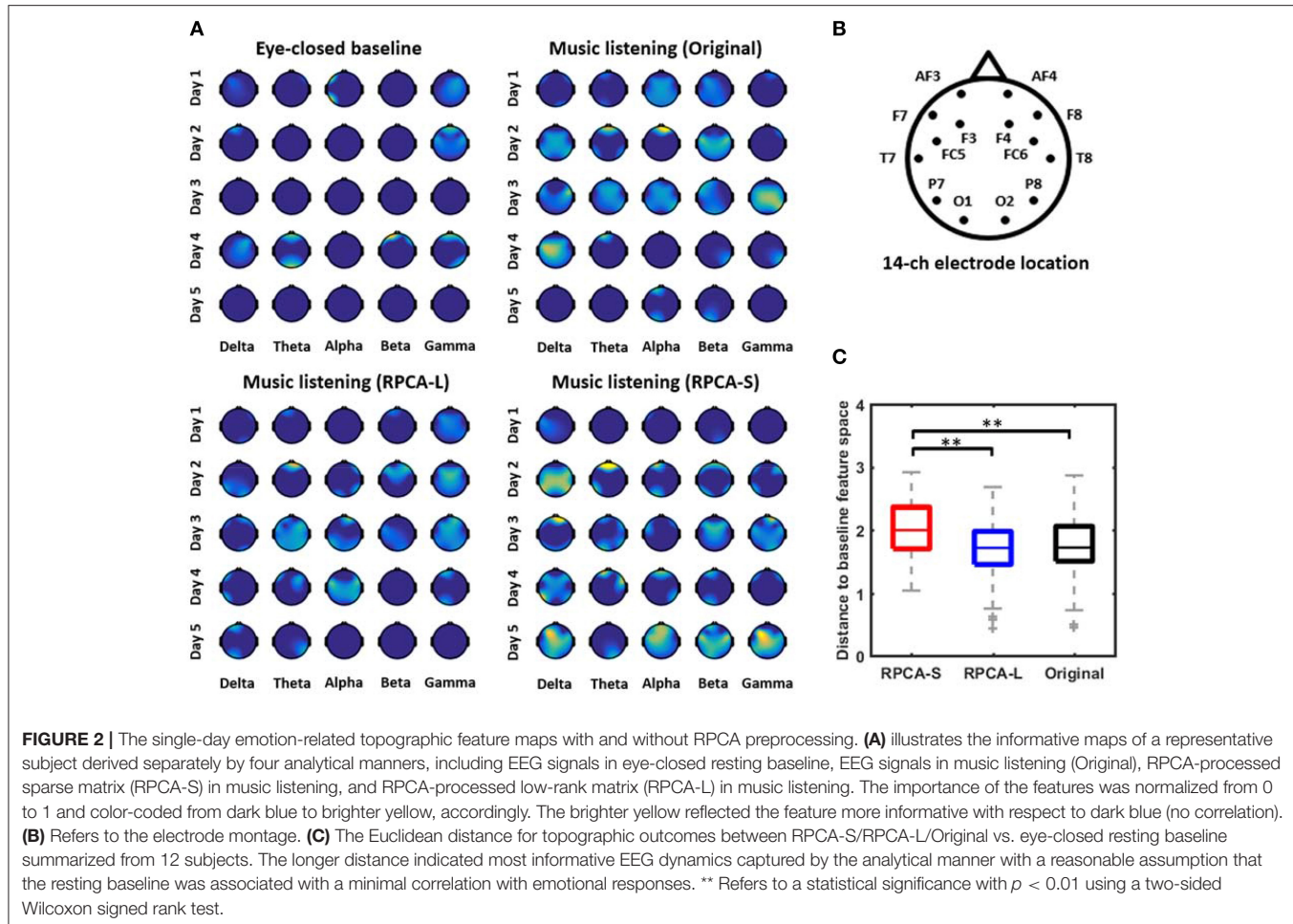
2) *Test the GNB classifier*
   The data from an unseen recording day were treated as test samples, and its initial MESH feature space was trimmed to fit the subspace optimized in the training phase. The trained GNB model was then tested on the trimmed data.

The ADI validation framework was applied to the EEG signals leveraged without and with RPCA processing for comparison.

Second, this study additionally visualized the emotion class distributions across days following the ADI manner. In this way, the variability in EEG signals between classes across days can be explored. We adopted the linear discriminative analysis (LDA) to reduce the original feature dimensionality (110) to a 2-D discriminative yet comprehensible feature space composed of the first two LDA components. Note that the LDA was simply involved in data visualization rather than in classification task. Furthermore, this study superimposed a decision boundary over the class clusters of the training data artificially. The boundary laid perpendicular to the vector of the means of the clusters and intercepted at their center. The multiple-day

FIGURE 2 | The single-day emotion-related topographic feature maps with and without RPCA preprocessing. **(A)** illustrates the informative maps of a representative subject derived separately by four analytical manners, including EEG signals in eye-closed resting baseline, EEG signals in music listening (Original), RPCA-processed sparse matrix (RPCA-S) in music listening, and RPCA-processed low-rank matrix (RPCA-L) in music listening. The importance of the features was normalized from 0 to 1 and color-coded from dark blue to brighter yellow, accordingly. The brighter yellow reflected the feature more informative with respect to dark blue (no correlation). **(B)** Refers to the electrode montage. **(C)** The Euclidean distance for topographic outcomes between RPCA-S/RPCA-L/Original vs. eye-closed resting baseline summarized from 12 subjects. The longer distance indicated most informative EEG dynamics captured by the analytical manner with a reasonable assumption that the resting baseline was associated with a minimal correlation with emotional responses. ** Refers to a statistical significance with $p < 0.01$ using a two-sided Wilcoxon signed rank test.

class distributions plus the conceptualized decision boundaries intended to demonstrate two facts: how the inter-day variability shaped the distributions of training and testing data, and to which extent this variability behaved in EEG signals with and without RPCA preprocessing.

Last, this study mapped the emotion-related EEG features that corresponded to high *F*-score values with statistical significance ($p < 0.05$) onto topography. The topographic mapping was done by using EEGLAB toolbox (Delorme and Makeig, 2004). Through comparing the topographic outcomes between a pre-stimulus baseline, i.e., eye-closed resting state, and a music-listening period, we could somehow elucidate the neurophysiological meanings underlying the RPCA-decomposed low-rank and sparse matrices. The low-rank matrix supposedly contained mostly background EEG dynamics, so that it barely had spectral characteristics about emotional responses. Thus, the maps of low-rank matrix exploited in music listening were presumably similar to those from the resting state. Furthermore, the ADI classification was also replicated on the eye-closed baseline. The baseline-music listening comparison can directly assess the validity of RPCA processing and *F*-score feature selection for cross-day emotion classification with more neurophysiological sense (i.e., EEG signals without and

with music elicitation). Note that for such analysis each of the pre-stimulus baseline trials was artificially assigned with an emotion label equal to the one rated right after the subsequent music-listening trial. In addition, for group analysis, this study vectorized each topographic outcome and objectively quantified their similarity using the Euclidean distance measurement. A longer distance referred to two distinct feature maps being compared.

RESULTS

Single-Day Topographic Feature Maps Underlying RPCA Matrices
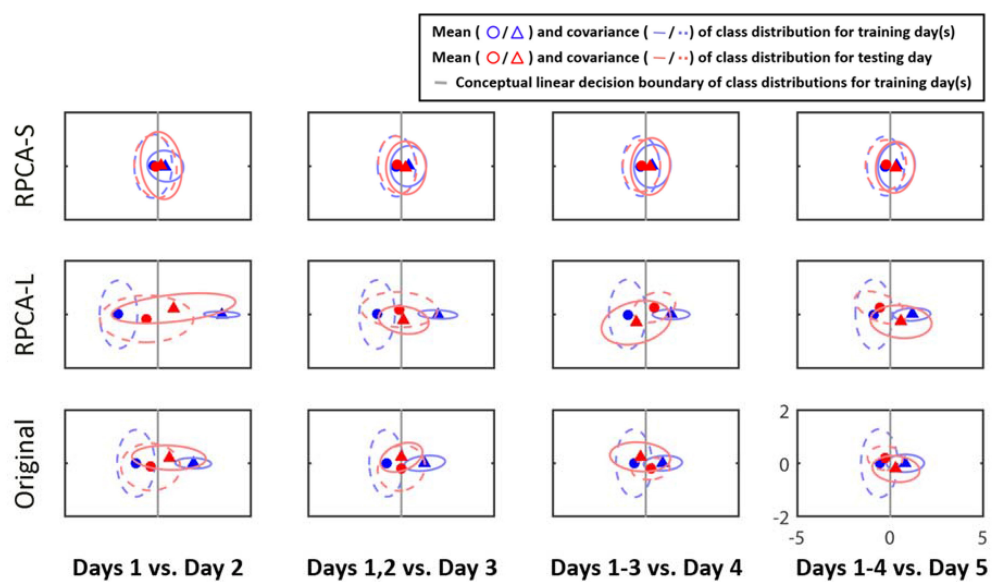
Figure 2 presents the single-day emotion-relevant EEG spatio-spectral features explored in music-listening vs. eye-closed resting scenarios. The comparative outcomes were obtained for four data matrices separately, including EEG signals in eye-closed resting baseline, EEG signals in music listening (Original), RPCA-processed sparse matrix (RPCA-S) in music listening, and RPCA-processed low-rank matrix (RPCA-L) in music listening. **Figure 2A** color-coded the importance (i.e., the *F*-score values) of the band-power features onto topography

(c.f. the electrode montage in **Figure 2B**) from a representative subject. All topographic values of four analytical outcomes were normalized concurrently to the range of 0 and 1 within each day so that the extent of each feature importance of all topographic outcomes could be compared across days. The brighter yellow indicates more informative features, compared to dark blue (no correlation). As can be seen in the topographic feature maps, the RPCA-S generally exhibited more emotion-related spectral features in each band and on each day, compared to its original input, i.e., Original. In contrast, the RPCA-L simply led to minor yet fewer informative features (with lighter yellow) on certain days. The benchmark scenario of eye-closed resting barely accompanied features. Most of the resting topographies were annotated with dark blue, similar to the outcomes of RPCA-L. Note that both the RPCA-L and RPCA-S of the resting baseline got analogous outcomes irrelevant to emotional responses (but not shown here).
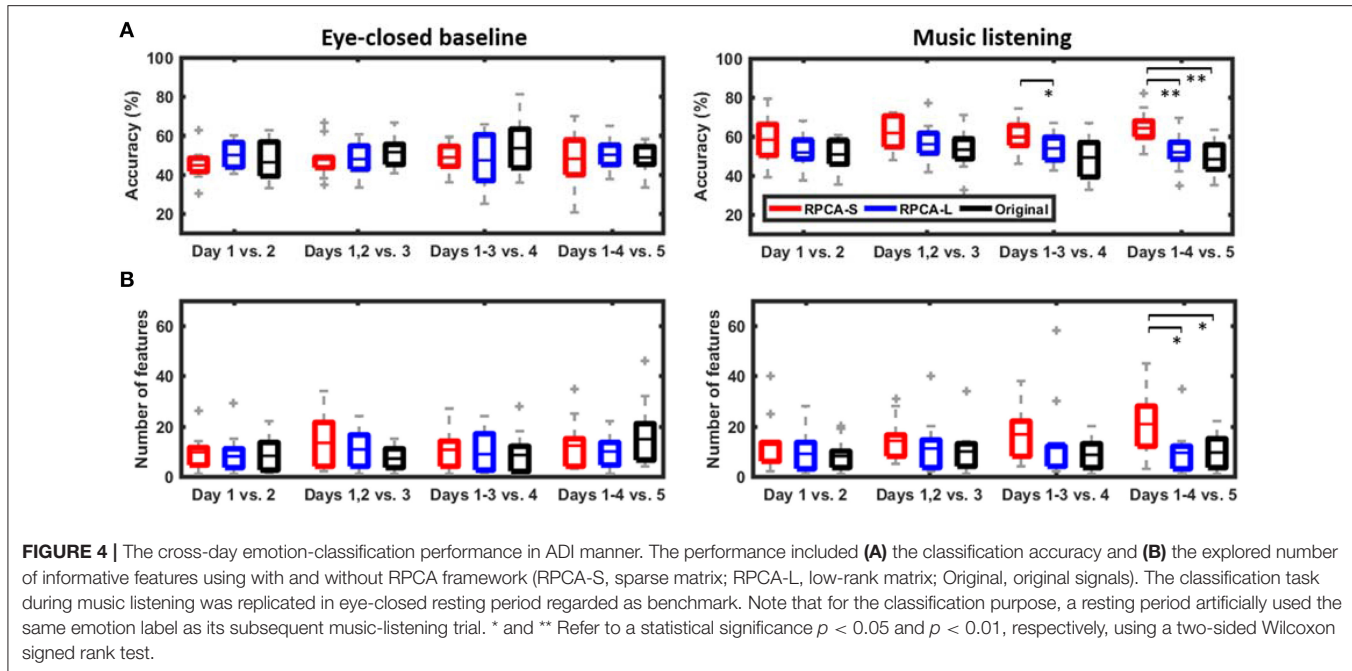
Figure 2C further quantified to which extent the emotion-related topographic maps with/without RPCA (i.e., RPCA-S, RPCA-L, and Original in music listening) were deviant from those of the benchmark (i.e., the eye-closed baseline) from the entire group of 12 subjects. To this end, the Euclidean distance measurement was adopted to calculate the distance between the vectorized topographic maps within each day. A longer distance value indicated the analytical matrix of interest being most informative under a reasonable assumption that the eye-closed resting state accounted for the minimal information regarding emotional responses. As can be seen, RPCA-S differed most from the eye-closed baseline than both the Original and RPCA-L did ($p < 0.01$). Due to the shortest distance, the RPCA-L's feature maps were the most similar to the baseline, followed by the Original.

Cross-Day Emotion Class Distributions with and Without RPCA Processing

Figure 3 illustrates the class distributions of the EEG signals projected to a 2D LDA feature space from a representative subject. The row of subplots from the bottom to the top represents the distributions of the original EEG signals (Original), its RPCA's low-rank matrix (RPCA-L), and its RPCA's sparse matrix (RPCA-S). The subplots along columns show the outcome with the ADI manner. As can be seen, the inter-day variability in Original did negatively shape the class distributions of the training data based on the relationship between the class centroids and distributions as the EEG signals were taken into account from more recording days. In the case of Day 1 vs. Day 2 in Original, the decision boundary (gray line) for Day 1 seemed to work for Day 2 because the two class centroids of the two days lined aside moderately. Nevertheless, the separable class centroids became misleading as considering the training data from one more recording day, i.e., Days 1–2 vs. Day 3, and even confusing by adding more days for the condition, i.e., Days 1–3 vs. Day 4, as referenced to their decision boundaries. While involving four recording days for training (Days 1–4 vs. Day 5), there was a smaller between-class margin than that of the initial outcome (Day 1 vs. Day 2). Next, after leveraging the EEG signals with RPCA processing, the inter-day variability tended to be mitigated to a certain extent. In the RPCA-S, the interplay of the class centroids of the training and testing days remained relatively stable to all ADI conditions, i.e., invulnerable to the number of recording days involved. Importantly, the decision boundary got improved marginally yet progressively when considering the data from more days as training dataset. On the contrary, the RPCA-L resembled the Original, but exhibited larger covariance

FIGURE 3 | The 2D projection of the cross-day class distributions of the EEG signals by LDA for a representative subject in ADI manner. The rows of subplots indicate the outcomes leveraged with or without RPCA processing (RPCA-S, sparse matrix; RPCA-L, low-rank matrix; Original, original signals). Triangles and circles are the centers of the happiness and sadness clusters, respectively, whereas the dotted and solid ellipses reflect their covariance values. The annotations in red and in blue referred to training and test days, respectively. The gray lines conceptualize the decision boundaries of the training data distributions.

FIGURE 4 | The cross-day emotion-classification performance in ADI manner. The performance included **(A)** the classification accuracy and **(B)** the explored number of informative features using with and without RPCA framework (RPCA-S, sparse matrix; RPCA-L, low-rank matrix; Original, original signals). The classification task during music listening was replicated in eye-closed resting period regarded as benchmark. Note that for the classification purpose, a resting period artificially used the same emotion label as its subsequent music-listening trial. * and ** Refer to a statistical significance $p < 0.05$ and $p < 0.01$, respectively, using a two-sided Wilcoxon signed rank test.

in class distributions. The above results evidently demonstrated the negative impact of the potential inter-day variability to a predictive emotion model, but the RPCA framework was capable of alleviating it to some extent.

Cross-Day Emotion Classification with and Without RPCA Processing

Figure 4 shows the cross-day emotion-classification performance with and without using the RPCA framework in the ADI manner. The classification performance includes the number of informative features and the binary classification accuracy explored during music listening vs. eye-closed resting. There were two main findings in the comparative results. First, the RPCA framework improved the cross-day classification accuracy. For the music-listening classification accuracy (right panel in **Figure 4A**), the RPCA-decomposed sparse matrix (RPCA-S, red box) improved the classification accuracy monotonically as more data were added from additional recording days (Day 1 vs. Day 2: $58.31 \pm 12.33\%$, Days 1–2 vs. Day 3: $61.53 \pm 8.62\%$, Days 1–3 vs. Day 4: $59.65 \pm 8.00\%$, and Days 1–4 vs. Day 5: $64.03 \pm 8.40\%$). Such improvement was up to around 6% ($p = 0.09$ using a two-sided Wilcoxon signed rank test) in the case of four training days. In contrast, the RPCA-decomposed low-rank matrix (RPCA-L, blue box) and the original EEG signals without RPCA preprocessing (Original, black box) did not replicate such improvement along ADI conditions. Their accuracies were apparently worse than those of RPAC-S. There was a statistically significant difference between RPCA-L and RPCA-S for Days 1–3 vs. Day 4 ($p < 0.05$) and between RPCA-L/Original and RPCA-S for Days 1–4 vs. Day 5 ($p < 0.01$), respectively. Opposed to the above music-listening outcomes, the benchmark of eye-closed resting (left panel in **Figure 4A**) neither exhibited distinct differences with and without RPCA preprocessing within each

ADI condition nor led to a tendency in classification accuracy along ADI conditions.

Second, the RPCA-S framework advanced the exploitation of informative features related to emotional responses. For the music-listening scenario (c.f. right panel of **Figure 4B**), the number of feature explored in RPCA-S was found to augment steadily as pooling EEG signals from one to four recording days (Day 1 vs. Day 2: 12.67 ± 5.99, Days 1–2 vs. Day 3: 14.17 ± 8.43, Days 1–3 vs. Day 4: 16.75 ± 5.74, and Days 1–4 vs. Day 5: 20.83 ± 7.18). The maximal increment was up to around 8 features for the ADI condition of four training days ($p = 0.06$). Unlike RPCA-S, both RPCA-L and Original exhibited features independent of the ADI conditions and typically yielded fewer features. Both of them were found significantly worse than RPCA-S for Days 1–4 vs. 5 ($p < 0.05$). For the eye-closed resting scenario, the number of features in RPCA-S tended to be comparable to those of RPCA-L and Original in each ADI condition and be independent to ADI conditions.

In sum, the RPCA-S led to progressive improvements in classification performance in terms of the number of informative features and the cross-day classification accuracy as long as the EEG signals leveraged from more recording days. This only worked for the music-listening scenario.

DISCUSSION

The present work studied how the inter-day EEG variability of emotional responses can be mitigated to facilitate cross-day emotion classification task, which was largely overlooked in the literature. This study extended our early proof-of-concept work (Jao et al., 2015) to validate the capability of the proposed RPCA-based signal filtering framework from the neurophysiological and

realistic BCI perspectives through a five-day EEG dataset of 12 subjects. We first validated that the RPCA-decomposed sparse signals returned representative EEG features reflecting emotional responses that were relatively consistent across days. We further demonstrated that such sparse signals helped a machine-learning framework to exploit more informative features and lead to a progressive improvement on cross-day emotion-classification accuracy as EEG signals were engaged from multiple-day sessions. In contrast, neither its accompaniment low-rank signals nor the raw EEG features (i.e., without RPCA preprocessing) could replicate the above cross-day classification outcomes. The following sections discussed the RPCA findings upon the neurophysiological validity and machine-learning practicability.

Neurophysiological Validity Underlying RPCA in Emotion Data

The present work aimed to exploit the underlying neurophysiological meanings associated with the two decomposed low-rank and sparse matrices using RPCA. By the mathematical definition of RPCA, the low-rank and sparse matrices account for the regular and sparse activities of the given streaming signals, respectively. The question herein was about what information the low-rank and sparse matrices actually account for in the EEG signals collected in an emotion-elicitation paradigm. There were three facets empirically indicating that the EEG oscillations captured in the sparse matrix were profitably linked to the implicit emotional responses. First, emotional responses elicited by music listening were considered as sparse activity. The induced EEG oscillations thus behaved as deviant activity to the concurrent intrinsic background activity, which presumably conformed to the mathematical role of the sparse matrix. As referred to the RPCA applications in other domains, the sparse matrix was also found to isolate sparse signal dynamics, such as, foreground moving objects in a video stream (Bouwmans and Zahzah, 2014), incoherent occlusion and disguise in a face image (Chen et al., 2012), neurocognitive lapses in driving (Wei et al., 2016), and a singing voice from music (Yang, 2012).

Second, the resultant music-baseline comparative outcomes of informative topographic feature maps (c.f., **Figure 2**) led to direct evidence. With respect to the sparse matrix, the low-rank matrix reciprocally dealt with regular activity in the given signals. Based on the results of this study, the low-rank matrix was found to reveal less informative features as compared to the sparse matrix and its original input (without RPCA processing), yet tended to be marginally similar to the control benchmark of the eye-closed baseline scenario (**Figures 2A,C**). This thus implied that the low-rank matrix relatively summarized intrinsic background EEG activity with a minimal relationship with emotional responses, like the eye-closed resting. However, one may argue a few features remained in the analytical scenarios of the eye-closed baseline and the RPCA-L from the illustrated individual. This may be attributed to the fact that most of the eye-closed baseline periods were interleaved with music excerpts (c.f., **Figure 1**).

The lingering emotion effects (Eryilmaz et al., 2011) might occur in our study. That is, the transit emotional responses induced in a regular music excerpt may remain and modulate the brain activity in subsequent resting state. In addition, as RPCA essentially involves a convex optimization problem (Candès et al., 2011), it may not lead to a perfect matrix-factorization decomposition. Some sparse activity may thus leak into the low-rank matrix (Han et al., 2017), contributing some minor information. Most critically, unlike the low-rank matrix, enormous emotion-relevant features emerged in the sparse matrix, which behaved most distinctly to the eye-closed condition.

Third, the music-baseline comparative cross-day classification performance in accuracy and the number of informative features (c.f., **Figure 4**) presented another conclusive evidence. The eye-closed resting periods barely provided discriminative information to conduct a binary emotion-classification task (i.e., around chance level) regardless of which analytical strategy (especially for the sparse matrix) was used and how much EEG-recording days were leveraged. Instead, the sparse matrix only worked valid for the EEG signals recorded in the music-listening period. Given more training days, the progressively increased number of informative features and the cross-day emotion-classification accuracy evidently inferred the discriminative yet emotional information exclusively captured by the sparse matrix.

Impact of the Inter-Day EEG Variability

Through the assessment to a five-day EEG dataset, the original EEG distributions (without RPCA processing) between training and test data across days (c.f., **Figure 3**) were found to be quite different. The binary clusters from an unseen day happened to be misleading or even reversal with the pre-learned class clusters, which exactly replicated the outcomes in Picard et al. (2001) and Christensen et al. (2012). Because of such the inconsistent class distributions, a classifier trained on one day may perform poorly on the test data collected from the same subject on another day. The resultant cross-day classification performance (c.f., **Figure 4**) reflected the negative impact of the inherent inter-day EEG variability, where involving more cross-day training sessions helped neither for exploring more robust informative features nor for optimizing the discriminative decision boundaries to yield a better classification accuracy. This implied that performing a multiple-day EEG collection and analysis barely worked without an efficient way to deal with day-to-day variability. It is worth noting that the aforementioned phenomenon may not emerge if an offline validation was adopted. For example, some works (Christensen et al., 2012; Liu et al., 2016) computed the cross-day classification accuracy by averaging the classification outcomes of all possible combinations of training and test days. Without a constraint on time ordering (e.g., allowing using Days 4, 5 to predict Day 1), the chance for including a day(s) having feature distributions compatible to those of a test day(s) likely increases (Lin et al., 2015). The plausible discrepancy of feature distributions on separate days and the

corresponding degradation in cross-day classification accuracy might thus be overlooked. Furthermore, such an offline manner is unlikely the case for an ecological, real-life scenario, i.e., we may not use the data of a later day(s) to predict the emotional responses on a prior day(s). In contrast, the ADI scheme adopted by the present work considers time ordering and facilitates more realistic assessment of the impact of inter-day EEG variability.

The RPCA-based signal-filtering framework was proposed in the present work for the above purpose. Following the demonstrated neurophysiological evidence underlying the RPCA (see detailed discussions in the last subsection), the RPCA-decomposed low-rank matrix predominantly accounted for the background EEG activity that seemed to contribute more to the concerned inter-day EEG variability. That is, the RPCA-L and Original (before RPCA processing) compared favorably in cluster distributions along the ADI manner (c.f., **Figure 3**). Our exploratory results were in line with the previous outcome in motor imagery study (Shenoy et al., 2006), in which different background EEG activity was reported to shift the data in the feature space. After mitigating the background EEG perturbations (c.f., **Figure 4**), the phenomenon gave a direct support to the outcome of the improved cross-day classification accuracy in the RPCA-decomposed sparse matrix (i.e., RPCA-S). The extent of the improvement in accuracy when given more training days was attributed to the fact that the RPCA-S elaborated the class clusters gently yet progressively. Accordingly, the class distributions and the cross-day classification performance empirically demonstrated the posed hypothesis that the more the intrinsic EEG perturbations can be alleviated in each day, the more the elicited emotion-related EEG oscillations can be revealed.

This work has a limitation in elucidating plausible causes contributing the background EEG perturbations in the analyzed dataset. Some studies (Shenoy et al., 2006; Ahn et al., 2016) mentioned that the mental states of the subjects, such as, mental fatigue, attention level, engagement to the task, and sleep quality, may alter EEG patterns. This thereby suggested that future emotion study may include a comprehensive behavioral and mental questionnaire along with emotional labels, facilitating a systematic assessment of realistic EEG oscillations of emotional responses.

Comparison to Previous Works

This work performed a binary emotion-classification task dedicated to an ecologically cross-day EEG dataset (five days). The realistic ADI validation manner was adopted to obtain the cross-day emotion-classification performance, which can straightforwardly infer the practicality of the proposed RPCA framework toward real-life applications. The study results showed that the optimal binary classification accuracy (using the sparse matrix, RPCA-S, c.f., **Figure 4**) was improved steadily from 58.31 ± 12.33% to 64.03 ± 8.40% as leveraging more EEG signals from one to four recording days for training. Nevertheless, most of previously related works (Koelstra et al., 2012; Koelstra and Patras, 2013; Lin et al., 2014; Gupta

et al., 2016), in which a binary task was also conducted on limited data trials (using a long-duration elicitation materials), performed the analysis on a single-day dataset only, so that the impact of the inter-day EEG variability was not considered. As such, this study cannot make a direct comparison to the previous works, but instead we summarized their reported within-day binary classification accuracies for reference as follows: 55.4∼62.0% for different emotion categories (referred to their Table 7 in Koelstra et al., 2012), 63.5∼71.5% for different categories and features (Koelstra and Patras, 2013 referred to their EEG results in Table 3), 67∼76% for different categories and features (referred to their Figure 2 in Lin et al., 2014), and 58∼69% for different categories and features (referred to their in Table 5 Gupta et al., 2016). It was expected that the within-day accuracies that were not negatively affected by the inter-day variability outperformed the cross-day outcomes. The resultant cross-day accuracies of 58.31∼64.03% using different training days in the present study seemed justifiable.

CONCLUSION

This study proposed a robust principal component analysis (RPCA)-based signal-filtering strategy and incorporated it into a machine-learning framework to improve cross-day EEG-based emotion-classification performance. Through applying a realistic add-day-in validation manner to a five-day EEG dataset of 12 subjects, this study first validated that the RPCA-decomposed sparse signals predominately captured the EEG oscillations of emotional responses that were relatively consistent across days, and suppressed the day-fluctuated background EEG perturbations in its accompaniment low-rank signals. By leveraging EEG signals from all four recording days for training and tested for the last unseen day, the maximal improvement in the number of informative features and the cross-day classification accuracy appeared up to ∼8 and ∼6%, respectively. The original EEG features (prior to RPCA processing) neither achieved the cross-day classification task (i.e., the accuracy was around chance level) nor replicated the encouraging improvement due to the inter-day EEG variability.

ETHICS STATEMENT

The study was conducted in accordance with the Declaration of Helsinki and approved by the local Ethics Committee of University of California, San Diego.

AUTHOR CONTRIBUTIONS

YL conceived analytical hypothesis, performed data analysis and interpretation, and drafted/revised the work; PJ performed data analysis and interpretation, and revised the work; YY contributed to data interpretation and revised the work. All authors approved the work for publication.

FUNDING

ACKNOWLEDGMENTS

REFERENCES

Ahn, S., Nguyen, T., Jang, H., Kim, J. G., and Jun, S. C. (2016). Exploring neurophysiological correlates of drivers' mental fatigue caused by sleep deprivation using simultaneous EEG, ECG, and fNIRS data. *Front. Hum. Neurosci.* 10:219. doi: 10.3389/fnhum.2016.00219

Bouwmans, T., and Zahzah, E. H. (2014). Robust PCA via principal component pursuit: a review for a comparative evaluation in video surveillance. *Comput. Vis. Image Underst.* 122, 22–34. doi: 10.1016/j.cviu.2013.11.009

Candès, E. J., Li, X. D., Ma, Y., and Wright, J. (2011). Robust principal component analysis? *J. ACM* 58:11. doi: 10.1145/1970392.1970395

Chanel, G., Kierkels, J. J. M., Soleymani, M., and Pun, T. (2009). Short-term emotion assessment in a recall paradigm. *Int. J. Hum. Comput. Stud.* 67, 607–627. doi: 10.1016/j.ijhcs.2009.03.005

Chen, C. F., Wei, C. P., and Wang, Y. C. F. (2012). "Low-rank matrix recovery with structural incoherence for robust face recognition", in *IEEE Conference on Computer Vision and Pattern Recognition* (Providence).

Chen, M., Ma, Y., Li, Y., Wu, D., Zhang, Y., and Youn, C. H. (2017). Wearable 2.0: enabling human-cloud integration in next generation healthcare systems. *IEEE Commun. Mag.* 55, 54–61. doi: 10.1109/MCOM.2017.1600410CM

Christensen, J. C., Estepp, J. R., Wilson, G. F., and Russell, C. A. (2012). The effects of day-to-day variability of physiological data on operator functional state classification. *Neuroimage* 59, 57–63. doi: 10.1016/j.neuroimage.2011.07.091

Das, R., Maiorana, E., and Campisi, P. (2016). EEG biometrics using visual stimuli: a longitudinal study. *IEEE Signal Process. Lett.* 23, 341–345. doi: 10.1109/LSP.2016.2516043

Delorme, A., and Makeig, S. (2004). EEGLAB: an open source toolbox for analysis of single-trial EEG dynamics including independent component analysis. *J. Neurosci. Methods* 134, 9–21. doi: 10.1016/j.jneumeth.2003.10.009

Eerola, T., and Vuoskoski, J. K. (2011). A comparison of the discrete and dimensional models of emotion in music. *Psychol. Music* 39, 18–49. doi: 10.1177/0305735610362821

Eryilmaz, H., Van De Ville, D., Schwartz, S., and Vuilleumier, P. (2011). Impact of transient emotions on functional connectivity during subsequent resting state: a wavelet correlation approach. *Neuroimage* 54, 2481–2491. doi: 10.1016/j.neuroimage.2010.10.021

Frantzidis, C. A., Bratsas, C., Papadelis, C. L., Konstantinidis, E., Pappas, C., and Bamidis, P. D. (2010). Toward emotion aware computing: an integrated approach using multichannel neurophysiological recordings and affective visual stimuli. *IEEE Trans. Inform. Technol. Biomed.* 14, 589–597. doi: 10.1109/TITB.2010.2041553

Gupta, R., Laghari, K. U. R., and Falk, T. H. (2016). Relevance vector classifier decision fusion and EEG graph-theoretic features for automatic affective state characterization. *Neurocomputing* 174, 875–884. doi: 10.1016/j.neucom.2015.09.085

Guyon, C., Bouwmans, T., and Zahzah, E.-H. (2012), "Robust principal component analysis for background subtraction: systematic evaluation and comparative analysis," in *Principal Component Analysis*, ed P. Sanguansat (InTech), 223–238. doi: 10.5772/38267

Han, N., Song, Y., and Song, Z. (2017). Bayesian robust principal component analysis with structured sparse component. *Comput. Stat. Data Anal.* 109, 144–158. doi: 10.1016/j.csda.2016.12.005

Hariri, A. R., Bookheimer, S. Y., and Mazziotta, J. C. (2000). Modulating emotional responses: effects of a neocortical network on the limbic system. *Neuroreport* 11, 43–48. doi: 10.1097/00001756-200001170-00009

Hu, X., Yu, J. W., Song, M. D., Yu, C., Wang, F., Sun, P., et al. (2017). EEG correlates of ten positive emotions. *Front. Hum. Neurosci.* 11:26. doi: 10.3389/fnhum.2017.00026

Ian, D., Duncan, W., Alexis, K., James, W., Asad, M., Faustina, H., et al. (2016). Affective brain–computer music interfacing. *J. Neural Eng.* 13:046022. doi: 10.1088/1741-2560/13/4/046022

Jao, P. K., Lin, Y. P., Yang, Y. H., and Jung, T. P. (2015). "Using robust principal component analysis to alleviate day-to-day variability in EEG based emotion classification," in *37th Annual International Conference of the IEEE Engineering in Medicine and Biology Society* (Milan), 570–573.

Jenke, R., Peer, A., and Buss, M. (2014). Feature extraction and selection for emotion recognition from EEG. *IEEE Trans. Affect. Comput.* 5, 327–339. doi: 10.1109/TAFFC.2014.2339834

Kim, J., and Andre, E. (2008). Emotion recognition based on physiological changes in music listening. *IEEE Trans. Pattern Anal. Mach. Intell.* 30, 2067–2083. doi: 10.1109/TPAMI.2008.26

Koelstra, S., Muhl, C., Soleymani, M., Lee, J. S., Yazdani, A., Ebrahimi, T., et al. (2012). DEAP: a database for emotion analysis using physiological signals. *IEEE Trans. Affect. Comput.* 3, 18–31. doi: 10.1109/T-AFFC.2011.15

Koelstra, S., and Patras, I. (2013). Fusion of facial expressions and EEG for implicit affective tagging. *Image Vis. Comput.* 31, 164–174. doi: 10.1016/j.imavis.2012.10.002

Lee, J. S., and Shin, D. H. (2013). "A study on the interaction between human and smart devices based on emotion recognition," in *Communications in Computer and Information Science*, ed C. Stephanidis (Berlin; Heidelberg: Springer Berlin Heidelberg), 352–356.

Lin, Y. P., Hsu, S. H., and Jung, T. P. (2015). "Exploring day-to-day variability in the relations between emotion and EEG signals," in *Lecture Notes in Computer Science*, eds D. D. Schmorrow and C. M. Fidopiastis (Cham: Springer International Publishing), 461–469.

Lin, Y. P., Wang, C. H., Jung, T. P., Wu, T. L., Jeng, S. K., Duann, J. R., et al. (2010). EEG-based emotion recognition in music listening. *IEEE Trans. Biomed. Eng.* 57, 1798–1806. doi: 10.1109/TBME.2010.2048568

Lin, Y. P., Yang, Y. H., and Jung, T. P. (2014). Fusion of electroencephalographic dynamics and musical contents for estimating emotional responses in music listening. *Front. Neurosci.* 8:94. doi: 10.3389/fnins.2014.00094

Liu, S., Tong, J., Xu, M., Yang, J., Qi, H., and Ming, D. (2016). "Improve the generalization of emotional classifiers across time by using training samples from different days," in *2016 38th Annual International Conference of the IEEE Engineering in Medicine and Biology Society (EMBC)* (Orlando, FL), 841–844.

Mühl, C., Allison, B., Nijholt, A., and Chanel, G. (2014). A survey of affective brain computer interfaces: principles, state-of-the-art, and challenges. *Brain Comput. Interfaces* 1, 66–84. doi: 10.1080/2326263X.2014.912881

Muñoz, K., Kevitt, P. M., Lunney, T., Noguez, J., and Neri, L. (2010). "PlayPhysics: an emotional games learning environment for teaching physics," in *Lecture Notes in Computer Science*, eds Y. Bi and M.-A. Williams (Berlin; Heidelberg: Springer Berlin Heidelberg), 400–411.

Petrantonakis, P. C., and Hadjileontiadis, L. J. (2010). Emotion recognition from brain signals using hybrid adaptive filtering and higher order crossings analysis. *IEEE Trans. Affect. Comput.* 1, 81–97. doi: 10.1109/T-AFFC.2010.7

Picard, R. W., Vyzas, E., and Healey, J. (2001). Toward machine emotional intelligence: analysis of affective physiological state. *IEEE Trans. Pattern Anal. Mach. Intell.* 23, 1175–1191. doi: 10.1109/34.954607

Pinheiro, P. G., Ramos, J. J. G., Donizete, V. L., Picanço, P., and De Oliveira, G. H. (2017). "Workplace emotion monitoring-an emotion-oriented system hidden behind a receptionist robot," in *Mechatronics and Robotics Engineering for Advanced and Intelligent Manufacturing*, eds D. Zhang and B. Wei (Cham: Springer International Publishing), 407–420.

Shenoy, P., Krauledat, M., Blankertz, B., Rao, R. P. N., and Muller, K. R. (2006). Towards adaptive classification for BCI. *J. Neural Eng.* 3, R13–R23. doi: 10.1088/1741-2560/3/1/R02

Soleymani, M., Pantic, M., and Pun, T. (2012). Multimodal emotion recognition in response to videos. *IEEE Trans. Affect. Comput.* 3, 211–223. doi: 10.1109/T-AFFC.2011.37

Torre, F. D. L., and Black, M. (2003). A framework for robust subspace learning. *Int. J. Computer Vis.* 54, 117–142. doi: 10.1023/A:1023709501986

Wei, C. S., Lin, Y. P., and Jung, T. P. (2016). "Exploring the EEG correlates of neurocognitive lapse with robust principal component analysis," in *Lecture Notes in Computer Science*, eds D. D. Schmorrow and C. M. Fidopiastis (Cham: Springer International Publishing), 113–120.

Yang, Y. H. (2012). "On sparse and low-rank matrix decomposition for singing voice separation," in *Proceedings of the 20th ACM International Conference on Multimedia* (Nara: ACM).

Yin, Z., and Zhang, J. (2017). Cross-session classification of mental workload levels using EEG and an adaptive deep learning model.

Biomed. Signal Process. Control 33, 30–47. doi: 10.1016/j.bspc.2016.11.013

Face Recognition, Musical Appraisal, and Emotional Crossmodal Bias

Sara Invitto [1]*, Antonio Calcagnì [2], Arianna Mignozzi [1], Rosanna Scardino [1], Giulia Piraino [3], Daniele Turchi [1], Irio De Feudis [4], Antonio Brunetti [4], Vitoantonio Bevilacqua [4] and Marina de Tommaso [5]

[1] Human Anatomy and Neuroscience Lab, Department of Environmental Science and Technology, University of Salento, Lecce, Italy, [2] Department of Psychology and Cognitive Sciences, University of Trento, Trento, Italy, [3] Santa Chiara Institute, Lecce, Italy, [4] Department of Electrical and Information Engineering, Polytechnic University of Bari, Bari, Italy, [5] Department of Medical Science, Neuroscience, and Sense Organs, University Aldo Moro, Bari, Italy

Recent research on the crossmodal integration of visual and auditory perception suggests that evaluations of emotional information in one sensory modality may tend toward the emotional value generated in another sensory modality. This implies that the emotions elicited by musical stimuli can influence the perception of emotional stimuli presented in other sensory modalities, through a top-down process. The aim of this work was to investigate how crossmodal perceptual processing influences emotional face recognition and how potential modulation of this processing induced by music could be influenced by the subject's musical competence. We investigated how emotional face recognition processing could be modulated by listening to music and how this modulation varies according to the subjective emotional salience of the music and the listener's musical competence. The sample consisted of 24 participants: 12 professional musicians and 12 university students (non-musicians). Participants performed an emotional go/no-go task whilst listening to music by Albeniz, Chopin, or Mozart. The target stimuli were emotionally neutral facial expressions. We examined the N170 Event-Related Potential (ERP) and behavioral responses (i.e., motor reaction time to target recognition and musical emotional judgment). A linear mixed-effects model and a decision-tree learning technique were applied to N170 amplitudes and latencies. The main findings of the study were that musicians' behavioral responses and N170 is more affected by the emotional value of music administered in the emotional go/no-go task and this bias is also apparent in responses to the non-target emotional face. This suggests that emotional information, coming from multiple sensory channels, activates a crossmodal integration process that depends upon the stimuli emotional salience and the listener's appraisal.

Keywords: music cognition, face recognition, N170 ERP, emotional salience, crossmodal integration, emotional biases, musical appraisal

INTRODUCTION

The wide discussion of recent research on the interaction between music and emotion addresses various issues, mainly those relating to comparisons between emotional processing and sensory experience, and the definition of music a process of "sense making" that involves and influences aspects of perception and cognition, as posited in a joint model of embodied mind (Reybrouck, 2005; Reybrouck and Brattico, 2015; Schiavio et al., 2016). Pioneering research on the crossmodal

integration of visual and auditory perception suggests that evaluations of emotional information in one sensory modality may tend toward the emotional value generated in another (de Gelder and Vroomen, 2000; Logeswaran and Bhattacharya, 2009; Balconi and Carrera, 2011). Ad example, a realistic model able to explain emotional recognition process and crossmodal integration is the model of Balconi (Balconi and Carrera, 2011). This model is based on an experiment of a face recognition task interfaced, in crossmodal condition, with prosody, and analyzed through P2 ERP. The model highlights how an early ERP component (i.e., P2) can be considered a cognitive marker in multisensory processing. Thus, the emotion produced by musical stimulation, as could be prosody in the previous model, may influence the stimuli perception of stimuli, presented in other sensory modalities, through a top-down process (Sekuler et al., 1997; Jolij and Meurs, 2011; Wong and Gauthier, 2012). Different musical genres can also modulate arousal and others psychophysiological parameters eliciting different emotions (Schellenberg, 2005; Caldwell and Riby, 2007; Sammler et al., 2007; Fritz et al., 2009; Ladinig and Schellenberg, 2012; Schellenberg and Mankarious, 2012; Kawakami et al., 2014; Bhatti et al., 2016). For example, Baumgartner and colleagues investigated the psychophysiological effect of the interaction between emotional visual images, music, and a crossmodal presentation (music and images; Baumgartner et al., 2006). More intensely perceived emotions emerged in the crossmodal condition, and this was accompanied by predominant alpha band activity in EEG.

It has been proposed that music primes emotional responses to information in the visual domain (Logeswaran

TABLE 1 | Independent-samples t-tests of VAS results.

Musician	Emotion	t	df	Two-tailed significance	Mean VAS score	
					Musicians	Non-musicians
Albeniz	Pleasant	2.138	22	0.044	9.09	7.23
Mozart	Happy	3.537	22	0.002	8.91	6.85
Chopin	Pleasant	2.690	22	0.013	9.27	7.46
Chopin	Sad	6.546	22	0.000	8.64	4.31

T-tests are conducted with respect to the Group variable (Non-Musicians vs. Musicians) over different emotional levels (Pleasant, Happy, Sad) and different Music (Albeniz, Chopin, Mozart). Note that T-value are computed with the t-statistics corrected for paired groups, df indicates the degree of freedom of the test, whereas p-values are computed considered alpha = 0.05

TABLE 2 | Mean of the behavioral reaction times (in millisecond) in response to neutral faces during the emo go/no-go task.

Group	Reaction time		
	Albeniz	Chopin	Mozart
Musicians	744.75	721.31	662.15
Non-Musicians	564.29	587.42	570.57

Mean of reaction time in musicians is slower than in non-musicians group.

TABLE 3 | Results of linear mixed-effects model: fixed effects for group and music on N170 amplitude.

ROI		B (SE)	t
L-Ant	Baseline	−1.423 (0.231)	−6.144
	Group		
	Non-Musicians vs. Musicians	−0.175 (0.279)	−0.628
	Music		
	Albeniz vs. Chopin	0.209 (0.137)	1.523
	Albeniz vs. Mozart	0.019 (0.141)	0.134
	Group × music		
	Non-Musicians × Albeniz vs. Musicians × Chopin	−0.456 (0.212)	−2.152*
	Non-Musicians × Albeniz vs. Musicians × Mozart	0.070 (0.212)	0.331
R-Ant	Baseline	−1.431 (0.208)	−6.868
	Group		
	Non-Musicians vs. Musicians	−0.419 (0.214)	−2.11*
	Music		
	Albeniz vs. Chopin	0.299 (0.114)	2.701**
	Albeniz vs. Mozart	0.003 (0.110)	0.282
	Group × music		
	Non-Musicians × Albeniz vs. Musicians × Chopin	−0.360 (0.168)	−2.133*
	Non-Musicians × Albeniz vs. Musicians × Mozart	0.541 (0.171)	3.161**
L-Post	Baseline	−2.245 (0.365)	−6.137
	Group		
	Non-Musicians vs. Musicians	−0.687 (0.285)	−2.412*
	Music		
	Albeniz vs. Chopin	0.123 (0.106)	1.155
	Albeniz vs. Mozart	0.024 (0.110)	0.225
	Group × music		
	Non-Musicians × Albeniz vs. Musicians × Chopin	0.514 (0.328)	1.568
	Non-Musicians × Albeniz vs. Musicians × Mozart	0.857 (0.330)	2.596**
R-Post	Baseline	−2.245 (0.379)	−5.920
	Group		
	Non-Musicians vs. Musicians	−1.187 (0.550)	−2.157*
	Music		
	Albeniz vs. Chopin	−0.105 (0.211)	0.617
	Albeniz vs. Mozart	−0.392 (0.225)	−1.741
	Group × music		
	Non-Musicians × Albeniz vs. Musicians × Chopin	0.286 (0.339)	0.845
	Non-Musicians × Albeniz vs. Musicians × Mozart	0.827 (0.341)	2.422*
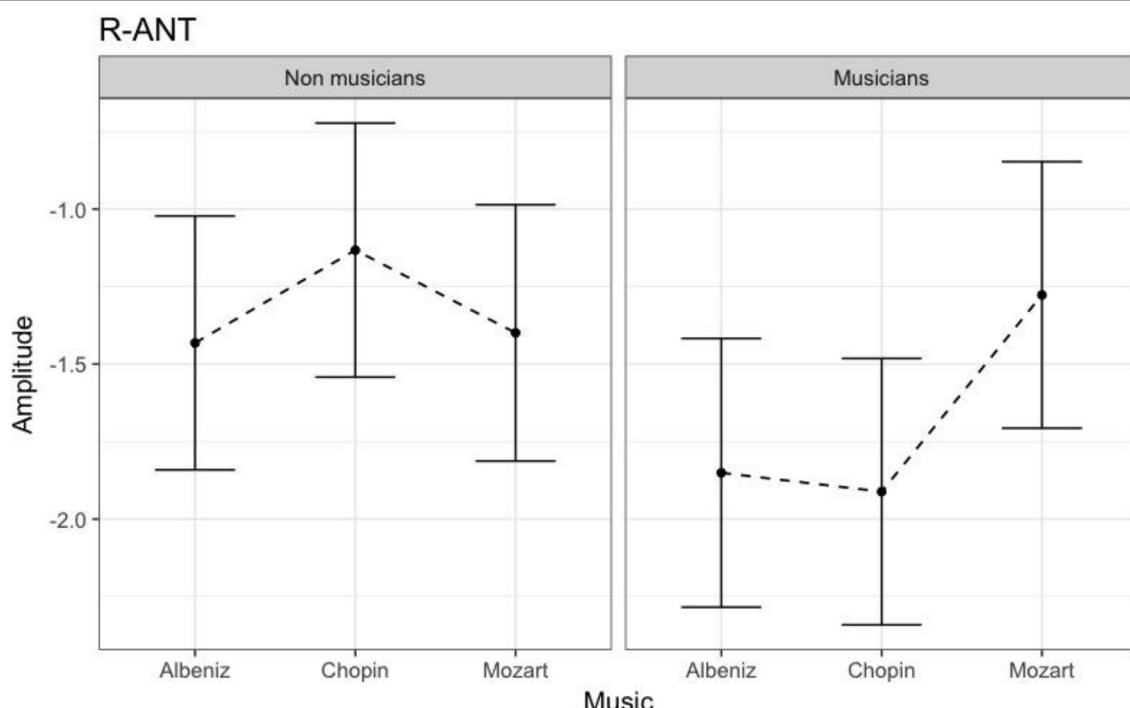
Participants and EEG channels were treated as random effects; degrees of freedom of the model were calculated with the Satterthwaite approximation. L-Ant: left-anterior; R-Ant: right-anterior; L-Post: left-posterior; R-Post: right-posterior.
*p < 0.05; **p < 0.01.*

and Bhattacharya, 2009). Logeswaran and Bhattacharya demonstrated that musical priming (positive or negative) can modulate perceptions of emotional faces. In their study, participants were asked to rate the emotional salience of the faces, and the results demonstrated the existence of a crossmodal priming effect. Happy faces were rated as happier when they were presented after a happy piece of music and vice versa. The priming effect of music is evident with neutral targets. Analysis of Event-Related Potential (ERP) components showed that the N1 response to neutral faces increases when stimulus presentation is preceded by happy music than when it was preceded by sad music. Previous studies have observed an increased N1 component in the auditory cortex during simultaneous presentation of an emotionally congruent face (i.e., face–voice pairs; Pourtois et al., 2002). The N1 component was distributed over the frontal regions, suggesting the involvement of top–down psychophysiological mechanisms (Zanto et al., 2011; Gilbert and Li, 2013). Moreover, the perception of music is affected by the listener's emotional and cognitive state (Kawakami et al., 2013, 2014). Many studies have highlighted differences between the cognitive processing and cortical responses of musicians and non-musicians (Pantev et al., 1998; Brattico et al., 2010; Müller et al., 2010; Pallesen et al., 2010; Herholz and Zatorre, 2012; Proverbio et al., 2013).

Recent studies suggest that musical stimulation may interact with fatigue and motor activity, thereby affecting the motivation of individuals who are under intense physical stress (Bigliassi et al., 2016a,b). Music can modulate perception and cognition

via a complex interaction between the perceptual and emotional characteristics of a musical stimulus and the physical (i.e., sex differences; Miles et al., 2016), psychophysiological, (Gosselin et al., 2007) and cognitive characteristics of the listener. Because of this interaction, the emotion invoked by music can result in biased responses (Chen et al., 2008). The aim of our study was to investigate how cross-modal perception—in this instance processing of emotional faces whilst performing a task that involves listening to music—varies with the subjective emotional salience of the music and with musical competence. This effect can be seen at cognitive and behavioral level, in decisions and appraisals, (Ellsworth and Scherer, 2003) and at motor level (in motor reaction time; Brattico et al., 2013). In fact, the motor and perceptual systems can be subject to early, top-down modulation induced by crossmodal stimulation, which can induce emotional bias, reflected at the behavioral level and in cortical responses (i.e., electrophysiological level). We also evaluated whether this bias could be modulated by the participant's appraisal of the musical stimulus (Brattico and Jacobsen, 2009) choosing an electrophysiological investigation of N170 ERP component. N170 ERP component is the most sensible ERP component able to be modulated in the Face Recognition Tasks (Eimer, 2000, 2011; Heisz et al., 2006; Kolassa et al., 2009; Ibanez et al., 2012; Leleu et al., 2015; Almeida et al., 2016). In particular, N170 is strictly linked to automatic processes (Heisz et al., 2006), instead of P2, that is a demonstrated cognitive marker in crossmodal cognition (Balconi and Carrera, 2011; Peretz, 2012). Still, in the condition in which music is perceived as a cognitive expertise, the emotional salience of the

FIGURE 1 | N170 amplitudes in non-musicians and musicians in R-ANT ROI (Right Anterior Region of Interest).

stimulus observed (i.e., face expression), may be affected by emotional bias, and this effect can be early observable through N170 modulations.
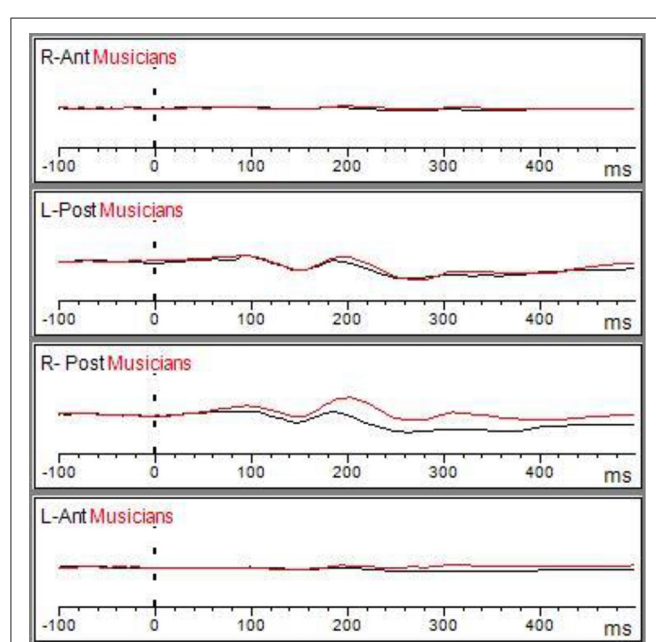
MATERIALS AND METHODS

Participants

Twenty-four participants were recruited in University and in Musical Conservatory, and were selected according to their musical skills. Twelve musicians, graduates in a Musical Conservatory, (5 men and 7 women; mean age = 29.8 years; $SD \pm 7.2$) were compared to a group of 12 non-musicians, University students (graduated of the three-year degree and attending the specialist degree) without educational musical training (7 men and 5 women; mean age = 26.9 years; $SD \pm 4.5$). The instruments played by the group of musicians included piano, guitar, trumpet, and trombone; one musician was a singer. All participants were right-handed, had normal hearing, and normal or corrected-to-normal vision. Participants provided written, informed consent to participation in accordance with the Helsinki Declaration. Participants did not receive any financial compensation. The local ethics committee (ASL Lecce, Apulia Region, Italy) approved the study.

Materials

Participants performed an emotional go/no-go task (emo go/no-go), presented using E-Prime 2.0 (Richard and Charbonneau, 2009), during the EEG recordings.
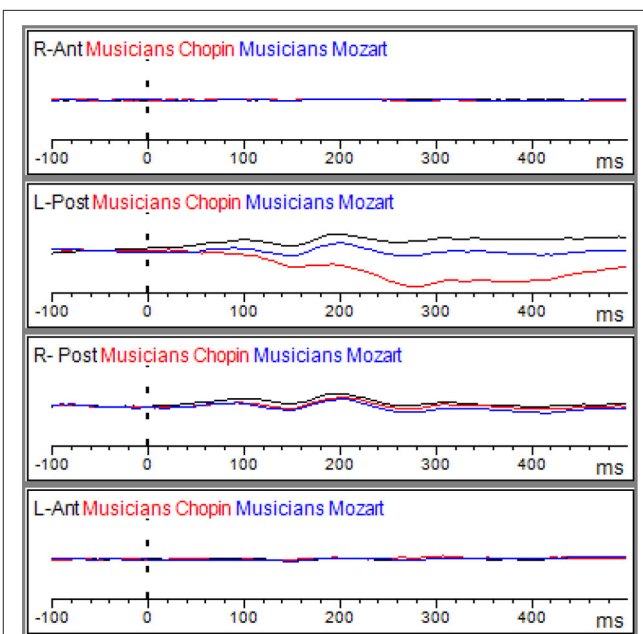
FIGURE 2 | Matching ERP of Grand average elicited by the emo go/no-go face recognition task in non-musicians in (black line) and musician (red line) in right anterior, right posterior, left anterior, and left posterior regions. The Graphic of ROIs Regions has been performed through the channels pooling processing.

The emotional go/no-go task (Schulz et al., 2007; Waters and Valvoi, 2009; Yerys et al., 2013) is a variant of the cognitive go/no-go task (Gomez et al., 2007) in which emotional information, measured through a decision-making process, is accompanied by a motor response. Generally, during an emo go/no-go task, the participant has to press the spacebar of a keyboard in response to an emotional face (neutral, angry, fearful, or happy). The choice of the face emotional expression depends on the task and on the process being investigated. The emo go/no-go task is a paradigm often used in ERP studies investigating a mismatch in response to stimulus salience (Jodo and Kayama, 1992; Smith et al., 2013; Moreno et al., 2014; Invitto et al., 2016). The N170 ERP component is the most sensitive in face recognition tasks (Eimer, 2000, 2011; Heisz et al., 2006; Blau et al., 2007). In this study, the computerized behavioral task required participants to press the spacebar when they identified a neutral face; EEG data were recorded whilst they were performing the task. Facial expressions were extracted from the NimStim Set of Facial Expressions (http://www.macbrain.org/resources.htm).

The NimStim Set is a collection of 672 images of the faces of 70 professional actors displaying various emotional expressions. The actors are of varying ethnicity and are represented in the same proportions by women and men. The collection consists of images of eight emotional facial expressions: fear, happiness, sadness, anger, surprise, disgust, neutral, and calm. In this experiment, we presented a sample of 64 images of fearful, happy and neutral faces, the expression categories were matched for sex and ethnicity.

In each condition the go-no-go task was accompanied by one of the following pieces from the classical piano repertoire:

FIGURE 3 | Grand average of the ERP components elicited by the emo go/no-go face recognition task in non-musicians in the Albeniz (black line), Chopin (red line), and Mozart condition (blue line) in right anterior, right posterior, left anterior, and left posterior regions.

- Chopin: Nocturne Op. 9 n. 1 and Nocturne Op. 9 n. 2.
- Mozart: Sonata in D major, K.V. 311.
- Albeniz: In Iberia, Rondeña.

Musical stimuli were delivered via two earphones, with a Windows 7 reproduction intensity of 60% (−6.4 dB), Conexant Smart Audio HD, Roland Sound Canvas, with a sampling rate of 48,000 Hz and 24-bit depth (system information: professional quality).
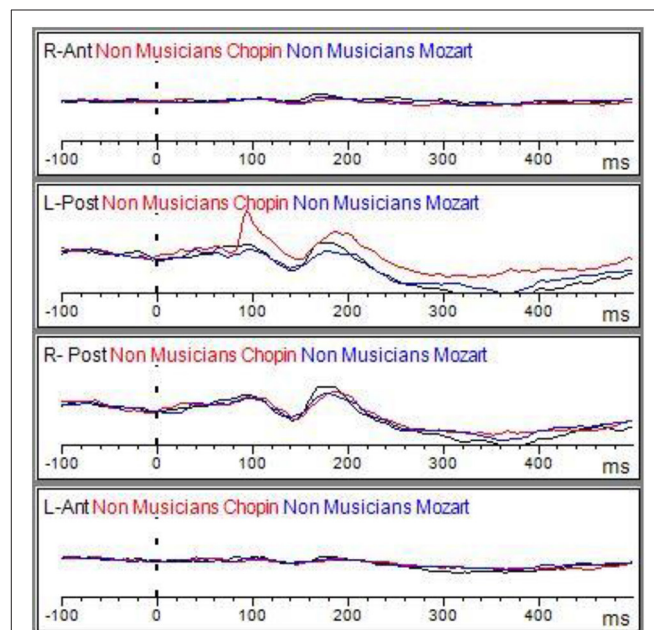
Each condition began with the listening of a musical piece, selected from the pieces above, whilst participants were performing the emo go/no-go task, looking at the emotional face displayed on the screen.

Participants rated the sadness and happiness each piece of music invoked using visual analog scales (VASs). The scales were administered immediately after each condition. The VASs consisted of a ten-centimeter line with the poles labeled 0 (absence of pleasure, sadness or happiness) and 10 (highest possible degree of pleasure, sadness, or happiness).
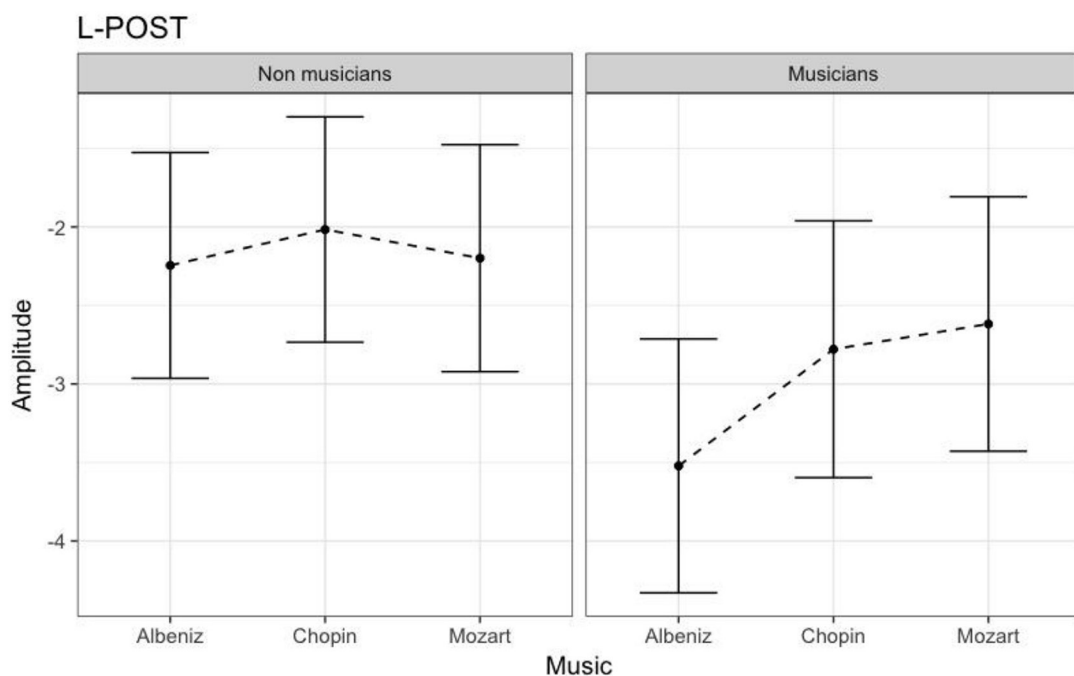
Each condition lasted approximately 500 s. Images of neutral (target), fearful and happy (non-target) faces were presented in pseudo-random order. Both target and non-target images were presented for 1,500 ms and the interstimulus interval was 1,500 ms.

Participants were instructed to sit so that there was a gap of about 75 cm between the front edge of the chair and the base of the computer screen. They had to listen to the pieces of classical music and respond to the presentation of neutral face on the screen by pressing the spacebar of the computer keyboard.

At the end of each condition participants rated the emotions the accompanying music had elicited using the VASs described above.

FIGURE 5 | Grand average of the ERP components elicited by the emo go/no-go face recognition task in non-musicians in the Albeniz (black line), Chopin (red line), and Mozart conditions (blue line) in right anterior, right posterior, left anterior, and left posterior regions.


FIGURE 4 | N170 amplitudes in non-musicians and musicians in L-POST ROI (Left Posterior Region of Interest).

N170 ERP Recording

EEGs were recorded from 64 active channels, mounted in an electrode cap according to the International 10–20-system. Signals were recorded through Brain Vision actiCHamp (Brain Products GmbH); the recording software was Brain Vision Recorder and the analysis software was Brain Vision Analyzer (Brain Products GmbH). Electrode impedance was kept below 15 kΩ. The EEG was amplified (band pass 0.1–40 Hz, 24 dB), with a sampling rate of 1000 Hz. Electrodes were referenced online to the FpZ. One electrode placed at the outer canthus of the right eye and used to monitor horizontal eye movements. Vertical eye movements and blinks were monitored by electrodes above and below the left eye. Trials contaminated by eye movements, amplifier conditioning, or other artifacts were rejected. The signal was filtered offline (0.01–50 Hz, 24 dB), and the threshold for artifact rejection was set at $> |125| \mu V$. The ocular rejection was performed through independent component analysis (ICA). The ERP epochs included a 100-ms pre-stimulus baseline period and a 500-ms post-stimulus segment. Separate averages were calculated for each facial expression (neutral, happy, and fearful) in each music condition (Albeniz, Mozart, and Chopin). The onset of ERP N170 peaks was estimated from grand average waveforms, according to the ERP latency definition (Heisz et al., 2006; De Vos et al., 2012; Smith et al., 2013). Peaks were automatically detected for all channels, using the global maxima in interval method (Giroldini et al., 2016).

DATA ANALYSIS AND RESULTS

To investigate the role of the experimental manipulation on behavioral and psychophysiological data, we combined a linear mixed modeling with a decision-tree learning approach. Statistical analyses on linear mixed-models were performed with lme4, car, and lmertest packages supplied in the R environment whereas the decision-tree model was built by means of a tailor-made algorithm (Menolascina et al., 2007).
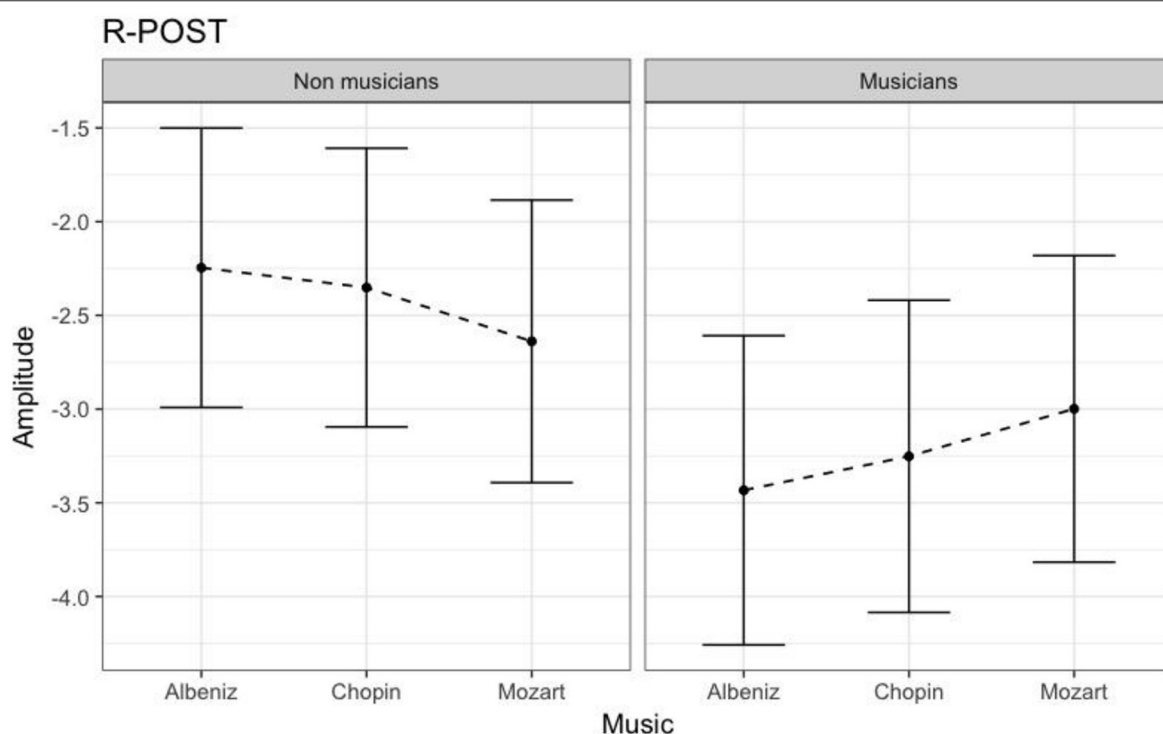
Behavioral Data

Independent-samples t-tests were used to analyze data from the three VASs for each condition (see **Table 1**).

A repeated measures ANOVA was performed to analyze behavioral Reaction Time to neuter faces in the Emo Go/No-Go paradigm. The analysis considered Music (Albeniz, Chopin, Mozart) as within factor (3 Levels) and Group (2 Levels) as between factor. The model showed significant results in Group ($F = 57.055$, df = 1, $p = 0.01$), results just over the limits of statistical significance in Music condition ($F = 2.947$, df = 2, $p = 0.053$) and an interaction Music condition × Group ($F = 3.012$, df = 2, $p = 0.049$). The results showed a trend in higher response times in the musicians group, with a slower reaction time in Chopin session (**Table 2**).
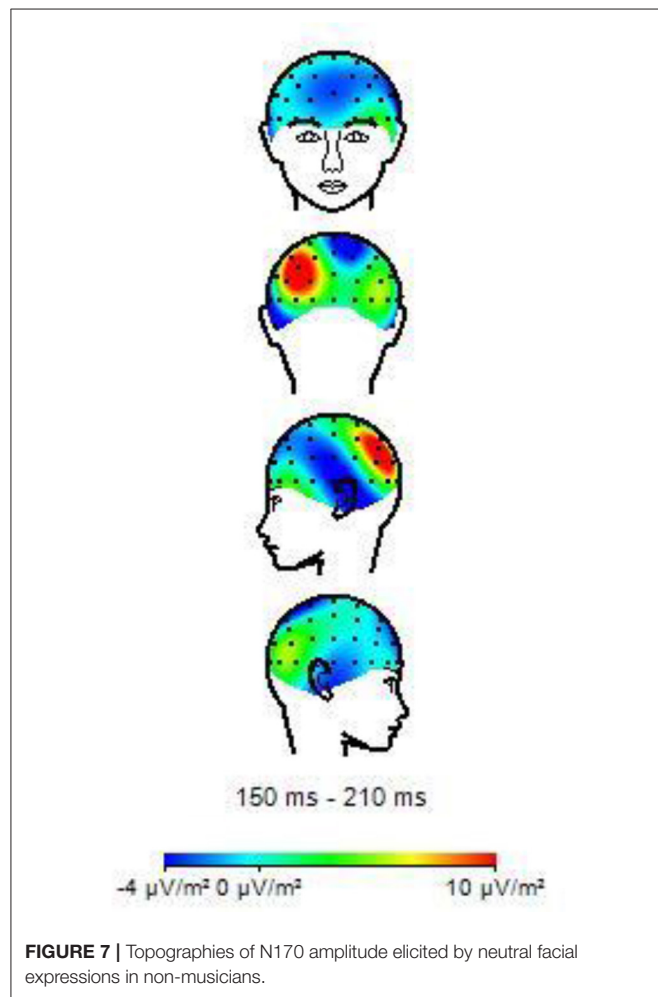
Psychophysiological Data

The latency and amplitude of the N170 component were analyzed using separate linear mixed-effects models (LMMs) lme4 package
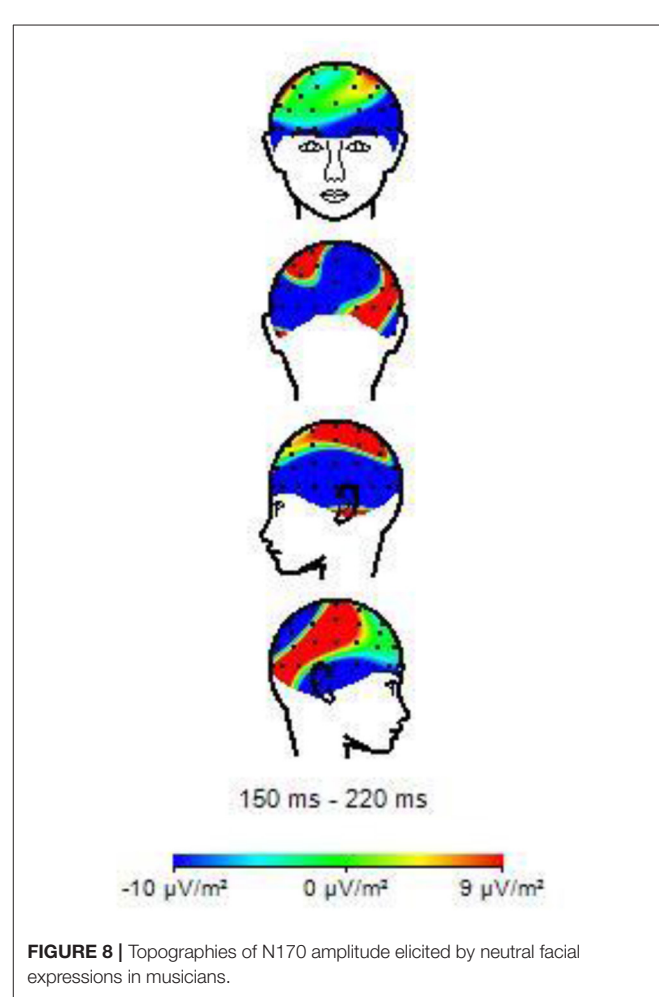
FIGURE 6 | N170 amplitudes in non-musicians and musicians in R-POST ROI (Right Posterior Region of Interest). N170 amplitudes in non-musicians and musicians in R-POST ROI (Right Posterior).

(Bates et al., 2015) supplied as part of the R package (Bates et al., 2013, 2014). In both models, Group (musicians; non-musicians) and Music (Albeniz; Mozart; Chopin) were defined as fixed factors and participant and channel were coded as random effects. The interaction between Group and Music was also examined in the models. Sixty-one EEG electrodes were clustered into four main regions (ROIs): left anterior (L-Ant), right anterior (R-Ant), left posterior (L-Post) and right posterior (R-Post). Left and right were defined according to the standard international 10–20 system whereas anterior and posterior were defined according to the following rule: ANT (F, Fp, FC, FT, C, T, AF) and POST (TP, CP, P, PO, O; Frömer et al., 2012; Bornkessel-Schlesewsky and Schlesewsky, 2013) and as according the recent suggestions about the reduction of data dimensions (Luck and Gaspelin, 2017). To investigate potential regional differences, separate LMM analyses were run for reach ROI. In all these models, the Face variable was kept fixed at the Neutral emotional level (i.e., Target variable in the behavioral task, as described in the Materials section). To identify graphically the Regions of interest (ROIs), were processes through Analyzer a Pooling Elaboration with the creation of 4 New areas: Right Anterior (R-Ant), Right Posterior (R-Post), Left Anterior (L-Ant) and Left Posterior (L-Post).

N170 Amplitude

Table 3 shows the results of LMMs for N170 amplitude. In the L-Ant region there was no effect of Group or Music, although there was an interaction ($B = -2.152$, $t_{896} = -2.152$, $p = 0.03$). In the R-Ant region there were main effects of Group ($B = -0.419$, $t_{32} = -2.11$, $p = 0.04$; **Figure 1**) and Music ($B = 0.299$, $t_{906} = 2.69$, $p = 0.007$), reflecting ampler N170 in the musicians group and in the Chopin condition (**Figure 2**). There was also an interaction between Group and Music: musicians, in Chopin condition, revealed an increased amplitude ($B = -0.360$, $t_{910} = -2.13$, $p = 0.03$) and a decreased amplitude elicited in Mozart condition ($B = 0.541$, $t_{913} = 3.16$, $p = 0.001$; **Figure 3**). In the L-Post region there was an effect of Group (**Figures 2, 4**), reflecting increased N170 amplitude in musicians ($B = -1.276$, $t_{26} = -6.13$, $p = 0.002$). There was also a Group × Music interaction reflecting an increase in N170 amplitude in non-musicians during the Mozart condition ($B = 0.857$, $t_{537} = 2.59$, $p = 0.009$; **Figure 5**). In the R-Post region there was an effect of Group (**Figure 6**): N170 amplitude was greater in the musicians ($B = -1.187$, $t_{25} = -2.16$, $p = 0.04$; **Figure 5**), and Group × Music interaction: non-musicians showed an increase in N170 amplitude in the Mozart condition ($B = 0.827$, $t_{552} = 2.42$, $p = 0.01$). Respect these results, more negative components are

FIGURE 7 | Topographies of N170 amplitude elicited by neutral facial expressions in non-musicians.

FIGURE 8 | Topographies of N170 amplitude elicited by neutral facial expressions in musicians.

visible through a Mapping imaging reconstruction in musicians vs. non-musicians (**Figures 7**, **8**).

N170 Latency

Table 4 shows the results of LMMs for N170 latency. There were no effects of Group or Music in the L-Ant region. In R-Ant latencies (**Figure 9**) were shorter in the Chopin condition ($B = -15.800$, $t_{919} = -4.25$, $p < 0.001$), the opposite effect was found in L-Post (**Figure 10**), with slower latencies in the Chopin condition ($B = -8.743$, $t_{730} = -2.16$, $p = 0.03$). Finally, in the R-Post (**Figure 11**) region latencies were shorter in both the Chopin ($B = -15.285$, $t_{741} = -4.88$, $p < 0.001$) and Mozart ($B = -15.543$, $t_{743} = -4.81$, $p < 0.001$) conditions.

Assessing the Gender Effect

In order to evaluate whether the bias could be related to a gender effect, we proceed by comparing the fixed-effects structure of the previous linear-mixed models by adding and excluding the factor *gender* from the models. The results were evaluated in terms of model fit by using an information theory based approach (McElreath, 2016). To do so, for each ROI we considered two models: M0 (Simple model: excluding Gender variable) and M1 (Complex Model: including the Gender variable) and we fit the model via maximum likelihood. The BIC information criterion was then computed on the log-likelihood of the models along with the Vuong's statistic (Vuong, 1989; Merkle et al., 2016). Finally, asymptotic confidence intervals (CIs) on the BIC differences of the models (ΔBIC) were also computed. All the computations involved were performed by means of the nonnest2 package in the R environment.

Table 5 shows results for the model comparisons considering Amplitude and Latency of N170. As for the previous analyses (see **Tables 2, 3**), four models were considered with respect to the four ROIs previously defined. Overall, the Vuong's test did not allow to reject the null hypothesis of indistinguishable between models with and without the Gender Variable. The model, in all ROI, showed very similar BICs. This strongly suggests that the evidence of the models is the same. Indeed, the 95% confidence intervals of ΔBIC overlapped the zero, implying that the models are enough close and M1s cannot be preferred over M0s. These results would suggest that including the gender variable in the models (M1s) did not improve their evidence with regards to the previous models (M0s). In this case, adding Gender Effect, don't significantly change the evidence of the model, when compared to the sample data. Therefore, using Occam's razor, we resorted to considering the simplest models in terms of parameters, according to the principle of simplifying the variables in an experiment (Srinagesh, 2006; Luck and Gaspelin, 2017).

Decision-Tree Modeling: Target and Non-target Stimuli
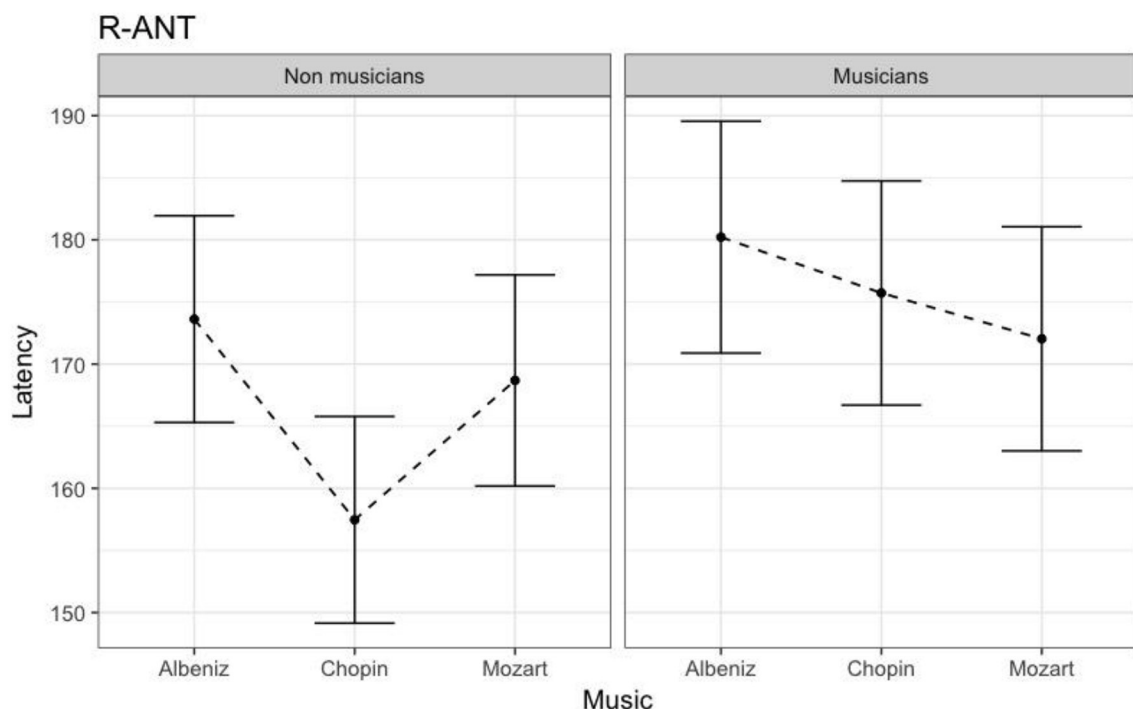
To validate that the emotional bias, generated by combined stimuli, is correlated with the class of participant (musicians/non-musicians), we processed the input data calculating, for each participant, the relative variation between the music conditions considering each EEG channel.

TABLE 4 | Results of linear mixed-effects model: fixed effects for group and music on N170 latency.
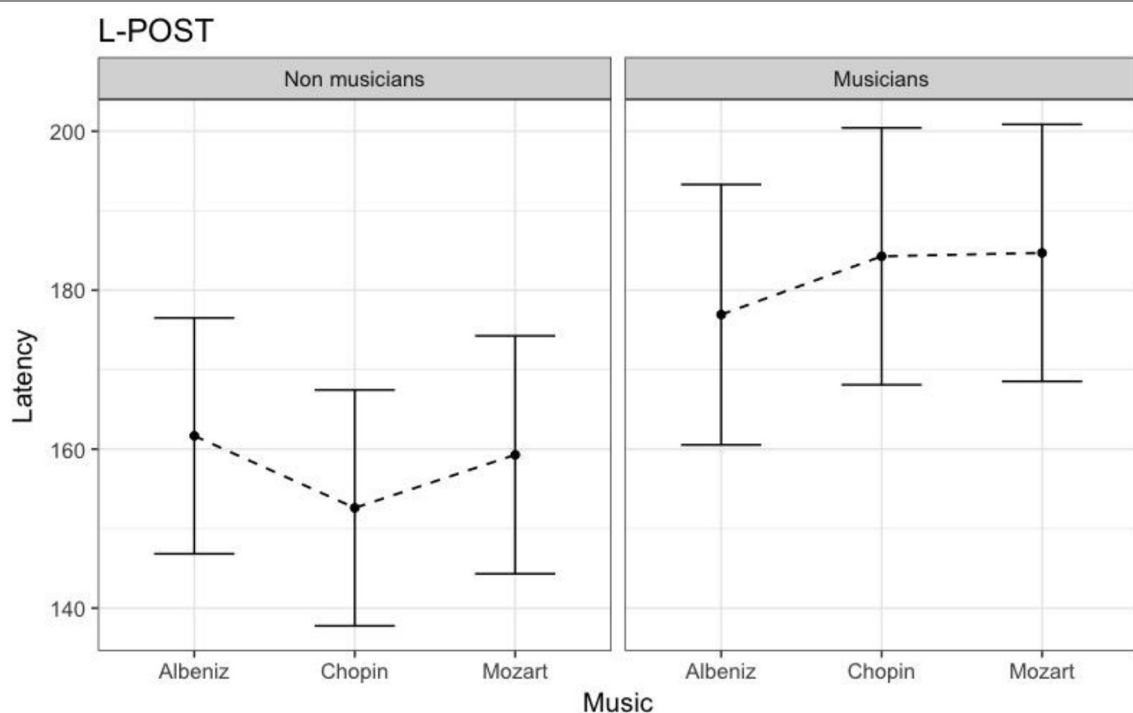
ROI		B (SE)	t
L-Ant	Baseline	166.283 (34.783)	−0.609
	Group		
	Non-Musicians vs. Musicians	9.178 (6.968)	1.317
	Music		
	Albeniz vs. Chopin	−6.022 (3.935)	−1.531
	Albeniz vs. Mozart	1.214 (4.057)	0.299
	Group × music		
	Non-Musicians × Albeniz vs. Musicians × Chopin	4.147 (5.958)	0.696
	Non-Musicians × Albeniz vs. Musicians × Mozart	4.111 (6.039)	0.681
R-Ant	Baseline	172.94 (4.38)	39.486
	Group		
	Non-Musicians vs. Musicians	8.612 (6.320)	1.363
	Music		
	Albeniz vs. Chopin	−15.80 (3.715)	−4.253***
	Albeniz vs. Mozart	−4.655 (3.829)	−1.216
	Group × music		
	Non-Musicians × Albeniz vs. Musicians × Chopin	9.990 (5.624)	1.776
	Non-Musicians × Albeniz vs. Musicians × Mozart	−4.621 (5.701)	−0.811
L-Post	Baseline	101.215 (7.47)	21.569
	Group		
	Non-Musicians vs. Musicians	16.991 (10.931)	1.554
	Music		
	Albeniz vs. Chopin	−8.743 (4.041)	−2.163*
	Albeniz vs. Mozart	−2.552 (4.174)	−0.611
	Group × music		
	Non-Musicians × Albeniz vs. Musicians × Chopin	14.881 (6.126)	2.430*
	Non-Musicians × Albeniz vs. Musicians × Mozart	9.282 (6.214)	1.493
R-Post	Baseline	169.701 (7.599)	22.332
	Group		
	Non-Musicians vs. Musicians	21.699 (11.314)	1.918
	Music		
	Albeniz vs. Chopin	−15.285 (3.216)	−4.889***
	Albeniz vs. Mozart	−15.543 (3.229)	−4.813***
	Group × music		
	Non-Musicians × Albeniz vs. Musicians × Chopin	15.226 (4.739)	3.213**
	Non-Musicians × Albeniz vs. Musicians × Mozart	14.184 (4.808)	2.950**
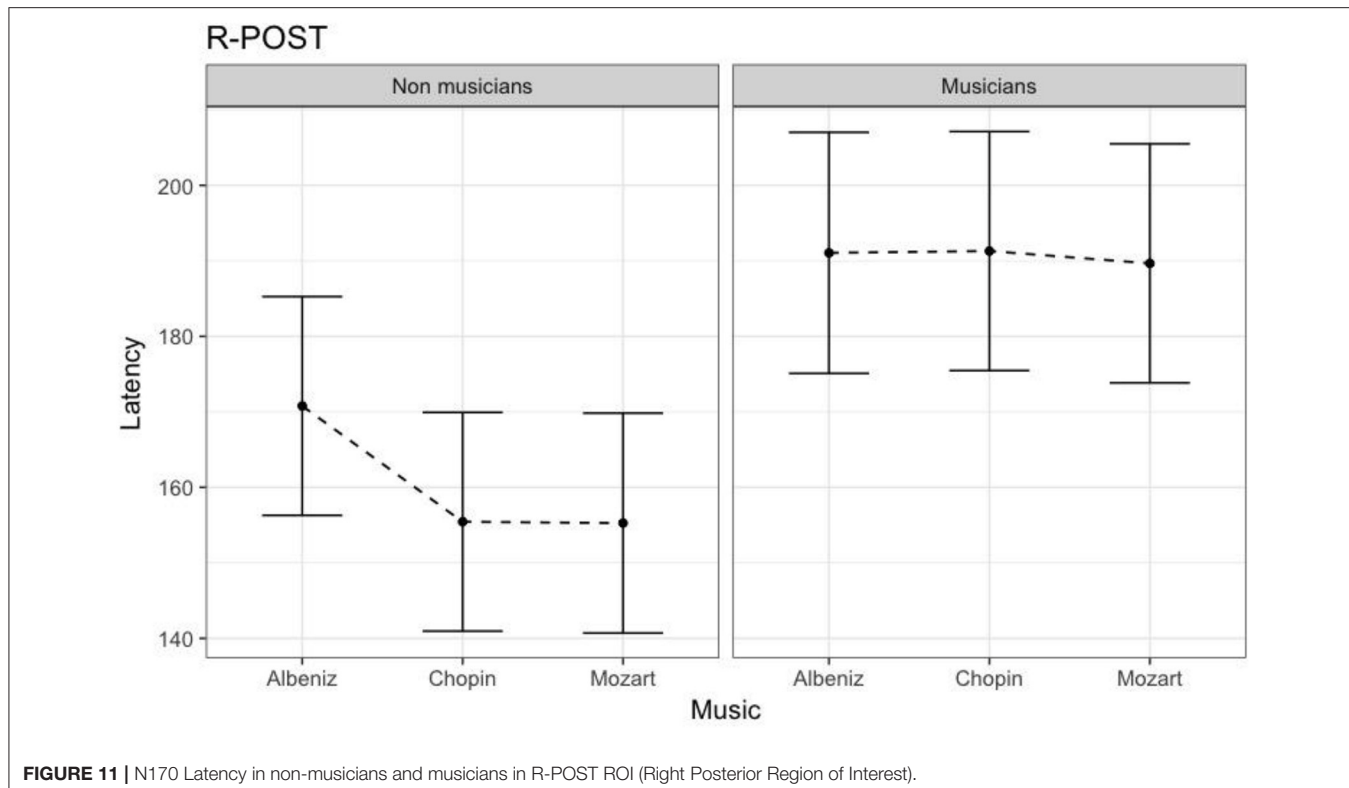
Participants and EEG channels were treated as random effects; degrees of freedom of the model were calculated with the Satterthwaite approximation. L-Ant: left-anterior; R-Ant: right-anterior; L-Post: left-posterior; R-Post: right-posterior.
*p < 0.05; **p < 0.01; ***p < 0.001.

FIGURE 9 | N170 Latency in non-musicians and musicians in R-ANT ROI (Right Anterior Region of Interest).

FIGURE 10 | N170 Latency in non-musicians and musicians in L-POST ROI (Left Posterior Region of Interest).

FIGURE 11 | N170 Latency in non-musicians and musicians in R-POST ROI (Right Posterior Region of Interest).

TABLE 5 | Comparison respect to gender effect.

		Gender effect			
	Model	**BIC M0**	**BIC M1**	**Vuong's statistic**	**95% CIs ΔBIC**
N170 Amplitude	L-ANT	3432.45	3448.54	0.026 (p = 0.994)	[−35.38, 3.20]
	R-ANT	3160.68	3157.28	0.053 (p = 0.3)	[−24.47, 31.26]
	L-POST	2323.46	2345.85	0.026 (p = 0.998)	[−37.30, −7.47]
	R-POST	2460.68	2461.10	0.048 (p = 0.997)	[−21.13, 20.30]
N170 Latency	L-ANT	9825.47	9826.65	0.042 (p = 0.5)	[−26.18, 23.83]
	R-ANT	9703.89	9719.64	0.017 (p = 0.6)	[−31.77, 0.27]
	L-POST	7927.17	7929.67	0.05 (p = 0.5)	[−26.69, 21.71]
	R-POST	7696.23	7675.25	0.09 (p = 0.6)	[−11.63, 53.0]

In the Table, M0 indicates the model without the gender variable whereas M1 the model where the gender variable was instead added. The Vuong's statistic considers the difference of two models in terms of log-likelihood. The statistic evaluates the hypothesis that the models M0 and M1 are indistinguishable with regards to the sample data. ΔBIC indicates the difference (M0-M1) in terms of their BIC values whereas 95% CIs are computed with the asymptotic formula.

To do this, we used the following equation (Equation 1):

$$\Delta x_{ij} = \left| \frac{x_k - x_a}{x_a} \right| \qquad (1)$$

where $i \in 1, \ldots, 24$ was the participant, $j \in 1, \ldots, 61$ was the EEG channel, a = Albeniz; k = Chopin or Mozart.

TABLE 6 | Mean performances of the predictive models – N170 amplitude.

Face	Dataset	Accuracy %	Sensitivity	Specificity	AUC
Fear	Albeniz vs. Mozart	32.75	0.28	0.38	0.31
	Albeniz vs. Chopin	**62.00**	0.52	0.73	0.72
Happy	Albeniz vs. Mozart	**66.88**	0.60	0.74	0.67
	Albeniz vs. Chopin	37.00	0.33	0.41	0.37
Neuter	Albeniz vs. Mozart	**63.50**	0.68	0.60	0.64
	Albeniz vs. Chopin	49.88	0.54	0.46	0.50

These models highlight that in happy faces ERP amplitude is modulated as in neuter faces (in Albeniz vs. Mozart predictive model).

TABLE 7 | Mean performances of the predictive models – N170 latency.

Face	Dataset	Accuracy %	Sensitivity	Specificity	AUC
Fear	Albeniz vs. Mozart	**64.50**	0.61	0.68	0.70
	Albeniz vs. Chopin	41.88	0.36	0.48	0.41
Happy	Albeniz vs. Mozart	**51.88**	0.47	0.57	0.53
	Albeniz vs. Chopin	**75.88**	0.70	0.81	0.76
Neuter	Albeniz vs. Mozart	42.88	0.41	0.45	0.41
	Albeniz vs. Chopin	**65.5**	0.46	0.85	0.66

These models highlight that in happy faces ERP latencies are modulated as in neuter faces (in Albeniz vs Chopin predictive model)

The output data was further processed to evaluate which EEG channels showed the best discrimination capability for the classification between the two groups. A predictive model was implemented using a tree-building algorithm (Menolascina et al., 2007), by generating prediction rules from partially pruned decision trees that were built using C4.5 Quinlan's heuristics (Quinlan, 1993), whose main goal consists in the minimization of the tree levels and nodes number, thereby maximizing data generalization. This technique uses an information theoretical procedure to select, at each choice point in the tree, the attribute that would maximize the information gained from splitting the data.

Predictive Model Results

The predictive model was trained and tested 200 times considering different random combinations of training and test sets, obtained from the input dataset considering a splitting percentage of 81.82%. The results are expressed as mean values, considering 200 iterations, of Accuracy, Sensitivity, Specificity and Area Under the Curve (AUC) and are reported in **Tables 6**, **7**.

We tried to improve the performance of the previous predictive model by reducing the number of the considered EEG channels using a correlation-based filter that selects the most highly correlated features. A fast correlation-based filter (FCBF) algorithm (Yu and Liu, 2003) was adopted.

The same procedure discussed in the previous section was applied considering the obtained subset of EEG channels, and a new predictive model was implemented and evaluated.

The performance of the new predictive model is reported in **Tables 8, 9**.

DISCUSSION

Our aim was to investigate modulation of emotional face recognition by cross-modal perception, treated as a function of background music. Synesthesia and crossmodal perception can have a strong modulatory effect on cortical processing, conditioning or facilitating perception and interpretation of the administered stimulus. We analyzed how musicians' recognition of facial expressions was affected by music-induced emotions. These data allow us to suggest that the presence of emotional information from another sensory channel (i.e., auditory information from background music) activates cross-modal integration of information and that this process can be modulated by the perception of the musical stimulus. This salience, for emotional face, could be explicable in terms adaptive: identify more early stage emotions is a skill that, developmentally, can be crucial for the survival and, proximal and contingent, is an indispensable social competence (Niu et al., 2012). So, in a condition where the participants are more "emotionally involved," the neuter face, that is ambiguous for a defined emotional recognition and that is more difficult to recognize, can be more affected by emotion music induced. This justifies the fact that the musicians evaluated music as more pleasant and emotional (happy and sad) than non-musicians, and this judgment on emotional engagement is in agreement with their musical appraisal and competence. This emotional involvement leads to a delay in reaction times. These results imply that the motor and perceptual systems can be modulated, in a top-down process, by music-induced emotions. The electrophysiological data revealed increased N170 amplitudes in musicians in all conditions. The background music had less impact in non-musicians, then can produce less bias in the task. Instead, an earlier onset of the global processing of the stimulus indicates that

TABLE 8 | Mean performances of the FCBF-filtered predictive models – N170 amplitude.

Face	Dataset	EEG channels	Accuracy %	Sensitivity	Specificity	AUC
Fear	*Albeniz* vs. *Mozart*	–	–	–	–	–
	Albeniz vs. *Chopin*	P3–CPz	71.65	0.70	0.74	0.77
Happy	*Albeniz* vs. *Mozart*	T8–F4	69.27	0.64	0.74	0.72
	Albeniz vs. *Chopin*	–	–	–	–	–
Neuter	*Albeniz* vs. *Mozart*	CP1	79.13	0.69	0.8925	0.81
	Albeniz vs. *Chopin*	FCz–CPz	66.38	0.73	0.60	0.67

In this amplitude dataset, we can see electrodes more sensible to predictive model. In Fear face, EEG channels are P3 and CPz, In Happy face T8 and F4 and in Neuter Face CP, FCz, and CPz.

TABLE 9 | Mean performances of the FCBF-filtered predictive models – N170 latency.

Face	Dataset	EEG channels	Accuracy %	Sensitivity	Specificity	AUC
Fear	*Albeniz* vs. *Mozart*	Fp1–AF7	79.75	0.84	0.76	0.80
	Albeniz vs. *Chopin*	F8	65.50	0.45	0.86	0.66
Happy	*Albeniz* vs. *Mozart*	CP5	61.13	0.94	0.45	0.69
	Albeniz vs. *Chopin*	CP1–C5–CPz–AF4	82.00	0.78	0.87	0.82
Neuter	*Albeniz* vs. *Mozart*	–	–	–	–	–
	Albeniz vs. *Chopin*	FC1–O2–F4–AF7–FT7–FT8–AF8	70.63	0.49	0.92	0.71

In this latency dataset we can see electrodes more sensible to predictive model. In Fear face, EEG channels are Fp1, AF7 and F8; in Happy face CP5, CPP1, C5, CPz, and AF4 and in Neuter Face FC1, O2, F4, AF7, FT7, FT8, and AF8.

music interacts with the interpretation of salience, producing a behavioral delay and an increased cortical arousal in musicians. This result suggests that perception of facial expressions can vary according to perceptions of a concurrent auditory stimulus and an individual's musical background.

The decreased ERP amplitude, faster reaction times and lower VAS scores in the non-musicians group, suggests that non-musicians found the background music less engaging and emotionally arousing. Hence their top-down processes (less modulated by musical listening), doesn't bias the face perception. The relative changes in arousal, during the face recognition process, are driven by the subjective emotional reaction and top-down processing. The evidence of this concept was obtained from the comparison of responses to the neutral face (Target) whilst listening to music by Albeniz (pleasant), Mozart (happy) and Chopin (judged, at the same time, both sad and pleasant). We also assessed whether, within our model, there was a gender effect (Miles et al., 2016), but, in our study, gender analysis did not improve evidence with regards to the simpler model. In this case, adding gender effect, don't significantly change the evidence of the model, when compared to the sample data. We chose to keep the simpler model, even in accordance with the latest methodological ERP guidelines (Luck, 2005; Luck and Gaspelin, 2017). Probably in a future study, increasing the number of the sample, so that we can analyze the gender effect within the model, we could implement the complex model.

In view of these results, to investigate other possible bias variable-related, we sought to determine whether the bias effect could be present not only on neutral faces, as literature highlight. According to this hypothesis, we tested, using the predictive model, the N170 components for the other face emotional expressions showed during the task (happy and fear).

The predictive model allowed us to determine the most significant decision-tree features; in fact, the classification performances obtained using the trained predictive model were high, regardless of training and test sets. In this case, we find modulation of the response even in happy faces, but not in fear faces. This could also be explained by theories on emotions where the stimulus that produces fear is the least susceptible to alterations because it is the one most immediately and easily perceived (Vuilleumier et al., 2001; Phelps and LeDoux, 2005; Almeida et al., 2016).

Emotional salience allows the recognition and discrimination of neutral expressions. Our data indicate that the simultaneous presence of emotional information from multiple sensory channels activates a process of crossmodal integration that could be facilitated by music. Further research using different neuroscientific and behavioral techniques and paradigms is needed to improve our understanding of emotional crossmodal integration.

ETHICS STATEMENT

Lecce Ethical Comittee, ASL Hospital Vito Fazzi, approved the study with Verbal n. 2 all.21 approved the study in date October, 02, 2013.

AUTHOR CONTRIBUTIONS

SI: Study design and coordination, whole data analysis design, manuscript preparation and editing and reviewing. AC: Statistical Data Analysis. AM: Subjects selection and data recording. GP: Subjects selections and data recording. RS: Subjects selection, Classical Music pieces choice. DT: Data recording. ID, AB, and VB: Machine Learning Data Analysis. MdT: Manuscript editing.

FUNDING

REFERENCES

Almeida, P. R., Ferreira-Santos, F., Chaves, P. L., Paiva, T. O., Barbosa, F., and Marques-Teixeira, J. (2016). Perceived arousal of facial expressions of emotion modulates the N170, regardless of emotional category: time domain and time–frequency dynamics. *Int. J. Psychophysiol.* 99, 48–56. doi: 10.1016/j.ijpsycho.2015.11.017

Balconi, M., and Carrera, A. (2011). Cross-modal integration of emotional face and voice in congruous and incongruous pairs: the P2 ERP effect. *J. Cogn. Psychol.* 23, 132–139. doi: 10.1080/20445911.2011.473560

Bates, D., Maechler, M., and Bolker, B. (2013). *Lme4: Linear Mixed-Effects Models using S4 Classes.* R Package version 0.999999–2.999999.

Bates, D., Maechler, M., Bolker, B., and Walker, S. (2014). *Lme4: Linear Mixed-Effects Models Using S4 Classes.* R package version 1.1-6. R.

Bates, D., Maechler, M., Bolker, B., and Walker, S. (2015). Fitting linear mixed-effects models using lme4. *J. Stat. Softw.* 67, 1–91. doi: 10.18637/jss.v067.i01

Baumgartner, T., Esslen, M., and Jäncke, L. (2006). From emotion perception to emotion experience: emotions evoked by pictures and classical music. *Int. J. Psychophysiol.* 60, 34–43. doi: 10.1016/j.ijpsycho.2005.04.007

Bhatti, A. M., Majid, M., Anwar, S. M., and Khan, B. (2016). Human emotion recognition and analysis in response to audio music using brain signals. *Comput. Hum. Behav.* 65, 267–275. doi: 10.1016/j.chb.2016.08.029

Bigliassi, M., Karageorghis, C. I., Nowicky, A. V., Orgs, G., and Wright, M. J. (2016a). Cerebral mechanisms underlying the effects of music during a fatiguing isometric ankle-dorsiflexion task. *Psychophysiology* 53, 1472–1483. doi: 10.1111/psyp.12693

Bigliassi, M., Silva, V. B., Karageorghis, C. I., Bird, J. M., Santos, P. C., and Altimari, L. R. (2016b). Brain mechanisms that underlie the effects of motivational audiovisual stimuli on psychophysiological responses during exercise. *Physiol. Behav.* 158, 128–136. doi: 10.1016/j.physbeh.2016.03.001

Blau, V. C., Maurer, U., Tottenham, N., and McCandliss, B. D. (2007). The face-specific N170 component is modulated by emotional facial expression. *Behav. Brain Funct.* 3:7. doi: 10.1186/1744-9081-3-7

Bornkessel-Schlesewsky, I., and Schlesewsky, M. (2013). Reconciling time, space and function: a new dorsal-ventral stream model of sentence comprehension. *Brain Lang.* 125, 60–76. doi: 10.1016/j.bandl.2013.01.010

Brattico, E., Brigitte, B., and Jacobsen, T. (2013). Toward a neural chronometry for the aesthetic experience of music. *Front. Psychol.* 4:206. doi: 10.3389/fpsyg.2013.00206

Brattico, E., and Jacobsen, T. (2009). Subjective appraisal of music: neuroimaging evidence. *Ann. N.Y. Acad. Sci.* 1169, 308–317. doi: 10.1111/j.1749-6632.2009.04843.x

Brattico, E., Jacobsen, T., De Baene, W., Glerean, E., and Tervaniemi, M. (2010). Cognitive vs. affective listening modes and judgments of music - An ERP study. *Biol. Psychol.* 85, 393–409. doi: 10.1016/j.biopsycho.2010.08.014

Caldwell, G. N., and Riby, L. M. (2007). The effects of music exposure and own genre preference on conscious and unconscious cognitive processes: a pilot ERP study. *Conscious. Cogn.* 16, 992–996. doi: 10.1016/j.concog.2006.06.015

Chen, J., Yuan, J., Huang, H., Chen, C., and Li, H. (2008). Music-induced mood modulates the strength of emotional negativity bias: an ERP study. *Neurosci. Lett.* 445, 135–139. doi: 10.1016/j.neulet.2008.08.061

de Gelder, B., and Vroomen, J. (2000). The perception of emotions by ear and by eye. *Cogn. Emot.* 14, 289–311. doi: 10.1080/026999300378824

De Vos, M., Thorne, J. D., Yovel, G., and Debener, S. (2012). Let's face it, from trial to trial: comparing procedures for N170 single-trial estimation. *Neuroimage* 63, 1196–1202. doi: 10.1016/j.neuroimage.2012.07.055

Eimer, M. (2000). The face-specific N170 component reflects late stages in the structural encoding of faces. *Neuroreport* 11, 2319–2324. doi: 10.1097/00001756-200007140-00050

Eimer, M. (2011). "The face-sensitive N170 component of the event-related brain potential," in *The Oxford Handbook of Face Perception,* eds A. J. Calder, G. Rhodes, M. Johnson, and J. V. Haxby (Oxford: Oxford University Press), 329–344.

Ellsworth, P. C., and Scherer, K. R. (2003). "Appraisal processes in emotion," in *Handbook of Affective Sciences,* eds R. J. Davidson, K. R. Scherer, and H. H. Goldsmith (New York, NY: Oxford University Press), 572–595.

Fritz, T., Jentschke, S., Gosselin, N., Sammler, D., Peretz, I., Turner, R., et al. (2009). Universal recognition of three basic emotions in music. *Curr. Biol.* 19, 573–576. doi: 10.1016/j.cub.2009.02.058

Frömer, R., Hafner, V., and Sommer, W. (2012). Aiming for the bull's eye: preparing for throwing investigated with event-related brain potentials. *Psychophysiology* 49, 335–344. doi: 10.1111/j.1469-8986.2011.01317.x

Gilbert, C. D., and Li, W. (2013). Top-down influences on visual processing. *Nat. Rev. Neurosci.* 14, 350–363. doi: 10.1038/nrn3476

Giroldini, W., Pederzoli, L., Bilucaglia, M., Melloni, S., and Tressoldi, P. (2016). A new method to detect event-related potentials based on Pearson's correlation. *EURASIP J. Bioinforma. Syst. Biol.* 11, 1–23. doi: 10.1186/s13637-016-0043-z

Gomez, P., Ratcliff, R., and Perea, M. (2007). A model of the Go/No-Go task. *J. Exp. Psychol. Gen.* 136, 389–413. doi: 10.1037/0096-3445.136.3.389

Gosselin, N., Peretz, I., Johnsen, E., and Adolphs, R. (2007). Amygdala damage impairs emotion recognition from music. *Neuropsychologia* 45, 236–244. doi: 10.1016/j.neuropsychologia.2006.07.012

Heisz, J. J., Watter, S., and Shedden, J. M. (2006). Automatic face identity encoding at the N170. *Vis. Res.* 46, 4604–4614. doi: 10.1016/j.visres.2006.09.026

Herholz, S. C., and Zatorre, R. J. (2012). Musical training as a framework for brain plasticity: behavior, function, and structure. *Neuron* 76, 486–502. doi: 10.1016/j.neuron.2012.10.011

Ibanez, A., Melloni, M., Huepe, D., Helgiu, E., Rivera-Rei, A., Canales-Johnson, A., et al. (2012). What event-related potentials (ERPs) bring to social neuroscience? *Soc. Neurosci.* 7, 632–649. doi: 10.1080/17470919.2012.691078

Invitto, S., Faggiano, C., Sammarco, S., De Luca, V., and De Paolis, L. (2016). Haptic, virtual interaction and motor imagery: entertainment tools and psychophysiological testing. *Sensors* 16:394. doi: 10.3390/s16030394

Jodo, E., and Kayama, Y. (1992). Relation of a negative ERP component to response inhibition in a Go/No-go task. *Electroencephalogr. Clin. Neurophysiol.* 82, 477–482. doi: 10.1016/0013-4694(92)90054-L

Jolij, J., and Meurs, M. (2011). Music alters visual perception. *PLoS ONE* 6:e18861. doi: 10.1371/journal.pone.0018861

Kawakami, A., Furukawa, K., Katahira, K., and Okanoya, K. (2013). Sad music induces pleasant emotion. *Front. Psychol.* 4:311. doi: 10.3389/fpsyg.2013.00311

Kawakami, A., Furukawa, K., and Okanoya, K. (2014). Music evokes vicarious emotions in listeners. *Front. Psychol.* 5:431. doi: 10.3389/fpsyg.2014.00431

Kolassa, I.-T., Kolassa, S., Bergmann, S., Lauche, R., Dilger, S., Miltner, W. H. R., et al. (2009). Interpretive bias in social phobia: an ERP study with morphed emotional schematic faces. *Cogn. Emot.* 23, 69–95. doi: 10.1080/02699930801940461

Ladinig, O., and Schellenberg, E. G. (2012). Liking unfamiliar music: effects of felt emotion and individual differences. *Psychol. Aesthetics Creat. Arts* 6, 146–154. doi: 10.1037/a0024671

Leleu, A., Godard, O., Dollion, N., Durand, K., Schaal, B., and Baudouin, J. Y. (2015). Contextual odors modulate the visual processing of emotional facial expressions: an ERP study. *Neuropsychologia* 77, 366–379. doi: 10.1016/j.neuropsychologia.2015.09.014

Logeswaran, N., and Bhattacharya, J. (2009). Crossmodal transfer of emotion by music. *Neurosci. Lett.* 455, 129–133. doi: 10.1016/j.neulet.2009.03.044

Luck, S. (2005). "Ten simple rules for designing ERP experiments," in *Event-Related Potentials A Methods Handbook*, ed T. C. Handy (Cambridge, MA; London, UK: The MIT Press), 17–32.

Luck, S. J., and Gaspelin, N. (2017). How to get statistically significant effects in any ERP experiment (and why you shouldn't). *Psychophysiology* 54, 146–157. doi: 10.1111/psyp.12639

McElreath, R. (2016). *Statistical Rethinking.* Boca Raton, FL: Chapman & Hall/CRC.

Menolascina, F., Tommasi, S., Paradiso, A., Cortellino, M., Bevilacqua, V., and Mastronardi, G. (2007). "Novel data mining techniques in aCGH based breast cancer subtypes profiling: the biological perspective," in *2007 IEEE Symposium on Computational Intelligence and Bioinformatics and Computational Biology* (Honolulu, HI), 9–16.

Merkle, E. C., You, D., and Preacher, K. J. (2016). Testing nonnested structural equation models. *Psychol. Methods* 21, 151–163. doi: 10.1037/met0000038

Miles, S. A., Miranda, R. A., and Ullman, M. T. (2016). Sex differences in music: a female advantage at recognizing familiar melodies. *Front. Psychol.* 7:278. doi: 10.3389/fpsyg.2016.00278

Moreno, S., Wodniecka, Z., Tays, W., Alain, C., and Bialystok, E. (2014). Inhibitory control in bilinguals and musicians: Event related potential (ERP) evidence for experience-specific effects. *PLoS ONE* 9:e94169. doi: 10.1371/journal.pone.0094169

Müller, M., Höfel, L., Brattico, E., and Jacobsen, T. (2010). Aesthetic judgments of music in experts and laypersons - an ERP study. *Int. J. Psychophysiol.* 76, 40–51. doi: 10.1016/j.ijpsycho.2010.02.002

Niu, Y., Todd, R. M., and Anderson, A. K. (2012). Affective salience can reverse the effects of stimulus-driven salience on eye movements in complex scenes. *Front. Psychol.* 3:336. doi: 10.3389/fpsyg.2012.00336

Pallesen, K. J., Brattico, E., Bailey, C. J., Korvenoja, A., Koivisto, J., Gjedde, A., et al. (2010). Cognitive control in auditory working memory is enhanced in musicians. *PLoS ONE* 5:e11120. doi: 10.1371/journal.pone.0011120

Pantev, C., Oostenveld, R., Engelien, A., Ross, B., Roberts, L. E., and Hoke, M. (1998). Increased auditory cortical representation in musicians. *Nature* 392, 811–814. doi: 10.1038/33918

Peretz, I. (2012). "Music, language, and modularity in action," in *Language and Music as Cognitive Systems,* eds P. Rebuschat, M. Rohmeier, J. A. Hawkins, and I. Cross (New York, NY: Oxford University Press), 254–268.

Phelps, E. A., and LeDoux, J. E. (2005). Contributions of the amygdala to emotion processing: from animal models to human behavior. *Neuron* 48, 175–187. doi: 10.1016/j.neuron.2005.09.025

Pourtois, G., Debatisse, D., Despland, P.-A., and de Gelder, B. (2002). Facial expressions modulate the time course of long latency auditory brain potentials. *Cogn. Brain Res.* 14, 99–105. doi: 10.1016/S0926-6410(02) 00064-2

Proverbio, A. M., Manfredi, M., Zani, A., and Adorni, R. (2013). Musical expertise affects neural bases of letter recognition. *Neuropsychologia* 51, 538–549. doi: 10.1016/j.neuropsychologia.2012.12.001

Quinlan, J. (1993). *C4. 5: Programs for Machine Learning.* San Mateo, CA: Morgan Kaufmann.

Reybrouck, M. (2005). Body, mind and music: musical semantics between experiential cognition and cognitive economy. *Rev. Transcult. Música* 9, 1–37.

Reybrouck, M., and Brattico, E. (2015). Neuroplasticity beyond sounds: neural adaptations following long-term musical aesthetic experiences. *Brain Sci.* 5, 69–91. doi: 10.3390/brainsci5010069

Richard, L., and Charbonneau, D. (2009). An introduction to E-Prime. *Tutor. Quant. Methods Psychol.* 5, 68–76. doi: 10.20982/tqmp.05.2.p068

Sammler, D., Grigutsch, M., Fritz, T., and Koelsch, S. (2007). Music and emotion: electrophysiological correlates of the processing of pleasant and unpleasant music. *Psychophysiology* 44, 293–304. doi: 10.1111/j.1469-8986.2007. 00497.x

Schellenberg, E. G. (2005). Music and cognitive abilities. *Curr. Dir. Psychol. Sci.* 14, 317–320. doi: 10.1111/j.0963-7214.2005.00389.x

Schellenberg, E. G., and Mankarious, M. (2012). Music training and emotion comprehension in childhood. *Emotion* 12, 887–891. doi: 10.1037/a0027971

Schiavio, A., van der Schyff, D., Cespedes-Guevara, J., and Reybrouck, M. (2016). Enacting musical emotions. sense-making, dynamic systems, and the embodied mind. *Phenomenol. Cogn. Sci.* doi: 10.1007/s11097-016-9477-8. [Epub ahead of print].

Schulz, K. P., Fan, J., Magidina, O., Marks, D. J., Hahn, B., and Halperin, J. M. (2007). Does the emotional go/no-go task really measure behavioral inhibition?. Convergence with measures on a non-emotional analog. *Arch. Clin. Neuropsychol.* 22, 151–160. doi: 10.1016/j.acn.2006.12.001

Sekuler, R., Sekuler, A. B., and Lau, R. (1997). Sound alters visual motion perception. *Nature* 385, 308. doi: 10.1038/385308a0

Smith, J. L., Jamadar, S., Provost, A. L., and Michie, P. T. (2013). Motor and non-motor inhibition in the Go/NoGo task: An ERP and fMRI study. *Int. J. Psychophysiol.* 87, 244–253. doi: 10.1016/j.ijpsycho.2012.07.185

Srinagesh, K. (2006). *The Principles of Experimental Research.* Amsterdam; Burlington, MA: Elsevier/Butterworth-Heinemann.

Vuilleumier, P., Armony, J. L., Driver, J., and Dolan, R. J. (2001). Effects of attention and emotion on face processing in the human brain: an event-related fMRI study. *Neuron* 30, 829–841. doi: 10.1016/S0896-6273(01)00328-2

Vuong, Q. H. (1989). Likelihood ratio tests for model selection and non-nested hypotheses. *Econom. J. Econom. Soc.* 57, 307–333. doi: 10.2307/1912557

Waters, A. M., and Valvoi, J. S. (2009). Attentional bias for emotional faces in paediatric anxiety disorders: an investigation using the emotional go/no go task. *J. Behav. Ther. Exp. Psychiatry* 40, 306–316. doi: 10.1016/j.jbtep.2008.12.008

Wong, Y. K., and Gauthier, I. (2012). Music-reading expertise alters visual spatial resolution for musical notation. *Psychon. Bull. Rev.* 19, 594–600. doi: 10.3758/s13423-012-0242-x

Yerys, B. E., Kenworthy, L., Jankowski, K. F., Strang, J., and Wallace, G. L. (2013). Separate components of emotional go/no-go performance relate to autism versus attention symptoms in children with autism. *Neuropsychology* 27, 537–545. doi: 10.1037/a0033615

Yu, L., and Liu, H. (2003). "Feature selection for high-dimensional data: a fast correlation-based filter solution," in *Proceedings of the Twentieth International Conference on Machine Learning (ICML-2003),* (Washington, DC), 856–863.

Zanto, T. P., Rubens, M. T., Thangavel, A., and Gazzaley, A. (2011). Causal role of the prefrontal cortex in top-down modulation of visual processing and working memory. *Nat. Neurosci.* 14, 656–661. doi: 10.1038/nn.2773

frontiers
in Computational Neuroscience

Automated Detection of Driver Fatigue Based on AdaBoost Classifier with EEG Signals

Jianfeng Hu *

The Center of Collaboration and Innovation, Jiangxi University of Technology, Nanchang, China

Purpose: Driving fatigue has become one of the important causes of road accidents, there are many researches to analyze driver fatigue. EEG is becoming increasingly useful in the measuring fatigue state. Manual interpretation of EEG signals is impossible, so an effective method for automatic detection of EEG signals is crucial needed.

Method: In order to evaluate the complex, unstable, and non-linear characteristics of EEG signals, four feature sets were computed from EEG signals, in which fuzzy entropy (FE), sample entropy (SE), approximate Entropy (AE), spectral entropy (PE), and combined entropies (FE + SE + AE + PE) were included. All these feature sets were used as the input vectors of AdaBoost classifier, a boosting method which is fast and highly accurate. To assess our method, several experiments including parameter setting and classifier comparison were conducted on 28 subjects. For comparison, Decision Trees (DT), Support Vector Machine (SVM) and Naive Bayes (NB) classifiers are used.

Results: The proposed method (combination of FE and AdaBoost) yields superior performance than other schemes. Using FE feature extractor, AdaBoost achieves improved area (AUC) under the receiver operating curve of 0.994, error rate (ERR) of 0.024, Precision of 0.969, Recall of 0.984, F1 score of 0.976, and Matthews correlation coefficient (MCC) of 0.952, compared to SVM (ERR at 0.035, Precision of 0.957, Recall of 0.974, F1 score of 0.966, and MCC of 0.930 with AUC of 0.990), DT (ERR at 0.142, Precision of 0.857, Recall of 0.859, F1 score of 0.966, and MCC of 0.716 with AUC of 0.916) and NB (ERR at 0.405, Precision of 0.646, Recall of 0.434, F1 score of 0.519, and MCC of 0.203 with AUC of 0.606). It shows that the FE feature set and combined feature set outperform other feature sets. AdaBoost seems to have better robustness against changes of ratio of test samples for all samples and number of subjects, which might therefore aid in the real-time detection of driver fatigue through the classification of EEG signals.

Conclusion: By using combination of FE features and AdaBoost classifier to detect EEG-based driver fatigue, this paper ensured confidence in exploring the inherent physiological mechanisms and wearable application.

Keywords: driver fatigue, electroencephalogram (EEG), adaboost, fuzzy entropy, receiver operating characteristic (ROC)

INTRODUCTION

Electroencephalogram (EEG) is a very important monitoring technique to reflect the instantaneous state of the brain. Various computational ways based on EEG signals have been successfully used to assist the diagnosis of seizure (Amal Feltane et al., 2013), stroke, Alzheimer's, schizophrenia (Boostani et al., 2009), epilepsy (Guo et al., 2010), depression, Attention Deficit Hyperactivity Disorder, and even fatigue. Driver fatigue is very important factor to traffic safety and automated detection is necessary urgently (Lal and Craig, 2001). Many EEG-based studies have been performed to analyze and detect driving fatigue (Kar et al., 2010; Mu et al., 2017a; Yin et al., 2017).

Correa et al. got 83.6% accuracy using a Neural Network classifier (Correa et al., 2014). Mousa Kadhim et al. yielded the highest accuracy of 85% using Discrete Wavelet Transforms method (Mousa Kadhim et al., 2013). Li et al. achieved the highest accuracy of 91.5% based on 12 types of energy parameters (Li et al., 2012). Fu et al. reached a highest accuracy of 92.5% based on Hidden Markov Model (HMM; Fu et al., 2016). Zhao et al. hit a higher accuracy (98.7%) based on a KPCA-SVM classifier (Zhao et al., 2010). Recently, entropy has been broadly applied in the analysis of EEG signals, considering the fact that EEG is a complex, unstable, and non-linear signal (Acharya et al., 2012; Hu et al., 2015; Mu et al., 2016). A diverse varied collection of these methods has been proposed in the last few decades, including spectral entropy (PE), permutation entropy, distribution entropy, fuzzy entropy (FE), Renyi entropy, approximate entropy (AE), sample entropy (SE), and some others. Specially, in the field of EEG processing, four of the most widely used and successful entropy estimators are FE (Chen et al., 2009), SE (Richman and Moorman, 2000), AE (Pincus, 1991), and PE (Reyes-Sanchez et al., 2016). AE has demonstrated its capability to detect complexity changes. SE is a similar statistic, which has not yet been used as extensively as AE. AE and SE are very successful entropy features, but they also have their weaknesses. AE is biased because it includes self-matching in the count, while SE needs to avoid the log(0) problem. They are also very sensitive to input parameters. More recently, FE has been proposed to alleviate these problems. FE is based on a continuous function to compute the dissimilarity between two zero-mean subsequences, so it is more stable in noise and parameter initialization.

Liu et al. got 84% accuracy with the combination of kernel principal component analysis and HMM utilizing AE and Kolmogorov complexity to detect the fatigue state (Liu et al., 2010). Mu et al. yielded accuracy of 85% with FE and Support Vector Machine (SVM) classifier (Mu et al., 2017a). Xiong et al. proposed a feature combination of AE and SE with SVM classifier to test driving fatigue, and achieved the best accuracy of 91.3% (Xiong et al., 2016). Khushaba et al. exploited a feature extraction by using fuzzy mutual-information method and achieved 92.8% (Khushaba et al., 2011). Hu hit highest accuracy of 96.6% with FE and Random Forest classifier (Hu, 2017).

Abbreviations: FE, Fuzzy entropy; SE, Sample entropy; AE, Approximate entropy; PE, Spectral entropy; EEG, Electroencephalogram; AUC, Areas under ROC curves; SVM, Support Vector Machine; DT, Decision Tree; NB, Naive Bayes; AdaBoost, Adaptive Boosting; ERR, Error rate.

From the literature review, it has been observed that few studies have been conducted for using ensemble classifier based on EEG to study driver fatigue detection. Keeping this in mind, the prime motivation of this work is to develop an automated detection system for driver fatigue based on ensemble classifier. The scheme employs four types of entropy for feature extraction and AdaBoost (Freund and Schapire, 1997; Hastie et al., 2009) for classification of EEG signals into normal and fatigue. Several experiments on 28 subjects indicate that the proposed scheme earns better detection performance and robustness in comparison to other existing schemes.

The rest of this article is described as below. In Materials and Methods, data acquisition, feature extraction, and classification are illustrated. The results are discussed in Section Results presents the evaluation of the method with the obtained results, followed by a general discussion about classifier accuracy in Section Discussion.

MATERIALS AND METHODS

Subjects

Twenty-eight university students (14 male, 19–24 years) participated in this experiment, which all had a current driver's license. Before the experiment, they practiced driving for several minutes to familiarize themselves with the process and purpose of the experiment. The experiment was approved by the Academic Ethics Committee of the Jiangxi University of Technology according to the standards of the Declaration of Helsinki. Written informed consent was obtained from each subject.

Experiment

In the static driving simulator (ZY-31D, ZhongYu CO., LTD, China), the driver's fatigue simulation test was performed on each subject, as shown in **Figure 1**. The driving environment selected for this work was a highway with low traffic density so as to induce monotonous driving, which easily leads to driver fatigue state.

Data Recording

Similar to former experiments (Chai et al., 2017; Hu, 2017; Mu et al., 2017b), when the driving procedure started 20 min, the last 5-min EEG recordings were marked as normal state. When

FIGURE 1 | Snapshot of the experimental setup.

the continuous driving procedure lasted 60–120 min until the questionnaire results (Lee's subjective fatigue scale and Borg's CR-10 scale; Borg, 1990; Lee et al., 1991), participants' responses and electrooculogram (EOG) signals show the subject was in driving fatigue state, the last 5-min recorded EEG recordings were marked as fatigue state. EOG signals were used to determine fatigue state using the blink rate and eye closure such as, the small and slow blinks.

All channel data were referenced to two reference electrodes A1 and A2, and digitized at 1 kHz from a 32-channel electrode cap (including 2 reference electrodes) based on the international 10–20 system.

After the acquisition of EEG signals, the main procedures of data preprocessing was implemented by Scan 4.3 software of Neuroscan (Compumedics, Australia). The original signals were first filtered and a 0.15–45 Hz band-pass filter was used. Then 5-min EEG signals from 30 channels were sectioned into 1-s epochs, resulting in 300 epochs. With the 28 subjects and 30 channels, a total of 504,000 units were randomly formed for dataset (each state having 252,000 units).

Feature Extraction

The EEG is assumed to be a non-stationary time series and most feature extraction methods are only applicable to stationary signal. To deal with this problem, the EEG time series were divided into several short windows and its statistics is assumed to be approximately stationary within each window. The following feature extraction methods are applied to each 1-s windowed signal. EEG signals are segmented without overlap, finally feature sets are extracted from all channels in each 1 s window.

The ability to distinguish between normal state and fatigue state depends mainly on the quality of the input vectors of the classifier. In order to capture EEG features, four feature sets are computed, including FE, SE, AE, and PE. In this section, the computational methods of these feature sets in EEG recordings are described in detail.

Spectral Entropy (PE)

PE is evaluated using the normalized Shannon entropy (Kannathal et al., 2005), which quantifies the spectral complexity of the time series. The power level of the frequency component is indicated by Y_i and y_i is normalized as:

$$y_i = \frac{Y_i}{\sum Y_i} \tag{1}$$

The PE of the time series is calculated using the following equation:

$$PE = \sum_i i y_i \log(\frac{1}{y_i}) \tag{2}$$

Approximate Entropy (AE)

AE, as proposed by Pincus (1991), is a statistically quantified non-linear dynamic parameter that measures the complexity of a time series. The procedure for the AE-based algorithm is described as follows:

(1) Considering a time series $t(i)$, a set of m-dimensional vectors are obtained according to the sequence order of $t(i)$:

$$T_i^m = [t(i), t(i+1), \ldots, t(i+m-1)]; i \leq L - m + 1 \tag{3}$$

$d[T_i^m, T_j^m]$ is the distance between two vectors T_i^m and T_j^m, defined as the maximum difference values between the corresponding elements of two vectors:

$$d[T_i^m, T_j^m] = \max_{k \in (0, m-1)}\{|t(i+k) - t(j+k)|\}, (i, j = 1 \sim L - m$$
$$+ 1, i \neq j) \tag{4}$$

(2) Define S_i is the number of vectors T_j that are similar to T_i, subject to the criterion of similarity $d[T_i^m, T_j^m] \leq s$

$$S_i^m(s) = \frac{1}{L - m + 1} S_i \tag{5}$$

(3) Define the function $\gamma^m(s)$ as:

$$\gamma^m(s) = \frac{1}{L - m + 1} \sum_{i=1}^{L-m+1} \ln S_i^m(s) \tag{6}$$

(4) Set $m = m + 1$, and repeat steps (3) to (6) to obtain $S_i^{m+1}(s)$ and $\gamma^{m+1}(s)$, then:

$$\gamma^{m+1}(s) = \frac{1}{L - m} \sum_{i=1}^{L-m} \ln S_i^{m+1}(s) \tag{7}$$

(5) The AE can be expressed as:

$$AE = \gamma^m(s) - \gamma^{m+1}(s) \tag{8}$$

Sample Entropy (SE)

SE's algorithm is similar to that of AE (Yentes et al., 2013), which is a new measure of time series complexity proposed by Richman and Moorman (2000). The step (1) can be defined in the same way as the AE-based algorithm; other steps in the SE-based algorithm are described as follows:

(1) Define A_i is the number of vectors T_j that are similar to T_i subject to the criterion of similarity $d[T_i^m, T_j^m] \leq s$

$$A_i^m(s) = \frac{1}{L - m - 1} A_i \tag{9}$$

(2) Define the function $\gamma^m(s)$ as:

$$\gamma^m(s) = \frac{1}{L - m} \sum_{i=1}^{L-m} A_i^m(s) \tag{10}$$

(3) Set $m = m + 1$, and repeat above steps to obtain $A_i^{m+1}(s)$ and $\gamma^{m+1}(s)$, then

$$\gamma^{m+1}(s) = \frac{1}{L - m - 1} \sum_{i=1}^{L-m-1} A_i^{m+1}(s) \tag{11}$$

(4) The SE can be expressed as:

$$SE = \log(\gamma^m(s) / \gamma^{m+1}(s)) \tag{12}$$

Fuzzy Entropy (FE)

To deal with some of the issues with SE, Xiang et al. proposed the use of fuzzy membership function in computing the vector similarity to replace the binary function in SE algorithm (Xiang et al., 2015), so that the entropy value is continuous and smooth. The procedure for the FE-based algorithm is described in detail as follows:

(1) Set a L-point sample sequence: $\{v(i) : 1 \leq i \leq L\}$;
(2) The phase-space reconstruction is performed on $v(i)$ according to the sequence order. The reconstructed vector can be written as:

$$T_i^m = \{v(i), v(i+1), ..., v(i+m-1)\} - v_0(i) \quad (13)$$

where $i = 1, 2, ..., L - m + 1$, and $v_0(i)$ is the average value described as the following equation:

$$v_0(i) = \frac{1}{m} \sum_{j=0}^{m-1} v(i+j) \quad (14)$$

(3) d_{ij}^m, the distance between two vectors T_i^m and T_j^m, is defined as the maximum difference values between the corresponding elements of two vectors:

$$d_{ij}^m = \mathrm{d}\left[T_i^m, T_j^m\right] = \max_{k \in (0, m-1)} \{|v(i+k) - v_0(i)$$
$$- (v(j+k) - v_0(j))|\}$$
$$(i, j = 1 \sim L - m, i \neq j) \quad (15)$$

(4) According to the fuzzy membership function $\sigma(d_{ij}^m, n, s)$, the similarity degree D_{ij}^m between two vectors T_i^m and T_j^m is defined as:

$$D_{ij}^m = \sigma(d_{ij}^m, n, s) = \exp(-(d_{ij}^m)^n/s) \quad (16)$$

where the fuzzy membership function $\sigma(d_{ij}^m, n, s)$ is an exponential function, while n and s are the gradient and width of the exponential function, respectively.

(5) Define the function $\gamma^m(n, s)$:

$$\gamma^m(n, s) = \frac{1}{L-m} \sum_{i=1}^{L-m} \frac{1}{L-m-1} \sum_{j=1, j \neq 1}^{L-m} D_{ij}^m] \quad (17)$$

(6) Repeat the steps from (1) to (4) in the same manner. Define the function:

$$\gamma^{m+1}(n, s) = \frac{1}{L-m} \sum_{i=1}^{L-m} \frac{1}{L-m-1} \sum_{j=1, j \neq 1}^{L-m} D_{ij}^{m+1}] \quad (18)$$

(7) The FE can be expressed as:

$$\mathrm{FE}(m, s, n) = \ln \gamma^m(n, s) - \ln \gamma^{m+1}(n, s) \quad (19)$$

In these four entropies, m and s are the dimensions of phase space and similarity tolerance, respectively. In the present study, $m = 2$, $n = 4$ while $s = 0.2 * SD$, where SD denotes the standard deviation of the time series.

For optimizing the detection quality, the feature sets were normalized for each subject and each channel by scaling between -1 and 1.

Classification

To avoid over-fitting problem, the datasets were separated into train sets and test sets in the following pattern. In the train phase, 10-fold cross validation applied on the features such that 10% feature vectors are dedicated as test set and other 90% feature vectors are considered as the train set. In the next iteration, another 10% feature vectors consider as test set and the rest for the train set, till all of feature vectors involved one time in the test process. The final result was obtained by averaging the results of corresponding turns. By this evaluation scheme, the dependencies of the train and test sets were eliminated.

Since there is no uniform classification method suitable for all subjects and all applications, usually it may be useful to test multiple methods (Zhang et al., 2017). In this work, three types of base classifiers namely Decision Trees (DT), Support Vector Machine (SVM), and Naive Bayes (NB) were used. DT is a non-parametric supervised learning method used for classification. DT establishes several binary decision functions on the features. DT1 and DT9 represent DT with the maximum depth of the tree being 1 and 9 in this work, respectively. In the case of non-linear classification, kernels, such as, radial basis functions (RBF), are used to map the data into a higher dimensional feature space in which a linear separating hyper-plane could be found. Naive Bayes method is based on applying Bayes' theorem with the "naive" assumption. The likelihood in NB of the features is assumed to be Gaussian. In this study, grid parameter search was used to achieve better results.

AdaBoost is an eminent ensemble learning based classification model (Amal Feltane et al., 2013; Yang et al., 2016), which was first proposed by Freund and Schapire (1997). AdaBoost produces the final output by weighting the decisions of all these weak classifiers using majority vote method. The AdaBoost algorithm is described as follow:

Algorithm *AdaBoost*
Definition train dataset $(X, Y) = \{(x_1, y_1), (x_2, y_2), (x_3, y_3), \ldots, (x_N, y_N)\}, y_i \, \varepsilon \, \{-1, 1\}$
    iterator: M;
  Initialize each weight $W_{1, i} = \frac{1}{N}$, $i = 1, 2, \ldots, N$,
  Linear combination function of basic classifiers $f_0(x) = 0$
for $m = 1$ to M do
    train a base learner: $D_m(x)$
    calculate error rate: $e_m = \sum_{i=1}^{N} W_{m,i} I(D_m(x_i) - y_i)$
    $\alpha_m = \frac{1}{2} \ln(\frac{1-e_m}{e_m})$
    update weight: $W_{m+1, i} = \frac{W_{m, i}}{Z_m} \exp(-\alpha_m y_i D_m(x_i))$,

normalization factor $Z_m = \sum_{i=1}^{N} W_{m,i} \exp(-\alpha_m y_i D_m(x_i))$
    $f_m(x) = f_{m-1}(x) + lr * \alpha_m D_m(x)$
end for
Output sign $(f_M(x)) = sign(\sum_{m=1}^{M} \alpha_m D_m(x))$
  In this work, the DT9 was used as base classifiers.
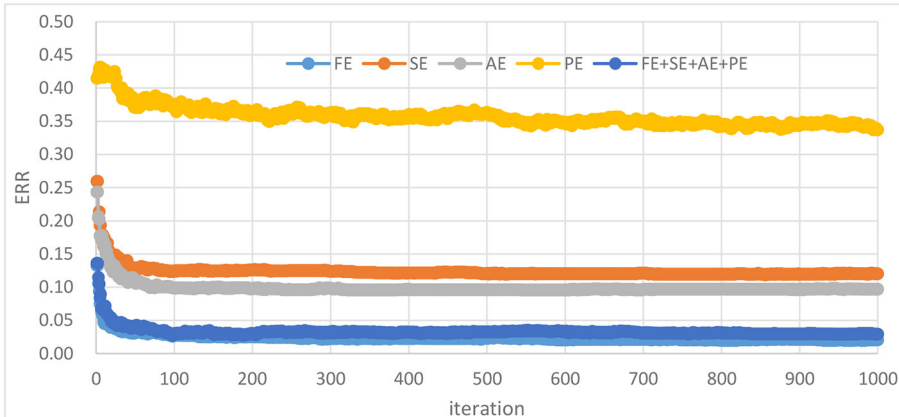
Performance Evaluation

To provide an easier-to-understand method to assess the classification quality, the results of classification and the performance of classifiers are expressed in terms of Error rate, Precision, Recall, F1 score, MCC, and AUC which are defined as follows:

FIGURE 2 | ERR for AdaBoost based on different feature sets.

Error rate (ERR) calculates the total number of EEG segments which are incorrectly classified

$$ERR = \frac{(FP + FN)}{(FP + TN + FP + FN)}$$

The precision intuitively reflects the ability of the classifier to determine the whole sample—which the positive is identified as positive and the negative is identified as negative.

$$Precision = \frac{TP}{TP + FP}$$

The recall intuitively reflects the proportion of positive samples that are correctly identified.

$$Recall = \frac{TP}{TP + FN}$$

The F1 score can be interpreted as a weighted average of precision and recall, where an F1 score reaches the optimum value at 1 and the worst score at 0.

$$F1 = \frac{2 * (Precision * Recall)}{(Precision + Recall)}$$

The Matthews correlation coefficient (MCC) is used in machine learning as a measure of the quality of two-class classifications. The MCC is in essence a correlation coefficient value between -1 and +1.

$$MCC = \frac{TP*TN - FP*FN}{\sqrt{(TP + FP)(TP + FN)(TN + FP)(TN + FN)}}$$

Where

TP (True Positive) = correctly identified normal segments
TN (True Negative) = correctly identified fatigue segments
FN (False Negative) = incorrectly identified normal segments
FP (False Positive) = incorrectly identified fatigue segments

AUC illustrates the performance of a binary classifier system as its discrimination threshold is varied. It is created by drawing true positive rates from positive (true positive rate) and false positive rates (false positive rates) in a variety of threshold settings.

Statistical Analysis

In order to investigate differences of average accuracy among various classifiers and feature sets, the paired sample t-test was used to evaluate effectiveness on each comparison. The results are averages over 10 independently turns of combination of train set and test set in each experiment.
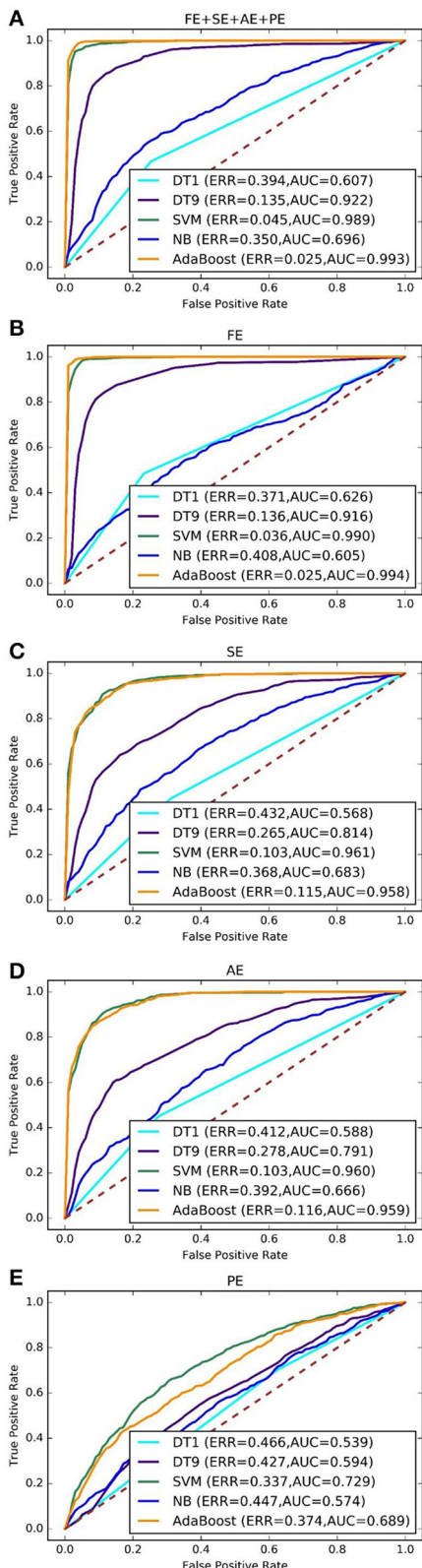
RESULTS

In order to verify the validity, effectiveness, and robust of proposed method, some experiments were performed on 28 subjects.

Comparison with Different Feature Sets and Different Classifiers

As shown in **Figure 2**. FE feature set performs slightly better than the combined entropy (FE + SE + AE + PE) feature set (0.020 against 0.029). A paired t-test across the 10 independent comparisons indicates a significant difference with p-value around 0.003. It can be seen that the FE feature set performs about 0.098 and 0.075 better than the SE and AE feature set at ERR index, respectively. A paired t-test over 10 independent comparisons shows a significant difference with p-value lower than 0.001. AE feature set performs slightly better than SE feature set. It can also show that the PE feature set performs worst with the lowest ERR being about 0.337.

The results of 10 independently rounds are used to draw mean ROC curves. Different feature sets or classifiers were compared by analyzing their ROC curves and areas under ROC curves (AUC). In **Figures 3A–E**, their performance in ROC curves produced was compared by different classifiers on combined entropy feature set, FE feature set, SE feature set, AE feature set

FIGURE 3 | ROC curves for different feature sets and different classifiers. **(A–E)** Represents combined feature set, FE feature set, SE feature set, AE feature set and PE feature set, respectively.

and PE feature set, respectively. It shows that the FE feature set and combined feature set outperform other feature sets, which similar to **Figure 2**. For example, the best ERR of FE feature set and combined feature set are both 0.025, while the best ERR of SE, AE, and PE are 0.115, 0.116, and 0.374, respectively. The best AUC of FE feature set and combined feature set is are 0.993 and 0.994, respectively while the best ERR of SE, AE, and PE are 0.961, 0.960, and 0.729, respectively. Consequently, adding more features makes nothing changes for driver fatigue detection. Therefore, the FE feature set is selected for the next experiments.

As shown in **Figure 4**, it illustrate that AdaBoost outperform other classifiers. For instance, the best ERR and AUC is 0.025 and 0.994 for AdaBoost based on FE feature set, while the best ERR and AUC is 0.036 and 0.990 for SVM based on FE feature set. The p-value is 0.0062 between AdaBoost and SVM. AdaBoost classifier is significantly better than other classifiers. The p-values are 0.0032 and 0.0001, by paired t-test between DT9 and AdaBoost, and between NB and AdaBoost, respectively. It's conjectured that AdaBoost models work best because they may be more robust than other models such as, DT and NB when dealing with scalar data sets that are not too larger.

To evaluate the effectiveness of AdaBoost in the classification of EEG signals, the classification indexes including ERR, Precision, Recall, F1, score and MCC of the four classifiers were compared based on FE feature set. As shown in **Figure 4** and **Table 1**, the overall performance of AdaBoost is the best of the four classifiers in terms of ERR, Precision, Recall, MCC, and F1 score. The ERR of AdaBoost can reach 0.024 ± 0.002, which is almost 0.011 lower than SVM (0.035 ± 0.005). The ERR of DT1, DT9, and NB is 0.0369 ± 0.014, 0.0142 ± 0.008, and 0.405 ± 0.012, respectively.
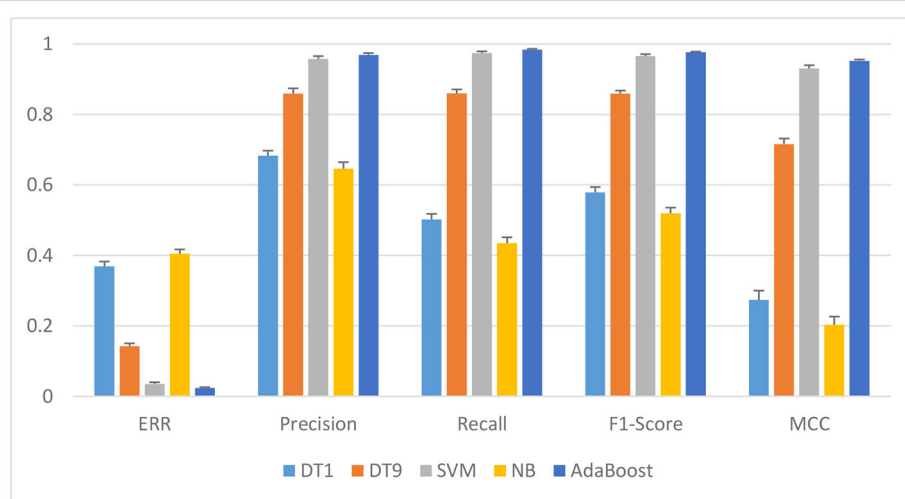
Parameter Setting

The main parameters to be adjusted in AdaBoost method are parameter *max_depth* of base classifier DT and *lr*. Best performance of AdaBoost model can be yielded through carefully choosing the optimal combination of these parameters. The parameter *max_depth* is the most important one in the DT, which controls the maximum depth of the tree. **Figure 5A** shows the error rates under different *max_depth* and fixed iteration (=500) based on FE feature set. It is showed that the average error rate attains the minimal point 0.022 ± 0.004 when *max_depth* equals to about 8. From **Figure 5B**, it can be seen that the average error rate starts to even out at 0.022 ± 0.003 when the value of *lr* smaller than about 1.5. According to these results, the final AdaBoost classifier in next experiments is set with the parameters *max_depth* = 9 (DT9) and *lr* = 1.0.

Comparison with Different Size of Test Samples

The ratio of train samples for test samples is important for the performance of classifier. To determine the robustness of the classifier against size of test sample or train size, the ratio of test samples for all samples is set varying from 0.03 to 0.97. The ERR of AdaBoost against different ratio is shown in **Figure 6**.

It is observed that the average error rate begins to stabilize at about 0.03 when the ratio being about 0.5. When the ratio

FIGURE 4 | Performance of different classifiers based on FE feature set.

TABLE 1 | *p*-value between AdaBoost and other classifiers with paired *t*-test.

Index Classifiers	ERR	Precision	Recall	F1 score	MCC
SVM	1.05e-5	4.81e-4	5.60e-4	1.31e-4	8.92e-5
DT1	2.12e-7	4.82e-7	4.10e-7	4.46e-7	4.41e-7
DT9	2.07e-7	1.32e-6	9.46e-7	6.61e-7	6.10e-7
NB	2.06e-7	5.33e-7	3.98e-7	4.27e-7	3.97e-7

becomes larger, the ERR also becomes larger, but when ratio reaches close to 1.0, the ERR is close to 10% and becomes worse, possibly because of the lack of training samples. On the contrary, when the ratio becomes smaller, ERR is stable at around 0.02, which indicating that ratio is more appropriate in the 0.1.

P-value between AdaBoost and SVM, between AdaBoost and DT9, are 3e-8 and 4e-16, respectively. Compared to SVM and DT, AdaBoost seems to have better robustness against changes of ratio of test samples for all samples.

Comparison with Different Number of Subjects

The number of subjects is also an important parameter in the driving fatigue detection system. More subjects can provide more information that may improve or reduce detection performance. Generally speaking, when average performance is poor, any subject with higher accuracy can improve the overall performance, and vice versa. Sometimes, the classifier model that is suitable for small samples may lose performance when large samples are used. However, when more subjects are involved, the system costs, including hardware and computation time, will also increase. Therefore, a tradeoff between the system performance and system cost should be based on the specificity of the application.

To answer the question of how many subjects are needed to train for a satisfactory detection system, system performance

was evaluated with respect to the number of subjects. For each number *n* (from 2 to 28), a random combination (*n* out of 28 subjects) was repeated 20 times for calculating classification accuracy using 10-fold cross validation. Three classifiers approaches were calculated for comparison. Furthermore, for each condition (*n* from 2 to 28), the paired *T*-test was used as a post-hoc test to evaluate if the performance of AdaBoost was significantly better than that of other two classifiers.
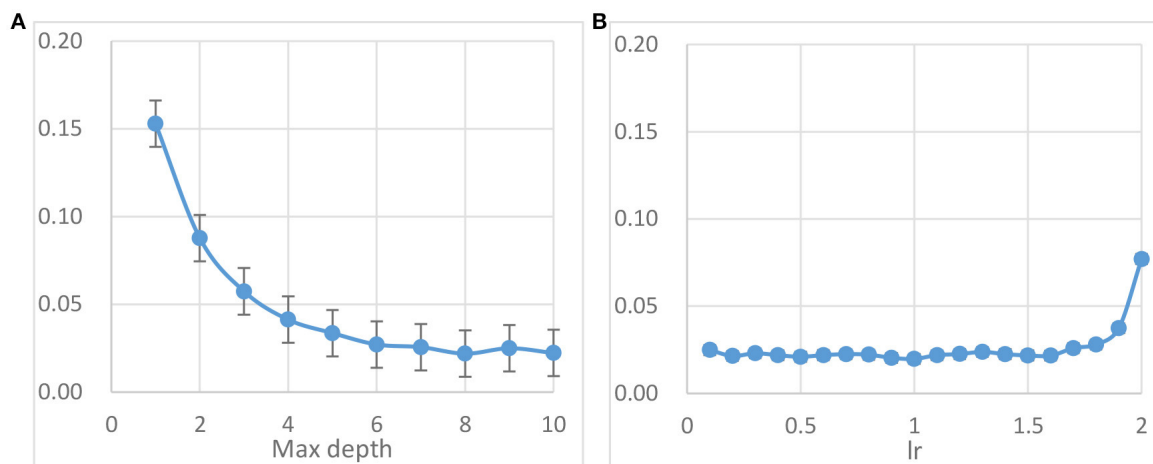
The ERR of AdaBoost against different number of subjects is shown in **Figure 7**. It can be seen that, for AdaBoost classifier, when the number of subjects is <13, ERR is <0.01, when the number of subjects continue to increase, ERR also increases, and is stable at about 0.02. ERR is not increasing monotonically with the number of subjects but tending to reach equilibrium.

P-values between AdaBoost and SVM, between AdaBoost and DT9, are 4.665e-8 and 1.409e-8, respectively. Compared to SVM and DT, AdaBoost seems to have better robustness against changes of number of subjects.
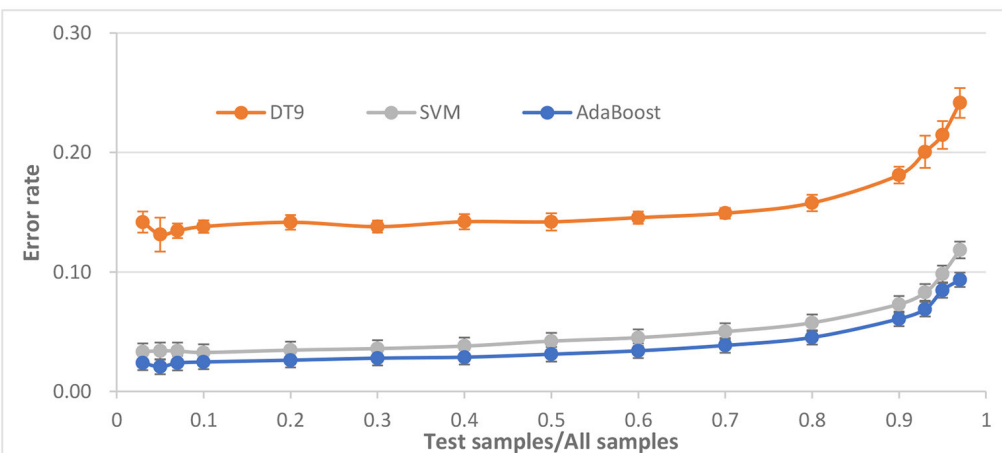
DISCUSSION

As see in **Table 2**, it is found that the classification performance of proposed method was better than that in the others research using entropy feature sets. Although, based on the existing EEG data, the optimal performance of detection of driving fatigue by using AdaBoost-based method showed well application on the real-time detection of driving fatigue.
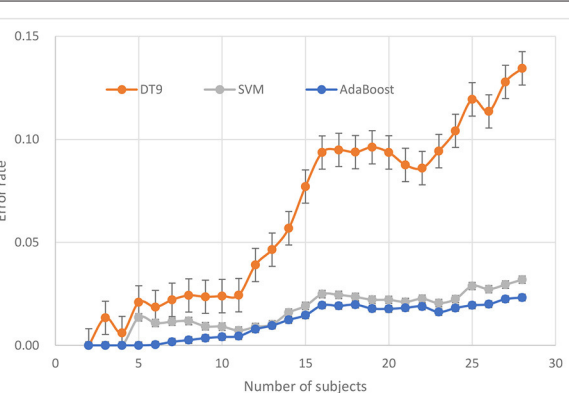
Among the state-of-art classifier schemes, four representative algorithms, DT, NB, SVM, and AdaBoost were experimented for classification tasks of some data sets. These classifiers have been shown very effective in many pattern recognition applications. These classifiers are applied on the extracted features and their results are shown in **Figures 3**, **4** in which AdaBoost

FIGURE 5 | AdaBoost method parameter tuning results based on FE feature set and DT base classifier. **(A)** The error rates for different *max_depth* with *lr* = 1.0. **(B)** The error rates with default *max_depth* (value = 9) for different *lr*.

FIGURE 6 | Performance evaluation with respect to the ratio of test samples for all samples.

FIGURE 7 | Performance evaluation in terms of number of subjects.

TABLE 2 | Studies regarding driver fatigue detection using entropy feature sets.

Research group	Feature method	Highest accuracy (%)
Liu et al., 2010	AE and others	84
Mu et al., 2017a	FE	85
Xiong et al., 2016	AE and SE	91.3
Khushaba et al., 2011	FE	92.8
Hu, 2017	FE	96.6
This paper	FE	97.5

showed a better results in comparison with the three other classifiers.

Also to evaluate robustness of the classifiers, different combinations of train set and test sets were employed and the classification results were brought in **Figures 6**, **7**. A repeated

progressive method with various sample sizes was applied to find out if there is any relationship between data set size and the performance. It can be seen that AdaBoost is also more robust than the three other classifiers.

The experiment confirmed that, in comparison with the AE, PE, and SE, the FE had a better consistency and better discrimination ability. The results also showed that the differences between the normal state and the fatigue state were relative larger from the FE from the AE, SE, or the PE, confirming that the FE had a better performance in distinguishing fatigue state. The result achieved in this study ensured confidence in probing the theoretical reason for the different discrimination ability and, hence, leads to new ideas for exploring the inherent physiological mechanisms when using the entropy methods. This indicated that the FE could be an effective method for the driver fatigue detection.

However, there are several limitations in this study. First, it is worth noting that the parameter settings for the SE, AE, and PE method are the local similarity and parameters may not be the optimal solution. Second, the number of subject is relatively small. Although according to the existing literature in the Introduction section, the 28 subjects are not too small, but the number still needs to be increased. Third, only three commonly used classifiers and the four feature sets were compared in this study. Last, the different impacts of different channels haven't been took into account.

CONCLUSION

In this paper, a method to develop an ensemble classifier for recognizing fatigue was proposed. A new EEG feature vector based on FE, SE, AE, and PE was used as input into four different classifiers: DT, NB, SVM, and AdaBoost. It was concluded that the combination of these feature sets or FE feature set with the AdaBoost provided the best performance on EEG dataset. The proposed method had very high accuracy classifying driver fatigue events. Further, it was showed how the method for detecting fatigue segments was robust.

AUTHOR CONTRIBUTIONS

JH conceived and designed the experiments; JH analyzed the data and wrote the paper.

ACKNOWLEDGMENTS

REFERENCES

Acharya, U. R., Molinari, F., Sree, S. V., Chattopadhyay, S., Ng, K. H., and Suri, J. S. (2012). Automated diagnosis of epileptic EEG using entropies. *Biomed. Signal Process. Control* 7, 401–408. doi: 10.1016/j.bspc.2011.07.007

Amal Feltane, G., Boudreaux-Bartels, F., and Besio, W. (2013). Automatic seizure detection in rats using laplacian EEG and verification with human seizure signals. *Ann. Biomed. Eng.* 41, 645–654. doi: 10.1007/s10439-012-0675-4

Boostani, R., Sadatnezhad, K., and Sabeti, M. (2009). An efficient classifier to diagnose of schizophrenia based on the EEG signals. *Expert Syst. Appl.* 36, 6492–6499. doi: 10.1016/j.eswa.2008.07.037

Borg, G. (1990). Psychophysical scaling with applications in physical work and the perception of exertion. *Scand. J. Work Environ. Health.* 16, 55–58. doi: 10.5271/sjweh.1815

Chai, R., Ling, S. H., San, P. P., Naik, G. R., Nguyen, T. N., Tran, Y., et al. (2017). Improving EEG-based driver fatigue classification using sparse-deep belief networks. *Front. Neurosci.* 11:103. doi: 10.3389/fnins.2017.00103

Chen, W., Zhuang, J., Yu, W., and Wang, Z. (2009). Measuring complexity using fuzzyen, apen, and sampen. *Med. Eng. Phys.* 31, 61–68. doi: 10.1016/j.medengphy.2008.04.005

Correa, A. G., Orosco, L., and Laciar, E. (2014). Automatic detection of drowsiness in EEG records based on multimodal analysis. *Med. Eng. Phys.* 36, 244–249. doi: 10.1016/j.medengphy.2013.07.011

Freund, F., and Schapire, R. (1997). A decision-theoretic generalization of on-line learning algorithms and an application to boosting. *J. Comput. Syst. Sci.* 55, 119–139. doi: 10.1006/jcss.1997.1504

Fu, R. R., Wang, H., and Zhao, W. B. (2016). Dynamic driver fatigue detection using hidden Markov model in real driving condition. *Expert Syst. Appl.* 63, 397–411. doi: 10.1016/j.eswa.2016.06.042

Guo, L., Rivero, D., and Pazos, A. (2010). Epileptic seizure detection using multiwavelet transform based approximate entropy and

artificial neural networks. *J. Neurosci. Methods* 193, 156–163. doi: 10.1016/j.jneumeth.2010.08.030

Hastie, T., Rosset, S., Zhu, J., and Zou, H. (2009). Multi-class AdaBoost. *Stat. Interf.* 2, 349–360. doi: 10.4310/sii.2009.v2.n3.a8

Hu, J. F. (2017). Comparison of different features and classifiers for driver fatigue detection based on a single EEG channel. *Comput. Math. Methods Med.* 2017:9. doi: 10.1155/2017/5109530

Hu, J. F., Mu, Z. D., and Wang, P. (2015). Multi-feature authentication system based on event evoked electroencephalogram. *J. Med. Imaging Health Inform.* 5, 862–870. doi: 10.1166/jmihi.2015.1471

Kannathal, N., Choo, M. L., Acharya, U. R., and Sadasivan, P. (2005). Entropies for detection of epilepsy in EEG. *Comput. Methods Programs Biomed.* 80, 187–194. doi: 10.1016/j.cmpb.2005.06.012

Kar, S., Bhagat, M., and Routray, A. (2010). EEG signal analysis for the assessment and quantification of driver's fatigue. *Transp. Res. F Traffic Psychol. Behav.* 13, 297–306. doi: 10.1016/j.trf.2010.06.006

Khushaba, R. N., Kodagoda, S., Lal, S., and Dissanayake, G. (2011). Driver drowsiness classification using fuzzy wavelet-packet-based feature-extraction algorithm. *IEEE Trans. Biomed. Eng.* 58, 121–131. doi: 10.1109/TBME.2010.2077291

Lal, S. K., and Craig, A. (2001). A critical review of the psychophysiology of driver fatigue. *Biol. Psychol.* 55, 173–194. doi: 10.1016/S0301-0511(00)00085-5

Lee, K. A., Hicks, G., and Nino-Murcia, G. (1991). Validity and reliability of a scale to assess fatigue. *Psychiatry Res.* 36, 291–298. doi: 10.1016/0165-1781(91)90027-M

Li, W., He, Q. C., Fan, X. M., and Fei, Z. M. (2012). Evaluation of driver fatigue on two channels of EEG data. *Neurosci. Lett.* 506, 235–239. doi: 10.1016/j.neulet.2011.11.014

Liu, J. P., Zhang, C., and Zheng, C. X. (2010). EEG-based estimation of mental fatigue by using KPCA–HMM and complexity parameters. *Biomed. Signal Process. Control* 5, 124–130. doi: 10.1016/j.bspc.2010.01.001

Mousa Kadhim, W., Murugappan, M., and Ahmmad, B. (2013). Wavelet packet transform based driver distraction level classification using EEG. *Mathem. Probl. Eng.* 3, 841–860. doi: 10.1155/2013/297587

Mu, Z. D., Hu, J. F., and Min, J. L. (2016). EEG-based person authentication using a fuzzy entropy-related approach with two electrodes. *Entropy* 18:432. doi: 10.3390/e18120432

Mu, Z., Hu, J., and Yin, J. (2017a). Driving fatigue detecting based on EEG signals of forehead area. *Int. J. Pattern Recognit. Artif. Intell.* 31:12. doi: 10.1142/S0218001417500112

Mu, Z., Hu, J., and Min, J. (2017b). Driver fatigue detection system using electroencephalography signals based on combined entropy features. *Appl. Sci.* 7:150. doi: 10.3390/app7020150

Pincus, S. M. (1991). Approximate entropy as a measure of system complexity. *Proc. Natl. Acad. Sci. U.S.A.* 88, 2297–2301. doi: 10.1073/pnas.88. 6.2297

Reyes-Sanchez, E., Alba, A., Mendez, M. O., Milioli, G., and Parrino, L. (2016). Spectral entropy analysis of the respiratory signal and its relationship with the cyclic alternating pattern during sleep. *Int. J. Mod. Phys. C* 27:10. doi: 10.1142/S0129183116501400

Richman, J. S., and Moorman, J. R. (2000). Physiological time-series analysis using approximate entropy and sample entropy. *Am. J. Physiol. Heart Circ. Physiol.* 278, H2039–H2049.

Xiang, J., Li, C., Li, H., Cao, R., Wang, B., Han, X., et al. (2015). The detection of epileptic seizure signals based on fuzzy entropy. *J. Neurosci. Methods* 243, 18–25. doi: 10.1016/j.jneumeth.2015.01.015

Xiong, Y., Gao, J., Yang, Y., Yu, X., and Huang, W. (2016). Classifying driving fatigue based on combined entropy measure using EEG signals. *Int. J. Control Autom.* 9, 329–338. doi: 10.14257/ijca.2016.9.3.30

Yang, T., Chen, W. T., and Cao, G. T. (2016). Automated classification of neonatal amplitude-integrated EEG based on gradient boosting method. *Biomed. Signal Process. Control.* 28, 50–57. doi: 10.1016/j.bspc.2016.04.004

Yentes, J. M., Hunt, N., Schmid, K. K., Kaipust, J. P., McGrath, D., and Stergiou, N. (2013). The appropriate use of approximate entropy and sample entropy with short data sets. *Ann. Biomed. Eng.* 41, 349–365. doi: 10.1007/s10439-012-0668-3

Yin, J. H., Hu, J. F., and Mu, Z. D. (2017). Developing and evaluating a mobile driver fatigue detection network based on electroencephalograph signals. *Healthcare Technol. Lett.* 4, 34–38. doi: 10.1049/htl.2016.0053

Zhang, C. S., Liu, C. C., Zhang, X. L., and Almpanidis, G. (2017). An up-to-date comparison of state-of-the-art classification algorithms. *Expert Syst. Appl.* 82, 128–150. doi: 10.1016/j.eswa.2017. 04.003

Zhao, C., Zheng, C., Zhao, M., and Liu, J. (2010). Physiological assessment of driving mental fatigue using wavelet packet energy and random forests. *Am. J. Biomed. Sci.* 2, 262–274. doi: 10.5099/aj100300262

frontiers
in Behavioral Neuroscience

Theta Oscillations Related to Orientation Recognition in Unattended Condition: A vMMN Study

Tianyi Yan[1]*, Yuan Feng[1], Tiantian Liu[1], Luyao Wang[2], Nan Mu[1], Xiaonan Dong[1], Zichuan Liu[3], Tianran Qin[4], Xiaoying Tang[1] and Lun Zhao[5,6]

[1]School of Life Science, Beijing Institute of Technology, Beijing, China, [2]Intelligent Robotics Institute, School of Mechatronical Engineering, Beijing Institute of Technology, Beijing, China, [3]Saddle River Day School, Saddle River, NJ, United States, [4]Beijing Royal School, Beijing, China, [5]School of Education, Beijing Normal University Zhuhai, Zhuhai, China, [6]School of Psychological Research, Beijing Yiran Sunny Technology Co., Ltd., Beijing, China

Orientation is one of the important elements of objects that can influence visual processing. In this study, we examined whether changes in orientation could be detected automatically under unattended condition. Visual mismatch negativity (vMMN) was used to analyze this processing. In addition, we investigated the underlying neural oscillatory activity. Non-phase-locked spectral power was used to explore the specific frequency related to unexpected changes in orientation. The experiment consisted of standard (0° arrows) and deviant (90°/270° arrows) stimuli. Compared with standard stimuli, deviant stimuli elicited a larger N170 component (negative wave approximately 170 ms after the stimuli started) and a smaller P2 component (positive wave approximately 200 ms after the stimuli started). Furthermore, vMMN was obtained by subtracting the event-related potential (ERP) waveforms in response to standard stimuli from those elicited in response to deviant stimuli. According to the time–frequency analysis, deviant stimuli elicited enhanced band power compared with standard stimuli in the delta and theta bands. Compared with previous studies, we concluded that theta activity plays an important role in the generation of the vMMN induced by changes in orientation.

Keywords: visual mismatch negativity (vMMN), wavelet analysis, event-related brain potentials (ERPs), time–frequency analysis, theta oscillation

INTRODUCTION

Object characteristics affect visual processing. In addition to color, shape and size, orientation is one important element. Furthermore, detecting orientation changes can be vital to survival, especially under unattended condition. This process can be studied using a component of event-related potential (ERP) called mismatch negativity (MMN).

MMN is a reliable indicator of change-detection processing (Näätänen et al., 2007; Fuentemilla et al., 2008). Visual MMN (vMMN) can be elicited by visual oddball tasks (20% deviant stimuli are inserted randomly in a sequence of 80% standard stimuli). Researchers found that the lateral N1b subcomponent (120–200 ms) and P2 component (200–300 ms) were related to vMMN (Czigler et al., 2006; Hietanen et al., 2008). However, the components varied for different

electrode sites and tasks (Shtyrov et al., 2013), especially in orientation oddball tasks (Takács et al., 2013). In addition, the N170 component is very common in orientation oddball tasks related to vMMN (Takács et al., 2013).

Recent studies have provided fairly convincing evidence that vMMN can be elicited by changes in many kinds of object characteristics (Stefanics et al., 2014). Czigler et al. (2002) used red-black and green-black checkerboards to elicit vMMN in 220–260 ms. Kimura et al. (2006) also found vMMN within 200 ms using different colors. Facial expression MMN could be obtained approximately 100–400 ms using neutral, happy and sad faces (Zhao and Li, 2006). In addition, Amenedo et al. (2007) investigated the vMMN that exists for motion-direction tasks. For studies of orientation, many researchers used bars as stimuli with different deviations from cardinal directions (vertical and horizontal; Astikainen et al., 2008; Kimura et al., 2009). The results showed that unattended changes in orientation could induce vMMN. Furthermore, changes from cardinal orientations could induce larger vMMN than oblique angles.
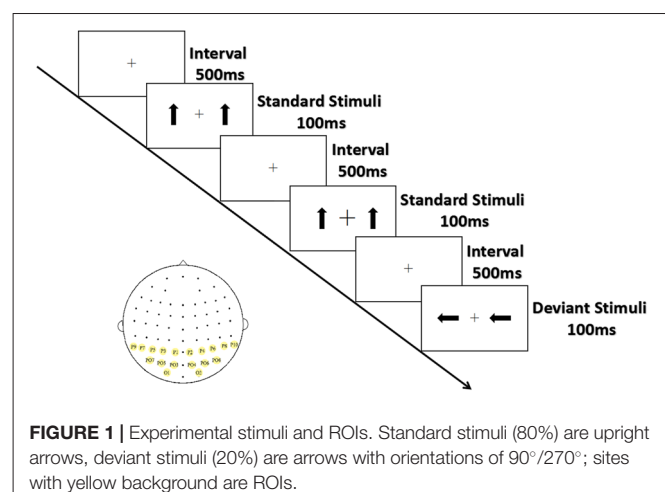
Most studies of vMMN were based on ERPs. Many studies have shown that neural oscillations are related to ERP results (Makeig et al., 2002; Fuentemilla et al., 2008). The amplitude of electrophysiological responses can be examined as a function of frequency to understand their oscillatory characteristics as a function of time. Stothart and Kazanina (2013) found that vMMN was associated with an early increase in theta power (75–175 ms post-stimulus) and that during the 450–600 ms post-stimulus interval, deviant stimuli elicited a stronger reduction in non-phase-locked alpha power than did standard stimuli, reflecting an attentional shift following the detection of change. These findings indicated that different oscillatory frequencies were involved in the vMMN. However, the specific frequency related to the vMMN induced by changes in orientation is still unknown.

To sum up, humans are capable of automatically detecting deviant stimuli. In this study, we hypothesized that changes in orientation could induce vMMN. We focused on the cardinal orientations and sought to investigate the role of neural oscillations in the vMMN response. To this end, a simple arrow symbol was used in this experiment; specifically, upright arrows (0°) served as standard stimuli, and arrows with rotations of 90°/270° served as deviant stimuli. We analyzed them based on ERP and electroencephalogram (EEG) oscillatory characteristics. Time-frequency analysis was used to explore the specific frequency related to the automatic detection of directional changes.

MATERIALS AND METHODS

Subjects

Fifteen students attending the Beijing Institute of Technology in China (six females; age range = 20–23 years old) participated in this experiment. All participants were right-handed, had normal or corrected-to-normal vision, and were free of neurological or psychiatric disorders. This study was reviewed and approved by

FIGURE 1 | Experimental stimuli and ROIs. Standard stimuli (80%) are upright arrows, deviant stimuli (20%) are arrows with orientations of 90°/270°; sites with yellow background are ROIs.

the School of Life Science Ethics Committee, Beijing Institute of Technology. Written informed consent was obtained from each participant after the nature of the study had been explained.

Stimuli and Procedure
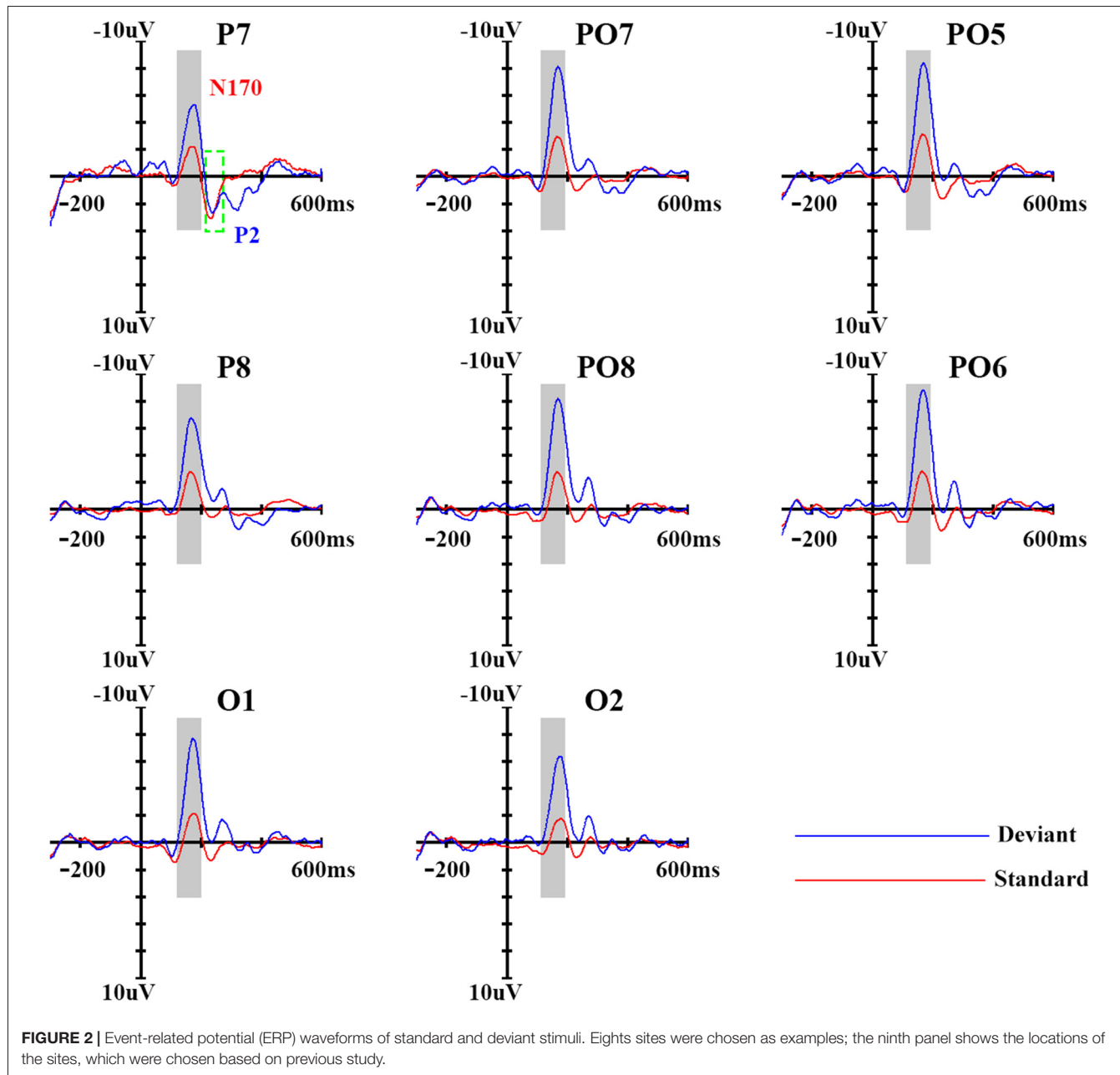
As shown in **Figure 1**, the arrows were presented from a viewing distance of 70 cm at a visual angle of 3.68° × 3.42° for 100 ms; they appeared on both sides of a cross that appeared at the center of the screen separated by an inter-stimulus interval (offset-to-onset) of 500 ms. The standards and the deviants were made symmetrical in terms of position about the target area to minimize the effect caused by the tendency to fix gaze away from the central square. Ten standard stimuli were presented at the start of the sequence, and at least two standard stimuli (0° orientation 80% probability) were presented between consecutive deviant stimuli (90° and 270° orientation, 10% probability for each). Three blocks of 300 trials (60 deviant and 240 standard stimuli) each were conducted, with the order of blocks counterbalanced across participants. The serial order of the stimuli was pseudo-random with one restriction: at least two standards had to occur between deviants.

The black cross at the center of screen, which was displayed throughout the stimulus blocks, unpredictably became bigger or smaller (mean frequency: 15/min; 22/block). To eliminate the potential effect peripheral stimuli might have on the outcome, participants were asked to respond as quickly and accurately as possible by pressing the left or the right button when the size of the cross changed. The response hands were counterbalanced across subjects.

EEG Recording

EEG data were continuously recorded (bandpass 1–100 Hz, sampling rate 1000 Hz) using as NeuroLab® Digital Amplifier[1] and an electrode cap with 64 Ag/AgCl electrodes mounted according to the extended international 10-20 system and referenced to the tip of the nose. Vertical electro-oculography

---

[1]www.brainstarbj.com

FIGURE 2 | Event-related potential (ERP) waveforms of standard and deviant stimuli. Eights sites were chosen as examples; the ninth panel shows the locations of the sites, which were chosen based on previous study.
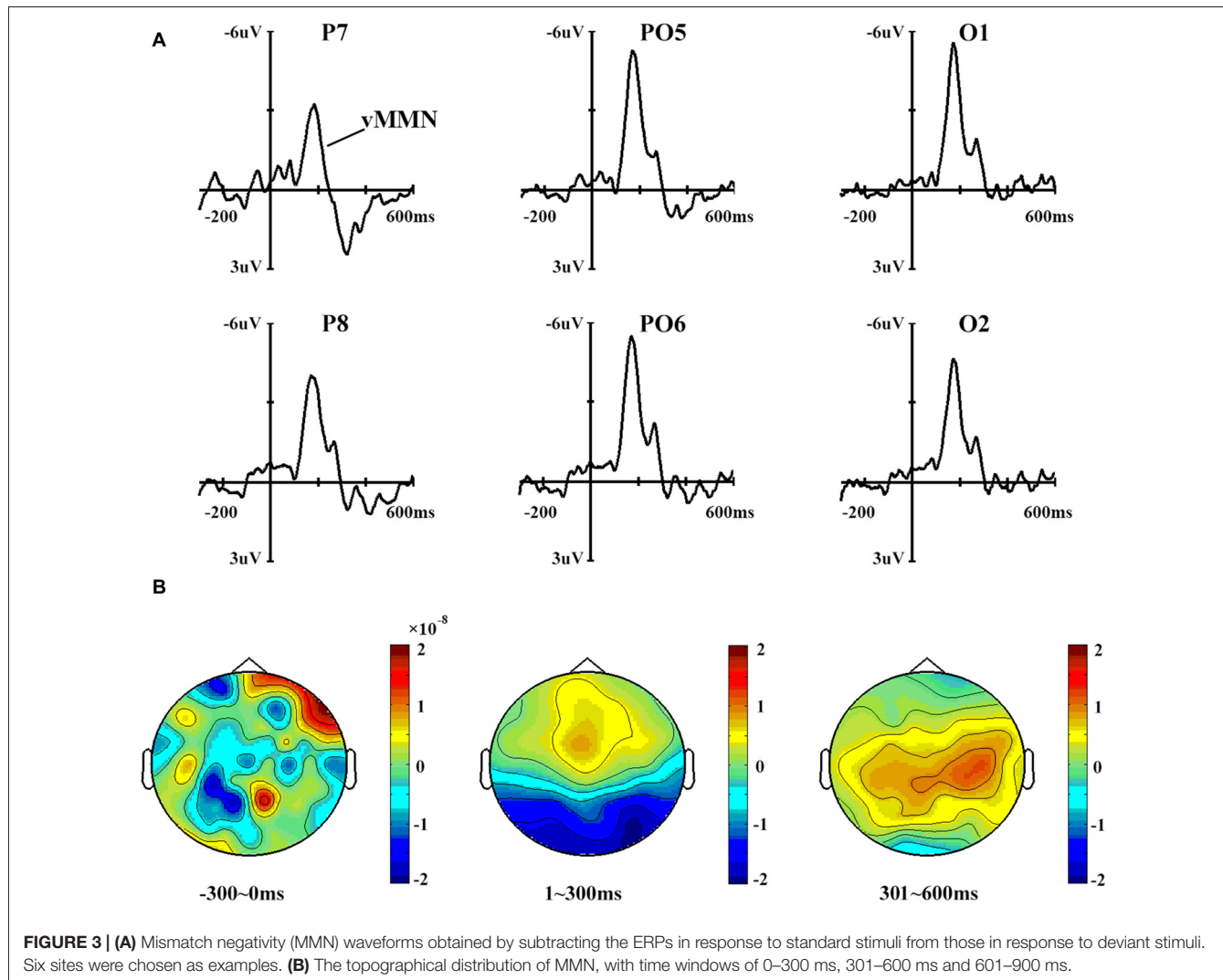
(VEOG) and horizontal electro-oculography (HEOG) were recorded with two pairs of electrodes; one pair was placed above and below the right eye, and the other was placed 10 mm from the lateral canthi. Electrode impedance was maintained below 5 kΩ throughout the experiment.

ERP Analysis

Independent component analysis using Matlab R2013a (MathWorks, Inc., Natick, MA, USA) with the open-source toolbox EEGLAB (Swartz Center for Computational Neuroscience, La Jolla, CA, USA)[2] was effectively used for

---

[2]http://sccn.ucsd.edu/eeglab/

EOG noise removal in the EEG. Traditionally, a digital low-pass filter at 30 Hz is applied to obtain a clean signal separated into 900-ms epochs, including a 300-ms pre-stimulus baseline time-locked to the subsequent onset of stimuli. Due to the bursts of EMG activity and amplifier clipping, affected trials were excluded from averaging. Additionally, trials contaminated by responses to changes in the fixation cross were also excluded. A total of 126 ± 15.8 and 565 ± 28.6 trials with deviant and standard stimuli, respectively, were included in the analysis. Based on analysis of the present N170 component (negative wave approximately 170 ms after the stimuli starts), P2 component (positive wave approximately 200 ms after the stimuli starts), and MMN distributions, the statistical

FIGURE 3 | (A) Mismatch negativity (MMN) waveforms obtained by subtracting the ERPs in response to standard stimuli from those in response to deviant stimuli. Six sites were chosen as examples. **(B)** The topographical distribution of MMN, with time windows of 0–300 ms, 301–600 ms and 601–900 ms.
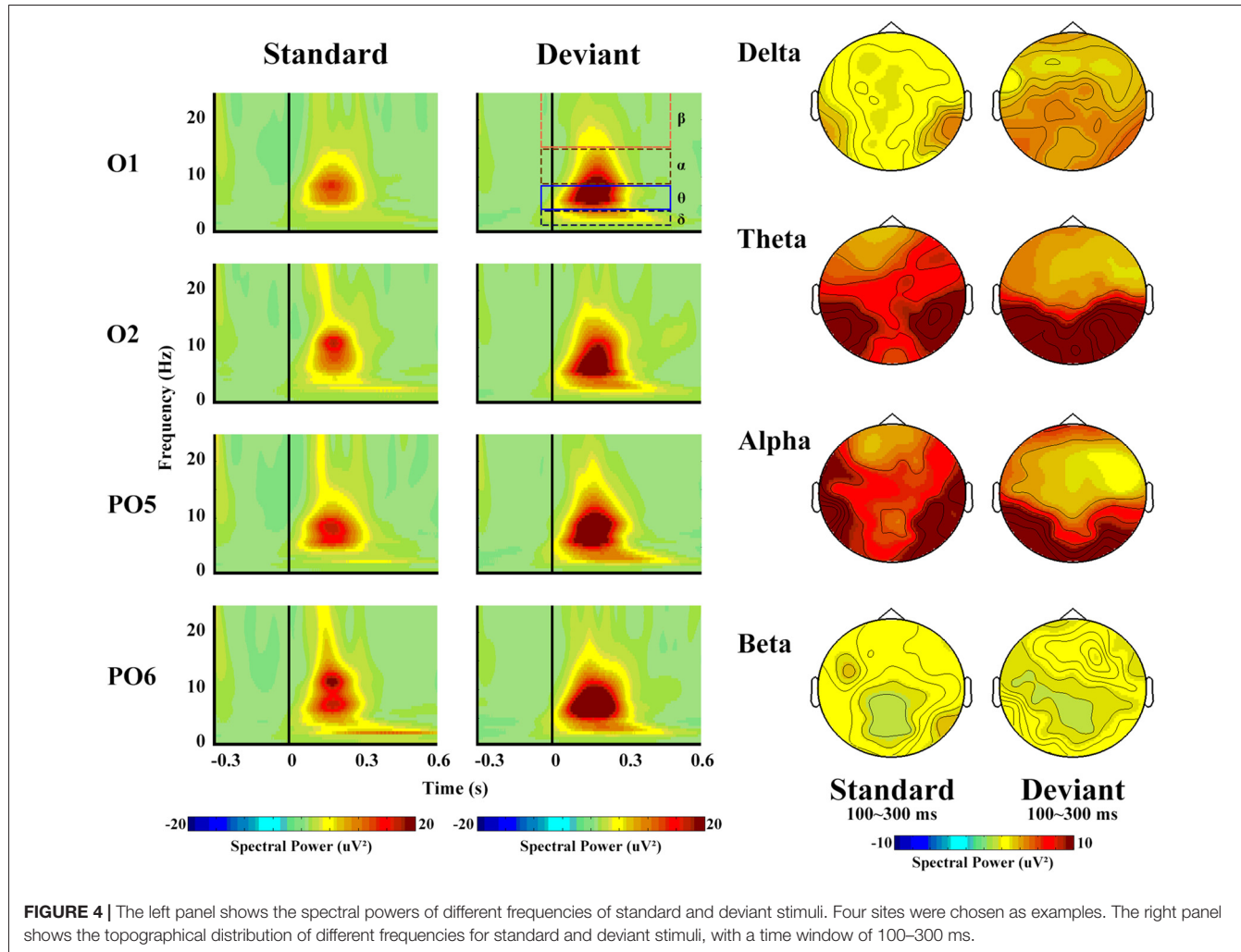
analysis was restricted to posterior regions (P4, PO4, P6, PO6, P8, PO8, P10 and O2 over the right hemisphere and the homolog sites over the left; Amenedo et al., 2007; Kimura et al., 2009). The peak amplitudes and latencies between 120 ms and 200 ms and between 200 ms and 300 ms for N170 and P2, respectively, were measured automatically. These measures were analyzed using a repeated-measures analysis of variance (ANOVA) with stimulus type (deviant, standard), hemisphere (left, right) and site (P3/4, PO3/4, P5/6, PO5/6, P7/8, PO7/8, P9/10 and O1/2) as within-subject factors.

The MMN waveforms were obtained by subtracting the ERPs in response to standard stimuli from those in response to deviant stimuli. Based on the grand average MMN waveforms (see **Figure 2**) for each subject, the peak of the MMN components was defined as the most negative peak between 100 ms and 300 ms (based on N170 and P2 component) after stimulus onset. Subsequent visual scrutiny ensured that the most negative values represented real peaks rather than end points of an epoch. The measurements of MMN amplitudes

and latencies were subjected to a repeated-measures ANOVA with hemisphere (left, right) and site (P3/4, PO3/4, P5/6, PO5/6, P7/8, PO7/8, P9/10 and O1/2) as within-subject factors. For factors with more than two levels, the degrees of freedom were corrected using the Greenhouse–Geisser procedure (for simplicity, the uncorrected degrees of freedom are presented). *Post hoc* comparisons were performed with the Bonferroni procedure.

Time–Frequency Analysis

For assessing non-stimulus phase-locked activity, we subtracted the participant's average response in the time-frequency domain from each individual trial, and then averaged the trials. Thus, we only created averages of the non-phase-locked spectral power (Stothart and Kazanina, 2013). Epochs were sorted according to stimulus condition to create a plot of time–frequency representations (TFRs). Total frequency band responses were analyzed via a Morlet wavelet using the Matlab wavelet toolbox (MathWorks). Morlet parameter c was set to 3 for low frequency analysis, and the final power was $\mu V2$. The TFRs of the delta

FIGURE 4 | The left panel shows the spectral powers of different frequencies of standard and deviant stimuli. Four sites were chosen as examples. The right panel shows the topographical distribution of different frequencies for standard and deviant stimuli, with a time window of 100–300 ms.

band power of each participant were calculated; these ranged from 1 Hz to 4 Hz in a time window between −300 ms pre- and 600 ms post-stimulus onset, whereas the theta band ranged from 4 Hz to 7 Hz, the alpha band from 8 Hz to 13 Hz and the beta band from 15 Hz to 30 Hz. Inverse Fourier transforms were subsequently performed. We calculated the synchrony among the medial, right and left electrodes and subtracted the frequency-specific baseline (−300 to 0 ms pre-stimulus). Wavelet activity was individually returned by wavelet decomposition for each trial.

Statistical Analysis

For all frequencies, a repeated-measures ANOVA with frequency band (delta, theta, alpha, beta), stimulus type (deviant, standard) and hemisphere (left, right) was used to examine the overall effects. For each EEG frequency band, the measurements were analyzed using a repeated-measures ANOVA treating stimulus type (deviant, standard), hemisphere (left, right) and site (P3/4, PO3/4, P5/6, PO5/6, P7/8, PO7/8, P9/10 and O1/2) as within-subject factors. For factors with more than two levels, the degrees of freedom were corrected using the Greenhouse–Geisser

procedure (for simplicity, the uncorrected degrees of freedom are presented). *Post hoc* comparisons were performed with the Bonferroni procedure.
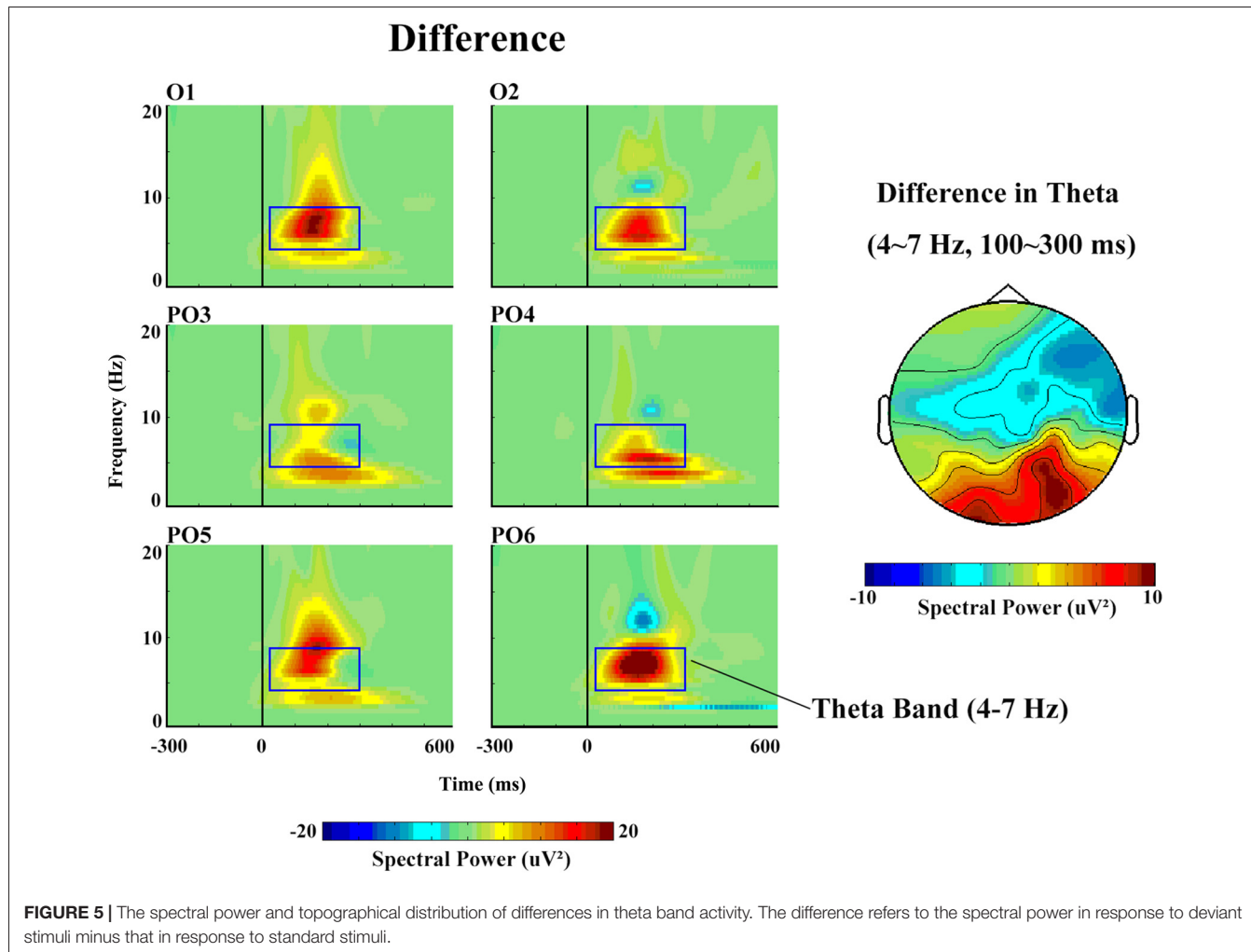
RESULTS

Behavioral Data

In this study, the degree of participant attention would influence our results. So the cross that became bigger or smaller was regarded as the target cross. Subjects were asked to respond to them. Thus the response accuracy was evaluated to determine the degree of participant attention. The results showed that accuracy was more than 93.5%, which means our ERP and EEG data were recorded under unattended condition.

ERP Data

In order to get a clear vMMN response, we used ERP analysis. As shown in **Figure 2**, the standard stimuli elicited N170 and subsequent P2 components at the posterior sites. Compared with standard stimuli, the deviant stimuli elicited larger N170 and smaller P2 components, representing a clear

FIGURE 5 | The spectral power and topographical distribution of differences in theta band activity. The difference refers to the spectral power in response to deviant stimuli minus that in response to standard stimuli.

vMMN response that had a more negative deflection from 100–300 ms.

In terms of N170 amplitudes, there was a significant main effect of stimulus type ($F_{(1,14)}$ = 50.30, $p < 0.001$, partial η = 0.81), and deviant stimuli elicited a larger N170 component ($-7.7\,\mu$V) than did standard stimuli ($-3.2\,\mu$V). The main effect of site was also significant ($F_{(3,42)}$ = 5.83, $p < 0.05$, partial η = 0.29), revealing a partial lateral distribution of N170 amplitudes. The ANOVA of N170 peak latencies showed that deviant stimuli were associated with longer N170 latencies (169 ms) compared with standard stimuli (164 ms; $F_{(1,14)}$ = 15.60, $p < 0.01$, partial η = 0.56). No other main effects or interactions were significant ($p > 0.1$).

A similar ANOVA analysis was conducted for the P2 component. We found a significant main effect of stimulus type ($F_{(1,14)}$ = 17.40, $p < 0.01$, partial η = 0.59), indicating that deviant stimuli elicited a smaller P2 component (2.0 μV) than did standard stimuli (3.80 μV). With regard to P2 peak latencies, the ANOVA revealed a significant main effect of stimulus type ($F_{(1,14)}$ = 10.77, $p < 0.05$, partial η = 0.47), indicating that deviant stimuli were associated with longer P2 latency (258 ms) compared with standard stimuli (236 ms). No other main

effects or interactions were significant for the P2 component ($p > 0.1$).

Figure 3 shows the vMMN waveforms and topographical distribution of vMMN. A one-way ANOVA showed that site had a significant effect on vMMN peak amplitudes ($F_{(3,42)}$ = 2.996, $p < 0.05$) but not on latencies ($p > 0.1$).

Time–Frequency Analysis

From the view of frequency domain, we could better know about vMMN. **Figure 4** shows the spectral activity of deviant and standard stimuli. The oscillation power occurred primarily between 100 ms and 300 ms, which is similar to the time window of the vMMN.

The spectral power revealed a clear difference in the frequency band, with maximum theta (14.49 μV2) and minimum beta (1.99 μV2, $F_{(3,42)}$ = 26.55, $p < 0.001$, partial η = 0.92). Deviant stimuli were more powerful (8.57 μV2) than standard ones (6.13 μV2, $F_{(1,14)}$ = 7.06, $p = 0.03$, partial η = 0.44), but no significant differences with regard to hemisphere or site were observed.

In terms of the delta band, only the main effect of stimulus type was significant ($F_{(1,14)}$ = 76.91, $p < 0.001$, partial η = 0.90),

as a greater increase in delta spectral power was observed in response to deviant (5.40 μV2) than to standard (3.14 μV2) stimuli.

With respect to the theta band (**Figure 5**), the ANOVA revealed a main effect of stimulus type ($F_{(1,14)}$ = 5.85, p = 0.04, partial η = 0.40), as a greater increase in theta spectral power was observed in response to deviant (17.57 μV2) than to standard (11.41 μV2) stimuli.

The same type of ANOVA analysis revealed no significant differences in the alpha and beta bands. However, the alpha band reflected a greater increase in power in response to deviant (9.46 μV2) than to standard (7.84 μV2) stimuli, whereas the beta band reflected the opposite pattern (2.14 μV2 in response to standard and 1.85 μV2 in response to deviant stimuli).

DISCUSSION

The aim of this study is to explore the vMMN related to the automatic detection of directional changes. We focused on the cardinal orientations, and the arrow symbol was used as the stimuli in this study. The EEG data were divided based on four oscillatory frequencies: delta, theta, alpha and beta. For each frequency band, the non-phase-locked spectral power was calculated independently. The results confirmed that changes in orientation under unattended condition could induce vMMN. In addition, our results further indicated that deviant stimuli could induce stronger spectral power in delta and theta bands.

In line with previous studies, deviant stimuli elicited larger N170 and smaller P2 components compared with standard stimuli. Based on the differences, we found that the participants could notice the orientation changes (0° and 90°/270°) easily. However, whether they could notice the arrow change (90°/270°) is not clear. Recently, researchers used arrow stimuli to find early attention direction negativity effects 220–260 ms after the arrow stimulus onset (Hietanen et al., 2008). Compared with our ERP results, we can infer that participants did not notice the arrow (we did not find an early attention direction negativity effect). Participants only noticed the orientation changes.

MMN is usually obtained through ERP analysis when an unexpected event occurs. It is analyzed by subtracting the ERP waveforms in response to standard stimuli from those in response to deviant stimuli. vMMN could be induced by changes in many kinds of object characteristics. Our study agrees with previous studies that showed that changes in orientation can induce vMMN (Kimura et al., 2009; Stefanics et al., 2014).

The time–frequency analysis showed that deviant stimuli elicited enhanced band power compared with standard stimuli; this was the case for the delta and theta bands, which may be attributable to the lower probability and novelty of deviant stimuli and which may have been influenced by principles of perception (Parmentier et al., 2011a,b). Replicating one recent report on auditory MMN (aMMN) response (Stothart and Kazanina, 2013), we also found that deviant stimuli induced an increase in theta power before 25–300 ms post-stimulus onset. These data indicate that theta activity appears to play a role in the generation of the vMMN response (Stothart and Kazanina, 2013). Thus, both aMMN and vMMN are related to theta bands.

We can infer that MMN is more associated with theta response. The present study found the greatest theta activity (i.e., enhanced theta oscillation) in response to deviant vs. standard stimuli, indicating that theta activity may play an important role in cognitive processes involving automatic change detection.

Although we also observed increased delta power in response to deviant vs. standard stimuli, we did not consider it correlated with MMN because delta oscillations constitute one of the major operating rhythms of the P300 component (Başar et al., 2001), which has historically been viewed as an important ERP component elicited by infrequent target stimuli in the auditory oddball paradigm (Öniz and Başar, 2009). However, this component was less evident in vMMN, and the P300 may be the main difference between aMMN and vMMN, but this possibility requires further investigation. Additionally, delta oscillations contribute to making a decision and detecting a signal (Başar et al., 2001). Therefore, delta response did not correlate with MMN. In some studies of MMN, researchers found changed post-auditory stimulus alpha/beta power using an oddball paradigm (Hsiao et al., 2009; Öniz and Başar, 2009; Stothart and Kazanina, 2013; Başar et al., 2015). However, in this study, we did not find a correlation between vMMN and alpha/beta bands. This difference may be caused by the different tasks.

In summary, to investigate the EEG oscillatory characteristics of vMMN, we analyzed ERP and EEG data elicited by standard (0° arrows) and deviant (90°/270° arrows) stimuli. Compared with standard stimuli, deviant stimuli elicited larger negative N170 and smaller P2. In addition, changes in orientation could induce vMMN as expected. According to the time–frequency analysis, deviant stimuli elicited enhanced band power compared with standard stimuli in delta and theta bands. Furthermore, theta activity played an important role in the generation of the vMMN induced by changes in orientation. Examination of both ERPs and EEG oscillation provides a more complete picture of the event-related changes in vMMN responses.

However, the present study has some limitations. For instance, the sample was small, although the present method of statistical analysis is reliable. It is necessary to further investigate the present results in a clinical evaluation of cognitive function using a larger sample size.

AUTHOR CONTRIBUTIONS

TY and LZ designed experiments; ZL, XT and TQ carried out experiments; NM and YF analyzed experimental results. TY, TL, LW and XD wrote the manuscript.

ACKNOWLEDGMENTS

REFERENCES

Amenedo, E., Pazo-Alvarez, P., and Cadaveira, F. (2007). Vertical asymmetries in pre-attentive detection of changes in motion direction. *Int. J. Psychophysiol.* 64, 184–189. doi: 10.1016/j.ijpsycho.2007.02.001

Astikainen, P., Lillstrang, E., and Ruusuvirta, T. (2008). Visual mismatch negativity for changes in orientation—a sensory memory-dependent response. *Eur. J. Neurosci.* 28, 2319–2324. doi: 10.1111/j.1460-9568. 2008.06510.x

Başar, E., Başar-Eroglu, C., Karakaş, S., and Schürmann, M. (2001). Gamma, alpha, delta, and theta oscillations govern cognitive processes. *Int. J. Psychophysiol.* 39, 241–248. doi: 10.1016/s0167-8760(00) 00145-8

Başar, E., Tülay, E., and Güntekin, B. (2015). Multiple gamma oscillations in the brain: a new strategy to differentiate functional correlates and p300 dynamics. *Int. J. Psychophysiol.* 95, 406–420. doi: 10.1016/j.ijpsycho. 2015.01.013

Czigler, I., Balázs, L., and Winkler, I. (2002). Memory-based detection of task-irrelevant visual changes. *Psychophysiology* 39, 869–873. doi: 10.1111/1469-8986.3960869

Czigler, I., Weisz, J., and Winkler, I. (2006). ERPs and deviance detection: visual mismatch negativity to repeated visual stimuli. *Neurosci. Lett.* 401, 178–182. doi: 10.1016/j.neulet.2006.03.018

Fuentemilla, L., Marco-Pallarés, J., Munte, T. F., and Grau, C. (2008). Theta EEG oscillatory activity and auditory change detection. *Brain Res.* 1220, 93–101. doi: 10.1016/j.brainres.2007.07.079

Hietanen, J. K., Leppänen, J. M., Nummenmaa, L., and Astikainen, P. (2008). Visuospatial attention shifts by gaze and arrow cues: an ERP study. *Brain Res.* 1215, 123–136. doi: 10.1016/j.brainres.2008. 03.091

Hsiao, F.-J., Wu, Z.-A., Ho, L.-T., and Lin, Y.-Y. (2009). Theta oscillation during auditory change detection: an MEG study. *Biol. Psychol.* 81, 58–66. doi: 10.1016/j.biopsycho.2009.01.007

Kimura, M., Katayama, J., and Murohashi, H. (2006). Probability-independent and -dependent ERPs reflecting visual change detection. *Psychophysiology* 43, 180–189. doi: 10.1111/j.1469-8986.2006.00388.x

Kimura, M., Katayama, J., Ohira, H., and Schroger, E. (2009). Visual mismatch negativity: new evidence from the equiprobable paradigm. *Psychophysiology* 46, 402–409. doi: 10.1111/j.1469-8986.2008.00767.x

Makeig, S., Westerfield, M., Jung, P., Enghoff, S., Townsend, J., Courchesne, E., et al. (2002). Dynamic brain sources of visual evoked responses. *Science* 295, 690–694. doi: 10.1126/science.1066168

Näätänen, R., Paavilainen, P., Rinne, T., and Alho, K. (2007). The mismatch negativity (MMN) in basic research of central auditory processing: a review. *Clin. Neurophysiol.* 118, 2544–2590. doi: 10.1016/j.clinph.2007. 04.026

Öniz, A., and Başar, E. (2009). Prolongation of alpha oscillations in auditory oddball paradigm. *Int. J. Psychophysiol.* 71, 235–241. doi: 10.1016/j.ijpsycho. 2008.10.003

Parmentier, F. B. R., Elsley, J. V., Andrés, P., and Barceló, F. (2011a). Why are auditory novels distracting? Contrasting the roles of novelty, violation of expectation and stimulus change. *Cognition* 119, 374–380. doi: 10.1016/j. cognition.2011.02.001

Parmentier, F. B. R., Turner, J., and Elsley, J. V. (2011b). Distraction by auditory novelty. The course and aftermath of novelty and semantic effects. *Exp. Psychol.* 58, 92–101. doi: 10.1027/1618-3169/a000072

Shtyrov, Y., Goryainova, G., Tugin, S., and Shestakova, A. (2013). Automatic processing of unattended lexical information in visual oddball presentation: neurophysiological evidence. *Front. Hum. Neurosci.* 7:421. doi: 10.3389/fnhum. 2013.00421

Stefanics, G., Kremláček, J., and Czigler, I. (2014). Visual mismatch negativity: a predictive coding view. *Front. Hum. Neurosci.* 8:666. doi: 10.3389/fnhum.2014. 00666

Stothart, G., and Kazanina, N. (2013). Oscillatory characteristics of the visual mismatch negativity: what evoked potentials aren't telling us. *Front. Hum. Neurosci.* 7:426. doi: 10.3389/fnhum.2013.00426

Takács, E., Sulykos, I., Czigler, I., Barkaszi, I., and Balázs, L. (2013). Oblique effect in visual mismatch negativity. *Front. Hum. Neurosci.* 7:591. doi: 10.3389/fnhum.2013.00591

Zhao, L., and Li, J. (2006). Visual mismatch negativity elicited by facial expressions under non-attentional condition. *Neurosci. Lett.* 410, 126–131. doi: 10.1016/j. neulet.2006.09.081

Cooperation and Competition with Hyperscanning Methods: Review and Future Application to Emotion Domain

Michela Balconi[1,2] and Maria E. Vanutelli[1,2,3*]

[1] Research Unit in Affective and Social Neuroscience, Catholic University of Milan, Milan, Italy, [2] Department of Psychology, Catholic University of Milan, Milan, Italy, [3] Department of Philosophy, Università degli Studi di Milano, Milan, Italy

Cooperation and competition, as two common and opposite examples of interpersonal dynamics, are thought to be reflected by different cognitive, neural, and behavioral patterns. According to the conventional approach, they have been explored by measuring subjects' reactions during individual performance or turn-based interactions in artificial settings, that don't allow on-line, ecological enactment of real-life social exchange. Considering the importance of these factors, and accounting for the complexity of such phenomena, the hyperscanning approach emerged as a multi-subject paradigm since it allows the simultaneous recording of the brain activity from multiple participants interacting. In this view, the present paper aimed at reviewing the most significant work about cooperation and competition by EEG hyperscanning technique, which proved to be a promising tool in capturing the sudden course of social interactions. In detail, the review will consider and group different experimental tasks that have been developed so far: (1) paradigms that used rhythm, music and motor synchronization; (2) card tasks taken from the Game Theory; (3) computerized tasks; and (4) possible real-life applications. Finally, although highlighting the potential contribution of such approach, some important limitations about these paradigms will be elucidated, with a specific focus on the emotional domain.

Keywords: EEG, emotions, hyperscanning, cooperation, competition, social interaction, synchronization

HYPERSCANNING AS A TOOL TO ASSESS SOCIAL DYNAMICS

Cooperation and competition are two common and opposite models of interpersonal exchange (Decety et al., 2004). In fact, according to the interaction type, individuals could facilitate, but also obstruct, others' goal achievement. Nonetheless, the two modalities share some important features. First, from an evolutionary point of view, they are both recognized as human behavioral patterns devoted to survival, although in different ways. Second, they both require some cognitive capacities such as monitoring and mentalizing abilities, to attribute independent mental states, such as thoughts, beliefs, and desires, to others (Flavell, 1999). This allows anticipating and predicting others' intentions and adjusting one's own action accordingly (Decety and Sommerville, 2003). For these reasons, many previous studies focused on these two models as a good example of social and emotional sharing. For example, Decety et al. (2004) asked subjects to participate in couples to a computer game in a functional Magnetic Resonance Imaging (fMRI) scan and compared

their neural responses during cooperation and competition. Results highlighted the presence of common networks related to executive functions, as well as a more specific recruitment of different brain areas according to the different mental framework engaged. Also, Liu et al. (2015), by using functional near infrared spectroscopy (fNIRS), found a differential activation of the right inferior frontal gyrus during cooperation and competition in a turn-taking game. Moreover, Cui et al. (2015) explored the role of these two context in modulating empathy for pain by using event-related potentials (ERP). Finally, Balconi and Pagani (2014, 2015) experimentally manipulated the perceived efficacy during a competitive task to investigate social hierarchies and ranking. However, it has been suggested that the study of social cognition could be reductive and partial by using single-subject or turn-taking paradigm (Schilbach, 2010).

Recent scientific evidence studied these forms of synchronous interactions by considering brain-to-brain coupling. In fact, it has been shown that observing the actions, emotions or feelings of other people can trigger corresponding cortical representations (Hasson et al., 2012), a mechanism defined as vicarious activation (Keysers and Gazzola, 2009). It appears clear that similar processes cannot be captured by conventional experimental approach on individual brains. In the attempt to move a step forward, the hyperscanning paradigm emerged in contrast to previous research approach to allow the simultaneous recording of the neural activation from two, but also multiple, participants interacting jointly (Montague, 2002). This technique permitted to discover typical patterns of inter-brain synchronization during social and emotional exchange thus providing data that can't be obtained by recording single brain activities alone (Babiloni and Astolfi, 2012).

Previous work conducted with imaging techniques such as fMRI allowed identifying the brain areas that are involved during emotional sharing. Nonetheless, fMRI can provide only partial support to this ambitious aim in that it lacks temporal resolution. Also, it is unable to provide a real-time ecological environment in that participants have to lie motionless in a noisy and often emotionally daunting scanner while the verbal communication is discouraged (Cui et al., 2012). Conversely, EEG hyperscanning studies provide higher temporal resolution that permits capturing real-time events. Prior findings showed inter-brain phase coherence across different frequencies, including delta, theta, alpha, beta, and gamma, that can be attributed to a series of different processes, from perception, to cognition, and especially emotion (Balconi et al., 2015). Among the most used techniques are correlation or coherence-based analyses (King-Casas et al., 2005; Funane et al., 2011; Cui et al., 2012), which move from the assumption that the modifications in the activity of certain cerebral regions in subjects can share the same generator/generative source.

Thus, the aim of the present review is to collect and describe existing research on cooperative/competitive dynamics conducted with a hyperscanning approach as a promising paradigm for social neuroscience. Previous reviews already explored the potentiality of such paradigm to social interactions (Dumas et al., 2011; Liu and Pelowski, 2014; Koike et al., 2015), but none of them explicitly focused on these two opposite

scenarios, which could provide some precious findings for everyday social life, from work environment, to prosocial behaviors, from collective performance, to affiliation and dyadic bonds. EEG will be valued as a promising technique to capture the sudden and unpredictable modification related to social interactions.

In the next section, the most important evidence in the field will be reviewed and grouped according to the different materials and experimental tasks.

EEG HYPERSCANNING TECHNIQUE: THE CASE OF COOPERATION AND COMPETITION

The selection criteria included: use of EEG technique; use of hyperscanning paradigm with real-time interactions; explicit use of cooperative and/or competitive paradigms. According to the different materials and experimental paradigms used to reproduce the social dynamics, available evidence has been grouped in four different categories: paradigms that used rhythm, music, and motor synchronization (section Rhythm, Music, and Motor Synchronization); paradigms based on card tasks taken from the Game Theory (section Evidence from the Game Theory); paradigms based on computerized tasks (section Computer-Based Paradigms); and possible real-life applications (section Real-Life Applications).

Rhythm, Music, and Motor Synchronization

Some previous studies used rhythmic synchronization to assess the capacity to cooperate each other. Lindenberger et al. (2009) found that, when playing a short melody together, dyads of guitarists showed increased phase synchronized theta and delta oscillations. The authors suggested that coordinated behaviors are characterized by inter-brain oscillatory coherence. Also, since the reported rhythms were all in lower frequency range, it is possible that the similarities in sensorimotor feedback could have enhanced between-brain synchronization.

To disambiguate this issue the same team (Sänger et al., 2012) later used a similar but advanced paradigm with a more complex piece of music such that the two members of the couple would have different roles, a leader, and a follower. The paradigm reduced similarities in movement, proprioception, and perception. Results extended previous data and attributed between-brain phase coherence to musical coordination periods. Also, since the effects were larger at frontal and central sites, it was proposed that the on-line representation of one's own and others' actions and their combination into a joint, coupled model, may help supporting interpersonal action coordination (IAC).

A recent finger-tapping experiment replicated this asymmetrical pattern in leader-follower dynamics (Konvalinka et al., 2014): it was demonstrated that it is possible to differentiate roles on the basis of the modulation of frontal alpha-suppression, being this latter prominent in leaders than followers. It has been hypothesized that leaders probably allocated more resources to self-processing to monitor their own rhythm, while followers should monitor the output of their partner.

Analogously, another study by Yun et al. (2012) used a leader-follower task to demonstrate the presence of implicit motor synchronization when interacting with another human. Seated face to face, a leader had to perform hand movements and another player had to imitate them at their best. Finally, both participants were asked to freeze. The behavioral results highlighted that the two mates implicitly synchronized their movements, mainly during the final phase that followed imitation. EEG results showed higher phase synchronization following the imitation phase within theta and beta frequency bands over the inferior frontal gyrus, anterior cingulate, parahippocampal gyrus, and post-central gyrus. Such results were considered as an improved coupling between the two cognitive representations.

Similarly, Dumas et al. (2010) used a video feedback system and asked subjects to imitate the other's hands movement. The researchers found higher inter-brain phase synchronization within mu, beta, and gamma range in the right centro-parietal areas of the two brains during behavioral synchrony.

Finally, a work by Kawasaki et al. (2013) explored the presence of inter-brain correlation during speech rhythm synchronization. Results showed that speech rhythms were more easily synchronized in the joint condition with respect to the individual condition where subjects performed the same task within a computerized session. Moreover, increased synchronized theta/alpha amplitudes were found in the same temporal and lateral-parietal regions known to be associated with social cognition, such as comprehending others' intentions, affects, and actions (Adolphs, 1999) (**Figure 1**).

The mentioned studies are relevant to neuropsychophysiology since they show how neural synchronization can emerge and be studied with simple matched behaviors involving motor and rhythmic coordination. Moreover, it has been shown that EEG technique can recognize the different roles assumed within the couple. In fact, the cognitive and behavioral states related to the joint task can modulate rhythm synchronization.

Evidence from the Game Theory

A series of studies conducted by Astolfi et al. (2009, 2010, 2011b,c) used the Prisoner's Dilemma paradigm: a cooperation/competition task that requires to decide whether to cooperate or defect. The game requires two players (or

groups) and two alternative choices: cooperate or defect. When both players decide to cooperate, they both gain small wins (cooperation condition). If only one player cooperates and the other retracts, the cooperator obtains a big loss and the defector a big win. If both players betray, they have small losses (defeat condition). The aim of the game is to gain the highest score. Through this sharp paradigm the research group obtained some important results: first, the defeat conditions elicited the higher cortical activity in the theta and alpha frequency band. This choice, in fact, can be related to major penalty and risky conditions when compared to cooperation. Also, this effect was mostly present over the frontal regions, in accordance with the decisional request (Astolfi et al., 2009, 2010).

A successive study with the same paradigm (Astolfi et al., 2011c) integrated such data with functional connectivity analyses and found that the pattern of inter-brain connectivity in the cooperation condition is denser than in the defect one. In fact, as an individualist act, the defect choice could produce a lower synchronization between brains. On the other hand, a cooperative act could elicit weaker brain activity, but a denser synchronization between the two brains.
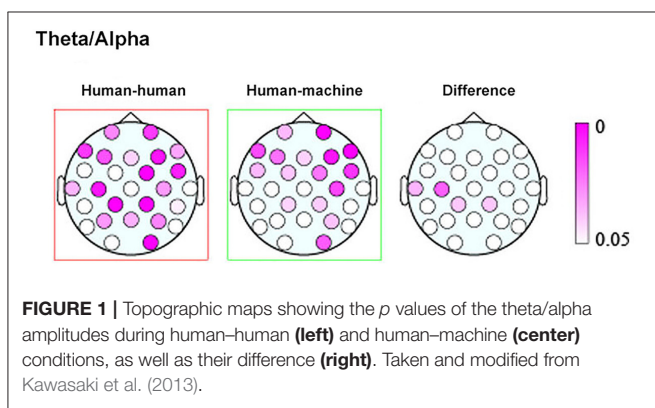
Research coming from the Game Theory tradition is relevant in that provides a standardized tool to directly compare cooperation and competition, but also different studies each other. Thus, it was possible to differentiate the two conditions, associating cooperation with increased neural connectivity between the two brains resonating each other.

Computer-Based Paradigms

A series of hyperscanning studies used computer-based paradigm to assess cooperation and competition in experimental settings. For example, Astolfi et al. (2014) asked participants to lift a rolling ball up to a particular target region placed at the top of the screen with a virtual bar. There was a joint condition, where both subjects played together on the same task, a solo condition, where both subjects were asked to complete the task individually, and a PC condition which was identical to the joint one, but subjects were told that they were playing against a computer. The comparison between joint and PC, as well as between joint and solo condition, revealed significant differences in terms of inter-brain functional causal relations.

In another study by Sinha et al. (2016) the authors investigated the effect of cooperative and competitive interactions with a game similar to table tennis. The aim is to defeat the competitor by striking a ball back and forth using a vertical bar (competition condition) or to act as a team to defeat a computer program (cooperative condition). Results showed that the cooperative condition was characterized by significantly higher synchronization as compared to competition.

Another computer-based task was proposed by Balconi and Vanutelli (2016) within a competitive scenario where participants coupled in dyads had to perform better than their opponent in a sustained-attention task. During the game they were continuously informed about their performance and, halfway through the task, they received a general feedback reinforcing the results obtained so far and the instruction for the second part of the game. The analyses showed a systematic response within

FIGURE 1 | Topographic maps showing the *p* values of the theta/alpha amplitudes during human–human **(left)** and human–machine **(center)** conditions, as well as their difference **(right)**. Taken and modified from Kawasaki et al. (2013).

the prefrontal regions (PFC) during competition. This effect was mainly present after receiving a positive feedback assessing a good performance and a winning situation. Also, considering the enhanced PFC responsiveness, a specific lateralized pattern was found in favor of the left hemisphere, compatible with positive emotions, and approach-related motivations. Accordingly, winners' behavioral performance was improved in terms of reduced reaction times (RTs).

With respect to card games, computer-based hyperscanning studies offer more controlled, even if less ecological, paradigms to study cooperation and competition. Also, they allow varying the experimental conditions according to specific research aims. In particular, it is possible to manipulate the cognitive scenarios to induce different and correspondent neural synchronization as in the last example (Balconi and Vanutelli, 2016) where the affective state could modulate both neural activation and performance.

Real-Life Applications

Finally, some promising real-life applications through hyperscanning methods are reviewed: a first contribution refers to flight simulations in couples of pilots and co-pilots (Astolfi et al., 2011a, 2012; Toppi et al., 2016). Results showed increased coherence in the alpha band over the parietal sites during the most demanding phases of the simulation, which can be attributed to higher cognitive load, as well as in the theta band over the frontal sites, which is compatible with increased resources engaged for information processing (Klimesch, 1999). Hyperconnectivity patterns linking frontal and parietal areas of the two participants emerged during the phases involving a close interaction between the two pilots, that is takeoff and landing. In particular, the strongest connections were located over the
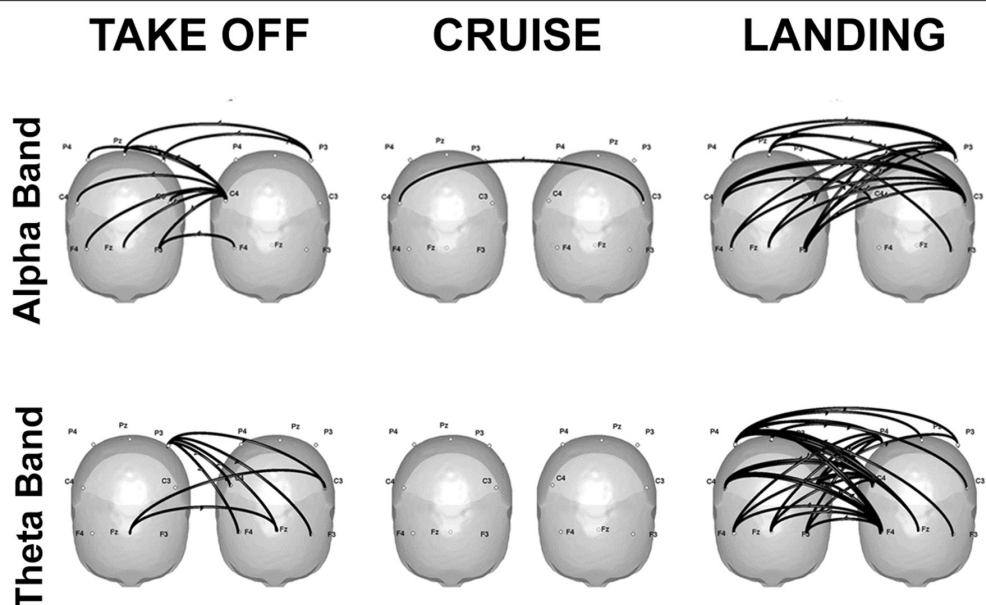
frontal sites, and were directed from the co-pilot toward the pilot (**Figure 2**).

Finally, an innovative application was proposed by Balconi et al. (Venturella et al., 2017) within a neuromanagement approach: the authors proposed a pilot study on the brain dynamics occurring during a role-played employees' evaluation in couples of manager-collaborator. Preliminary results showed greater delta and theta response to positive and constructive inter-subjective exchange, as well as to the conversational moments while sharing the company mission and aims.

Such examples are particularly relevant in that they can be used to get neuroscience closer to real-life situations and to improve specific work environment where the performance depends on good cooperative/competitive dynamics. In fact, it has been demonstrated that specific phases or topics during dyadic work simulation can be identified by specific neural markers which can be indicative of higher or lower cognitive demand, emotional involvement and interactive skills.

Methodological and Statistical Caveats

However, how were these results obtained? Being a very complex and innovative paradigm, a few methodological and statistical considerations about hyperscanning should be discussed. First, hyperscanning conventionally means both the experimental paradigm including the simultaneous registration of multiple brain activities, and/or the specific connectivity analyses performed on resulting multiple data. In this second case, the most used techniques are based on correlation or coherence analyses (King-Casas et al., 2005; Funane et al., 2011; Cui et al., 2012). Since the computation is made on time series, the paradigm should include a high number of frames for each experimental condition. This issue can be solved

FIGURE 2 | Significant connectivity elicited in the alpha **(top)** and theta **(bottom)** frequencies during takeoff **(left)**, cruise **(center)**, and landing **(right)** of one exemplificative couple composed by the first officer **(left)** and the captain **(right)**. Taken and modified from Toppi et al. (2016).

by (a) using EEG or other techniques which can provide a high sampling rate: the higher, the better; (b) reducing the experimental factors. For example, the number of brain regions could be simplified by creating regions of interests (ROI), or performing specific computations such as principal component analysis (PCA). Finally, since couples are the cases for statistics instead of single subjects, the number of participants should be improved. Anyway, to solve these criticalities, before performing the experiment a power analysis would be recommended.

EMOTIONS IN HYPESCANNING STUDIES: THE BIG ABSENTEE

As already discussed in previous sections, EEG-based hyperscanning technique provides a valid and innovative tool for exploring coupled responses and obtaining real-time results in highly-ecological paradigms. Nonetheless, it seems that most experimental paradigms did not explicitly taken into account the affective component (Acquadro et al., 2016) in terms of emotional contagion, sharing, and social exchange. Moreover, the pioneeristic nature of these studies often led to adopt an explorative approach and, accordingly, to vague and sparse findings.

However, previous research on both animals and humans has suggested that the psychophysiological connection between two individuals is an intrinsic element of affective bonding (Coan et al., 2006; McAssey et al., 2013). In fact, when we interact with someone else, our brains and bodies can no longer be considered independent, but must be viewed as part of a new environment with the other person, in which we become coupled through a continuous and mutual adaptation (Konvalinka and Roepstorff, 2012). Besides neural synchronization, such dynamic and interactive process has been also shown to result in an alignment of behavior (Konvalinka et al., 2010), posture (Shockley et al., 2003), autonomic systems such as respiration

(McFarland, 2000; Giuliano et al., 2015) and cardiac rhythms (Konvalinka et al., 2011; Müller and Lindenberger, 2011).

For these reasons, it should be important that hyperscanning paradigms would also consider the affective components related to cooperative and competitive scenarios, and, possibly, to combine other autonomic or behavioral measures (Niedenthal, 2007; Keysers et al., 2010).

From a clinical point of view such results are particularly relevant. In fact, such inter-personal couplings generate social bonds that could facilitate or obstruct future successful exchange. For example, higher synchronization in heart rate variability is associated with the length of romantic relationship (Anderson et al., 2003). On the contrary, few developmental studies found that mother–child synchrony decreases in particular conditions (Feldman, 2007).

Thus, the adoption of clear theoretical approach and specific research questions about the role of emotions in modifying neural and bodily synchronization would help designing hyperscanning protocols with different emotional conditions or clinical groups to be compared. Accordingly, the methods could be refined by including some subjective factors such as the motivation in participating to the task, the effective involvement in the role or the experimental condition, but also all those psychological variables which could differentiate subjects or couples by their personality, affective style, dominance, and so on. To conclude, the need for experimental situations leading to emotional engagement is still urgent in a way to enhance the understanding of emotions within social interactions, and improve the ecological validity of cooperative and competitive settings.

AUTHOR CONTRIBUTIONS

MB and MV critically discussed the literature and wrote the paper.

REFERENCES

Acquadro, M. A. S., Congedo, M., and De Riddeer, D. (2016). Music performance as an experimental approach to hyperscanning *Studies* 10, 1–13. doi: 10.3389/fnhum.2016.00242

Adolphs, R. (1999). Social cognition and the human brain. *Trends Cogn. Sci.* 3, 469–479. doi: 10.1016/S1364-6613(99)01399-6

Anderson, C., Keltner, D., and John, O. P. (2003). Emotional convergence between people over time. *J. Pers. Soc. Psychol.* 84, 1054–1068. doi: 10.1037/0022-3514.84.5.1054

Astolfi, L., Cincotti, F., Mattia, D., Fallani, F. D. V., Salinari, S., Marciani, M. G., et al. (2009). "Estimation of the cortical activity from simultaneous multi-subject recordings during the prisoner's dilemma," in *Engineering in Medicine and Biology Society, 2009. EMBC 2009. Annual International Conference of the IEEE* (Minneapolis, MN), 1937–1939.

Astolfi, L., Cincotti, F., Mattia, D., Fallani, F. D. V., Salinari, S., Vecchiato, G., et al. (2010). "Simultaneous estimation of cortical activity during social interactions by using EEG hyperscannings," in *Engineering in Medicine and Biology Society (EMBC), 2010 Annual International Conference of the IEEE* (Buenos Aires), 2814–2817.

Astolfi, L., Toppi, J., Borghini, G., Vecchiato, G., He, E. J., Roy, A., et al. (2012). Cortical activity and functional hyperconnectivity by simultaneous EEG

recordings from interacting couples of professional pilots. *Conf. Proc. IEEE Eng. Med. Biol. Soc.* 2012, 4752–4755. doi: 10.1109/EMBC.2012.6347029

Astolfi, L., Toppi, J., Borghini, G., Vecchiato, G., Isabella, R., Fallani, F. D. V., et al. (2011a). Study of the functional hyperconnectivity between couples of pilots during flight simulation: an EEG hyperscanning study. *Conf. Proc. IEEE Eng. Med. Biol. Soc.* 2011, 2338–2341. doi: 10.1109/IEMBS.2011.6090654

Astolfi, L., Toppi, J., Cincotti, F., Mattia, D., Salinari, S., Fallani, F. D. V., et al. (2011b). "Methods for the EEG hyperscanning," in *Simultaneous Recordings from Multiple Subjects during Social Interaction* (Piscataway, NJ), 8–11.

Astolfi, L., Toppi, J., De Vico Fallani, F., Vecchiato, G., Cincotti, F., Wilke, C. T., et al. (2011c). Imaging the social brain by simultaneous hyperscanning during subject interaction. *IEEE Intell. Syst.* 26, 38–45. doi: 10.1109/MIS.2011.61

Astolfi, L., Toppi, J., Vogel, P., Mattia, D., Babiloni, F., Ciaramidaro, A., et al. (2014). "Investigating the neural basis of cooperative joint action. An EEG hyperscanning study," in *Engineering in Medicine and Biology Society (EMBC), 2014 36th Annual International Conference of the IEEE* (Chicago, IL: IEEE), 4896–4899.

Babiloni, F., and Astolfi, L. (2012). Social neuroscience and hyperscanning techniques: past, present and future. *Neurosci. Biobehav. Rev.* 44, 76–93. doi: 10.1016/j.neubiorev.2012.07.006

Balconi, M., and Pagani, S. (2014). Personality correlates (BAS-BIS), self-perception of social ranking, and cortical (alpha frequency band)

modulation in peer-group comparison. *Physiol. Behav.* 133C, 207–215. doi: 10.1016/j.physbeh.2014.05.043

Balconi, M., and Pagani, S. (2015). Social hierarchies and emotions: cortical prefrontal activity, facial feedback (EMG), and cognitive performance in a dynamic interaction. *Soc. Neurosci.* 10, 166–178. doi: 10.1080/17470919.2014.977403

Balconi, M., and Vanutelli, M. E. (2016). Competition in the brain. The contribution of EEG and fNIRS modulation and personality effects in social ranking. *Front. Psychol.* 7:1587. doi: 10.3389/fpsyg.2016.01587

Balconi, M., Grippa, E., and Vanutelli, M. E. (2015). What hemodynamic (fNIRS), electrophysiological (EEG) and autonomic integrated measures can tell us about emotional processing. *Brain Cogn.* 95, 67–76. doi: 10.1016/j.bandc.2015.02.001

Coan, J. A., Schaefer, H. S., and Davidson, R. J. (2006). Lending a hand: social regulation of the neural response to threat. *Psychol. Sci.* 17, 1032–1039. doi: 10.1111/j.1467-9280.2006.01832.x

Cui, F., Zhu, X., Duan, F., and Luo, Y. (2015). Instructions of cooperation and competition influence the neural responses to others' pain: an ERP study. *Soc. Neurosci.* 11, 289–296. doi: 10.1080/17470919.2015.1078258

Cui, X., Bryant, D. M., and Reiss, A. L. (2012). NIRS-based hyperscanning reveals increased interpersonal coherence in superior frontal cortex during cooperation. *Neuroimage* 59, 2430–2437. doi: 10.1016/j.neuroimage.2011.09.003

Decety, J., and Sommerville, J. A. (2003). Shared representations between self and other: a social cognitive neuroscience view. *Trends Cogn. Sci.* 7, 527–533. doi: 10.1016/j.tics.2003.10.004

Decety, J., Jackson, P. L., Sommerville, J. A., Chaminade, T., and Meltzoff, A. N. (2004). The neural bases of cooperation and competition: an fMRI investigation. *Neuroimage* 23, 744–751. doi: 10.1016/j.neuroimage.2004.05.025

Dumas, G., Lachat, F., Martinerie, J., Nadel, J., and George, N. (2011). From social behaviour to brain synchronization: review and perspectives in hyperscanning. *IRBM* 32, 48–53. doi: 10.1016/j.irbm.2011.01.002

Dumas, G., Nadel, J., Soussignan, R., Martinerie, J., and Garnero, L. (2010). Inter-brain synchronization during social interaction. *PLoS ONE* 5:e12166. doi: 10.1371/journal.pone.0012166

Feldman, R. (2007). Parent–infant synchrony and the construction of shared timing; physiological precursors, developmental outcomes, and risk conditions. *J. Child Psychol. Psychiatry* 48, 329–354. doi: 10.1111/j.1469-7610.2006.01701.x

Flavell, J. H. (1999). Cognitive development: children's knowledge about the mind. *Annu. Rev. Psychol.* 50, 21–45. doi: 10.1146/annurev.psych.50.1.21

Funane, T., Kiguchi, M., Atsumori, H., Sato, H., Kubota, K., and Koizumi, H. (2011). Synchronous activity of two people's prefrontal cortices during a cooperative task measured by simultaneous near-infrared spectroscopy. *J. Biomed. Opt.* 16:77011. doi: 10.1117/1.3602853

Giuliano, R. J., Skowron, E. A., and Berkman, E. T. (2015). Growth models of dyadic synchrony and mother-child vagal tone in the context of parenting at-risk. *Biol. Psychol.* 105, 29–36. doi: 10.1016/j.biopsycho.2014.12.009

Hasson, U., Ghazanfar, A. A., Galantucci, B., Garrod, S., and Keysers, C. (2012). Brain-to-brain coupling: A mechanism for creating and sharing a social world. *Trends Cogn. Sci.* 16, 114–121. doi: 10.1016/j.tics.2011.12.007

Kawasaki, M., Yamada, Y., Ushiku, Y., Miyauchi, E., and Yamaguchi, Y. (2013). Inter-brain synchronization during coordination of speech rhythm in human-to-human social interaction. *Sci. Rep.* 3, 1–8. doi: 10.1038/srep01692

Keysers, C., and Gazzola, V. (2009). Expanding the mirror: vicarious activity for actions, emotions, and sensations. *Curr. Opin. Neurobiol.* 19, 666–671. doi: 10.1016/j.conb.2009.10.006

Keysers, C., Kaas, J. H., and Gazzola, V. (2010). Somatosensation in social perception. *Nat. Rev. Neurosci.* 11, 417–428. doi: 10.1038/nrn2833

King-Casas, B., Tomlin, D., Anen, C., Camerer, C. F., Quartz, S. R., and Montague, P. R. (2005). Getting to know you: reputation and trust in a two-person economic exchange. *Science* 308, 78–83. doi: 10.1126/science.1108062

Klimesch, W. (1999). EEG alpha and theta oscillations reflect cognitive and memory performance: a review and analysis. *Brain Res. Rev.* 29, 169–195. doi: 10.1016/S0165-0173(98)00056-3

Koike, T., Tanabe, H. C., and Sadato, N. (2015). Hyperscanning neuroimaging technique to reveal the two-in-one system in social interactions. *Neurosci. Res.* 90, 25–32. doi: 10.1016/j.neures.2014.11.006

Konvalinka, I., and Roepstorff, A. (2012). The two-brain approach: how can mutually interacting brains teach us something about social interaction? *Front. Hum. Neurosci.* 6:215. doi: 10.3389/fnhum.2012.00215

Konvalinka, I., Bauer, M., Stahlhut, C., Hansen, L. K., Roepstorff, A., and Frith, C. D. (2014). Frontal alpha oscillations distinguish leaders from followers: multivariate decoding of mutually interacting brains. *Neuroimage* 94, 79–88. doi: 10.1016/j.neuroimage.2014.03.003

Konvalinka, I., Vuusta, P., Roepstorffa, A., and Frith, C. D. (2010). Follow you, follow me: continuous mutual prediction and adaptation in joint tapping. *Q. J. Exp. Psychol.* 63, 2220–2230. doi: 10.1080/17470218.2010.497843

Konvalinka, I., Xygalatasa, D., Bulbuliac, J., Schjødta, U., Jegindøa, E.-M., Wallotd, S., et al. (2011). Synchronized arousal between performers and related spectators in a fire-walking ritual. *Proc. Natl. Acad. Sci. U.S.A.* 108, 8514–8519. doi: 10.1073/pnas.1016955108

Lindenberger, U., Li, S.-C., Gruber, W., and Müller, V. (2009). Brains swinging in concert: cortical phase synchronization while playing guitar. *BMC Neurosci.* 10:22. doi: 10.1186/1471-2202-10-22

Liu, T., and Pelowski, M. (2014). A new research trend in social neuroscience: towards an interactive-brain neuroscience. *PsyCh. J.* 3, 177–188. doi: 10.1002/pchj.56

Liu, T., Saito, H., and Oi, M. (2015). Role of the right inferior frontal gyrus in turn-based cooperation and competition: a near-infrared spectroscopy study. *Brain Cogn.* 99, 17–23. doi: 10.1016/j.bandc.2015.07.001

McAssey, M. P., Helm, J., Hsieh, F., Sbarra, D. A., and Ferrer, E. (2013). Methodological advances for detecting physiological synchrony during dyadic interactions. *Methodology* 9, 41–53. doi: 10.1027/1614-2241/a000053

McFarland, D. H. (2000). Respiratory markers of conversational interaction. *J. Speech Lang. Hear. Res.* 44, 128–143. doi: 10.1044/1092-4388(2001/012)

Montague, P. (2002). Hyperscanning: simultaneous fMRI during linked social interactions. *Neuroimage* 16, 1159–1164. doi: 10.1006/nimg.2002.1150

Müller, V., and Lindenberger, U. (2011). Cardiac and respiratory patterns synchronize between persons during choir singing. *PLoS ONE* 6:e24893. doi: 10.1371/journal.pone.0024893

Niedenthal, P. M. (2007). Embodying Emotion. *Science* 316, 1002–1005. doi: 10.1126/science.1136930

Sänger, J., Müller, V., and Lindenberger, U. (2012). Intra- and interbrain synchronization and network properties when playing guitar in duets. *Front. Hum. Neurosci.* 6:312. doi: 10.3389/fnhum.2012.00312

Schilbach, L. (2010). A second-person approach to other minds. *Nat. Rev. Neurosci.* 11:449. doi: 10.1038/nrn2805-c1

Shockley, K., Santana, M.-V., and Fowler, C. A. (2003). Mutual interpersonal postural constraints are involved in cooperative conversation. *J. Exp. Psychol. Hum. Percept. Perform.* 29, 326–332. doi: 10.1037/0096-1523.29.2.326

Sinha, N., Maszczyk, T., Wanxuan, Z., Tan, J., and Dauwels, J. (2016). "EEG hyperscanning study of inter-brain synchrony during cooperative and competitive interaction," in *Systems, Man, and Cybernetics (SMC), 2016 IEEE International Conference on IEEE* (Budapest), 4813–4818.

Toppi, J., Borghini, G., Petti, M., He, E. J., De Giusti, V., He, B., et al. (2016). Investigating cooperative behavior in ecological settings: an EEG hyperscanning study. *PLoS ONE* 11:e0154236. doi: 10.1371/journal.pone.0154236

Venturella, I., Gatti, L., Vanutelli, M. E., and Balconi, M. (2017). When brains dialogue by synchronized or unsynchronized languages. Hyperscanning applications to neuromanagement. *Neuropsychol. Trends* 21, 35–52. doi: 10.7358/neur-2017-021-vent

Yun, K., Watanabe, K., and Shimojo, S. (2012). Interpersonal body and neural synchronization as a marker of implicit social interaction. *Sci. Rep.* 2:959. doi: 10.1038/srep00959

Check for updates

Insensitivity to Fearful Emotion for Early ERP Components in High Autistic Tendency Is Associated with Lower Magnocellular Efficiency

Adelaide Burt*, Laila Hugrass, Tash Frith-Belvedere and David Crewther

Centre for Human Psychopharmacology, Faculty of Health, Arts and Design, Swinburne University of Technology, Melbourne, VIC, Australia

Low spatial frequency (LSF) visual information is extracted rapidly from fearful faces, suggesting magnocellular involvement. Autistic phenotypes demonstrate altered magnocellular processing, which we propose contributes to a decreased P100 evoked response to LSF fearful faces. Here, we investigated whether rapid processing of fearful facial expressions differs for groups of neurotypical adults with low and high scores on the Autistic Spectrum Quotient (AQ). We created hybrid face stimuli with low and high spatial frequency filtered, fearful, and neutral expressions. Fearful faces produced higher amplitude P100 responses than neutral faces in the low AQ group, particularly when the hybrid face contained a LSF fearful expression. By contrast, there was no effect of fearful expression on P100 amplitude in the high AQ group. Consistent with evidence linking magnocellular differences with autistic personality traits, our non-linear VEP results showed that the high AQ group had higher amplitude K2.1 responses than the low AQ group, which is indicative of less efficient magnocellular recovery. Our results suggest that magnocellular LSF processing of a human face may be the initial visual cue used to rapidly and automatically detect fear, but that this cue functions atypically in those with high autistic tendency.

Keywords: spatial frequency, event related potentials, P100, autistic tendency, fearful face perception, magnocellular inefficiency

INTRODUCTION

Autism spectrum disorder (ASD) is a broad group of disorders, characterized by impairments in communication and social awareness, and by repetitive stereotyped behaviors (American Psychiatric Association, 2013). In addition to these well-known impairments, there are some differences in perceptual functioning, particularly in the visual domain (Dakin and Frith, 2005; Kellerman et al., 2005; Pellicano et al., 2005; Dale and Salt, 2008; McCleery et al., 2009; Simmons et al., 2009). These perceptual differences extend to the neurotypical population (Almeida et al., 2010; Sutherland and Crewther, 2010; Jackson et al., 2013) for individuals with high scores on the Autism Spectrum Quotient (AQ) personality scale (Baron-Cohen et al., 2001). This suggests that the underlying physiology of ASD may be distributed throughout a broader autistic phenotype, which contributes to visual differences in these individuals (Bailey et al., 1995; Braddick et al., 2003).

Detection of potentially threatening stimuli, such as fearful or angry faces involves a distributed network of cortical and subcortical regions (LeDoux, 1998; Johnson, 2005; Kragel et al., 2016).

Several researchers have proposed that rapid processing of threat occurs via a direct, subcortical route from the pulvinar and superior colliculus to the amygdala (LeDoux, 1998; Morris et al., 1998a; Öhman, 2005). Direct evidence of a subcortical (retino-collicular-pulvinar) route to the amygdala has come from animal studies (LeDoux, 1998), whereas functional evidence in humans has been inferred based on evidence of emotional face processing in cortically blind participants (Morris et al., 2001), unconscious processing of emotional stimuli (Morris et al., 1998a), and magnetoencephalographic (MEG) responses to fearful stimuli in the amygdala and subcortical structures (Streit et al., 2003). Clear anatomical evidence from *in vivo* DTI tractography conducted in humans demonstrates connections between the amygdala and superior colliculus (Rafal et al., 2015); and amygdala and pulvinar (Tamietto et al., 2012). In support of this model, connectivity analyses have shown that fearful stimuli engage a distributed network of brain sites including the bilateral fusiform gyrus, dorsal/anterior precuneus, amygdala, hippocampus, and parahippocampal regions (Kragel and LaBar, 2015).

In order to compare cortical and subcortical routes for affective information processing, several researchers have taken advantage of the tuning properties of cells in the subcortical structures (Vuilleumier et al., 2003; Öhman, 2005; Vlamings et al., 2009). Cells in the input layers of the superior colliculus receive input from the magnocellular pathway (Schiller et al., 1979). Magnocellular neurons have relatively large receptive fields and respond preferentially to low spatial frequency (LSF) input, compared with parvocellular neurons which have smaller receptive fields and respond preferentially to high spatial frequency (HSF) input (Livingstone and Hubel, 1988). Processing of coarse information contained in the LPFs precedes processing of more detailed information contained in the HSFs, with magnocellular input reaching V1 25–31 ms earlier than parvocellular input (Klistorner et al., 1997; Bullier, 2001; Bar et al., 2006; Sutherland and Crewther, 2010; Crewther et al., 2016). This temporal precedence has been termed the 'magnocellular advantage' (Laycock et al., 2007).

In support of a magnocellular route for fearful face processing, Vuilleumier et al. (2003) found enhanced BOLD responses in the superior colliculus and amygdala structures for LSF, but not HSF, fearful expressions. However, the amygdala also receives input from the anterior inferotemporal cortex (Aggleton, 1993), so it is not 'blind' to HSF fearful face representations. In fact, the amygdala is likely to have numerous connections with subcortical and cortical structures, which process and integrate both LSF and HSF, to form a 'whole' fearful face percept. Evidence for multiple pathways comes from connectivity analyses demonstrating that fearful stimuli engage a distributed network of brain sites including the bilateral fusiform gyrus, dorsal/anterior precuneus, amygdala, hippocampus, and parahippocampal regions (Kragel and LaBar, 2015). In addition, evidence for multiple pathways is presented by one fMRI study demonstrating that during unconscious processing using binocular rivalry and backward masking, when visual input must be processed via a subcortical route, the amygdala has limited capacity to differentiate between facial emotions (Morris et al., 1998b; Williams et al., 2004).

Sets of hybrid face stimuli have been used in numerous studies in order to investigate the relative contributions of LSF and HSF information to various aspects of emotional face processing, while controlling the natural variation of spatial frequencies within the images (Pourtois et al., 2005; Laeng et al., 2010, 2013; Prete et al., 2014, 2015a,b,c, 2016). LSF information generally includes coarse, global visual features whereas HSF information includes finer, more detailed features (De Valois and De Valois, 1988). Hybrid face stimuli are created from different combinations of the LSF and HSF filtered components of neutral and emotional faces. By equating the luminance and contrast of LSF and HSF within one image, only the change in emotional expression of the face remains (Pourtois et al., 2005). Hybrid faces have been used to assess conscious report of fearful face perception, where HSF fearful and neutral expressions are more rapidly discriminated than LSF expressions (Stein et al., 2014). However, behavioral report does not necessarily reflect the rapid, neural processing that occurs prior to conscious perception of a fearful face, which can be investigated with electroencephalogram (EEG). For consistency, throughout this paper we will refer to hybrids created from LSF and HSF, fearful (F) and neutral (N) face stimuli as follows: $F_{LSF}-F_{HSF}$, $F_{LSF}-N_{HSF}$, $N_{LSF}-F_{HSF}$, and $N_{LSF}-N_{HSF}$.

To elucidate the time course of rapid fear perception, electrophysiological studies have primarily focused on the P100 and N170 waveforms. The visual P100 is a fast response, typically evoked between 90 and 140 ms, that is maximal over lateral–occipital–parietal sites, and appears to originate from striate and extrastriate neural generators (Clark and Hillyard, 1996; Mangun et al., 1997; Allison et al., 1999). Cueing studies suggest the P100 amplitude is an index of the attentional gain mechanisms that suppress responses to irrelevant stimuli (Hillyard and Anllo-Vento, 1998). In addition, the P100 is sensitive to affect, with greater amplitude responses to fearful face presentation, compared to other emotions including neutral, happy, angry, sad, disgust, and surprise faces (Pizzagalli et al., 1999; Batty and Taylor, 2003; Pourtois et al., 2004; Magnée et al., 2008; Feng et al., 2009; Forscher and Li, 2012; Meaux et al., 2013; Smith et al., 2013; Zhang et al., 2013). The N170 is negative peak that occurs approximately 170 ms post-stimulus, originating from a network of face/object processing regions including the fusiform gyrus, superior temporal sulcus and inferior, middle and superior temporal gyri (Henson et al., 2003). N170 amplitude is sensitive to configural processing of faces, as evidenced by higher amplitude response to upright over inverted faces (Bentin et al., 1996). Affective input also modulates these early waveforms, with greater amplitude P100 and N170 responses to fearful or angry expressions (Batty and Taylor, 2003; Pegna et al., 2008).

Several studies have investigated whether fearful face modulation of visual ERPs relies on LSF (i.e., magnocellular) input. The P100 amplitude is enhanced for $F_{LSF}-N_{HSF}$ hybrid faces compared to $N_{LSF}-N_{HSF}$ hybrid faces in the right hemisphere, but not for $N_{LSF}-F_{HSF}$ hybrids (Pourtois et al., 2005); however, this effect is only observed when the images have been equated for luminance and contrast (Vlamings et al., 2009). In addition, Vlamings et al. (2009) found shorter P100

latency for $F_{LSF}-N_{HSF}$ compared to $N_{LSF}-F_{HSF}$ hybrids, which trended toward significance in the fearful expression condition. Findings regarding the effects of emotion and spatial frequency on the N170 amplitude have been mixed. Some studies reported no effect of emotion on the N170 response (Holmes et al., 2005; Pourtois et al., 2005), however, Vlamings et al. (2009) reported N170 enhancement for $F_{LSF}-N_{HSF}$ but not $N_{LSF}-F_{HSF}$ faces, regardless of whether the stimuli were equated for luminance and contrast.

Early electrophysiological responses to fearful faces vary across the autistic spectrum, indicating there are individual differences in the neural pathways that produce these responses. In autistic individuals, the P100 tends to be delayed, reduced in amplitude and less lateralized than in neurotypical groups (Bailey et al., 2005; Wong et al., 2008; McCleery et al., 2009; Luo et al., 2010; Batty et al., 2011; Fujita et al., 2013; Tye et al., 2013; Wagner et al., 2013; Key and Corbett, 2014; Bonnard-Couton et al., 2015; Lassalle and Itier, 2015; Anzures et al., 2016). In an investigation of face processing in the broader autistic phenotype, Stavropoulos et al. (2016) found that P100 and N170 latencies tended to be slower and decreased for people with high AQ scores, compared to people with low AQ scores. They found that non-consciously perceived emotional faces elicited enhanced neural responses regardless of AQ score, yet they did not use hybrid faces so it is unclear whether the two groups utilized LSF information in the same way. De Jong et al. (2008) investigated the effects of gaze cueing on ERPs and found that for neurotypical observers, gaze cueing had a stronger effect on ERPs for LSF filtered faces; whereas for autistic observers, cueing effects were stronger for HSF filtered faces. These findings indicate that the P100 and N170 responses to fearful emotional faces may be particularly affected in individuals with high autistic tendency. Therefore, we aimed to compare the effects of LSF and HSF fearful expressions on ERP responses for high and low AQ groups.

Several visual studies provide evidence for magnocellular/dorsal stream abnormalities in ASD (Pellicano et al., 2005; Milne et al., 2006; McCleery et al., 2009) and in the broader autistic phenotype (Almeida et al., 2010; Sutherland and Crewther, 2010; Jackson et al., 2013; Thompson et al., 2015; Stavropoulos et al., 2016). Other studies have indicated that the relationship between magnocellular function and ASD is more complicated (Bertone et al., 2003; Del Viva et al., 2006). The current view is that ASD involves complex interactions between multiple visual pathways, rather than a specific magnocellular/dorsal stream impairment (Simmons et al., 2009; Thye et al., 2017). Despite the nature of magnocellular impairment remaining unresolved, there are differences in the rapid output of magnocellular neurons to V1 in high autistic tendency (Sutherland and Crewther, 2010; Jackson et al., 2013). Moreover, as discussed above, magnocellular neurons have a preference for LSF input, resulting in rapid V1 activation. Neural efficiency of magnocellular neurons can be studied through Weiner kernel analysis of multifocal visual evoked potentials (mfVEP) (Sutherland and Crewther, 2010; Jackson et al., 2013). The first slice of the second order, non-linear VEP kernel (K2.1) measures non-linearity in neural recovery (referenced one video frame back). Studies of the contrast

response function indicate that the N60 K2.1 waveform, and early components (with the same latency) of the K2.2 waveform (second slice- referenced two frames back) are of magnocellular origin (Baseler and Sutter, 1997). Higher amplitudes of these waveforms indicate a greater degree of inefficiency in neural recovery by magnocellular neurons. The amplitude of the N60 negativity in the first slice of the second order kernel (K2.1) is elevated in high AQ observers, indicative of poor magnocellular recovery rate (Jackson et al., 2013). Hence, Jackson et al.'s (2013) findings are consistent with the lack of efficiency of the magnocellular pathway in ASD.

Based on prior research by Vlamings et al. (2009) we hypothesized that the low AQ group would exhibit significantly higher amplitude and shorter latency P100 and N170 responses to $F_{HSF}-F_{LSF}$ hybrids compared to $N_{HSF}-N_{LSF}$ hybrids, and to $F_{LSF}-N_{HSF}$ compared to $F_{HSF}-N_{LSF}$ hybrids. Based on the findings by Stavropoulos et al. (2016), it was hypothesized that the P100 and N170 would be lower for the high AQ group than for the low AQ group. Furthermore, we predicted that $F_{LSF}-N_{HSF}$ expressions would have a greater influence on response amplitudes in the low AQ group than in the high AQ group. We aimed to use non-linear VEP to assess magnocellular recovery, as indexed by the amplitude of the K2.1 waveform. It was hypothesized, the K2.1 response amplitude would be higher in the high AQ group, which is indicative of inefficient recovery rate of neurons within the magnocellular system.

MATERIALS AND METHODS

Participants

Participants were recruited through advertising and social media to complete an online AQ survey (Baron-Cohen et al., 2001). Thirty-seven participants with normal or corrected to normal vision completed the hybrid face EEG study conducted at Swinburne University of Technology, Melbourne, Australia. Two participants were excluded from the analysis because of very high movement artifact (one recording was actually discontinued for this reason), and a further two participants were excluded because their scores were in the mid-range of AQ (which we only established after recording). The final sample included 16 low AQ participants (3 male; 13 female; $M = 24.19$ years, $SD = 5.41$) and 17 high AQ participants (11 male; 6 female; $M = 25.29$ years, $SD = 5.72$). MfVEP data collection commenced after we had already began collecting data for the facial emotion study; hence only 12 low AQ and 12 high AQ participants completed the mfVEP recordings. For the behavioral data, two participants were excluded due to corrupted data files and a further participant was excluded due to misunderstanding task instructions, leaving a sample of 31 participants (17 high AQ and 14 low AQ). All participants gave informed consent in accordance with the Declaration of Helsinki, and the Swinburne Human Research Ethics Committee approved the study.

Autistic Quotient Online Survey
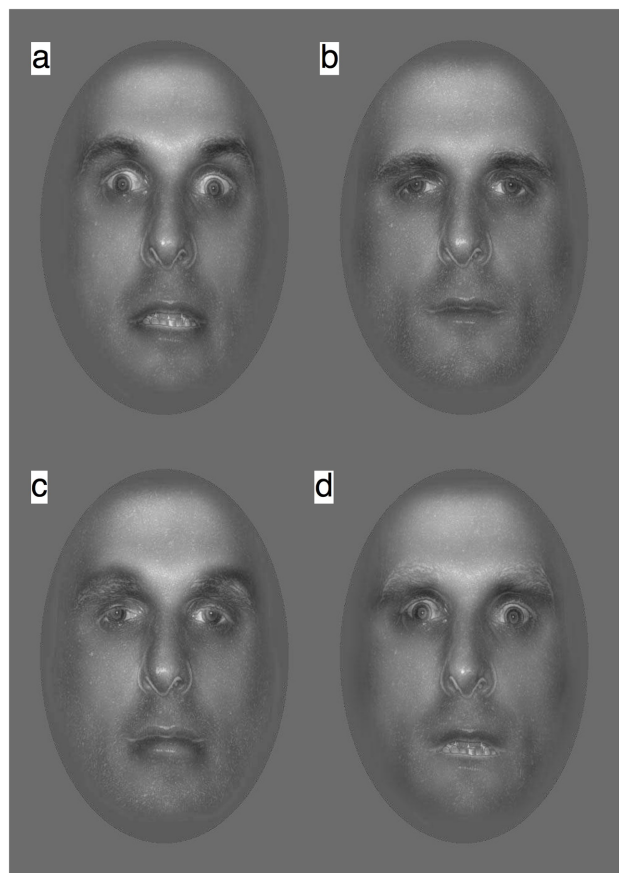
The AQ (Baron-Cohen et al., 2001) is a 50-item measure of autistic trait levels across the normal adult population. Low

and high group cut-offs for the EEG study were based on the population mean ($M = 17$, $SD = 6$) for the AQ groups (Ruzich et al., 2015). The low AQ group ($n = 16$) had a mean AQ score of 6.88 ($SD = 3.22$) and the high AQ ($n = 17$) group had a mean AQ score of 29.00 ($SD = 5.95$).
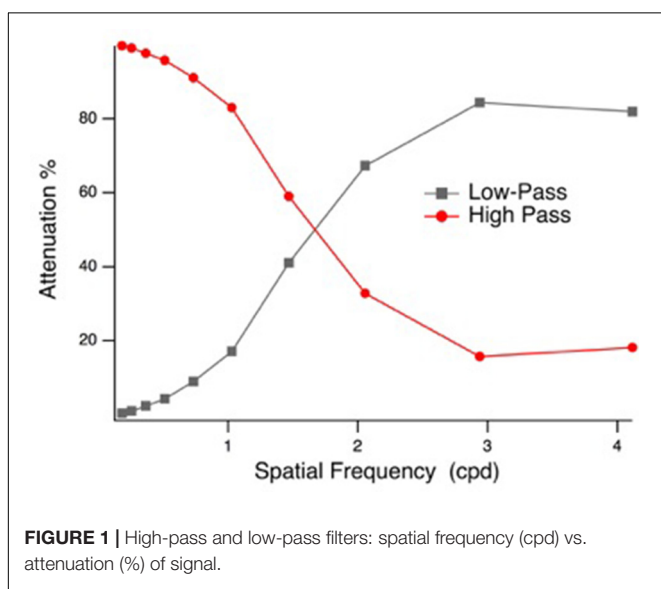
Hybrid Face Stimuli

Fourteen images of neutral and fearful faces were selected from the NimStim Face Set (Tottenham et al., 2009). The images were transformed to gray-scale and cropped with a smoothed edge to remove external features (e.g., hair, neck) using Adobe Photoshop. The fearful faces were altered to have a 30% increase in pupil size, to reproduce a physiologically accurate fearful response (Demos et al., 2008).

Face stimuli were spatial frequency filtered (Gaussian blur, low-pass filter preserving spatial frequencies <2 cpd and high pass filter preserving spatial frequencies >1.9 cpd, based on the point of 1 octave attenuation) using Photoshop (Adobe Systems Inc., San Jose, CA, United States), similar to prior investigations (Schyns and Oliva, 1999; Vlamings et al., 2009). The high- and low-pass filter characteristics are illustrated in **Figure 1**. The LSF and HSF images were matched for mean luminance (57 cd/m^2) and RMS contrast in Matlab (The Mathworks, Natick, MA, United States), before they were fused to create hybrid face stimuli. Four sets of F (fearful) and N (neutral) hybrid stimuli were created for each of the seven identities: F_{LSF}–F_{HSF}, F_{LSF}–N_{HSF}, N_{LSF}–F_{HSF}, and N_{LSF}–N_{HSF}. Example hybrid stimuli are presented in **Figure 2**. A phase-scrambled neutral face (luminance and RMS contrast matched) was presented during the baseline period. The tasks were created and presented using VPixx software (version 3.15, VPixx Technologies, Montreal, QC, Canada), and displayed on a 27 cm × 48 cm LCD monitor with linearized output, at a viewing distance of 70 cm. Face images were centrally displayed in a 20 × 19.5 degree (500 × 700 pixels) mid-gray frame (47 cd/m^2) on a gray background (65 cd/m^2).

FIGURE 2 | Hybrid face stimuli were created by recombining the LSF and HSF components of fearful (F) and neutral (N) faces into hybrids as: **(a)** F_{LSF}–F_{HSF} **(b)** N_{LSF}–N_{HSF} **(c)** F_{LSF}–N_{HSF}, and **(d)** N_{LSF}–F_{HSF}.

FIGURE 1 | High-pass and low-pass filters: spatial frequency (cpd) vs. attenuation (%) of signal.

Multifocal VEP

A 9-patch dartboard stimulus was programmed in VPixx, with a 4-degree central patch and two outer rings of four patches. Each patch fluctuated between two gray levels (70% Michelson contrast). The luminance for each patch was updated every video frame (60 Hz), following a pseudorandom binary m-sequence ($m = 14$). The m-sequences for each patch were maximally offset, so we could record independent responses. For the purpose of this paper, only the central patch was analyzed. The m-sequences were broken into four approximately 1-min recording segments. Participants were instructed to blink and rest in between recordings, and to maintain careful fixation during the recordings.

Procedure

Prior to the task, participants were shown example hybrid stimuli. Although participants were not explicitly informed about the different hybrid face conditions, they were told that some faces might appear distorted, due to different spatial frequency content. During the experiment, a behavioral task was used to confirm participants were attending to the

emotional content of the hybrid faces. Participants were verbally instructed that a hybrid face image would appear on screen for 500 ms, and after the image disappeared, they were to make 2AFC RESPONSEPixx button box decision between neutral and fearful expressions, where red button = *neutral* and green button = *fear*. Participants were instructed that this was not a timed response test, but that they should respond as accurately as possible, and guess when they were unsure of the facial expression. Participants were instructed to respond with their preferred hand, however, handedness was not measured. Following response selection, a phase-scrambled face was presented during a 1.8 s inter-stimulus interval.

To prevent fatigue, the recording was split into two blocks of 100 trials, so in total there were 50 trials for each of the four hybrid face conditions. Stimulus presentations were randomized, with set constraints on the number of trials for each hybrid condition. Trials with more than one button response were identified and removed from the analyses. For the second experiment, participants were instructed to passively view the multifocal dartboard stimulus. The m-sequences were broken into four approximately 1-min recording segments. Participants were instructed to blink and rest in between recordings, and to maintain careful fixation during the recordings.

EEG Recordings and Analyses

Electroencephalogram was recorded from parietal and occipital sites (Oz, O1, O2, P3, P4, P5, P6, P7, P8, PO1, PO2, PO3, PO4, PO5, PO6, PO7, PO8) using a 32 channel Quickcap recording cap (Neuroscan, Compumedics). The data were band-pass filtered from 0.1 to 200 Hz, and sampled at 1 KHz. The ground electrode was positioned at AFz and linked mastoid electrodes served as a reference. Eye blinks were monitored with EOG electrodes, attached to the sub and supra orbital regions of the right eye.

Data analysis was performed with Brainstorm (Tadel et al., 2011), which is documented and freely available for download online under the GNU general public license[1]. Data were band-pass filtered (1–30 Hz) and signal space projection was applied to reduce eye-blink artifact. Segments of data containing low-frequency artifact were excluded from the analysis. For the facial emotion experiment, we extracted ERP epochs from −200 ms pre to 450 ms post-stimulus presentation. Baseline corrections were made for each epoch, by subtracting the mean amplitude present during the 200 ms period before stimulus presentation (i.e., −200 to 0 ms). Any epochs containing high amplitude noise (>75 μV) were excluded from the analysis. Separate ERP averages were computed for the low and high AQ groups, for each hybrid face condition: F_{LSF}–F_{HSF} (Low AQ: 730 epochs, High AQ: 820 epochs), N_{LSF}–N_{HSF} (Low AQ: 744 epochs, High AQ: 817 epochs), F_{LSF}–N_{HSF} (Low AQ: 728 epochs, High AQ: 813 epochs) and N_{LSF}–F_{HSF} (Low AQ: 744 epochs, High AQ: 819 epochs).

Consistent with previous research (Vlamings et al., 2009, 2010) visual inspection revealed P100 amplitudes were the greatest at electrodes P8, PO8, PO7, P7, O1, O2 and Oz,

and N170 amplitudes were the greatest at P8, PO8, PO7, P7. To improve signal to noise ratio, the mean cluster responses were extracted. To reduce high frequency noise in these pre-processed waveforms, an additional 10 Hz low-pass filter was applied, prior to extracting the waveforms for the statistical amplitude and latency comparisons (Vlamings et al., 2010). The additional low-pass filter did not distort the P100 and N170 traces, indeed similar patterns of results were obtained regardless of whether this filter was applied. However, this step enabled more robust estimation of peak latencies at the individual level.
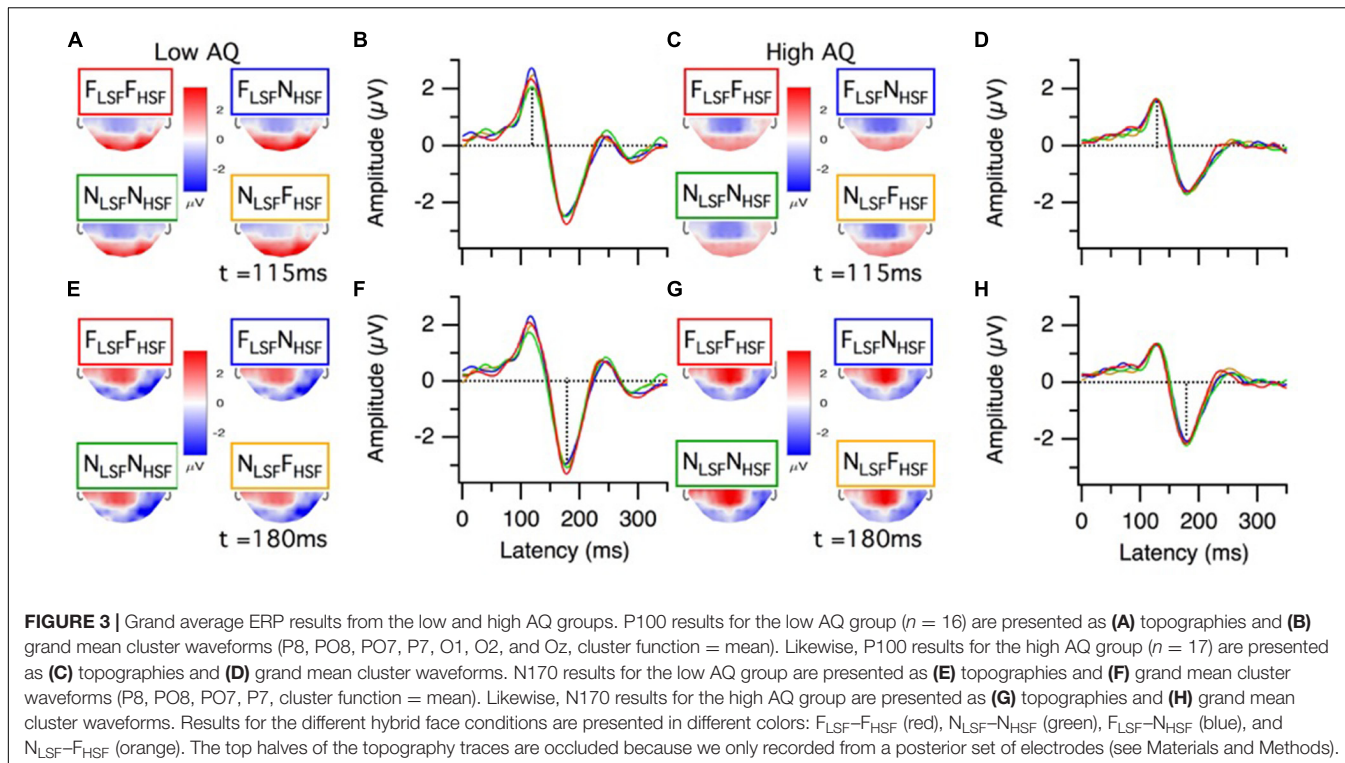
P100 and N170 amplitudes and latencies were detected using LabVIEW (National Instruments). P100 was detected as the maximum amplitude within the 90–150 ms time window, and N170 was detected as the minimum amplitude within the 160–240 ms time window. Peak amplitudes can be affected by noise, and emotion effects are not limited to the peaks, so we used the area under the P100 and N170 waveforms (60 ms window) as a measure of amplitude in the statistical comparisons (Vlamings et al., 2010). Due to individual differences in peak latencies, 60 ms time windows for P100 and N170 area measurements were centered separately on their peak latencies for each participant.

For the non-linear VEP analyses, custom Matlab/Brainstorm scripts were written to extract K1, K2.1 and K2.2 kernels for the central patch of the dartboard stimulus. The first order kernel (K1) is the difference in response when the patch was light (S1) or dark (S2) throughout the m-sequence, i.e., $0.5*(S_1 − S_2)$. As described in previous papers (Klistorner et al., 1997; Jackson et al., 2013), the first slice of the second order kernel (K2.1) compares consecutive frames when a transition did and did not occur, i.e., $K2.1 = 0.25*(S_{11} + S_{22} − S_{12} − S_{21})$. The second slice of the second order kernel (K2.2) is similar, but compares frames with an interleaving frame of either polarity. In other words, K2.1 measures neural recovery over one frame (16.67 ms on a 60 Hz monitor) and K2.2 measures neural recovery over two frames (33.33 ms).

RESULTS

Grand mean ERP topographies and waveforms for the low and high AQ groups are presented in **Figure 3**. The P100 topographies for the low and high AQ groups (**Figures 3A,C**, respectively) show there was a bilateral, occipital positivity at 115 ms latency for each of the hybrid face conditions. The N170 topographies for the low and high AQ groups (**Figures 3D,G**, respectively) show there was a right lateralized negativity, with strongest activations at electrode sites P8 and PO8, for each of the hybrid face conditions. Means and standard deviations for the low and high AQ groups are presented in **Figure 4**, with comparisons for P100 amplitude and latency, N170 amplitude and latency, and behavioral performance. As explained in the analyses section, we defined ERP amplitude as the area under the waveform (peak or trough latency ± 30 ms); however, it should be noted that we observed a similar pattern of results when we compared the waveform areas

---

[1]http://neuroimage.usc.edu/brainstorm

FIGURE 3 | Grand average ERP results from the low and high AQ groups. P100 results for the low AQ group ($n = 16$) are presented as **(A)** topographies and **(B)** grand mean cluster waveforms (P8, PO8, PO7, P7, O1, O2, and Oz, cluster function = mean). Likewise, P100 results for the high AQ group ($n = 17$) are presented as **(C)** topographies and **(D)** grand mean cluster waveforms. N170 results for the low AQ group are presented as **(E)** topographies and **(F)** grand mean cluster waveforms (P8, PO8, PO7, P7, cluster function = mean). Likewise, N170 results for the high AQ group are presented as **(G)** topographies and **(H)** grand mean cluster waveforms. Results for the different hybrid face conditions are presented in different colors: F_{LSF}–F_{HSF} (red), N_{LSF}–N_{HSF} (green), F_{LSF}–N_{HSF} (blue), and N_{LSF}–F_{HSF} (orange). The top halves of the topography traces are occluded because we only recorded from a posterior set of electrodes (see Materials and Methods).

or the peak voltages across hybrid face conditions and AQ groups.
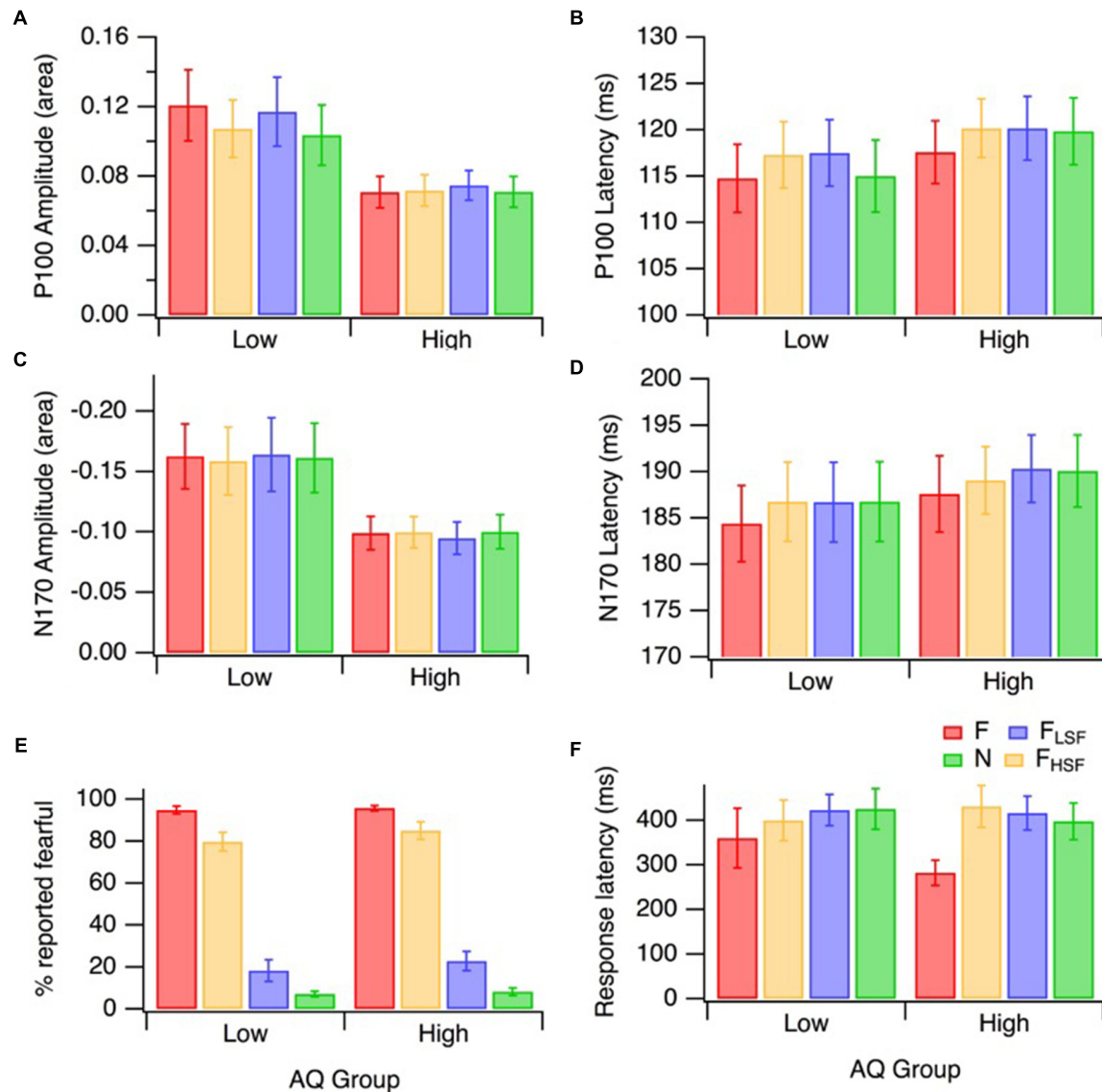
Behavioral Performance

The emotion identification data (i.e., the percentage of trials in which fearful expression was reported) are presented in **Figure 4E**. A mixed factorial design 2 (AQ group) by 4 (hybrid face condition) ANOVA (with Greenhouse–Geisser corrections for unequal variance) was performed on emotion identification. There was a significant main effect of hybrid face condition on fear identification [$F(2.23, 64.55) = 435.79$, $p < 0.001$, $\eta_p^2 = 0.94$]. There was no significant interaction between the effects of hybrid face condition and AQ group on the fear identification [$F(2.23, 64.55) = 0.31$, $p = 0.758$]; nor was there a main effect of AQ group [$F(1, 29) = 0.82$, $p = 0.372$]. This shows that both AQ groups performed similarly. As one would expect, planned comparisons showed that F_{LSF}–F_{HSF} hybrids were identified as 'fearful' significantly more often than N_{LSF}–N_{HSF} [$F(1, 29) = 2423.73$, $p < 0.001$, $\eta_p^2 = 0.99$], F_{LSF}–N_{HSF} [$F(1, 29) = 486.39$, $p < 0.001$, $\eta_p^2 = 0.94$], and N_{LSF}–F_{HSF} hybrids [$F(1, 29) = 29.45$, $p < 0.001$, $\eta_p^2 = 0.50$]. However, it was interesting that observers reported fearful expression substantially more often in the N_{LSF}–F_{HSF} condition than in the F_{LSF}–N_{HSF} condition [$F(1, 29) = 341.05$, $p < 0.001$, $\eta_p^2 = 0.92$]. This indicates that HSF information plays a more important role in conscious identification of facial emotion than LSF information. Please note that response latencies (**Figure 4F**) were not similarly analyzed because interpretation of the data could be confused by the stipulation that participants should wait until the stimulus disappeared before responding.

P100 Amplitude

A mixed factorial design 2 (AQ group) by 4 (hybrid face condition) ANOVA was performed on P100 amplitude (area), with means displayed in **Figure 4A**. The analysis revealed a significant difference in mean P100 amplitude across the four hybrid face conditions, [$F(3, 93) = 3.86$, $p = 0.012$, $\eta_p^2 = 0.11$]. Across hybrid conditions, the P100 amplitude was lower in the high AQ group than in the low AQ group, and this difference was approaching significance [$F(1, 31) = 4.08$, $p = 0.052$, $\eta_p^2 = 0.17$], as can be seen in **Figure 4A**. The interaction between AQ group and hybrid face condition was significant, [$F(3, 93) = 3.02$, $p = 0.034$, $\eta_p^2 = 0.09$].

As the effect of the hybrid face conditions on P100 amplitude area was different for the two AQ groups, separate ANOVAs were performed for each group. For the low AQ group, there was a significant effect of the hybrid face conditions on the mean P100 amplitude, [$F(3, 45) = 3.83$, $p = 0.016$, $\eta_p^2 = 0.20$]. Analytical contrasts revealed that, as predicted, mean P100 amplitude was significantly greater for F_{LSF}–F_{HSF} hybrids compared to N_{LSF}–N_{HSF} hybrids, [$F(1, 15) = 10.75$, $p = 0.005$, $\eta_p^2 = 0.42$]. Interestingly, while P100 amplitude was significantly lower with N_{LSF}–F_{HSF} than F_{LSF}–F_{HSF} faces [$F(1, 15) = 5.36$, $p = 0.035$, $\eta_p^2 = 0.26$], P100 amplitudes were not significantly different for F_{LSF}–F_{HSF} and F_{LSF}–N_{HSF} faces [$F(1, 15) = 0.43$, $p = 0.523$]. This suggests that the effect of fearful emotion on P100 amplitude is mostly due to the LSF fearful input. Contrary to our hypothesis on hybrid face differences, the low AQ group produced no significant amplitude area mean difference between F_{LSF}–N_{HSF} and N_{LSF}–F_{HSF} [$F(1, 15) = 2.87$, $p = 0.111$].

FIGURE 4 | Mean ERP and behavioral responses for the low ($n = 16$) and high ($n = 17$) AQ groups to the different hybrid face sets: F_{LSF}–F_{HSF} (red), N_{LSF}–N_{HSF} (green), F_{LSF}–N_{HSF} (blue), and N_{LSF}–F_{HSF} (orange). The error bars on all panels represent ± 1 SE. P100 amplitudes and latencies are displayed in **(A)** and **(B)**. N170 amplitudes and latencies are displayed in **(C)** and **(D)**. Behavioral results for the percentage of trials in which fear was identified, and the associated reactions times are presented in **(E)** and **(F)**, respectively.

The ANOVA for the high AQ group revealed that, as hypothesized, there was no significant mean difference in P100 amplitude area across the four hybrid face conditions [$F(3,48) = 0.85$, $p = 0.473$]. This suggests an overall lack of fear affect or spatial frequency modulation of the early P100 ERP component in high autistic tendency.

P100 Latency

A mixed factorial design 2 (AQ group) by 4 (hybrid face condition) ANOVA was performed on P100 latency, with the means and standard errors displayed in **Figure 4B**. Greenhouse–Geisser corrections were applied when Mauchly's Test of

Sphericity was violated. There was a significant difference in mean P100 latency across the four hybrid face conditions for the whole sample [$F(2.32, 71.86) = 6.05$, $p = 0.002$, $\eta_p^2 = 0.16$]. Planned contrasts revealed a faster P100 latency for F_{LSF}–F_{HSF} compared to N_{LSF}–F_{HSF} [$F(1,31) = 12.94$, $p = 0.002$ $\eta_p^2 = 0.29$] and F_{LSF}–N_{HSF} [$F(1,31) = 18.52$, $p < 0.001$, $\eta_p^2 = 0.37$] hybrids, respectively. The mean P100 latency for fearful hybrids F_{LSF}–F_{HSF} was faster than for N_{LSF}–N_{HSF} hybrids, however, this comparison did not reach significance [$F(1,31) = 3.23$, $p = 0.082$, $\eta_p^2 = 0.09$] The hybrid face by AQ group interaction was not significant [$F(2.32, 71.86) = 0.99$, $p = 0.388$]. This indicates that facial emotion affected P100 latency in similar ways for the two

groups. The between-groups ANOVA was also not significant $[F(1,31) = 0.448, p = 0.508]$. In summary, the effect of hybrid faces on P100 latency was similar for the low and high AQ group, with the whole sample producing significantly quicker latency to fear displayed at both LSF and HSF.

N170 Amplitude
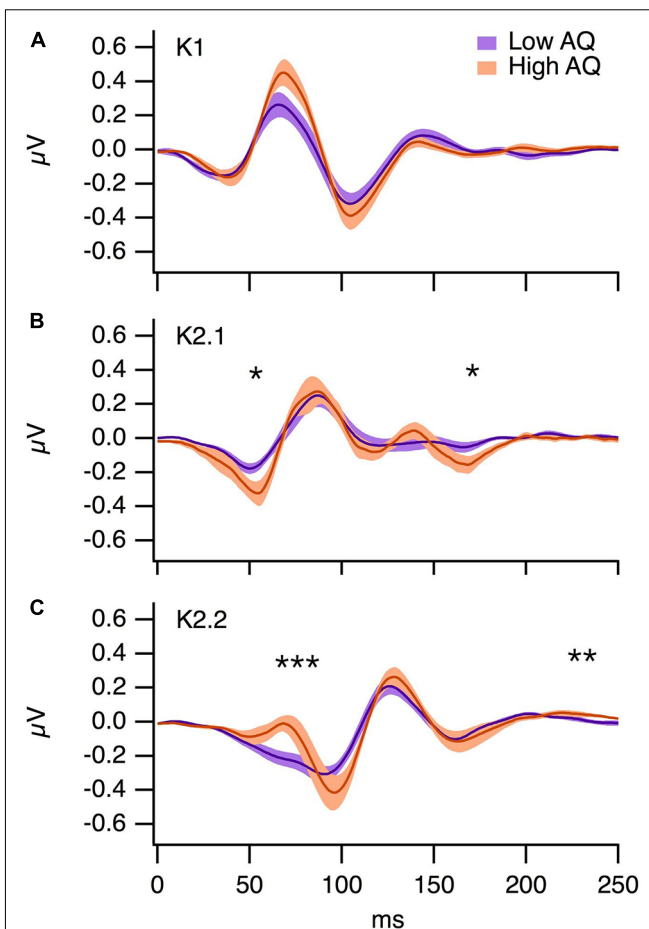
A mixed factorial design 2 (AQ group) by 4 (hybrid face condition) ANOVA (with Greenhouse–Geisser correction) was performed on N170 amplitude area, with means displayed in **Figure 4C**. There was no significant difference in mean N170 amplitude across the four hybrid face conditions $[F(2.17,67.37) = 0.13, p = 0.898]$. While there was no significant interaction $[F(2.17,67.37) = 0.77, p = 0.479]$; there was a significant effect of AQ group on mean N170 amplitude $[F(1,31) = 4.23, p = 0.048, \eta_p^2 = 0.12]$. As illustrated in **Figure 4C**, across conditions, mean N170 amplitudes tended to be lower in the high AQ group.

N170 Latency

A mixed factorial design 2 (AQ group) by 4 (hybrid face condition) ANOVA (with Greenhouse–Geisser correction) was performed on N170 latency, with means displayed in **Figure 4D**. The analysis revealed a significant difference in mean N170 latency, across the four hybrid face conditions in the whole sample $[F(2.33,72.29) = 6.28, p = 0.002, \eta_p^2 = 0.17]$. Planned contrasts of the whole sample revealed a significantly faster N170 latency in response to fearful hybrids compared with $N_{LSF}–N_{HSF}$ $[F(1,31) = 12.19, p = 0.001, \eta_p^2 = 0.28]$, $N_{LSF}–F_{HSF}$ $[F(1,31) = 11.18, p = 0.002, \eta_p^2 = 0.27]$ and $F_{LSF}–N_{HSF}$ hybrids $[F(1,31) = 15.89, p < 0.001, \eta_p^2 = 0.34]$. No significant interaction was observed $[F(2.33,72.29) = 0.36, p = 0.733, \eta_p^2 = 0.01]$. The between-groups ANOVA was also not significant $[F(1,31) = 0.303, p = 0.586]$. In summary, the effects of facial emotion on N170 latency were similar for the low and high AQ groups, with more rapid latency responses to hybrids with both LSF and HSF fear.

Multifocal VEP

The grand average K1, K2.1, and K2.2 Wiener kernel responses to the central multifocal patch for the low and high AQ groups are illustrated in **Figure 5**. For each participant, we selected the electrode with the highest amplitude response (Oz, O1, O2, or POz). The majority of participants showed maximal VEPs at Oz (Low AQ: Oz $n = 9$, POz $n = 1$ O1 $n = 2$, High AQ: Oz $n = 7$, POz $n = 4$, O2 $n = 1$). Independent samples t-tests were performed on kernel responses from the low and high AQ groups. For K1, the P70 peak was slightly higher in the high AQ group, but this difference was not statistically significant ($p > 0.05$). For K2.1, the amplitude of the N60 was significantly greater in the high AQ group $[t(22) = 2.09, p < 0.05]$, a negativity at approximately 180 ms was also lower in the high AQ group $[t(22) = 2.29, p < 0.05]$. The early component of the K2.2 [which reflects magnocellular processing (Jackson et al., 2013)] was significantly higher in amplitude for the high AQ group

FIGURE 5 | Grand averages from the low ($n = 12$) and high ($n = 12$) AQ groups for **(A)** K1, **(B)** K2.1, and **(C)** K2.2 VEP kernels. The shading represents ±1 SE, *$p < 0.05$, **$p < 0.01$, ***$p < 0.001$.

$[t(22) = 2.26, p < 0.05]$, yet there were no significant between-group differences in the parvocellularly driven N95 or P150 waveforms. These larger amplitude second-order non-linearities in the high AQ group are consistent with previous findings (Jackson et al., 2013), which suggests less efficient neural recovery within the magnocellular pathway for observers with high AQ.

DISCUSSION

Here, we conducted two investigations in groups with low and high autistic tendency recruited from within the neurotypical population. Firstly, we asked whether fearful expression affects the P100 and N170 ERP responses in the same way for low and high AQ groups. As expected, fearful expression modulated P100 amplitude in the low AQ group, but not in the high AQ group. In the low AQ group, P100 amplitudes were significantly greater for $F_{LSF}–F_{HSF}$ faces than for $N_{LSF}–N_{HSF}$ faces. Interestingly, while P100 amplitude was significantly greater with $F_{LSF}–F_{HSF}$ than $N_{LSF}–F_{HSF}$ faces, it was not significantly different with $F_{LSF}–F_{HSF}$ and $F_{LSF}–N_{HSF}$ faces. This suggests that the effect

of fearful expression on producing greater P100 amplitude is mostly via fearful expression being carried by LSF. By contrast, in the high AQ group there was an overall reduction in P100 and N170 amplitude and there was no effect of fearful expression on ERP amplitudes. P100 and N170 latencies were faster for the F_{LSF}–F_{HSF} hybrids than for the other conditions, but there were no significant latency differences between the two groups. We used Wiener kernel analysis of the visual evoked potential to investigate whether differences between the low and high AQ groups could reflect differences in magnocellular processing. The K2.1 non-linear VEP response amplitude was higher in the high versus low AQ group, which suggests inefficient neural recovery within the magnocellular stream (Sutherland and Crewther, 2010; Jackson et al., 2013).

We demonstrated that for people with low levels of autistic personality traits, fearful emotion tends to affect the P100 amplitude but not the N170 amplitude. Differences in the effects of our hybrid emotional stimuli on the P100 and N170 can be interpreted in terms of what we know about these early potentials. The literature suggests that P100 amplitude modulation reflects both rapid orienting to salient information (Hillyard and Anllo-Vento, 1998) and rapid identification of threat-related input, such as fearful facial expression (Batty and Taylor, 2003; Pourtois et al., 2004; Magnée et al., 2008; Feng et al., 2009; Luo et al., 2010; Forscher and Li, 2012; Meaux et al., 2013; Zhang et al., 2013). Consistent with this literature, our findings suggest that differences in facial emotion can be processed as early as the P100, but only in groups with low levels of autistic tendency. The N170 amplitude is sensitive to configural processing of faces, yet there are mixed findings as to whether it is influenced by facial emotion (Holmes et al., 2005; Pourtois et al., 2005). Vlamings et al. (2009) found increased N170 amplitude responses to fearful hybrids compared to neutral hybrids, yet in our experiment, these differences were not observed for either AQ group. On the contrary, we did observe some latency differences for the whole sample, with faster N170 responses for F_{LSF}–F_{HSF} hybrids than for the other hybrid conditions. The slower N170 responses for the hybrids with mixed expressions (i.e., F_{LSF}–N_{HSF} and N_{LSF}–F_{HSF}) might reflect disruptions in configural processing of these stimuli (Bentin et al., 1996).

Consistent with Stavropoulos et al. (2016), the P100 and N170 amplitudes were lower in the high AQ group than in the low AQ group, yet contrary to their findings we did not observe any clear P100 or N170 latency differences between the two AQ groups. There are several differences between our experiments that may explain these differences in results. First of all, we used hybrid face stimuli, whereas they used unaltered (i.e., broadband spatial frequency) face stimuli. Secondly, they observed the greatest between-groups differences when the stimuli were presented non-consciously (16 ms presentation time), whereas our stimuli were presented for 500 ms. Finally, their high AQ sample had very low amplitude/high noise ERP results. This may imply that their high AQ sample had greater face processing impairments than our high AQ sample. Given that we recorded clear P100 and N170 responses from both groups, we were able to make meaningful comparisons for the effects of facial emotion on ERP responses in the low and high AQ neurotypical groups.

Differences in the effects of facial emotion on P100 responses for the low and high AQ groups may reflect underlying differences in magnocellular function. In the low AQ group, P100 amplitudes were greater for F_{LSF}–F_{HSF} than N_{LSF}–F_{HSF} faces, yet there was no difference in P100 amplitude for F_{LSF}–F_{HSF} and F_{LSF}–N_{HSF} faces. This is consistent with evidence from Vlamings et al. (2009) that LSF input contributes to rapid detection of fearful expression. Recent studies have demonstrated magnocellular projections from the pulvinar to the orbitofrontal cortex, which allow for rapid feedback to bias visual processing toward behaviorally relevant stimuli (Bar et al., 2006; Kveraga et al., 2007). Given the spatial frequency preferences of the magnocellular and parvocellular pathways (Livingstone and Hubel, 1988), our results are consistent with evidence that the effects of fearful expression on early visual processing are likely to be carried by the magnocellular pathway. The K2.1 non-linear VEP response amplitude was higher in the high AQ group, which suggests inefficient neural recovery within the magnocellular stream (Sutherland and Crewther, 2010; Jackson et al., 2013).

In addition, fearful expression did not tend to affect P100 amplitudes in the high AQ group in any hybrid condition, compared to the low AQ group, which demonstrated sensitivity to hybrid conditions. This suggests that even within the neurotypical population, very early processing of fear-related input varies for individuals with different levels of autistic personality traits. While the exact nature of magnocellular impairment in high autistic tendency individuals remains unresolved (Simmons et al., 2009; Thye et al., 2017); the differences in early ERP responses to fearful faces that we observed for low and high AQ groups could reflect a magnocellular difference in processing LSF facial emotion.

Our results for the non-linear VEP analysis are consistent with magnocellular differences between the low and high AQ groups. Previous investigations of the contrast-response functions for non-linear VEP components (Klistorner et al., 1997; Jackson et al., 2013) indicate that the K2.1 and early components of the K2.2 waveform are of magnocellular origin, whereas the later K2.2 components are of parvocellular origin. Our results are consistent with previous findings that magnocellularly driven VEP non-linearities tend to be greater in groups with high AQ, but parvocellularly driven VEP non-linearities tend to be similar for both groups (Jackson et al., 2013). This implies that the magnocellular pathway recovers less efficiently from rapid stimulation in individuals with high AQ than in individuals with low AQ. Our results suggest that magnocellular projections, which would normally enable rapid detection of threatening stimuli, are less efficient within the broader autistic phenotype. This may contribute to explaining why the high AQ group produced reduced P100 ERP responses to all hybrid face conditions.

The results of our behavioral task are seemingly at odds with our ERP results. Both high and low AQ groups performed similarly in detecting fearful expression in the F_{LSF}–F_{HSF}, F_{LSF}–N_{HSF}, N_{LSF}–F_{HSF}, and N_{LSF}–N_{HSF} hybrid faces. More interestingly, our results indicated that both AQ groups relied upon HSF information to recognize fearful expressions. This HSF preference, however, was elicited in a task that required a

500 ms wait time before response. The conscious detection and report of fearful expression within a hybrid face, as described in prior studies of conscious perception, has demonstrated reliance on HSF facial information (Williams et al., 2004). However, these behavioral measures are not sensitive to very early visual processing stages that precede conscious awareness. We demonstrated differences in ERP responses to fearful and neutral face stimuli as early as 100 ms post-presentation in the low AQ group, but not in the high AQ group. Our non-linear VEP experiment found no significant between-group differences in the parvocellularly driven K2.2 N95 or P150 waveforms, which suggests the differences in the fearful face P100 are magnocellularly driven.

CONCLUSION

In conclusion, for observers with low AQ, we found that fearful expression enhances rapid electrophysiological responses to faces. Our results suggest that this enhancement is likely to occur via rapidly processed, magnocellular input. For observers with high AQ, we did not find any difference in ERP responses to fearful and neutral faces. Consistent with previous studies

(Jackson et al., 2013), our high AQ group showed abnormal temporal processing in the magnocellular pathway. These results support the notion that autism involves differences in processing of LSF information. Our results suggest that magnocellular projections, which would normally enable rapid detection of threatening stimuli, are not utilized efficiently for those with higher autistic tendency. Hence, visual processing differences may underlie some of the socio-cognitive aspects of autism.

AUTHOR CONTRIBUTIONS

AB contributed to this manuscript, including creating the first experimental design, conducting literature review, participant testing sessions, EEG and behavioral analysis and the preparation of this manuscript. LH contributed this manuscript by creating the second experimental design, programming analysis, EEG analysis of second experiment, creating manuscript figures, manuscript section for second experiment and manuscript editing. TF-B contributed by assisting in research participant testing sessions. DC contributed by supervising second experiment design and manuscript editing.

REFERENCES

Aggleton, J. P. (1993). The contribution of the amygdala to normal and abnormal emotional states. *Trends Neurosci.* 16, 328–333. doi: 10.1016/0166-2236(93)90110-8

Allison, T., Puce, A., Spencer, D. D., and McCarthy, G. (1999). Electrophysiological studies of human face perception. I: potentials generated in occipitotemporal cortex by face and non-face stimuli. *Cereb. Cortex* 9, 415–430. doi: 10.1093/cercor/9.5.415

Almeida, R. A., Dickinson, J. E., Maybery, M. T., Badcock, J. C., and Badcock, D. R. (2010). A new step towards understanding Embedded Figures Test performance in the autism spectrum: the radial frequency search task. *Neuropsychologia* 48, 374–381. doi: 10.1016/j.neuropsychologia.2009.09.024

American Psychiatric Association (2013). *Diagnostic and Statistical Manual of Mental Disorders*, 5th Edn. Washington, DC: American Psychiatric Association.

Anzures, G., Goyet, L., Ganea, N., and Johnson, M. H. (2016). Enhanced ERPs to visual stimuli in unaffected male siblings of ASD children. *Child Neuropsychol.* 22, 220–237. doi: 10.1080/09297049.2014.988609

Bailey, A., Le Couteur, A., Gottesman, I., Bolton, P., Simonoff, E., Yuzda, E., et al. (1995). Autism as a strongly genetic disorder: evidence from a British twin study. *Psychol. Med.* 25, 63–77. doi: 10.1017/S0033291700028099

Bailey, A. J., Braeutigam, S., Jousmäki, V., and Swithenby, S. J. (2005). Abnormal activation of face processing systems at early and intermediate latency in individuals with autism spectrum disorder: a magnetoencephalographic study. *Eur. J. Neurosci.* 21, 2575–2585. doi: 10.1111/j.1460-9568.2005.04061.x

Bar, M., Kassam, K. S., Ghuman, A. S., Boshyan, J., Schmid, A. M., Dale, A. M., et al. (2006). Top-down facilitation of visual recognition. *Proc. Natl. Acad. Sci. U.S.A.* 103, 449–454. doi: 10.1073/pnas.0507062103

Baron-Cohen, S., Wheelwright, S., Skinner, R., Martin, J., and Clubley, E. (2001). The autism-spectrum quotient (AQ): evidence from asperger syndrome/high-functioning autism, males and females, scientists and mathematicians. *J. Autism Dev. Disord.* 31, 5–17.

Baseler, H. A., and Sutter, E. E. (1997). M and P components of the VEP and their visual field distribution. *Vision Res.* 37, 675–690.

Batty, M., Meaux, E., Wittemeyer, K., Roge, B., and Taylor, M. J. (2011). Early processing of emotional faces in children with autism: an event-related potential study. *J. Exp. Child Psychol.* 109, 430–444. doi: 10.1016/j.jecp.2011.02.001

Batty, M., and Taylor, M. J. (2003). Early processing of the six basic facial emotional expressions. *Cogn. Brain Res.* 17, 613–620. doi: 10.1016/S0926-6410(03)00174-5

Bentin, S., Allison, T., Puce, A., Perez, E., and McCarthy, G. (1996). Electrophysiological studies of face perception in humans. *J. Cogn. Neurosci.* 8, 551–565. doi: 10.1162/jocn.1996.8.6.551

Bertone, A., Mottron, L., Jelenic, P., and Faubert, J. (2003). Motion perception in autism: a "complex" issue. *J. Cogn. Neurosci.* 15, 218–225. doi: 10.1162/089892903321208150

Bonnard-Couton, V., Iakimova, G., Le Gall, E., Dor-Nedonsel, E., and Askenazy, F. (2015). Emotional face perception: event-related potentials (ERPS) contribution to differentiate schizophrenia and autism spectrum disorders in adolescents. *Eur. Child Adolesc. Psychiatry* 24, S196–S196.

Braddick, O., Atkinson, J., and Wattam-Bell, J. (2003). Normal and anomalous development of visual motion processing: motion coherence and 'dorsal-stream vulnerability'. *Neuropsychologia* 41, 1769–1784. doi: 10.1016/S0028-3932(03)00178-7

Bullier, J. (2001). Integrated model of visual processing. *Brain Res. Rev.* 36, 96–107. doi: 10.1016/S0165-0173(01)00085-6

Clark, V. P., and Hillyard, S. A. (1996). Spatial selective attention affects early extrastriate but not striate components of the visual evoked potential. *J. Cogn. Neurosci.* 8, 387–402. doi: 10.1162/jocn.1996.8.5.387

Crewther, D. P., Brown, A., and Hugrass, L. (2016). Temporal structure of human magnetic evoked fields. *Exp. Brain Res.* 234, 1987–1995. doi: 10.1007/s00221-016-4601-0

Dakin, S., and Frith, U. (2005). Vagaries of visual perception in autism. *Neuron* 48, 497–507. doi: 10.1016/j.neuron.2005.10.018

Dale, N., and Salt, A. (2008). Social identity, autism and visual impairment (VI) in the early years. *Br. J. Vis. Impair.* 26, 135–146. doi: 10.1177/0264619607088282

De Jong, M. C., van Engeland, H., and Kemner, C. (2008). Attentional effects of gaze shifts are influenced by emotion and spatial frequency, but not in autism. *J. Am. Acad. Child Adolesc. Psychiatry* 47, 443–454. doi: 10.1097/CHI.0b013e31816429a6

De Valois, L., and De Valois, K. K. (1988). Spatial vision. *Exp. Physiol.* 74, 85. doi: 10.1113/expphysiol.1989.sp003247

Del Viva, M. M., Igliozzi, R., Tancredi, R., and Brizzolara, D. (2006). Spatial and motion integration in children with autism. *Vision Res.* 46, 1242–1252. doi: 10.1016/j.visres.2005.10.018

Demos, K. E., Kelley, W. M., Ryan, S. L., Davis, F. C., and Whalen, P. J. (2008). Human amygdala sensitivity to the pupil size of others. *Cereb. Cortex* 18, 2729–2734. doi: 10.1093/cercor/bhn034

Feng, W., Luo, W., Liao, Y., Wang, N., Gan, T., and Luo, Y. J. (2009). Human brain responsivity to different intensities of masked fearful eye whites: an ERP study. *Brain Res.* 1286, 147–154. doi: 10.1016/j.brainres.2009.06.059

Forscher, E. C., and Li, W. (2012). Hemispheric asymmetry and visuo-olfactory integration in perceiving subthreshold (micro) fearful expressions. *J. Neurosci.* 32, 2159–2165. doi: 10.1523/JNEUROSCI.5094-11.2012

Fujita, T., Kamio, Y., Yamasaki, T., Yasumoto, S., Hirose, S., and Tobimatsu, S. (2013). Altered automatic face processing in individuals with high-functioning autism spectrum disorders: evidence from visual evoked potentials. *Res. Autism Spectr. Disord.* 7, 710–720. doi: 10.1016/j.rasd.2013.03.001

Henson, R. N., Goshen-Gottstein, Y., Ganel, T., Otten, L. J., Quayle, A., and Rugg, M. D. (2003). Electrophysiological and haemodynamic correlates of face perception, recognition and priming. *Cereb. Cortex* 13, 793–805. doi: 10.1093/cercor/13.7.793

Hillyard, S. A., and Anllo-Vento, L. (1998). Event-related brain potentials in the study of visual selective attention. *Proc. Natl. Acad. Sci. U.S.A.* 95, 781–787.

Holmes, A., Winston, J. S., and Eimer, M. (2005). The role of spatial frequency information for ERP components sensitive to faces and emotional facial expression. *Cogn. Brain Res.* 25, 508–520. doi: 10.1016/j.cogbrainres.2005.08.003

Jackson, B. L., Blackwood, E. M., Blum, J., Carruthers, S. P., Nemorin, S., Pryor, B. A., et al. (2013). Magno- and parvocellular contrast responses in varying degrees of autistic trait. *PLOS ONE* 8:e66797. doi: 10.1371/journal.pone.0066797

Johnson, M. H. (2005). Subcortical face processing. *Nat. Rev. Neurosci.* 6, 766–774. doi: 10.1038/nrn1766

Kellerman, G. R., Fan, J., and Gorman, J. M. (2005). Auditory abnormalities in autism: toward functional distinctions among findings. *CNS Spectr.* 10, 748–756. doi: 10.1017/S1092852900019738

Key, A. P., and Corbett, B. A. (2014). ERP responses to face repetition during passive viewing: a nonverbal measure of social motivation in children with autism and typical development. *Dev. Neuropsychol.* 39, 474–495. doi: 10.1080/87565641.2014.940620

Klistorner, A., Crewther, D. P., and Crewther, S. G. (1997). Separate magnocellular and parvocellular contributions from temporal analysis of the multifocal VEP. *Vision Res.* 37, 2161–2169. doi: 10.1016/S0042-6989(97)00003-5

Kragel, P. A., Knodt, A. R., Hariri, A. R., and LaBar, K. S. (2016). Decoding spontaneous emotional states in the human brain. *PLOS Biol.* 14:e2000106. doi: 10.1371/journal.pbio.2000106

Kragel, P. A., and LaBar, K. S. (2015). Multivariate neural biomarkers of emotional states are categorically distinct. *Soc. Cogn. Affect. Neurosci.* 10, 1437–1448. doi: 10.1093/scan/nsv032

Kveraga, K., Boshyan, J., and Bar, M. (2007). Magnocellular projections as the trigger of top-down facilitation in recognition. *J. Neurosci.* 27, 13232–13240. doi: 10.1523/jneurosci.3481-07.2007

Laeng, B., Profeti, I., Saether, L., Adolfsdottir, S., Lundervold, A. J., Vangberg, T., et al. (2010). Invisible expressions evoke core impressions. *Emotion* 10, 573–586. doi: 10.1037/a0018689

Laeng, B., Saether, L., Holmlund, T., Wang, C. E. A., Waterloo, K., Eisemann, M., et al. (2013). Invisible emotional expressions influence social judgments and pupillary responses of both depressed and non-depressed individuals. *Front. Psychol.* 4:291. doi: 10.3389/fpsyg.2013.00291

Lassalle, A., and Itier, R. J. (2015). Autistic traits influence gaze-oriented attention to happy but not fearful faces. *Soc. Neurosci.* 10, 70–88. doi: 10.1080/17470919.2014.958616

Laycock, R., Crewther, S. G., and Crewther, D. P. (2007). A role for the 'magnocellular advantage' in visual impairments in neurodevelopmental and psychiatric disorders. *Neurosci. Biobehav. Rev.* 31, 363–376. doi: 10.1016/j.neubiorev.2006.10.003

LeDoux, J. E. (1998). *The Emotional Brain: The Mysterious Underpinnings of Emotional Life,* 1st Edn. New York, NY: Simon & Schuster.

Livingstone, M., and Hubel, D. (1988). Segregation of form, color, movement, and depth: anatomy, physiology, and perception. *Science* 240, 740–749.

Luo, W. B., Feng, W. F., He, W. Q., Wang, N. Y., and Luo, Y. J. (2010). Three stages of facial expression processing: ERP study with rapid serial visual presentation. *Neuroimage* 49, 1857–1867. doi: 10.1016/j.neuroimage.2009.09.018

Magnée, M. J., de Gelder, B., van Engeland, H., and Kemner, C. (2008). Atypical processing of fearful face–voice pairs in Pervasive Developmental Disorder: an ERP study. *Clin. Neurophysiol.* 119, 2004–2010. doi: 10.1016/j.clinph.2008.05.005

Mangun, G. R., Hopfinger, J. B., Kussmaul, C. L., Fletcher, E. M., and Heinze, H. J. (1997). Covariations in ERP and PET measures of spatial selective attention in human extrastriate visual cortex. *Hum. Brain Mapp.* 5, 273–279. doi: 10.1002/(SICI)1097-019319975:4

McCleery, J. P., Akshoomoff, N., Dobkins, K. R., and Carver, L. J. (2009). Atypical face versus object processing and hemispheric asymmetries in 10-month-old infants at risk for autism. *Biol. Psychiatry* 66, 950–957. doi: 10.1016/j.biopsych.2009.07.031

Meaux, E., Roux, S., and Batty, M. (2013). Early visual ERPs are influenced by individual emotional skills. *Soc. Cogn. Affect. Neurosci.* 9, 1089–1098. doi: 10.1093/scan/nst084

Milne, E., White, S., Campbell, R., Swettenham, J., Hansen, P., and Ramus, F. (2006). Motion and form coherence detection in autistic spectrum disorder: relationship to motor control and 2: 4 digit ratio. *J. Autism Dev. Disord.* 36, 225–237. doi: 10.1007/s10803-005-0052-3

Morris, J. S., DeGelder, B., Weiskrantz, L., and Dolan, R. J. (2001). Differential extrageniculostriate and amygdala responses to presentation of emotional faces in a cortically blind field. *Brain* 124, 1241–1252. doi: 10.1093/brain/124.6.1241

Morris, J. S., Friston, K. J., Buchel, C., Frith, C. D., Young, A. W., Calder, A. J., et al. (1998a). A neuromodulatory role for the human amygdala in processing emotional facial expressions. *Brain* 121, 47–57. doi: 10.1093/Brain/121.1.47

Morris, J. S., Ohman, A., and Dolan, R. J. (1998b). Conscious and unconscious emotional learning in the human amygdala. *Nature* 393, 467–470. doi: 10.1038/30976

Öhman, A. (2005). The role of the amygdala in human fear: automatic detection of threat. *Psychoneuroendocrinology* 30, 953–958. doi: 10.1016/j.psyneuen.2005.03.019

Pegna, A. J., Landis, T., and Khateb, A. (2008). Electrophysiological evidence for early non-conscious processing of fearful facial expressions. *Int. J. Psychophysiol.* 70, 127–136. doi: 10.1016/j.ijpsycho.2008.08.007

Pellicano, E., Gibson, L., Maybery, M., Durkin, K., and Badcock, D. R. (2005). Abnormal global processing along the dorsal visual pathway in autism: a possible mechanism for weak visuospatial coherence? *Neuropsychologia* 43, 1044–1053. doi: 10.1016/j.neuropsychologia.2004.10.003

Pizzagalli, D., Regard, M., and Lehmann, D. (1999). Rapid emotional face processing in the human right and left brain hemispheres: an ERP study. *Neuroreport* 10, 2691–2698. doi: 10.1097/00001756-199909090-00001

Pourtois, G., Dan, E. S., Grandjean, D., Sander, D., and Vuilleumier, P. (2005). Enhanced extrastriate visual response to bandpass spatial frequency filtered fearful faces: time course and topographic evoked-potentials mapping. *Hum. Brain Mapp.* 26, 65–79. doi: 10.1002/hbm.20130

Pourtois, G., Grandjean, D., Sander, D., and Vuilleumier, P. (2004). Electrophysiological correlates of rapid spatial orienting towards fearful faces. *Cereb. Cortex* 14, 619–633. doi: 10.1093/cercor/bhh023

Prete, G., Capotosto, P., Zappasodi, F., Laeng, B., and Tommasi, L. (2015a). The cerebral correlates of subliminal emotions: an eleoencephalographic study with emotional hybrid faces. *Eur. J. Neurosci.* 42, 2952–2962. doi: 10.1111/ejn.13078

Prete, G., D'Ascenzo, S., Laeng, B., Fabri, M., Foschi, N., and Tommasi, L. (2015b). Conscious and unconscious processing of facial expressions: evidence from two split-brain patients. *J. Neuropsychol.* 9, 45–63. doi: 10.1111/jnp.12034

Prete, G., Laeng, B., Fabri, M., Foschi, N., and Tommasi, L. (2015c). Right hemisphere or valence hypothesis, or both? The processing of hybrid faces in the intact and callosotomized brain. *Neuropsychologia* 68, 94–106. doi: 10.1016/j.neuropsychologia.2015.01.002

Prete, G., Laeng, B., and Tommasi, L. (2014). Lateralized hybrid faces: evidence of a valence-specific bias in the processing of implicit emotions. *Laterality* 19, 439–454. doi: 10.1080/1357650X.2013.862255

Prete, G., Laeng, B., and Tommasi, L. (2016). Modulating adaptation to emotional faces by spatial frequency filtering. *Psychol. Res.* doi: 10.1007/s00426-016-0830-x [Epub ahead of print].

Rafal, R. D., Koller, K., Bultitude, J. H., Mullins, P., Ward, R., Mitchell, A. S., et al. (2015). Connectivity between the superior colliculus and the amygdala in humans and macaque monkeys: virtual dissection with probabilistic DTI tractography. *J. Neurophysiol.* 114, 1947–1962. doi: 10.1152/jn.01016.2014

Ruzich, E., Allison, C., Smith, P., Watson, P., Auyeung, B., Ring, H., et al. (2015). Measuring autistic traits in the general population: a systematic review of the Autism-Spectrum Quotient (AQ) in a nonclinical population sample of 6,900 typical adult males and females. *Mol. Autism* 6:2.

Schiller, P. H., Malpeli, J. G., and Schein, S. J. (1979). Composition of geniculostriate input ot superior colliculus of the rhesus monkey. *J. Neurophysiol.* 42, 1124–1133.

Schyns, P. G., and Oliva, A. (1999). Dr. Angry and Mr. Smile: when categorization flexibly modifies the perception of faces in rapid visual presentations. *Cognition* 69, 243–265. doi: 10.1016/S0010-0277(98)00069-9

Simmons, D. R., Robertson, A. E., McKay, L. S., Toal, E., McAleer, P., and Pollick, F. E. (2009). Vision in autism spectrum disorders. *Vision Res.* 49, 2705–2739. doi: 10.1016/j.visres.2009.08.005

Smith, E., Weinberg, A., Moran, T., and Hajcak, G. (2013). Electrocortical responses to NIMSTIM facial expressions of emotion. *Int. J. Psychophysiol.* 88, 17–25. doi: 10.1016/j.ijpsycho.2012.12.004

Stavropoulos, K. K. M., Viktorinova, M., Naples, A., Foss-Feig, J., and McPartland, J. C. (2016). Autistic traits modulate conscious and nonconscious face perception. *Soc. Neurosci.* doi: 10.1080/17470919.2016.1248788 [Epub ahead of print].

Stein, T., Seymour, K., Hebart, M. N., and Sterzer, P. (2014). Rapid fear detection relies on high spatial frequencies. *Psychol. Sci.* 25, 566–574. doi: 10.1177/0956797613512509

Streit, M., Dammers, J., Simsek-Kraues, S., Brinkmeyer, J., Wolver, W., and Ioannides, A. (2003). Time course of regional brain activations during facial emotion recognition in humans. *Neurosci. Lett.* 342, 101–104. doi: 10.1016/S0304-3940(03)00274-X

Sutherland, A., and Crewther, D. P. (2010). Magnocellular visual evoked potential delay with high autism spectrum quotient yields a neural mechanism for altered perception. *Brain* 133, 2089–2097. doi: 10.1093/brain/awq122

Tadel, F., Baillet, S., Mosher, J. C., Pantazis, D., and Leahy, R. M. (2011). Brainstorm: a user-friendly application for MEG/EEG analysis. *Comput. Intell. Neurosci.* 2011:879716. doi: 10.1155/2011/879716

Tamietto, M., Pullens, P., De Gelder, B., Weiskrantz, L., and Goebel, R. (2012). Subcortical connections to human amygdala and changes following destruction of the visual cortex. *Curr. Biol.* 22, 1449–1455. doi: 10.1016/j.cub.2012.06.006

Thompson, J. I., Peck, C. E., Karvelas, G., Hartwell, C. A., Guarnaccia, C., Brown, A., et al. (2015). Temporal processing as a source of altered visual perception in high autistic tendency. *Neuropsychologia* 69, 148–153. doi: 10.1016/j.neuropsychologia.2015.01.046

Thye, M. D., Bednarz, H. M., Herringshaw, A. J., Sartin, E. B., and Kana, R. K. (2017). The impact of atypical sensory processing on social impairments in Autism Spectrum Disorder. *Dev. Cogn. Neurosci.* doi: 10.1016/j.dcn.2017.04.010 [Epub ahead of print].

Tottenham, N., Tanaka, J. W., Leon, A. C., McCarry, T., Nurse, M., Hare, T. A., et al. (2009). The NimStim set of facial expressions: judgments from untrained research participants. *Psychiatry Res.* 168, 242–249. doi: 10.1016/j.psychres.2008.05.006

Tye, C., Mercure, E., Ashwood, K. L., Azadi, B., Asherson, P., Johnson, M. H., et al. (2013). Neurophysiological responses to faces and gaze direction differentiate children with ASD, ADHD and ASD plus ADHD. *Dev. Cogn. Neurosci.* 5, 71–85. doi: 10.1016/j.dcn.2013.01.001

Vlamings, P. H., Goffaux, V., and Kemner, C. (2009). Is the early modulation of brain activity by fearful facial expressions primarily mediated by coarse low spatial frequency information? *J. Vis.* 9, 12.1–12.13. doi: 10.1167/9.5.12

Vlamings, P. H. J. M., Jonkman, L. M., van Daalen, E., van der Gaag, R. J., and Kemner, C. (2010). Basic abnormalities in visual processing affect face processing at an early age in Autism Spectrum Disorder. *Biol. Psychiatry* 68, 1107–1113. doi: 10.1016/j.biopsych.2010.06.024

Vuilleumier, P., Armony, J. L., Driver, J., and Dolan, R. J. (2003). Distinct spatial frequency sensitivities for processing faces and emotional expressions. *Nat. Neurosci.* 6, 624–631. doi: 10.1038/nn1057

Wagner, J. B., Hirsch, S. B., Vogel-Farley, V. K., Redcay, E., and Nelson, C. A. (2013). Eye-tracking, autonomic, and electrophysiological correlates of emotional face processing in adolescents with Autism Spectrum Disorder. *J. Autism Dev. Disord.* 43, 188–199. doi: 10.1007/s10803-012-1565-1

Williams, M. A., Morris, A. P., McGlone, F., Abbott, D. F., and Mattingley, J. B. (2004). Amygdala responses to fearful and happy facial expressions under conditions of binocular suppression. *J. Neurosci.* 24, 2898–2904. doi: 10.1523/JNEUROSCI.4977-03.2004

Wong, T. K. W., Fung, P. C. W., Chua, S. E., and McAlonan, G. M. (2008). Abnormal spatiotemporal processing of emotional facial expressions in childhood autism: dipole source analysis of event-related potentials. *Eur. J. Neurosci.* 28, 407–416. doi: 10.1111/j.1460-9568.2008.06328.x

Zhang, D., Luo, W., and Luo, Y. (2013). Single-trial ERP analysis reveals facial expression category in a three-stage scheme. *Brain Res.* 1512, 78–88. doi: 10.1016/j.brainres.2013.03.044

Conflict of Interest Statement: The authors declare that the research was conducted in the absence of any commercial or financial relationships that could be construed as a potential conflict of interest.

frontiers
in Behavioral Neuroscience

Frontal EEG Asymmetry of Mood: A Mini-Review

Massimiliano Palmiero [1,2]* and Laura Piccardi [1,3]

[1] *Neuropsychology Unit, IRCCS Fondazione Santa Lucia, Rome, Italy,* [2] *Department of Biotechnological and Applied Clinical Sciences, University of L'Aquila, L'Aquila, Italy,* [3] *Department of Life, Health and Environmental Sciences, University of L'Aquila, L'Aquila, Italy*

The present mini-review was aimed at exploring the frontal EEG asymmetry of mood. With respect to emotion, interpreted as a discrete affective process, mood is more controllable, more nebulous, and more related to mind/cognition; in addition, causes are less well-defined than those eliciting emotion. Therefore, firstly, the rational for the distinction between emotion and mood was provided. Then, the main frontal EEG asymmetry models were presented, such as the motivational approach/withdrawal, valence/arousal, capability, and inhibition asymmetric models. Afterward, the frontal EEG asymmetry of mood was investigated following three research lines, that is considering studies involving different mood induction procedures, dispositional mood (positive and negative affect), and mood alterations in both healthy and clinical populations. In general, results were found to be contradictory, no model is unequivocally supported regardless the research line considered. Different methodological issues were raised, such as: the composition of samples used across studies, in particular, gender and age were found to be critical variables that should be better addressed in future studies; the importance of third variables that might mediate the relationship between frontal EEG asymmetries and mood, for example bodily states and hormonal responses; the role of cognition, namely the interplay between mood and executive functions. In light of these issues, future research directions were proposed. Amongst others, the need to explore the neural connectivity that underpins EEG asymmetries, and the need to include both positive and negative mood conditions in the experimental designs have been highlighted.

Keywords: emotion, disposition, frontal asymmetry, mood induction, individual differences, depression, gender, pre-frontal cortex

In these last decades, the cognitive neuroscience of emotion has enormously increased, aiming at improving the understanding of the biological basis of emotional processing in both healthy and clinical populations. A variety of approaches have been used so far, including functional Magnetic Resonance Imaging (fMRI). However, given the high temporal resolution of the electroencephalography (EEG), the change of EEG signals has been extensively used to detect real-time emotional processes that arise following a series of external/internal stimuli or events. One of the most prolific research lines has focused on the investigation of frontal EEG asymmetries of emotion and affect-related phenomena (e.g., mood). In this vein, moving from the rational that emotion and mood are distinct affective processes, the present mini-review was aimed at clarifying the EEG frontal asymmetry of mood. At the aim a selection of those EEG studies focused on mood induction, dispositional mood (e.g., positive and negative affect) and mood alterations in

both healthy and clinical populations (e.g., depression and anxiety) were reviewed. Of course, the goal was not to systematically review all studies on the mood frontal asymmetry, but rather provide examples for the most important research lines in order to get insights about the current status of the research, in order to detect possible methodological- or theoretical-related issues and to draw possible future scenarios.

DIFFERENCES BETWEEN EMOTION AND MOOD

Emotion and mood are two distinct affective processes for different reasons. Beedie et al. (2005) revealed that eight themes were cited by both non-academics and academics (scientific literature). Excluding duration (emotion was evaluated both shorter and longer than mood) and function (intrinsic property to both processes), at least six reliable criteria were identified: causes, consequences, intentionality, intensity, physiology, and awareness of the cause. On the one hand, emotion involves specific causes, consequences on behavior, direction at something, high intensity, physical chemical response (e.g., adrenaline/fear), identification of the cause. On the other hand, mood is characterized by no specific causes, consequences on cognition, no specific direction at something, low intensity, psychological response and hormonal influences, no identification of the cause. In addition, emotion cannot be controlled (Ekman and Davidson, 1994), whereas mood can be controlled (Parkinson et al., 1996) and experimentally manipulated via different induction procedures, for example using music (e.g., Thompson et al., 2001; Palmiero et al., 2015, 2016). Emotion is mostly showed by facial expressions (Ekman, 1994), is clearly defined (Parkinson et al., 1996), whereas mood is hidden to others or expressed via body postures (Parkinson et al., 1996), and is more nebulous (Vallerand and Blanchard, 2000). Emotion is related to the heart and feeling, mood to the mind and thinking (Beedie et al., 2005). In addition, according to Scherer (2005) emotion is also characterized by response synchronization, that would play a key role on the preparation of the organism in order to face the emotional situation that has arisen by a specific cause; on the contrary, response synchronization is not important for mood because the organism must not prepare appropriate responses to unidentifiable eliciting causes.

EEG FRONTAL ASYMMETRY OF EMOTION: THE BASIC MODELS

The pioneristic frontal EEG asymmetry model (Davidson, 1983, 1993) supports the view that the activity of brain systems both moderates motivational trait tendencies to approach/withdraw novel emotional stimuli and mediate approach/withdrawal motivational tendencies underlying emotion. According to this model, an increase of the left prefrontal activity, either as a trait or as a state, is associated to approach-related emotions (e.g., positive), whereas an increase of the right prefrontal activity is associated to withdrawal-related emotions (e.g., negative).

According to the valence-arousal model (e.g., Heller, 1990, 1993; Berntson et al., 2011) the valence of emotions would be more important than the motivational tendencies: positive emotions are specifically associated with more left than right hemispheric activity, whereas negative emotions are associated with more right than left hemispheric activity.

In general, these two models diverge conceptually but overlap in terms of empirical predictions (Spielberg et al., 2008), that is, positive emotions are linked to approach-related motivation, whereas negative emotions to withdrawal-related motivation. With a few exceptions (e.g., Mller et al., 1999; Elgavish et al., 2003), the most of studies confirmed these asymmetry models (for review see Davidson et al., 2000; Coan and Allen, 2004). However, results collected with anger, which involves a negative valence but also an approach tendency (e.g., Berkowitz, 1999), raised doubt on the assumptions of the asymmetry models. Indeed, different studies demonstrated that anger yielded an increase of left rather than of right frontal EEG activity (e.g., Harmon-Jones, 2004a; Hewig et al., 2004; Gable and Poole, 2014; for a review see Harmon-Jones, 2004b). Collectively, these results show that EEG frontal asymmetry reflects the direction of the motivation rather than the valence of emotion.

More recently, Coan et al. (2006) proposed the capability model, which basically posits that, besides affective dispositions under resting condition, the situational variable plays a key role on the frontal EEG asymmetry. In other words, frontal EEG activity would rely on specific emotional contexts and individuals' capacity to respond emotionally (approaching vs. withdrawal responses) or to inhibit responses to the situation that has contributed to elicit emotions.

Yet, moving from the evidence that inhibitory processes are very important for emotional asymmetries (Jackson et al., 2003; Davidson, 2004; Coan et al., 2006), Grimshaw and Carmel (2014) proposed the asymmetric inhibition model, by which asymmetries can be interpreted in terms of executive control: mechanisms in left frontal cortex would inhibit negative distractors, whereas mechanisms in right frontal cortex would inhibit positive distractors. Different studies supported these predictions. For example, difficulty in releasing attention from negative stimuli was found to rely on low left frontal activity, as occurs in depression and anxious arousal (e.g., Cisler and Koster, 2010), whereas difficulty in inhibiting positive distractions was found to rely on low right frontal activity, as occurs in poor self-regulation and addiction (e.g., Goldstein and Volkow, 2011).

FRONTAL EEG ASYMMETRY OF MOOD

Three research lines were followed, that is studies exploring the relationships between frontal EEG asymmetries and: (1) mood states induced by different experimental procedures (e.g., film clips, music, faces); (2) dispositional mood (positive and negative affect); (3) mood alterations in both healthy and clinical populations (see **Table 1** for details).

TABLE 1 | List of studies for each research line.

MOOD INDUCTION

Study	Method	Subjects	Main result
Tucker et al., 1981	Textbook descriptions of euphoria and depression	10 (6 females); Students	Depression: ↑RFA
Tomarken et al., 1990	Positive and negative film clips Subjective emotional responses to film clips	32 females 17–41 years	NA: ↑RFA
Wheeler et al., 1993	As in Tomarken et al. (1990), but baseline EEG recorded twice 3 weeks apart; subjects with stable patterns of asymmetry	26 females 17–21 years	NA: ↑RFA; PA: ↑LFA
Gotlib et al., 1998: Study 2	Sad mood induced using negative music Non-verbal fluency task for control condition	59 females divided in: high vulnerable ↓LFA; low vulnerable ↑LFA	No relationship between EEG asymmetry, mood, cognitive functioning
Gale et al., 2001	Pictures of sad and happy faces Eysenck Personality Inventory Subjective emotional response to faces	30 females 18–36 years	Negative mood: ↑LFA Extraversion: ↑RFA for PA; Neuroticism: ↑left/right ratios and ↓RFA
Dennis and Solomon, 2010	Emotion regulation: self-reported change in negative mood induced using fearful, sad, neutral film clips; attention interference in a task with mood congruent emotional distractors	66 (40 females) 18–59 years	↑FA during mood inductions vs. baseline: more emotion regulation No significant asymmetry
Kop et al., 2011	Recall of happy and anger incidents	20/30 (55% females) Mean age 25 years	Positive mood: RFA
Rodriguez et al., 2015	Sadness induced while participants virtually navigated through a park by music, Velten self-statements, pictures, movies	24 (12 females) 19–36 years 9 controls; 9 reappraisal; 9 expressive/suppression	Sadness: ↑RFA only in controls
Warden-Smith et al., 2017	Light-pleasant smell to optimize positive psychophysiological benefit	24 for stage 1 64 for stage 2 NFA (difference between Alpha-wave activity in the right and left frontal hemispheres) and PFA groups.	Negative group (NFA): ↓RFA and ↑LFA No significant effect on the positive group

DISPOSITIONAL MOOD

Study	Mood Measures	Subjects	Main Results
Tomarken et al., 1992a	Baseline EEG on two occasions 3 weeks apart; PANAS	90 females 17–21 years	LFA: ↑PA, ↓NA compared with RFA
Tomarken et al., 1992b	As in Tomarken et al. (1992a)	85 females 17–21 years	As in Tomarken et al. (1992a)
Jacobs and Snyder, 1996	PANAS; BDI	40 males 18–53 years	↑LFA: ↓NA and ↓BDI
Sutton and Davidson, 1997	Baseline EEG on two occasions 6 weeks apart PANAS first session; BIS/BAS scales second session	46 (23 females) 18–22 years	No relationship between Pre-Frontal EEG asymmetry and PA or NA
Hagemann et al., 1999	Transient Mood assessed on a 0-9 scale; PANAS Eysenck Personality Questionnaire	36 (24 females) Mean age 24.7	Subjects with ↑NA: ↑LTA (but not LFA) than in subjects with ↓NA. No relation between asymmetry and PA
Hall and Petruzzello, 1999	PASE; STAI-Y2; PANAS; GDS; SWLS	41 (26 females) Mean age 68.7	LFA predicted PA High-active group: FA predicted affective valence and SWL Low active group: FA predicted NA
Mikolajczak et al., 2010	Trait Emotional Intelligence Questionnaire	31 (25 females) Mean age 22.4	No relationship between EEG FA and well-being subscale

MOOD ALTERATIONS

Study	Method	Subjects	Main Results
Schaffer et al., 1983	BDI	15 (10 females)	↑RFA: ↑BDI

(Continued)

TABLE 1 | Continued

Study	Method	Subjects	Main Results
Henriques and Davidson, 1990	BDI; Hamilton Rating Scale for Depression	14 (6 previously depressed) Mean age previously depressed 37.4 Mean age controls 34.7	↓LFA in previously depressed subjects relative to controls; no difference between groups on self-reported emotional state
Henriques and Davidson, 1991	BDI; Hamilton Rating Scale for Depression	28 (18 females) 15 currently depressed: 33–57 years 13 controls: 40–61 years	↓LFA in currently depressed subjects relative to controls; no correlation between FA and state ratings of emotion at the time of the baseline recording and depression
Allen et al., 1993	Pre-post bright light treatment	8 females (4 with Seasonal Affective Disorder)	↓LFA in Seasonal Affective Disorder relative to Control
Tomarken and Davidson, 1994	MC; STAI; BDI	90 females	Repressors ↑LFA than non-repressors No asymmetry difference between high-anxiety and low-anxiety, high-depression and low-depression groups
Gotlib et al., 1998: Study 1	Inventory to Diagnose Depression (IDD); Lifetime version of the IDD; 2 modules of the DSMIII-R: Major Depressive Disorder and Dysthymic Disorder	77 females 30 never depressed; 31 previously depressed; 16 currently depressed	↓LFA in currently depressed and previously depressed subjects compared to never depressed subjects
Reid et al., 1998	Study 1: BDI Study 2: DSM-III-R	Study 1: 36 females (17 depressed) Mean age 18.53 Study 2: 27 females (13 depressed) Mean age 27.54	No frontal asymmetry between depressed and non-depressed subjects in both studies
Papousek and Schulter, 2002	Study 1: Anxious tension anchored 17-point bipolar rating scale; Negative mood assessed by an adjective checklist Study 2: separate scales for state depression and state anxiety	Study 1: 56 (30 female): 18–36 years Study 2: 128 (68 female): 18–31 years	Anxiety, tension, and depression decrease when frontopolar activation asymmetry shifted to the right hemisphere
Mathersul et al., 2008	Depression Anxiety Stress Scales (DASS-21)	428 (214 females) 18–60 years	↑RFA associated to anxious arousal ↑LFA associated to anxious apprehension and to non-depression Symmetrical frontal activity associated to depression and comorbidity

↑, Increased; ↓, Decreased; LFA, Left Frontal Activation; RFA, Right Frontal Activation; LTA, Left Temporal Activation; NFA, Negative Frontal Asymmetry; PFA, Positive Frontal Asymmetry; PANAS, Positive and Negative Affect Schedule; NA, Negative Affect; PA, Positive Affect; EEG, Electroencephalography; BIS, Behavioral Inhibition System; BAS, Behavioral Activation system; PASE, Physical Activity Scale for Elderly; STAY-Y2, State-Trait Anxiety Inventory (Trait); GDS, Geriatric Depression Scale; MC, Marlowe-Crowne Social Desirability Scale; SWLS, Satisfaction with Life Scale.

EEG FRONTAL ASYMMETRY AND INDUCTION OF MOOD STATE

In one of the first studies, Tucker et al. (1981) revealed that the induced euphoria mood state generated symmetry, whereas the induced depression mood state was associated with greater activation of the right frontal lobe. Tomarken et al. (1990) also found that subjects' asymmetry predicted the level of negative affect in response to the negative film clips, which was related to greater activation in the right hemisphere. Using data from those subjects with stable patterns of asymmetry across 3-weeks period, Wheeler et al. (1993) replicated Tomarken et al. (1990) results, and also found greater left frontal activation associated with reports of more intense positive affect in response to the positive films. Rodriguez et al. (2015) also found significant activations in different right frontal regions due to the induction of negative mood in the control group but not in cognitive

reappraisal and expressive suppression groups. Collectively, these results suggest that hypoactivation of the left frontal region is an individual predisposition that underlies elevated responsivity to negative stimuli, increasing the risk for mood disorders, especially depression. However, Gale et al. (2001) revealed greater activation of the left frontal hemisphere with negative mood, whereas participants' personality (and gender of the face viewed) mediated the direction of the differentiation between positive and negative mood in the right hemisphere. Indeed, extraverts showed greater right hemisphere activation for positive affect, whereas, neurotics showed increased left/right ratios and less activated right hemisphere. Kop et al. (2011) also found increased right frontal activation during induced positive mood induction, which was associated with a decrease in low frequency/high frequency ratio of the heart rate variability. Interestingly, Warden-Smith et al. (2017) showed that a positive mood induction yielded a decrease of right frontal asymmetry

and an increase of left frontal asymmetry in negative alpha fontal group, as if a change in alphawave activity in the direction of positive affect occurred in people susceptible to negative affect. Yet, Gotlib et al. (1998) found in the study 2 that frontal EEG asymmetry was unrelated to mood reactivity and cognitive functioning. Dennis and Solomon (2010) also found that induced fear and anger were not related to greater right frontal asymmetry, but rather to bilateral activity.

EEG FRONTAL ASYMMETRY AND DISPOSITIONAL MOOD

In one large research project (e.g., Tomarken et al., 1992a,b), females with stable greater right frontal activation across two different sessions reported increased Negative Affect (NA), whereas females with stable left frontal activation reported increased Positive Affect (PA). However, Jacobs and Snyder (1996) only revealed that left lateral-frontal activation yielded lower score of NA in men, whereas Hall and Petruzzello (1999) showed that left frontal activation predicted PA in older adults of both sexes. In addition, other studies failed to observe significant relationships between the affective dimensions and frontal asymmetry in a sample of both sexes (e.g., Sutton and Davidson, 1997; Hagemann et al., 1999). More recently, also Mikolajczak et al. (2010) found that frontal EEG asymmetries were not related to the factor of wellbeing, which is a trait pertaining to dispositional mood. In addition, in the attempt to support more specifically the assumption of an asymmetry/personality relationship, Hagemann et al. (1999) found that while extraversion correlated with positive affect scores, neither extraversion nor neuroticism correlated with any of the EEG measures.

EEG FRONTAL ASYMMETRY AND MOOD ALTERATIONS

Comparing high vs. low scorers on the Beck Depression Inventory (BDI) on measures of resting EEG activation asymmetry, Schaffer et al. (1983) revealed that depressed subjects yielded greater right frontal activation than non-depressed subjects. In this direction, less left frontal activation was found in a sample of six euthymic individuals with a past history of depressive episodes relative to healthy subjects (Henriques and Davidson, 1990), in currently depressed (Henriques and Davidson, 1991; Gotlib et al., 1998) and previously depressed subjects (Gotlib et al., 1998), as well as in dysphoric patients with bipolar seasonal affective disorder relative to non-depressed controls, both before and after successful phototherapy (Allen et al., 1993). These results support the view that hypoactivation of the left frontal region represents a marker for mood disorders. However, once again contradictory results have been collected across years. For example, subjects classified as repressors showed relative left anterior cortical activation than non-repressors (Tomarken and Davidson, 1994), no asymmetry differences were not found between high-depression and low-depression groups using both Beck Depression Inventory scores (Tomarken

and Davidson, 1994; Reid et al., 1998) and subjects diagnosed with DSM-III-R depression relative to controls (Reid et al., 1998). In addition, no difference was found between high-anxiety and low-anxiety groups (Tomarken and Davidson, 1994). Interestingly, negative spontaneous mood (e.g., anxiety, tension, depression) was found to decrease across two different sessions when frontopolar activation asymmetry spontaneously shifted to the right hemisphere (Papousek and Schulter, 2002). More recently, Mathersul et al. (2008) found that anxious arousal subjects showed higher right frontal asymmetry, anxious apprehension and non-depression subjects showed higher left frontal asymmetry, whereas symmetry was found for depression and comorbid subjects.

CONCLUSIONS

From the studies reviewed on the EEG correlates of mood it appears that, regardless the research line considered, there are contrasting results that cannot be unequivocally interpreted according to one frontal asymmetry model rather than to another. The motivational approach/withdrawal and valence/arousal models appear to be the most supported ones (Tucker et al., 1981; Schaffer et al., 1983; Henriques and Davidson, 1990, 1991; Tomarken et al., 1990, 1992a,b; Allen et al., 1993; Wheeler et al., 1993; Gotlib et al., 1998—Study 1; Mathersul et al., 2008; Rodriguez et al., 2015; Warden-Smith et al., 2017). However, it is difficult to disentangle the contributions of specific studies to the two models given that the models overlap in terms of empirical predictions (Spielberg et al., 2008). The most of these studies might be also explained in light of the inhibition model of asymmetric differences, given that they revealed right frontal asymmetry or hypoactivation of the left hemisphere for negative mood, as if positive or approach-related distractors would be inhibited when there is a predisposition that supports elevated responsivity to negative stimuli. In addition, the capability model might also explain the most of results (e.g., Dennis and Solomon, 2010), as individual dynamic differences that are challenged by arousing situations, such as those relying on mood induction procedures. Nevertheless, the extent to which this model is appropriate to explain results when the situational variable is absent (e.g., dispositional mood) is unclear. Finally, some studies found results that do not fit with the models discussed (e.g., Papousek and Schulter, 2002; Kop et al., 2011), whereas other studies found frontal EEG asymmetry unrelated to mood (Tomarken and Davidson, 1994; Sutton and Davidson, 1997; Gotlib et al., 1998—Study 2; Reid et al., 1998; Hagemann et al., 1999; Mikolajczak et al., 2010).

These contradictory results depend on different reasons. Following Hagemann et al. (1998), firstly results vary according to methodological variables, such as different measurement procedures of asymmetry and affective variables. Secondly, it also appears that sample should be better composed. Indeed, different studies reviewed used only females (e.g., Tomarken et al., 1990; Wheeler et al., 1993; Gotlib et al., 1998; Reid et al., 1998; Gale et al., 2001), or much more females than males (e.g.,

Dennis and Solomon, 2010; Mikolajczak et al., 2010); one study enrolled only males (Jacobs and Snyder, 1996), and one study reported no information about gender (Warden-Smith et al., 2017). Only recently studies have increased the interest in gender-related brain mechanisms and cerebral lateralization subserving emotional processing (e.g., Gasbarri et al., 2006, 2007; Arnone et al., 2011). In particular, unpleasant stimuli (negatively valenced IAPS pictures) were found to elicit higher P300 amplitude and shorter P300 latency at left frontal site than pleasant and neutral stimuli in women than in men, while a stronger P300 component was elicited in the right hemisphere in men compared to women (e.g., Gasbarri et al., 2007; Arnone et al., 2011). In addition, participants' age might also be another confounding factor because different wide age ranges are reported across studies, even including over 50 (e.g., Jacobs and Snyder, 1996; Dennis and Solomon, 2010) or 60-year people (e.g., Hall and Petruzzello, 1999; Mathersul et al., 2008).

Thirdly, the relationships between frontal asymmetries and mood are also mediated by third variables that have been rarely considered beyond personality (e.g., Gotlib et al., 1998), emotion regulation-capabilities (e.g., Dennis and Solomon, 2010). For example, Hall and Petruzzello (1999) found that in older adults the relationships between frontal brain activity and dispositional affect is influenced by physical activity. This leads to suppose that although mood is generally associated to mind and thoughts, bodily states might also play a key role. Indeed, mood (and of course emotion—e.g., Neal and Chartrand, 2011; Palmiero and Borsellino, 2014) has been described as an embodied experience (e.g., Veenstra et al., 2016). At our knowledge, only Kop et al. (2011) included the measure of the heart rate variability in the study of EEG correlates of mood.

Therefore, the interplay between cognition and emotion should also be considered when studying the EEG asymmetries of mood. Cognition and emotion interact in prefrontal cortex. In particular, according to Grimshaw and Carmel (2014), the left dorsolateral prefrontal cortex (dlPFC) should inhibit negative distractors, whereas the right dlPFC should inhibit positive distractors. Consistent with this prediction, Compton et al. (2003) revealed the presentation of negative words in an emotional Stroop task yielded increased activation in the left dlPFC. Yet, different studies revealed that failures to recruit the left dlPFC during negative distractions are due to mood alterations, which yield higher activation of the right dlPFC (e.g., Engels et al., 2010). In this vein, it appears that frontal EEG asymmetries of mood must be also considering the underlying neural network organization.

In light of these issues, inferences drawn from data previously discussed are potentially limited by the scarce research examining EEG correlates of mood using standard procedures and samples, as well as the interplay with third variables and cognition. Then, frontal EEG asymmetries of mood might be better understood considering the extent to which parietal, temporal, and occipital asymmetries are also investigated. Indeed, Hagemann et al. (1999) showed significant greater relative left activation in the temporal lobe (but not in frontal lobe) in participants of both sexes with high negative affect than in participants with low negative affect. This means that also the neural connectivity between different brain areas should be investigated using more sophisticated neuroimaging approaches. Yet, given that the majority of studies used only negative stimuli, it is important that future research includes in the paradigm both positive and negative mood conditions, unless it is impossible to determine the extent to which hemispheric differences are related to valence.

In conclusion, pursuing more systematically the investigation of EEG asymmetries of mood adopting a wider perspective seems to be mandatory in order to achieve more consistent and reliable outcomes.

AUTHOR CONTRIBUTIONS

MP collected studies and write up the minireview. LP contributed to write up the mini-review.

FUNDING

REFERENCES

Allen, J. J., Iacano, W. G., Depue, R. A., and Arbisi, P. (1993). Regional electroencephalographic asymmetries in bipolar seasonal affective disorder before and after exposure to bright light. *Biol. Psychiatry* 33, 642–646. doi: 10.1016/0006-3223(93)90104-L

Arnone, B., Pompili, A., Tavares, M. C., and Gasbarri, A. (2011). Sex-related memory recall and talkativeness for emotional stimuli. *Front. Behav. Neurosci.* 5:52. doi: 10.3389/fnbeh.2011.00052

Beedie, C., Terry, P., and Lane, A. (2005). Distinctions between emotion and mood. *Cogn. Emot.* 19, 847–878. doi: 10.1080/02699930541000057

Berkowitz, L. (1999). "Anger," in *Handbook of Cognition and Emotion,* eds T. Dalgleish and M. Power (West Sussex: John Wiley & Sons), 411–428.

Berntson, G. G., Norman, G. J., and Cacioppo, J. T. (2011). Comment: laterality and evaluative bivalence: a neuroevolutionary perspective. *Emot. Rev.* 3, 344–346. doi: 10.1177/1754073911402401

Cisler, J. M., and Koster, E. H. W. (2010). Mechanisms of attentional biases towards threat in anxiety disorders: an integrative review. *Clin. Psychol. Rev.* 30, 203–216. doi: 10.1016/j.cpr.2009.11.003

Coan, J. A., and Allen, J. J. B. (2004). Frontal EEG asymmetry as a moderator and mediator of emotion. *Biol. Psychol.* 67, 7–49. doi: 10.1016/j.biopsycho.2004.03.002

Coan, J. A., Allen, J. J. B., and McKnight, P. E. (2006). A capability model of individual differences in frontal EEG asymmetry. *Biol. Psychol.* 72, 198–207. doi: 10.1016/j.biopsycho.2005.10.003

Compton, R. J., Banich, M. T., Mohanty, A., Milham, M. P., Herrington, J., Miller, G. A., et al. (2003). Paying attention to emotion: an fMRI investigation of cognitive and emotional stroop tasks. *Cogn. Affect. Behav. Neurosci.* 3, 81–96. doi: 10.3758/CABN.3.2.81

Davidson, R. J. (1983). "Hemispheric specialization for cognition and affect," in *Physiological Correlates of Human Behavior*, eds A. Gale and J. Edwards (London: Academic Press), 203–216.

Davidson, R. J. (1993). Cerebral asymmetry and emotion: conceptual and methological conundrums. *Cogn. Emot.* 7, 115–138. doi: 10.1080/02699939308409180

Davidson, R. J. (2004). What does the prefrontal cortex "do" in affect: perspectives on frontal EEG asymmetry research. *Biol. Psychol.* 67, 219–233. doi: 10.1016/j.biopsycho.2004.03.008

Davidson, R. J., Jackson, D. C., and Kalin, N. H. (2000). Emotion, plasticity, context, and regulation: perspectives from affective neuroscience. *Psychol. Bull.* 126, 890–909. doi: 10.1037/0033-2909.126.6.890

Dennis, T. A., and Solomon, B. (2010). Frontal EEG and emotion regulation: electrocortical activity in response to emotional film clips is associated with reduced mood induction and attention interference effects. *Biol. Psychol.* 85, 456–464. doi: 10.1016/j.biopsycho.2010.09.008

Ekman, P. (1994). Strong evidence for universals in facial expressions: a reply to Russell's mistaken critique. *Psychol. Bull.* 115, 268–287. doi: 10.1037/0033-2909.115.2.268

Ekman, P., and Davidson, R. J. (1994). *The Nature of Emotion*. Oxford: Oxford University Press.

Elgavish, E., Halpern, D., Dikman, Z., and Allen, J. J. B. (2003). Does frontal EEG asymmetry moderate or mediate responses to the international affective picture system (TAPS)? *Psychophysiology* 40:38. doi: 10.1111/1469-8986.40.s1.1

Engels, A. S., Heller, W., Spielberg, J. M., Warren, S. L., Sutton, B. P., Banich, M. T., et al. (2010). Co-occurring anxiety influences patterns of brain activity in depression. *Cogn. Affect. Behav. Neurosci.* 10, 141–156. doi: 10.3758/CABN.10.1.141

Gable, P. A., and Poole, B. D. (2014). Influence of trait behavioral inhibition and behavioral approach motivation systems on the LPP and frontal asymmetry to anger pictures. *Soc. Cogn. Affect. Neurosci.* 9, 182–190. doi: 10.1093/scan/nss130

Gale, A., Edwards, J., Morris, P., and Forrester, D. (2001). Extraversion-introversion, neuroticism-stability, and EEG indicators of positive and negative empathic mood. *Pers. Indiv. Diff.* 30, 449–461. doi: 10.1016/S0191-8869(00)00036-2

Gasbarri, A., Arnone, B., Pompili, A., Marchetti, A., Pacitti, F., Calil, S. S., et al. (2006). Sex-related lateralized effect of emotional content on declarative memory: an event related potential study. *Behav. Brain Res.* 168, 177–184. doi: 10.1016/j.bbr.2005.07.034

Gasbarri, A., Arnone, B., Pompili, A., Pacitti, F., Pacitti, C., and Cahill, L. (2007). Sex-related hemispheric lateralization of electrical potentials evoked by arousing negative stimuli. *Brain Res.* 1138, 178–186. doi: 10.1016/j.brainres.2006.12.073

Goldstein, R. Z., and Volkow, N. D. (2011). Dysfunction of the prefrontal cortex in addiction: neuroimaging findings and clinical implications. *Nat. Rev. Neurosci.* 12, 652–669. doi: 10.1038/nrn3119

Gotlib, I. H., Ranganath, C., and Rosenfeld, J. P. (1998). Frontal EEG alpha asymmetry, depression, and cognitive functioning. *Cogn. Emot.* 12, 449–478. doi: 10.1080/026999398379673

Grimshaw, G. M., and Carmel, D. (2014). An asymmetric inhibition model of hemispheric differences in emotional processing. *Front. Psychol.* 5:489. doi: 10.3389/fpsyg.2014.00489

Hagemann, D., Naumann, E., Becker, G., Maier, S., and Bartussek, D. (1998). Frontal brain asymmetry and affective style: a conceptual replication. *Psychophysiology* 35, 372–388. doi: 10.1111/1469-8986.3540372

Hagemann, D., Naumann, E., Luèrken, A., Becker, G., Maier, S., and Bartussek, D. (1999). EEG asymmetry, dispositional mood and personality. *Pers. Individ. Diff.* 27, 541–568. doi: 10.1016/S0191-8869(98)00263-3

Hall, E. E., and Petruzzello, S. J. (1999). Frontal asymmetry, dispositional affect, and physical activity in older adults. *J. Aging Phys. Act.* 7, 76–90. doi: 10.1123/japa.7.1.76

Harmon-Jones, E. (2004a). On the relationship of frontal brain activity and anger: examining the role of attitude toward anger. *Cogn. Emot.* 18, 337–361. doi: 10.1080/02699930341000059

Harmon-Jones, E. (2004b). Contributions from research on anger and cognitive dissonance to understanding the motivational functions of asymmetrical frontal brain activity. *Biol. Psychol.* 67, 51–76. doi: 10.1016/j.biopsycho.2004.03.003

Heller, W. (1990). "The neuropsychology of emotion: developmental patterns and implications for psychopathology," in *Psychological and Biological Approaches to Emotion,* eds N. Stein, B. L. Leventhal, and T. Trabasso (Hillsdale, NJ: Lawrence Erlbaum Associates), 167–211.

Heller, W. (1993). Neuropsychological mechanisms of individual differences in emotion, personality, and arousal. *Neuropsychology* 7, 476–489. doi: 10.1037/0894-4105.7.4.476

Henriques, J. B., and Davidson, R. J. (1990). Regional brain electrical asymmetries discriminate between previously depressed and healthy control subjects. *J. Abnorm. Psychol.* 99, 22–31. doi: 10.1037/0021-843X.99.1.22

Henriques, J. B., and Davidson, R. J. (1991). Left frontal hypoactivation in depression. *J. Abnorm. Psychol.* 100, 535–535. doi: 10.1037/0021-843X.100.4.535

Hewig, J., Hagemann, D., Seifert, J., Naumann, E., and Bartussek, D. (2004). On the selective relation of frontal cortical asymmetry and anger-out versus anger-control. *J. Pers. Soc. Psychol.* 87, 926–939. doi: 10.1037/0022-3514.87.6.926

Jackson, D. C., Mueller, C. J., Dolski, I., Dalton, K. M., Nitschke, J. B., Urry, H. L., et al. (2003). Now you feel it, now you don't frontal brain electrical asymmetry and individual differences in emotion regulation. *Psychol. Sci.* 14, 612–617. doi: 10.1046/j.0956-7976.2003.psci_1473.x

Jacobs, G. D., and Snyder, D. (1996). Frontal brain asymmetry predicts affective style in men. *Behav. Neurosci.* 110, 3–6. doi: 10.1037/0735-7044.110.1.3

Kop, W. J., Synowski, S. J., Newell, M. E., Schmidt, L. A., Waldstein, S. R., and Fox, N. A. (2011). Autonomic nervous system reactivity to positive and negative mood induction: the role of acute psychological responses and frontal electrocortical activity. *Biol. Psychol.* 86, 230–238. doi: 10.1016/j.biopsycho.2010.12.003

Mathersul, D., Williams, L. M., Hopkinson, P. J., and Kemp, A. H. (2008). Investigating models of affect: relationships among EEG alpha asymmetry, depression, and anxiety. *Emotion* 8, 560–572. doi: 10.1037/a0012811

Mikolajczak, M., Bodarwe, K., Laloyaux, O., Hansenne, M., and Nelis, D. (2010). Association between frontal EEG asymmetries and emotional intelligence among adults. *Pers. Individ. Diff.* 48, 177–181. doi: 10.1016/j.paid.2009.10.001

Mller, M. M., Keil, A., Gruber, T., and Elbert, T. (1999). Processing of affective pictures modulates right-hemispheric gamma band EEG activity. *Clin. Neurophysiol.* 110, 1913–1920. doi: 10.1016/S1388-2457(99)00151-0

Neal, D. T., and Chartrand, T. L. (2011). Embodied emotion perception: amplifying and dampening facial feedback modulates emotion perception accuracy. *Soc. Psychol. Pers. Sci.* 2, 673–678. doi: 10.1177/1948550611406138

Palmiero, M., and Borsellino, M. C. (2014). *Embodied Cognition: Comprendere la Mente Incarnata*. Fano (Pu): ARAS Edizioni.

Palmiero, M., Nori, R., Rogolino, C., D'Amico, S., and Piccardi, L. (2015). Situated navigational working memory: the role of positive mood. *Cogn. Process.* 16, 327–330. doi: 10.1007/s10339-015-0670-4

Palmiero, M., Nori, R., Rogolino, C., D'Amico, S., and Piccardi, L. (2016). Sex differences in visuospatial and navigational working memory: the role of mood induced by background music. *Exp. Brain Res.* 234, 2381–2389. doi: 10.1007/s00221-016-4643-3

Papousek, I., and Schulter, G. (2002). Covariations of EEG asymmetries and emotional states indicate that activity at frontopolar locations is particularly affected by state factors. *Psychophysiology* 39, 350–360. doi: 10.1017/S0048577201393083

Parkinson, B., Totterdell, P., Briner, R. B., and Reynolds, S. (1996). *Changing Moods: The Psychology of Mood and Mood Regulation*. Harlow: Addison Wesley Longman.

Reid, S. A., Duke, L. M., and Allen, J. J. (1998). Resting frontal electroencephalographic asymmetry in depression: inconsistencies suggest the need to identify mediating factors. *Psychophysiology* 35, 389–404. doi: 10.1111/1469-8986.3540389

Rodriguez, A., Rey, B., Clemente, M., Wrzesien, M., and Alcaniz, M. (2015). Assessing brain activations associated with emotional regulation during virtual reality mood induction procedures. *Expert Syst. Appl.* 42, 1699–1709. doi: 10.1016/j.eswa.2014.10.006

Schaffer, C. E., Davidson, R. J., and Saron, C. (1983). Frontal and parietal electroencephalogram asymmetry in depressed and nondepressed subjects. *Biol. Psychiatry* 18, 753–762.

Scherer, K. R. (2005). What are emotions? And how can they be measured? *Soc. Sci. Inf*. 44, 695–729. doi: 10.1177/0539018405058216

Spielberg, J. M., Stewart, J. L., Levin, R. L., Miller, G. A., and Heller, W. (2008). Prefrontal cortex, emotion, and approach/withdrawal motivation. *Soc. Pers. Psychol. Compass* 2, 135–153. doi: 10.1111/j.1751-9004.2007.00064.x

Sutton, S. K., and Davidson, R. J. (1997). Prefrontal brain asymmetry: a biological substrate of the behavioral approach and inhibition system. *Psychol. Sci.* 8, 204–210. doi: 10.1111/j.1467-9280.1997.tb00413.x

Thompson, W. F., Schellenberg, E. G., and Husain, G. (2001). Arousal, mood and the Mozart effect. *Psychol. Sci.* 12, 248–251. doi: 10.1111/1467-9280.00345

Tomarken, A. J., and Davidson, R. J. (1994). Frontal brain activation in repressors and nonrepressors. *J. Abnorm. Psychol.* 103, 339–349. doi: 10.1037/0021-843X.103.2.339

Tomarken, A. J., Davidson, R. J., and Henriques, J. B. (1990). Resting frontal brain asymmetry predicts affective responses to films. *J. Pers. Soc. Psychol.* 59, 791–801. doi: 10.1037/0022-3514.59.4.791

Tomarken, A. J., Davidson, R. J., Wheeler, R. E., and Doss, R. C. (1992a). Individual differences in anterior brain asymmetry and fundamental dimensions of emotion. *J. Pers. Soc. Psychol.* 62, 676–687. doi: 10.1037/0022-3514.62.4.676

Tomarken, A. J., Davidson, R. J., Wheeler, R. E., and Kinney, L. (1992b). Psychometric properties of resting anterior EEG asymmetry: temporal stability and internal consistency. *Psychophysiology* 29, 576–592. doi: 10.1111/j.1469-8986.1992.tb02034.x

Tucker, D. M., Stenslie, C. E., Roth, R. S., and Shearer, S. L. (1981). Right frontal lobe activation and right hemisphere performance. Decrement during a depressed mood. *Arch. Gen. Psychiatry* 38, 169–174. doi: 10.1001/archpsyc.1981.01780270055007

Vallerand, R. J., and Blanchard, C. M. (2000). "The study of emotion in sport and exercise: historical, definitional, and conceptual perspectives," in *Emotions in Sport*, ed Y. L. Hanin (Champaign, IL: Human Kinetics), 3–37.

Veenstra, L., Schneider, I. K., and Koole, S. L. (2016). Embodied mood regulation: the impact of body posture on mood recovery, negative thoughts, and mood-congruent recall. *Cogn. Emot.* 14, 1–16. doi: 10.1080/02699931.2016.1225003

Warden-Smith, J., Laboni, P., Olukogbon, K., Bointon, E. S., Cole, R. H., John, S. R., et al. (2017). Light and smell stimulus protocol reduced negative frontal EEG asymmetry and improved mood. *Open Life Sci.* 12, 51–61. doi: 10.1515/biol-2017-0006

Wheeler, R. E., Davidson, R. J., and Tomarken, A. J. (1993). Frontal brain asymmetry and emotional reactivity: a biological substrate of affective style. *Psychophysiology* 30, 82–89. doi: 10.1111/j.1469-8986.1993.tb03207.x

Conflict of Interest Statement: The authors declare that the research was conducted in the absence of any commercial or financial relationships that could be construed as a potential conflict of interest.

Your Brain on the Movies: A Computational Approach for Predicting Box-office Performance from Viewer's Brain Responses to Movie Trailers

Christoforos Christoforou [1,2]*, Timothy C. Papadopoulos [3,4], Fofi Constantinidou [3,4] and Maria Theodorou [2]

[1] Division of Computer Science, Mathematics and Science, St. John's University, New York, NY, United States, [2] Division of Research and Development, R.K.I Leaders Ltd., Larnaca, Cyprus, [3] Center for Applied Neuroscience, University of Cyprus, Nicosia, Cyprus, [4] Department of Psychology, University of Cyprus, Nicosia, Cyprus

The ability to anticipate the population-wide response of a target audience to a new movie or TV series, before its release, is critical to the film industry. Equally important is the ability to understand the underlying factors that drive or characterize viewer's decision to watch a movie. Traditional approaches (which involve pilot test-screenings, questionnaires, and focus groups) have reached a plateau in their ability to predict the population-wide responses to new movies. In this study, we develop a novel computational approach for extracting neurophysiological electroencephalography (EEG) and eye-gaze based metrics to predict the population-wide behavior of movie goers. We further, explore the connection of the derived metrics to the underlying cognitive processes that might drive moviegoers' decision to watch a movie. Towards that, we recorded neural activity—through the use of EEG—and eye-gaze activity from a group of naive individuals while watching movie trailers of pre-selected movies for which the population-wide preference is captured by the movie's market performance (i.e., box-office ticket sales in the US). Our findings show that the neural based metrics, derived using the proposed methodology, carry predictive information about the broader audience decisions to watch a movie, above and beyond traditional methods. In particular, neural metrics are shown to predict up to 72% of the variance of the films' performance at their premiere and up to 67% of the variance at following weekends; which corresponds to a 23-fold increase in prediction accuracy compared to current neurophysiological or traditional methods. We discuss our findings in the context of existing literature and hypothesize on the possible connection of the derived neurophysiological metrics to cognitive states of focused attention, the encoding of long-term memory, and the synchronization of different components of the brain's rewards network.

Beyond the practical implication in predicting and understanding the behavior of moviegoers, the proposed approach can facilitate the use of video stimuli in neuroscience research; such as the study of individual differences in attention-deficit disorders, and the study of desensitization to media violence.

INTRODUCTION

Anticipating the behavior of large audiences to video stimuli, such as movies, movie trailers and TV series, is critical for the film industry. Movie trailers serve as a primary marketing tool to promote a movie, and often capture the core characteristic of the movie and motivate its storyline. Thus, evaluating the responses of moviegoers to movie trailers can provide a convenient means of predicting an audience response to the actual movie and hence to anticipate its potential commercial success, before its release. Traditionally, film testing relies on measurements of consumers' stated preferences, obtained via questionnaires, and focus groups conducted during a test screening of the movie or the movie trailer (Eastman and Ferguson, 2012). However, with more than 75% of new movie releases earning a net loss during their run in theaters (Boksem and Smidts, 2015), there is a need for new methods for predicting moviegoer's behavior.

Recently, there has been a growing interest in using neural and biometric measures to identify metrics that predict the performance and effectiveness of video stimuli. These methods have been employed in a diverse set of applications, including investigating cross-culture (Vecchiato et al., 2014a) and gender (Vecchiato et al., 2014b) differences during the observation of video advertisements, analyzing movies to inform cognitive film theory (Smith, 2013), measuring engagement levels during video viewing (Dmochowski et al., 2012), predicting viewership of TV series (Dmochowski et al., 2014), predicting video advertising appreciation potential (Christoforou et al., 2015), and studying affective processing in individuals with high callous-unemotional traits (Fanti et al., 2016), among others. As movie trailers are a type of video stimuli, neuroscience metrics obtained while people are observing movie trailers might provide an alternative framework for predicting the overall performance of a film.

A testing framework based on neuroscience metrics can have several advantages over traditional methods. First, the noise variance of neuroscience metrics is thought to be smaller[1] than data obtained through traditional measures (Boksem and Smidts, 2015). Thus, these metrics could provide more accurate insights with smaller sample sizes, making them potentially cheaper, faster to implement, and likely to provide more accurate predictions. Second, it is thought that neuroscience measurements have the potential to provide additional information that is not obtainable through conventional methods (i.e., questionnaires and focus groups). The rationale of this assertion relies on the assumptions that

people cannot fully articulate their preferences when asked to express them explicitly and that consumers' brain contains hidden information about their actual preferences. Also, stated preferences can be thought of as being the result of the underlying subconscious response of the brain "contaminated" by conscious cognitive control processes and individual biases. In this context, neuronal measures might be thought of as providing the direct, raw and unfiltered impression of viewers to video stimuli. Thus, neural measures might obtain information that better reflects viewers' responses to stimuli, uncontaminated by personal biases. Finally, neuroscience measures may provide second-by-second responses to video stimuli, yielding information processing details that are not available through conventional methods. With these potential advantages in mind, this study proposes a novel approach for extracting meaningful neurophysiology and eye-gaze based metrics to predict the population-wide behavior of moviegoers.

To date, the most common methods used to measure preferences through neural activity have been electroencephalography (EEG) and functional magnetic resonance imaging (fMRI). For example, neural activity in response to advertisements, measured in the ventromedial Prefrontal Cortex (vmPFC) via fMRI, has been shown to be predictive of the population-wide success of commercials (Berns and Moore, 2012; Falk et al., 2012). Moreover, some methods have been proposed to extract informative metrics from neuronal activity captured in EEG measures. Such methods typically rely on obtaining spatial or temporal projections of the raw or pre-processed EEG measures to isolate neuronal activity relevant to a task (Dyrholm et al., 2007; Christoforou et al., 2008, 2013). Resulting metrics have been used in different applications such as Brain-computer interfaces (Blankertz et al., 2008), Robotic-telepresence (Christoforou et al., 2010) and maximization of throughput in performance tasks (Parra et al., 2008). In the context of video stimuli evaluation, EEG-based neuronal activity has been used to characterize the effects of video advertising on consumers. For example, Vecchiato et al. (2011) investigated the changes of EEG frontal asymmetry in the alpha and theta bands, during the observation of pleasant and unpleasant videos. Their analysis showed that an asymmetrical increase in the alpha and theta bands was negatively correlated with the degree of pleasances perceived by the participant. Similarly, Kong et al. (2012) proposed metrics which rely on the overall power in the theta band in EEG signals, as an index of memorization, and as an index of attention. In subsequent work, Kong et al. (2012) proposed the impression index, which combines both the memorization and attention indices. The authors suggested that the aggregate

---

[1]Even though the underlying measurements (i.e., raw EEG) tend to be noisy, the extracted metric/features' noise across participants are expected to be relatively small.

index tracks variations in cerebral activity, measured while subjects are observing video advertisements, could help judge whether scenes in the video advertising are impressive or not.

Recent efforts aim to identify measures of neuronal activity that carry predictive information regarding the performance of video stimuli. For example, Dmochowski et al. (2014) proposed the use of inter-subject correlation (ISC) to extract EEG components that are maximally correlated across participants during video viewing. The extracted ISC components are then used to define a metric that carries predictive information about viewership size and tweet frequency rates during a television broadcast. The same parameter calculated during observation of video advertisements could provide predictive information about the post-air preference rating of each advertisement. In another study, Boksem and Smidts (2015) investigated whether neural measures carry predictive information about the commercial success of movies, above and beyond information obtained through traditional, stated preference measures. In particular, they explored the overall power of high-frequency components (in beta and gamma bands) of EEG measurements obtained during the observation of a movie trailer as predictors of the box-office success of the film. Their results indicated that overall beta activity in EEG could provide predictive information about individual preferences, while overall gamma activity could carry predictive information about the population-wide success of the movie. The authors recognized that in both instances the predictive power of the neuronal measures was small (explained variance <2%), despite being statistically significant.

Various metrics which rely on eye-tracking measurements during video viewing have also been proposed as indicators of video content performance. Typically, these metrics rely on calculating a measure of consistency of eye-movements across different observers. Suggested metrics include: clustering-based methods (Goldstein et al., 2007), which measures the percentage of fixations falling within a cluster; string editing methods (Clauss et al., 2004), where gaze paths are encoded in string representation; attentional synchrony (Smith and Mital, 2013) and information theoretic metrics (Rajashekar et al., 2004); and other methods such as Dorr et al. (2010). A fundamental problem with such methods is that there is no direct (known) mapping between the eye-position and its perceptual consequences, and more importantly, none of these metrics has been shown to carry predictive information of the population-wide audience preferences (Dorr et al., 2010). More recently, Christoforou et al. (2015) proposed the eye-gaze divergence index; a metric that relies on the dispersion of eye-gaze points during video viewing across participants, and that has been shown to carry predictive information on the likability of narrative videos, in particular, video commercials.

In this study, we introduce a new approach for extracting neural-based and eye-gaze-based metrics to predict the population-wide behavior of moviegoers on new movie releases; as captured by the movie's ticket sales. We evaluate the predictive power of the derived metrics and discuss, based on existing literature, their potential connection to the underlying cognitive processes that might drive moviegoers' decision to watch a movie.

MATERIALS AND METHODS

Experimental Paradigm

We record neural activity—through the use of EEG—and eye-gaze activity from a group of naive individuals while watching movie trailers of pre-selected movies for which the population-wide preference is captured by the film's market performance (i.e., box-office ticket sales in the US).

Participants

A total of 27 participants (16 female, 11 male) were recruited for the study. All participants were recruited in Cyprus, were fluent in English and had self-reported normal or corrected-to-normal vision. The minimum, median and maximum ages of the participants were 19, 22 and 24, respectively. Participants were compensated for their participation in the study.

Video Stimuli

A database of 15 movie trailers, split into two stimuli sets, were used in this study. Movies were selected using a search of the boxofficemojo.com website. Specifically, we searched for movies in the action, adventure or thriller genre that premiered during the second or third quarter of 2014. The search focused only on the top 100 movies of each quarter, as ranked by their box office results. Movies that were released in less than 1000 theaters or had total revenue less than $10 million were excluded from the search results. This selection was made to ensure that only movies of reasonable quality and market reach were included in the final dataset. Movies that met the genre and inclusion criteria were ordered based on their box-office performance. To ensure maximum variability in commercial success, in the final database we included movies that came from both the highest and the lowest rankings of the resulting list. Official English trailers for the selected films were used in the study.

Data Collection Procedure

Data were collected in two different sessions to keep the duration of the experiment short and to minimize participant fatigue. Each of the sessions involved the presentation of a distinct set of movie trailers. Participants were randomly assigned to one of the sessions. Movie trailers were split into two stimuli sets; set A included eight of the fifteen trailers, and set B included the remaining seven. During the first session, 14 participants were exposed to movie trailers of set A, while in the second session 13 participants were presented with the movie trailers of set B.

At the onset of the testing, participants were seated in a comfortable chair and briefed on the objectives of the study. Participants were told that they would watch a set of movie trailers and that after each trailer they would have to answer a short questionnaire indicating the preferences about each trailer. Moreover, they were told that we would be collecting

EEG and eye-tracking measures while watching those trailers. A quick preparation and calibration procedure (explained below), before the presentation of the movie trailers (7 or 8 trailers depending on the session) followed next. At the end of each trailer, an on-screen questionnaire was presented asking the participants to report the following: (a) the degree to which they liked the movie trailer; (b) whether they intended to watch the movie promoted by the movie trailer; and (c) whether they would share the movie trailers video on their Facebook account. After having watched all of the movie trailers once, the participants were shown the same trailers for the second time. The order of the movie trailers was randomized across participants, but the order was preserved for each participant in both presentations. The open source software OpenSesame (Mathôt et al., 2012) was used to present the trailers. The trailers were shown at a frame rate of 23 Hz and an aspect ratio of 4:3, with sound (through on monitor speakers). Screen resolution was set to 1024 × 758 for all movie trailers. The present study is carried out in accordance with the ethical standards and the study procedures were approved by the Cyprus Bioethics Committee, and a consent form was obtained from all participants prior to the experiment in accordance with the Declaration of Helsinki.

Behavioral Measures

Participants reported their preferences about the movie by completing an on-screen questionnaire, immediately after watching each trailer. Participants expressed their preferences for the film twice (once after the first viewing of the movie trailer and once after the second viewing). The questionnaire was composed of three questions. For the first question, participants indicated their liking of the film on a scale of 1–10 using a sequence of radio-buttons. For the second and third questions, the participants indicated their willingness-to-watch the film, and their willingness-to-refer the movie (i.e., to share the video on their Facebook account), by selecting either a yes or a no check box on the screen. Three behavioral metrics were constructed based on participants stated preferences. The *likeability metric (LM)* is defined as the average liking score across all participants and viewings of each movie-trailer. The *willingness-to-watch metric (WTW)* and the *willingness-to-refer metric* (WTR) were calculated as the fraction of yes-responses, across participants and viewings, to the willingness-to-watch and willingness-to-refer questions, respectively.

The reported liking scores of participants ranged between 0 and 9 (M = 4.6, SD = 2.4). There were no significant differences in reported liking scores between the first and second viewing for either collection sessions (first session: $F_{(1,179)}$ = 0.02, $p > 0.87$ or second session $F_{(1,221)}$ = 0.01, $p > 0.93$). Thus, the likability metric was calculated using the average participant responses from the two viewings.

Eye-Tracking Measures and Pre-Processing

During the experiment, eye-gaze data were collected at a sampling rate of 60 Hz and spatial accuracy below 0.5°. The eye-tracking unit was placed in front of the participant and below the stimulus presentation monitor, with the camera-to-eye-distance at about 60 cm. A 9-point calibration was executed before the experiment to ensure a correct mapping of the gaze data points and screen coordinates. Also, event markers were sent to the eye-gaze stream to allow synchronization of video frames and gaze data. The recorded eye-gaze-data stream was epoched between −2000 ms before each video start time and 2000 ms after the video finish time and then re-referenced to the video's starting time. The Attentional-asynchrony metric (see "Statistical Analysis of the Prediction Metrics and Key Performance Indicators" section for details) was then calculated as a function of the epoched eye-gaze stream of all participants and viewings. The data analysis was performed using a custom Matlab code (Mathworks Inc., Natick, MA, USA; MATLAB, 2010).

EEG Measures and Pre-Processing

EEG data were collected using a BioSemi Active-two system (BioSemi, Amsterdam, Netherlands) at a sampling rate of 512 Hz. Participants were fitted with a standard 32-electrode cap following the international 10/20 system. The preparation procedure took about 10 min, during which time all electrodes were placed, and the DC offset of all sensors was kept below 20 μV. EEG data were collected for the entire duration of the experiment.

All EEG data preprocessing was performed offline using custom Matlab code (Mathworks Inc., Natick, MA, USA, MATLAB, 2010). As part of the preprocessing, the data were first downsampled to 256 Hz, and a software-based 1.5 Hz high-pass filter was employed on the continuous EEG signal, to remove DC drifts. Subsequently, 50 Hz and 100 Hz notch filters were applied to minimize the power-line noise interference, and all channels were then re-referenced to the average channel. The continuous EEG data was then epoched between 2000 ms prior the movie trailer's start time and 2000 ms after its finish time and the baseline amplitude (i.e., from −2000 ms to 0 ms of the movie trailers onset) was removed from each epoch. Meta-data reflecting the exact timings of each epoch relative to the video-trailer timing were kept throughout the preprocessing procedure.

Following the preprocessing of the temporal signal, each epoch was transformed into the spectro-temporal domain by convolving the EEG signal of each epoch with a complex morlet kernel. The spectrotemporal coefficients were estimated for every half Hz between 1–80 Hz and resulted in a temporal resolution of 8 Hz. The instantaneous power of each spectrotemporal coefficient was calculated as the product of that coefficient with its complex conjugate. Thus, the EEG response of each participant on each movie-trailer was represented as the collection on instantaneous power measures at different channels, time and frequency combination. In our study, we considered the instantaneous power for the subset of frequency's that corresponded to the beta and gamma bands. Specifically, we segmented the data into the following frequency bands 14–8 Hz, 16–18 Hz and 18–20 Hz for the beta band, and 40–48 Hz, 52–60 Hz, 52–70 Hz and 60–70 Hz for the gamma band.

Attentional-Asynchrony and Cognitive-Congruency Metrics

Eye-Gaze Measurements and the Attentional-Asynchrony Metric

The calculation of Attentional-asynchrony metric was based on the Eye-Gaze Divergence Index introduced by Christoforou et al. (2015), which was shown to carry predictive information on the likability of narrative videos. Similar to the Eye-Gaze Divergence Index (Christoforou et al., 2015), Attentional-asynchrony was calculated as the proportion of the movie-trailer on which the visual attention of a group of viewer's diverged. To quantify this proportion, the eye-gaze stream for each movie-trailer was first segmented into small overlapping windows, obtained in a time-resolved fashion by employing a sliding window with 250 ms duration and a shift of the window occurring every 50 ms (80% overlap between successive windows). Each window was subsequently classified as being either divergent or non-divergent; however, for the calculation of Attentional-asynchrony, a different classification criterion was used. Specifically, for each window, the set of pairwise Euclidian distances between all eye-gaze points of all participant was calculated, and a window was classified as being divergent if a fraction (in our study 30%) of the pairwise distances fell within a 90% confidence interval of the null-distribution. The null-distribution over pairwise distances was estimated by randomizing the order of windows, participants, and viewings for each movie trailer. Finally, the Attentional-asynchrony metric was calculated as the fraction of windows identified as being divergent.

EEG Measurements and Cognitive-Congruency Metric

Similarly, we used the epoched EEG measurement collected for each movie-trailer from all participants to define an aggregate metric of Cognitive-congruency. The objective of Cognitive-congruency metric was to identify and quantify coherence in the modulation patterns of instantaneous powers within the selected frequency bands. The rationale was that the presence of neuronal activity that was congruent across participants was an indication of the ability of the movie trailer to guide the viewer's cognitive response consistently. We calculated the Cognitive-congruency of each movie trailer for different frequency bands (14–18 Hz, 16–18 Hz and 18–20 Hz covering the beta band and 40–48 Hz, 52–60 Hz, 52–70 Hz and 60–70 Hz covering the gamma band). This selection was motivated by recent results (Boksem and Smidts, 2015) that suggest the overall power in the beta and gamma bands might carry predictive information about the performance of movie trailers.

To calculate the Cognitive-congruency, we first identified a multivariate spatial component that maximizes the correlation of the instantaneous power of EEG measures between the first and second viewing of the movie-trailer across all participants. Specifically, we estimated a spatial component (projection) $\boldsymbol{w} \in \mathbb{R}^D$ such that $\boldsymbol{w}^T \boldsymbol{R}_{(1,2)} \boldsymbol{w}/N(\boldsymbol{w})$ is maximized, where $\boldsymbol{w}$ is a weight vector, D corresponds to the number of EEG channels recorded, $\frac{1}{|S|.T} \sum_{s \in S} \boldsymbol{X}_{(1,s)} \boldsymbol{X}_{(2,s)}^T$ is the subject-aggregated covariance matrix of instantaneous powers, $\boldsymbol{X}_{(i,s)} \in \mathbb{R}^{D \times T}$ corresponds to the epoched EEG trails (capturing instantaneous power in a particular frequency band) of the sth participant during the ith viewing of a movie-trailer, and $N(\boldsymbol{w}) = \boldsymbol{w}^T (\boldsymbol{R}_{(1,1)} + \boldsymbol{R}_{(2,2)}) \boldsymbol{w}$ is a normalizing factor. The optimal $\boldsymbol{w}$ then refers to the solution to the generalized eigenvalue problem $\lambda(\boldsymbol{R}_{(1,1)} + \boldsymbol{R}_{(2,2)}) \boldsymbol{w} = \boldsymbol{R}_{(1,2)} \boldsymbol{w}$ (Dmochowski et al., 2012). The Cognitive-congruency then corresponded to the eigenvalue which corresponded to the optimal projection vector $\boldsymbol{w}$. Moreover, with the optimal $\boldsymbol{w}$, we could recover its corresponding "forwards model" (Parra et al., 2008), which could be used to visualize the topographic distribution of maximally correlated EEG activity. All calculations for cognitive-congruency were implemented using custom Matlab code (Mathworks Inc.; MATLAB, 2010).

TABLE 1 | Sales Performance key performance indicator (KPI) of each movie on Movie's Premiere, and on subsequent weekends.

Movie	Premiere	WKND$_1$	WKND$_2$	WKND$_3$	WKND$_4$	WKND$_5$	WKND$_6$	WKND$_7$	WKND$_8$
		WKND$_j$: J$_{th}$ weekends after movie's premiere							
1	1.0975	0.4563	0.2372	0.1373	0.0866	0.0691	0.0489	0.0386	0.0184
2	0.3857	0.1907	0.1028	0.0717	0.0465	0.0342	0.0232	0.0180	0.0102
3	0.6737	0.2872	0.1867	0.0468	0.0086	0.0020	0.0006	0.0021	0.0007
4	0.5548	0.2478	0.1477	0.1012	0.1005	0.0609	0.0477	0.0308	0.0222
5	0.6207	0.3409	0.1764	0.0979	0.0505	0.0324	0.0166	0.0084	0.0051
6	0.5246	0.2282	0.1338	0.0953	0.0521	0.0388	0.0212	0.0116	0.0062
7	0.1034	0.0433	0.0159	0.0059	0.0013	0.0009	0.0007	0.0004	0.0003
8	0.3399	0.1318	0.0587	0.0181	0.0056	0.0007	0.0028	0.0020	0.0011
9	0.4271	0.2133	0.0986	0.0511	0.0255	0.0117	0.0063	0.0051	0.0031
10	0.2980	0.1101	0.0575	0.0213	0.0085	0.0064	0.0028	0.0021	0.0028
11	0.3469	0.1578	0.0761	0.0510	0.0293	0.0181	0.0066	0.0029	0.0045
12	0.3006	0.1514	0.0885	0.0589	0.0372	0.0137	0.0045	0.0018	0.0022
13	0.3938	0.1772	0.0577	0.0167	0.0086	0.0029	0.0013	0.0008	0.0026
14	0.2704	0.1203	0.0640	0.0274	0.0103	0.0045	0.0026	0.0015	0.0018
15	0.5529	0.1628	0.0758	0.0491	0.0308	0.0166	0.0095	0.0051	0.0036

Key performance indicators (KPI) of each movie in the dataset used in the study. The ith row shows the sales performance KPI (revenue/budget) of the ith movie on the movie's premiere weekend (column "Premiere"), and on the eight following weekends (columns WKND$_1$,.. WKND$_8$).

Statistical Analysis of the Prediction Metrics and Key Performance Indicators

To evaluate the ability of Cognitive-congruency and Attentional-asynchrony to predict the commercial success of films, we used linear regression to model the relationship between these two metrics and a measure of box-office performance. We analyzed the relationship of between commercial success and each metric individually, and then we estimated a multiple regression model using both metrics.

Key Performance Indicators of Commercial Success

The commercial success of movies is typically measured regarding box-office sales. The film industry has long used a comprehensive system for measuring the post-air success of a movie; these measurements are collectively known as box-office performance and include the number of tickets sold and the total sales revenue from tickets on a daily, weekly and monthly basis. These metrics are of particular importance to the film industry as they provide a concrete framework for measuring changes in the overall success of the films.

In the present study, we used a key performance indicator (KPI) based on box-office measurements. This KPI is comprised of the movie's recorded revenues during the opening weekend, divided by the total budget of the film to account for variability of marketing capacity and reach of different movies. Moreover, we used the same KPI for movie revenues for the first eight weekends after the movies' release. All relevant data were obtained from the website boxofficemojo.com. **Table 1** shows the titles of the movies used in the study along with their corresponding KPI score.

Statistical Models

In the first model, Attentional-asynchrony served as the independent variable and KPI during the premiere weekend of the movie served as the dependent variable. We explored the Attentional-asynchrony metric calculated on data from the first viewing and second viewing separately. Moreover, we examined

the same model where the depended variable corresponded to the KPI of the movie during the first nine weekends.

In the second model, the Cognitive-congruency metric served as the independent variable and the sales performance KPI during the premiere weekend of the movie was the dependent variable. We explored the Cognitive-congruency metric calculated on beta and gamma frequency bands (see section on Cognitive-congruency); a separate univariate model was fitted for each of the selected instantiations of the Cognitive-congruency. As with Attentional-asynchrony, we also estimated a model where the depended variable corresponded to the sales performance KPIs of the movie during the first nine weekends. We report the explained variance of the model and regression statistics corrected for multiple comparisons using false discovery rate.

Finally, we considered a bivariate model where both Attentional-asynchrony and Cognitive-congruency served as independent variables and used the same dependent variable as in the univariate model. In the bivariate model, we only considered the Attentional-asynchrony from the first viewing of the trailer and Cognitive-congruency in the gamma band (60–70 Hz).

RESULTS
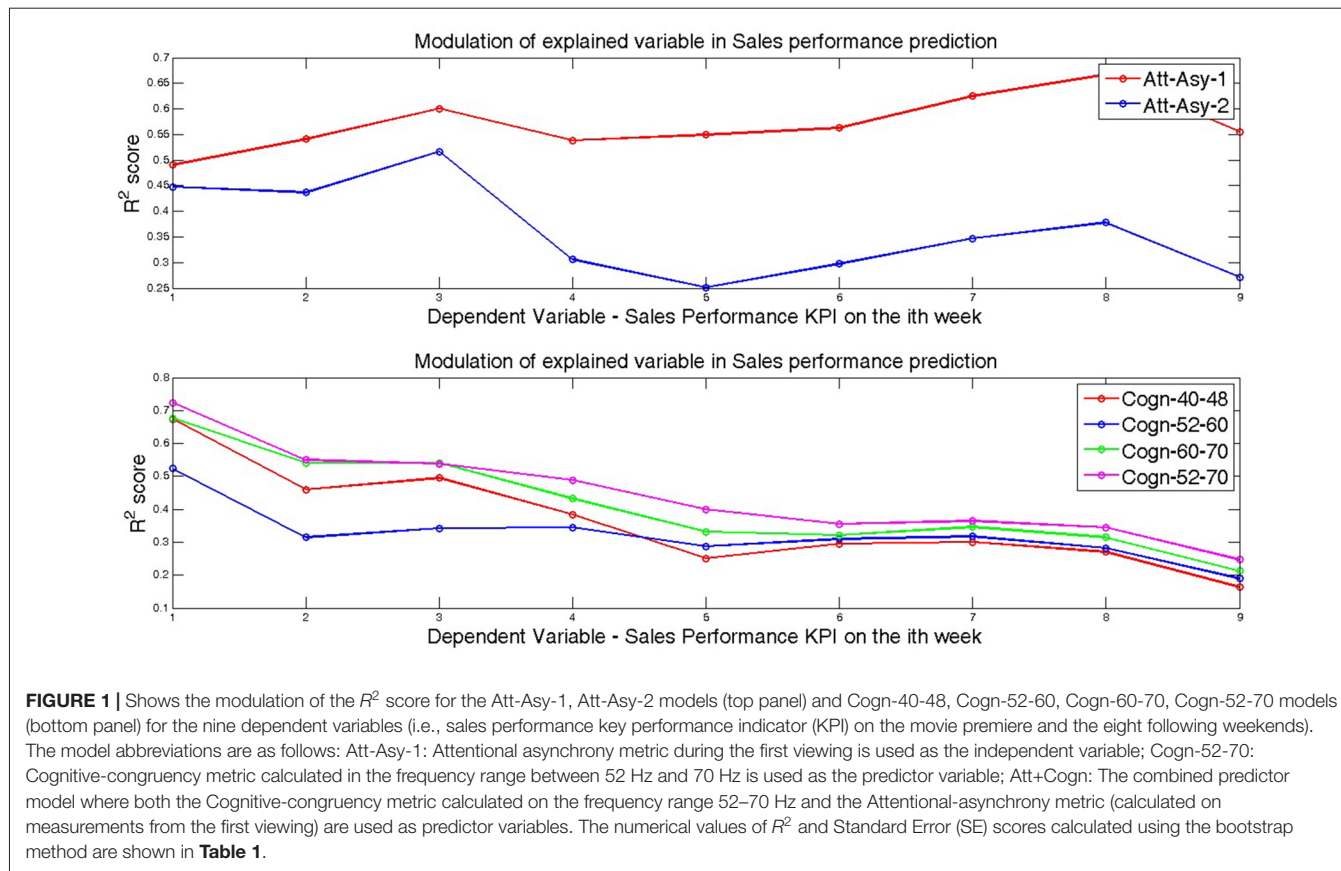
Behavioral Results

Using the *LM* as an independent variable and the KPI during the premiere weekend as the dependent variable, the regression model showed that the LM was not a significant predictor of sales performance, $F_{(1,12)} = 0.39$, $R^2 = 0.02$, $p > 0.54$). Similarly, in regression models where the *WTW* and WTR metric are the dependent variables, neither metric was a significant predictor of the sales performance KPI during the premiere weekend, WTW: $F_{(1,12)} = 1.76$, $R^2 = 0.11$, $p > 0.20$, WTR: $F_{(1,12)} = 1.75$, $R^2 = 0.11$, $p > 0.20$. Finally, correlation analysis showed a strong correlation among the three behavioral metrics, LM-WTW: $r = 0.87$, $p < 0.001$, LM-WTR: $r = 0.67$, $p < 0.01$, WTW-WTR: $r = 0.79$, $p < 0.001$.

TABLE 2 | R^2 scores of each of the the seven models when predicting sales performance KPI on each movie's premiere and on subsequent weekends.

Model	Premiere	WKND$_1$	WKND$_2$	WKND$_3$	WKND$_4$	WKND$_5$	WKND$_6$	WKND$_7$	WKND$_8$
		WKND$_j$: J$_{th}$ weekends after movie's premiere							
Att-Asy-1	0.49* (0.14)	0.54** (0.11)	0.60** (0.10)	0.53** (0.15)	0.55** (0.25)	0.56** (0.25)	0.62** (0.25)	0.66** (0.22)	0.55** (0.25)
Att-Asy-2	0.44* (0.16)	0.43* (0.16)	0.51* (0.15)	0.30 (0.17)	0.25 (0.21)	0.29 (0.24)	0.34 (0.24)	0.37 (0.21)	0.27 (0.20)
Cogn-40-48	0.67* (0.09)	0.45* (0.13)	0.49* (0.15)	0.38 (0.18)	0.25 (0.16)	0.29 (0.17)	0.29 (0.16)	0.27 (0.16)	0.16 (0.13)
Cogn-52-60	0.52* (0.18)	0.31 (0.17)	0.34 (0.19)	0.34 (0.17)	0.28 (0.17)	0.30 (0.17)	0.31 (0.17)	0.28 (0.17)	0.18 (0.16)
Cogn-60-70	0.67** (0.11)	0.54* (0.14)	0.54* (0.15)	0.43 (0.17)	0.33 (0.18)	0.32 (0.19)	0.34 (0.18)	0.31 (0.18)	0.21 (0.17)
Cogn-52-70	0.72** (0.07)	0.55* (0.17)	0.54* (0.19)	0.49* (0.17)	0.40 (0.19)	0.35 (0.19)	0.36 (0.18)	0.34 (0.17)	0.24 (0.18)
Att+Cogn	0.73** (0.07)	0.63** (0.10)	0.66** (0.09)	0.59* (0.15)	0.57* (0.24)	0.57* (0.24)	0.63** (0.23)	0.66** (0.19)	0.56* (0.23)

The modulation of the R^2 score for the seven prediction models. Single-starred R^2 scores are significant at 0.05 threshold level, while doubled-starred R^2 scores are significant at 0.01 threshold level. The significance is reported after correcting for multiple comparisons (using false-recovery-rate method). Within the parenthesis, below each R^2 score, is the SE of R^2 calculated using the bootstrap method. The model abbreviations are as follows: Att-Asy-1: Attentional-asynchrony metric during the first viewing is used as the independent variable; Att-Asy-2: Attentional-asynchrony metric during the first viewing is used as the independent variable; Cogn-X-Y: Cognitive-congruency metric calculated in the frequency range between X Hz and Y Hz is used as the predictor variable; Att+Cogn: the combined predictor model where both the Cognitive-congruency metric calculated on the frequency range 52–70 Hz and the Attentional-asynchrony metric (calculated on measurements from the first viewing) are used as predictor variables.

FIGURE 1 | Shows the modulation of the R^2 score for the Att-Asy-1, Att-Asy-2 models (top panel) and Cogn-40-48, Cogn-52-60, Cogn-60-70, Cogn-52-70 models (bottom panel) for the nine dependent variables (i.e., sales performance key performance indicator (KPI) on the movie premiere and the eight following weekends). The model abbreviations are as follows: Att-Asy-1: Attentional asynchrony metric during the first viewing is used as the independent variable; Cogn-52-70: Cognitive-congruency metric calculated in the frequency range between 52 Hz and 70 Hz is used as the predictor variable; Att+Cogn: The combined predictor model where both the Cognitive-congruency metric calculated on the frequency range 52–70 Hz and the Attentional-asynchrony metric (calculated on measurements from the first viewing) are used as predictor variables. The numerical values of R^2 and Standard Error (SE) scores calculated using the bootstrap method are shown in **Table 1**.

In all analyses, regression results are reported on data from 14 out of the 15 videos movie trailers. Trailer with vid:1 was removed as an outlier because its KPI score was four standard deviation above the mean KPI scores of the rest of the movies.

Correlational Analysis Results
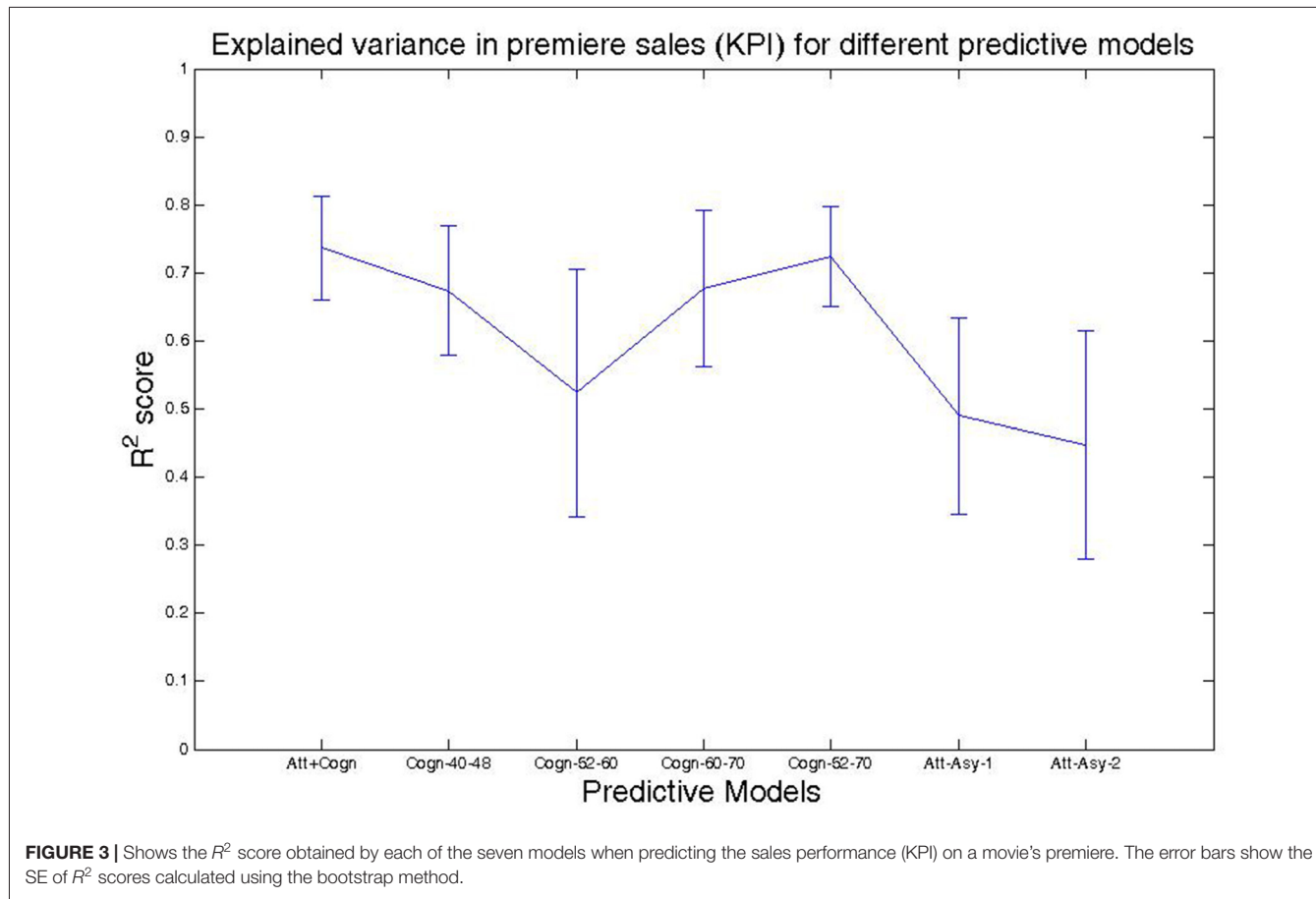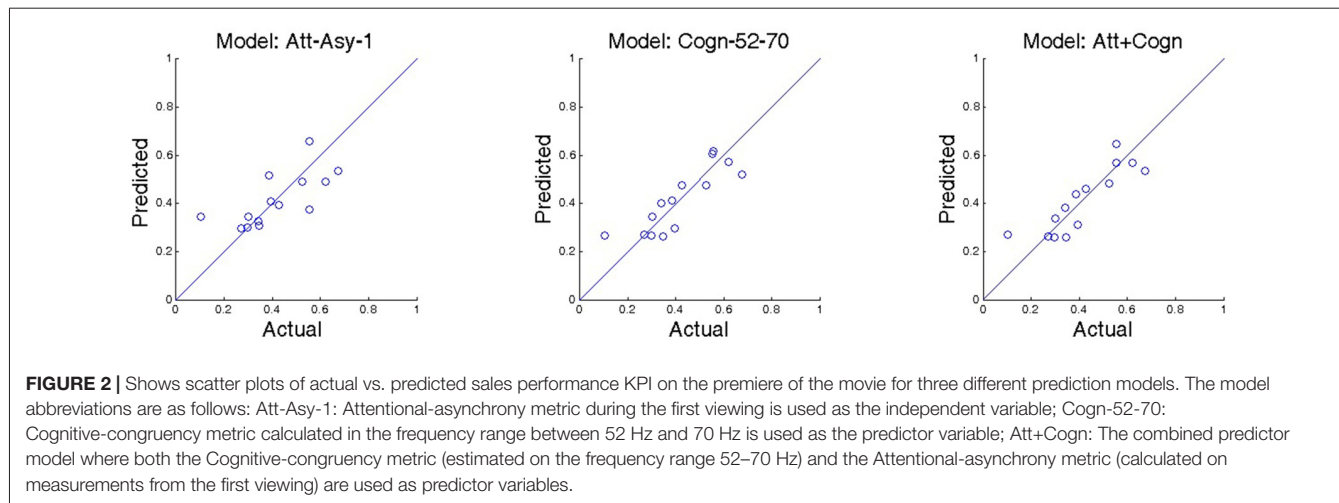
We first investigate the correlation between the sales performance KPI during the movie's premiere and the proposed metrics. Correlation analysis showed a strong negative correlation between the attentional-asynchrony metrics and the sales performance KPI (Asy-viewing-1: $r = -0.70$, $p < 0.01$; Asy-viewing-2: $r = -0.67$, $p < 0.01$). The analysis also showed a strong positive correlation between the KPI and cognitive-congruency metrics, calculated on each of the four gamma band ($r = 0.82–0.85$, $p < 0.001$). A moderate negative correlation was observed between the KPI and the cognitive-congruency metric calculated on the beta range (16–18 Hz). However, it failed to reach significance ($r = -0.45$, $p > 0.09$). No correlation was established between the other two beta-band metrics.

Attentional-Asynchrony Prediction Model Results

To investigate the capacity of Attentional-asynchrony metric to predict the sales performance KPI during the movie's

premiere, we employed two univariate regression models. In the first model, we considered the Attentional-asynchrony metric calculated on the first viewing of each movie trailer as the predictor, while in the second model we used Attentional-asynchrony calculated on data from the second viewing of the movie trailer. In both models, Attentional-asynchrony was regressed onto the sales performance KPI for the film's premiere weekend. The results showed that Attentional-asynchrony was a significant predictor of sales performance KPI at the movie's premiere. Specifically, Attentional-asynchrony calculated on eye-gaze data from the first viewing of the movie trailer predicted 49% of the model variance, $R^2 = 0.49$, $F_{(1,12)} = 11.53$, $p < 0.01$, R^2-adjusted $= 0.44$, $SE = 0.14$, Standard Error (SE) on R^2 computer using bootstrap, while the corresponding metric calculated on eye-gaze data from the second viewing of the trailer predicted 44% of the variance, $R^2 = 0.44$, $F_{(1,12)} = 9.72$, $p < 0.01$, R^2-adjusted $= 0.40$, $SE = 0.16$. The attentional-asynchrony metrics for the two viewings were strongly correlated ($r = 0.91$, $p < 0.001$).

Subsequently, we investigated whether the capacity of Attentional-asynchrony (calculated on the first- and second-viewing independently) to predict the sales performance KPI during the movie premiere propagates to the sales performance KPIs of subsequent weeks. **Table 2** shows the results of the mass-univariate regression where the Attentional-asynchrony

FIGURE 2 | Shows scatter plots of actual vs. predicted sales performance KPI on the premiere of the movie for three different prediction models. The model abbreviations are as follows: Att-Asy-1: Attentional-asynchrony metric during the first viewing is used as the independent variable; Cogn-52-70: Cognitive-congruency metric calculated in the frequency range between 52 Hz and 70 Hz is used as the predictor variable; Att+Cogn: The combined predictor model where both the Cognitive-congruency metric (estimated on the frequency range 52–70 Hz) and the Attentional-asynchrony metric (calculated on measurements from the first viewing) are used as predictor variables.

FIGURE 3 | Shows the R^2 score obtained by each of the seven models when predicting the sales performance (KPI) on a movie's premiere. The error bars show the SE of R^2 scores calculated using the bootstrap method.

acts as a predictor of the sales performance KPI of the movie for each one of the first 9 weeks.
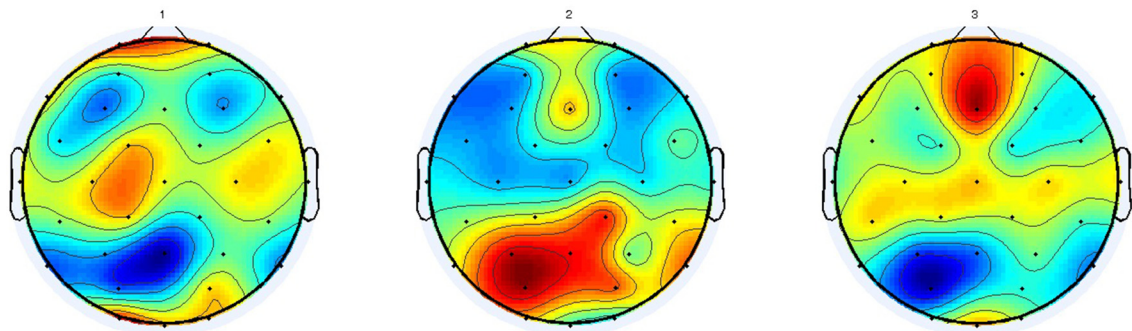
Cognitive-Congruency Prediction Model Results

First, we report results on the ability of the Cognitive-congruency EEG metric, calculated on gamma and beta bands, to predict sales performance KPI during the movie premiere. The univariate regression analysis shows that Cognitive-congruency calculated on each of the four gamma-band ranges significantly predicted the sales performance KPI during the premiere weekend. Specifically, Cognitive-congruency calculated in the gamma range 40–48 Hz was shown to predict 67% of the model variance, $R^2 = 0.67$, $F_{(1,12)} = 24.81$, $p < 0.001$, R^2-adjusted $= 0.65$,

FIGURE 4 | Shows the modulation of the R^2 score for the Att-Asy-1, Cogn-52-70 and Att+Cogn models and the nine dependent variables (i.e., sales performance KPI on the movie premiere and the eight following weekends). The model abbreviations are as follows: Att-Asy-1: Attentional-asynchrony metric during the first viewing is used as the independent variable; Cogn-52-70: Cognitive-congruency metric calculated in the frequency range between 52 Hz and 70 Hz is used as the predictor variable; Att+Cogn: The combined predictor model where both the Cognitive-congruency metric calculated on the frequency range 52–70 Hz and the Attentional-asynchrony metric (calculated on measurements from the first viewing) are used as predictor variables.


FIGURE 5 | The average forward model of the spatial components used in calculating Cognitive-congruency scores.

$SE = 0.09$), while the corresponding metric calculated on the 52–60 Hz range predicted 52% of the variance, $R^2 = 0.52$, $F_{(1,12)} = 13.20$, $p < 0.01$, R^2-adjusted $= 0.48$, $SE = 0.18$) and on the 60–70 Hz range predicted 67% of the variance, $R^2 = 0.67$, $F_{(1,12)} = 25.17$, $p < 0.001$, R^2-adjusted $= 0.65$, $SE = 0.11$). Moreover, regression analysis on Cognitive-congruency calculated in the broader gamma range (52–70 Hz) was found to explain 72% of the variance, $R^2 = 0.72$, $F_{(1,12)} = 31.45$, $p < 0.001$, R^2-adjusted $= 0.70$, $SE = 0.07$). On the other hand, Cognitive-congruency calculated on each of the two beta-band (14–16 Hz and 16–18 Hz) failed to predict the sales performance KPI during the movie premiere

$R^2 = 0.01$, $F_{(1,12)} = 0.13$, ns; $R^2 = 0.21$, $F_{(1,12)} = 3.28$, ns, respectively).

Subsequently, we investigated if the capacity of Cognitive-congruency (calculated on the four gamma-band ranges) to predict the sales performance KPI during the premiere weekend also applies to subsequent weeks. **Table 2** shows the results of the univariate regressions where the Cognitive-congruency acts as a predictor of the sales performance KPI of the movie for each of the first 9 weeks. The analysis showed that, indeed, Cognitive-congruency in the gamma-band continued to carry significant predictive power on sales performance KPI of the movie for up to 4 weeks, although the level of variance explained decrease every

week. **Figure 1** plots the R^2 of explained variance under the model where Cognitive-congruency (for each of the four gamma-band ranges) served as a predictor, as a function of the nine subsequent weeks.

Combined Eye-Tracking and EEG Prediction Model

Lastly, we consider the model where both Cognitive-congruency (calculated on the gamma band) and Attentional-asynchrony (computed on the first viewing of each movie trailer) serve as predictor variables of sales performance KPI for the film premiere weekend and subsequent weeks. The analysis shows that the combined model predicts 73% of the variance, $R^2 = 0.7370$, $F_{(2,11)} = 15.51$, $p < 0.001$, R^2-adjusted $= 0.69$, $SE = 0.07$, in sales performance KPI during the opening weekend. Subsequently, we investigated if the capacity of the combined model to predict the sales performance KPI during subsequent weeks. **Table 2** shows the results of the regressions for the combined model for each one of the first 9 week. **Figure 2** shows scattered plots of actual vs. predicted sales performance KPI on the movies premiere for three different prediction models. **Figure 3** compares the of R^2 score obtained by each of the seven models when predicting the sales performance (KPI) on a movie's premiere. **Figure 4** illustrates the modulation in explained variance across the 9 weeks for the Attentional-asynchrony model, the Cognitive-congruency model and the combined model, respectively. The forward model of the Cognitive-congruency model is illustrated in **Figure 5**.

DISCUSSION

In this study, we proposed a novel computational approach for extracting neurophysiological and eye-gaze based metrics to predict the population-wide behavior of movie goers. In particular, we derived two metrics, termed "Attentional-asynchrony"—calculated on eye-gaze data- and "Cognitive-congruency"—estimated on EEG data—and, evaluated the degree to which these metrics carry predictive information about the broader audience decisions to watch a movie. Towards that, we recorded neural activity—through the use of EEG—and eye-gaze activity from a group of naive individuals while watching movie trailers of pre-selected movies for which the population-wide preference is captured by the movie's market performance (i.e., box-office ticket sales in the US). In this section, we discuss our key findings and the connection of the derived metrics to the underlying cognitive processes that might drive moviegoers' decision to watch a movie.

A significant finding of this study is that neuroscience metrics obtained while people are observing movie trailers provides an alternative framework for predicting the overall performance of a film. Indeed, the results demonstrate that the proposed neuroscience-based metrics of Attentional-asynchrony and Cognitive-congruency can predict the commercial success of a given movie and explain a significant percentage of sales variability in box-office sales.

Specifically, when relating the Attentional-asynchrony metric to the commercial success of the films, we found that the metric carries significant predictive power. These results highlight the capacity of a movie trailer to guide viewers' visual attention consistently as an important factor in predicting the success of a film. Moreover, because movie trailers are composed (primarily) of scenes from the actual movie, they act as indicators of the capacity of the movie itself to guide viewers' attention in a consistent way. Further, the Attentional-asynchrony metric calculated on eye-gaze data obtained either during the first viewing or the second viewing exhibit equal predictive power and are highly correlated. This finding provides evidence for the robustness and consistency in the calculation of the metrics.

Intuitively, attentional-asynchrony quantifies the difficulty of a video stimuli to guide viewer's visual attention consistently for the duration of the video. fMRI research corroborates the close link between eye-gaze and attention (Eckstein et al., 2017). Moreover, eye-gaze asynchrony measures have been associated with biological process relating to the allocation of attention (Christoforou et al., 2015). In this context, our finding might suggest that movie-trailers that are likely to influence the general population to decide to watch the film, are able to engage viewer's visual in a consistent visual path, throughout the movie-trailer narrative.

We also tested the Cognitive-congruency metric, calculated on beta and gamma bands, as a predictor of the sales performance. Traditionally, researchers have related gamma-band activity to states of enhanced arousal and focused attention (Engel et al., 2001). Gamma-band synchronization between brain areas could reflect top-down control of attention modulated by the relevance of stimulus representation (Rodriguez et al., 1999). Moreover, gamma-band power was found to be enhanced during tasks involving object recognition (Rodriguez et al., 1999) and emotional evaluation tasks (Müller et al., 2000); both processes are most likely engaged during the viewing of movie clips (Boksem and Smidts, 2015). In this context, the proposed Cognitive-congruency metric—calculated on the gamma band—can be thought of as reflecting the capacity of the movie trailer to attract and maintain a viewer's attention, and to engage an audience's emotions. Thus, our finding suggests that the ability of the movie trailer to engage viewers, as quantified by the Cognitive-congruency metric, affects the likelihood that the general population will decide to watch the film, once exposed to movie-trailer.

Gamma activity is also strongly related to activation of the medial PFC (Mantini et al., 2007), an area in the brain which fMRI studies have found to be related to population-wide preferences and choices (Berns and Moore, 2012; Falk et al., 2012). Also, Howard et al. (2003) have reported that power in the gamma band is related to committing viewed materials to memory. Indeed, the medial PFC is strongly connected to the hippocampus (a brain area critically involved in memory formation) while gamma synchronization between the hippocampus and other brain regions are correlated with successful encoding of long-term memory (Fell et al., 2001). In this context, our findings suggest that gamma-modulation captured by the Cognitive-congruency metric

reflects the capacity of the movie trailer to both capture and maintain viewer's attention over time, and its ability to assist in memorability of the viewed materials. In turn, these characteristics of the movie trailer affect the likelihood that people will go and see the film.

When comparing the Cognitive-congruency metric (calculated on beta band power) to the population-wide commercial success of the movie, we found that the metric carried no predictive power. Previous research has linked medial frontal beta activity to reward processing including reward anticipation, rewards delivery, rewards evaluation and choice. Moreover, high-frequency oscillation (beta and gamma bands) are thought of being well suited to synchronize the different components of the reward network, as they allow for the communication and integration of information across distant brain areas. In fact, Boksem and Smidts (2015) have reported that medial frontal beta during viewing of a movie trailer relates to the individual's preferences about the film. However, they note that beta activity carries no predictive information about the population-wide success of the film. Taken together, these findings might suggest that short-term rewards, revealed by higher beta activity, might reflect the immediate (short-term) evaluation of the movie. However, the effect of the rewards is temporary and does not affect the likelihood of viewers to go and watch the film.

Putting all the above together, the findings suggest that movie-trailers are more successful in influencing viewer's to watch a movie when they capture and retain viewer's attention and potentially engage viewer's emotion; as attentional-asynchrony and cognitive-congruency metrics measure those. The most successful movie-trailers though, also trigger the long-term memory encoding process in the brain, as the gamma-band cognitive-congruency metrics capture that, and thus facilitate memorization of the film's narrative. On the other hand, movie-trailers that engage the reward system of viewer's brain, as captured by the beta-band cognitive-congruency metric, do not necessarily translate to increase in the likelihood of viewers to go and watch the film.

Finally, we explored a combined model where both Attentional-asynchrony and Cognitive-congruency metrics are used as predictors of population-wide success of the movies. The findings suggest that the two predictors provide complementary predictive information and likely capture different factors affecting the population's decision to see a movie. The combined model explained significantly higher variability in sales performance of the movie for the first three weekends after the film's premiere, while it explained at least as much variability as either of the individual models on the remaining weekend sales. Interestingly, by inspecting the modulation of explained variance under the different models (i.e., Att-Asy-1 and Cogn-52-70) across consecutive weekend sales performance, we found that Cognitive-congruency was a significantly stronger predictor of sales performance during the movie opening weekend. In turn, Attentional-asynchrony was a more reliable predictor of the sales performance on the weekends after the premiere. These findings provide additional evidence on the complementarity of predictive information from the two metrics. On the one

hand, these results suggest that Cognitive-congruency, and thus the capacity of the trailer to both capture and maintain viewer's attention over time, functions as a robust metric for the decision made by frequent moviegoers about the quality of a movie. Our results also suggest that this applies in particular during the movie's opening weekend when the movie is usually attended by regular movie–goers and fans of the film. On the other hand, the decisions of infrequent or casual moviegoers, which are likely to attend the film in following weekends after the movie's opening weekend, are better characterized by Attentional-asynchrony metric. From a practical point of view, given that the opening weekend accounts for 30%–50% of the total sales within the first nine weekends of a movie's release, the power of the Cognitive-congruency metric to predict sales during the film's opening weekend remains particularly important from a financial point of view.

Finally, the results showed a high correlation between the three behavioral measures of likeability, WTW and WTR metrics. However, none of the traditional behavioral measures were found to be significant predictors of population-wide commercial success of the movies. That the stated preference-based measures did not predict commercial success could be attributed to the sample size of the present study. Indeed, our findings are consistent with the work of Boksem and Smidts (2015), in which behavioral measures obtained on a small sample size (comparable to the current study) fail to predict broad population preferences. Current industry practices that rely on traditional behavioral measures require much larger sample sizes (>400 respondents) than the sample size used in this study. Our result could be seen as evidence of the reasonable variability that exists among stated preference measures. In contrast, the neuronal based metrics proposed in this article were found to extract predictive information of commercial success on different movies from a small sample size, suggesting that neural based metrics better reflect more accurate measures of the effect of a movie trailer on viewers.

Like previous research in neuromarketing research, the present study exhibits the limitations of correlational studies. For example, in the present study, we recorded participants' likeness of a movie, but we did not use this data to screen participants or movies. Our approach was based on the assumption that most of what we think we know is what we have been conditioned to know (Das, 2016). Nevertheless, future studies should control for the possible effects of movie likeness. Also, a future direction of the work in this area is to implement a broad range of criteria for movie selection that relate to the production technique of the movies (e.g., loudness, montage, sound effects), apart from those used in the present study. Another future research direction would be to study the relationship of the proposed metrics to pertinent factors of a movie's sales performance, such as film familiarity, the popularity of the actors and cultural familiarity (Hennig-Thurau et al., 2007). Factoring into the equation such features will help to examine further not only the direction but also the causality of the relations identified in this and other studies.

In summary, in this article, we propose a new computational approach for extracting a neural-based and an eye-gaze-based metrics and investigated their capacity to provide valuable and significant insights in predicting the population-wide behavior of movie goers. The first metric termed "Attentional-asynchrony" relies on eye-gaze data while the second metric termed "Cognitive-congruency" is estimated on selected frequency bands from the raw-EEG data. We provide evidence that such metrics provide significant and valuable insights in predicting sales performance of the movie during premiere as well as subsequent weekends, thus anticipating the commercial success of each film. Moreover, we discuss, in the context of existing literature, the possible relations of the derived neural metrics to cognitive states of enhanced arousal and focused attention, the encoding of long-term memory and the synchronization of different areas of the brain's rewards network. The proposed approach can be employed to pre-test a movie-trailer and anticipate the commercial success of the movie or TV series, thereby helping to inform the marketing strategy of the film before its release. Moreover, the proposed neurophysiological and eye-gaze based metrics could be used as markers in cinematics studies to help investigate the impact of movie features and filming techniques (scene transition/animations/special effect) to moviegoers' behavior. Finally, beyond the practical implication in predicting and understanding the behavior of moviegoers, the proposed approach can facilitate the use of video stimuli in neuroscience research; such as the study of individual differences in attention-deficit disorders, and the study of desensitization to media violence.

AUTHOR CONTRIBUTIONS

FUNDING

REFERENCES

Berns, G. S., and Moore, S. E. (2012). A neural predictor of cultural popularity. *J. Consum. Psychol.* 22, 154–160. doi: 10.1016/j.jcps.2011.05.001

Blankertz, B., Tomioka, R., Lemm, S., Kawanabe, M., and Muller, K.-R. (2008). Optimizing spatial filters for robust EEG single-trial analysis. *IEEE Signal Process. Mag.* 25, 41–56. doi: 10.1109/msp.2008.4408441

Boksem, M. A. S., and Smidts, A. (2015). Brain responses to movie trailers predict individual preferences for movies and their population-wide commercial success. *J. Mark. Res.* 52, 482–492. doi: 10.1509/jmr.13.0572

Christoforou, C., Christou-Champi, S., Constantinidou, F., and Theodorou, M. (2015). From the eyes and the heart: a novel eye-gaze metric that predicts video preferences of a large audience. *Front. Psychol.* 6:579. doi: 10.3389/fpsyg.2015.00579

Christoforou, C., Constantinidou, F., Shoshilou, P., and Simos, P. G. (2013). Single-trial linear correlation analysis: application to characterization of stimulus modality effects. *Front. Comput. Neurosci.* 7:15. doi: 10.3389/fncom.2013.00015

Christoforou, C., Mavridis, N., Machado, E. L., and Spanoudis, G. (2010). "Android tele-operation through brain-computer interfacing: a real-world demo with non-expert users," in *Proceedings of the 2010 International Symposium on Robotics and Intelligent Sensors (IRIS2010)* (Nagoya), 294–299.

Christoforou, C., Sajda, P., and Parra, L. C. (2008). "Second order bilinear discriminant analysis for single trial EEG analysis," in *Advances in Neural Information Processing Systems 20*, eds J. Platt, D. Koller, Y. Singer and S. Roweis (Vancouver, BC: Curran Associates, Inc.), 313–320.

Clauss, M., Bayerl, P., and Neumann, H. (2004). "A statistical measure for evaluating regions-of-interest based attention algorithms," in *Pattern Recognition*, (Vol. 3175) eds C. E. Rasmussen, H. H. Bülthoff, B. Schölkopf and M. A. Giese (Berlin, Heidelberg: Springer Berlin Heidelberg), 383–390.

Das, J. P. (2016). *Consciousness Quest: Where East Meets West, on Mind, Meditation, and Neural Correlates.* New Delhi: Sage Publications.

Dmochowski, J. P., Bezdek, M. A., Abelson, B. P., Johnson, J. S., Schumacher, E. H., and Parra, L. C. (2014). Audience preferences are predicted by temporal reliability of neural processing. *Nat. Commun.* 5:4567. doi: 10.1038/ncomms5567

Dmochowski, J. P., Sajda, P., Dias, J., and Parra, L. C. (2012). Correlated components of ongoing EEG point to emotionally laden attention—a possible marker of engagement? *Front. Hum. Neurosci.* 6:112. doi: 10.3389/fnhum.2012.00112

Dorr, M., Martinetz, T., Gegenfurtner, K. R., and Barth, E. (2010). Variability of eye movements when viewing dynamic natural scenes. *J. Vis.* 10:28. doi: 10.1167/10.10.28

Dyrholm, M., Christoforou, C., and Parra, L. C. (2007). Bilinear discriminant component analysis. *J. Mach. Learn. Res.* 8, 1097–1111. Available online at: http://www.jmlr.org/papers/volume8/dyrholm07a/dyrholm07a.pdf

Eastman, S. T., and Ferguson, D. A. (2012). *Media Programming: Strategies and Practices.* Available online at: http://books.google.com/books?id=xqslYAAACAAJ

Eckstein, M. K., Guerra-Carrillo, B., Miller Singley, A. T., and Bunge, S. A. (2017). Beyond eye gaze: what else can eyetracking reveal about cognition and cognitive development? *Dev. Cogn. Neurosci.* 25, 69–91. doi: 10.1016/j.dcn.2016.11.001

Engel, A. K., Fries, P., and Singer, W. (2001). Dynamic predictions: oscillations and synchrony in top-down processing. *Nat. Rev. Neurosci.* 2, 704–716. doi: 10.1038/35094565

Falk, E. B., Berkman, E. T., and Lieberman, M. D. (2012). From neural responses to population behavior: neural focus group predicts population-level media effects. *Psychol. Sci.* 23, 439–445. doi: 10.1177/0956797611434964

Fanti, K. A., Panayiotou, G., Lombardo, M. V., and Kyranides, M. N. (2016). Unemotional on all counts: evidence of reduced affective responses in individuals with high callous-unemotional traits across emotion systems and valences. *Soc. Neurosci.* 11, 72–87. doi: 10.1080/17470919.2015.1034378

Fell, J., Klaver, P., Lehnertz, K., Grunwald, T., Schaller, C., Elger, C. E., et al. (2001). Human memory formation is accompanied by rhinal-hippocampal coupling and decoupling. *Nat. Neurosci.* 4, 1259–1264. doi: 10.1038/nn759

Goldstein, R. B., Woods, R. L., and Peli, E. (2007). Where people look when watching movies: do all viewers look at the same place? *Comput. Biol. Med.* 37, 957–964. doi: 10.1016/j.compbiomed.2006.08.018

Hennig-Thurau, T., Houston, M. B., and Walsh, G. (2007). Determinants of motion picture box office and profitability: an interrelationship approach. *Rev. Manage. Sci.* 1, 65–92. doi: 10.1007/s11846-007-0003-9

Howard, M. W., Rizzuto, D. S., Caplan, J. B., Madsen, J. R., Lisman, J., Aschenbrenner-Scheibe, R., et al. (2003). Gamma oscillations correlate

with working memory load in humans. *Cereb. Cortex* 13, 1369–1374. doi: 10.1093/cercor/bhg084

Kong, W., Zhao, X., Hu, S., Zhang, J., Dai, G., Vecchiato, G., et al. (2012). "The study of memorization index based on W-GFP during the observation of TV commercials," in *Proceedings of the International Conference on Systems and Informatics (ICSAI2012)* (Yantai, China: IEEE), 2198–2202.

Mantini, D., Perrucci, M. G., Del Gratta, C., Romani, G. L., and Corbetta, M. (2007). Electrophysiological signatures of resting state networks in the human brain. *Proc. Natl. Acad. Sci. U S A* 104, 13170–13175. doi: 10.1073/pnas. 0700668104

Mathôt, S., Schreij, D., and Theeuwes, J. (2012). OpenSesame: an open-source, graphical experiment builder for the social sciences. *Behav. Res. Methods* 44, 314–324. doi: 10.3758/s13428-011-0168-7

Müller, M. M., Gruber, T., and Keil, A. (2000). Modulation of induced gamma band activity in the human EEG by attention and visual information processing. *Int. J. Psychophysiol.* 38, 283–299. doi: 10.1016/s0167-8760(00)00171-9

Parra, L., Christoforou, C., Gerson, A., Dyrholm, M., Luo, A., Wagner, M., et al. (2008). Spatiotemporal linear decoding of brain state. *IEEE Signal Process. Mag.* 25, 107–115. doi: 10.1109/msp.2008.4408447

Rajashekar, U., Cormack, L. K., and Bovik, A. C. (2004). "Point-of-gaze analysis reveals visual search strategies," in *Electronic Imaging 2004*, eds E. B. Rogowitz and T. N. Pappas (San Jose, CA: International Society for Optics and Photonics), 296–306.

Rodriguez, E., George, N., Lachaux, J. P., Martinerie, J., Renault, B., and Varela, F. J. (1999). Perception's shadow: long-distance synchronization of human brain activity. *Nature* 397, 430–433. doi: 10.1038/17120

Smith, T. J. (2013). "Watching you watch movies: using eye tracking to inform cognitive film theory," in *Psychocinematics: Exploring Cognition at the Movies, Chapter 9*, ed. A. P. Shimamura (New York, NY: Oxford University Press), 165–191.

Smith, T. J., and Mital, P. K. (2013). Attentional synchrony and the influence of viewing task on gaze behavior in static and dynamic scenes. *J. Vis.* 13:16. doi: 10.1167/13.8.16

Vecchiato, G., Kong, W., Giulio Maglione, A., Cherubino, P., Trettel, A., and Babiloni, F. (2014a). Cross-cultural analysis of neuroelectrical cognitive and emotional variables during the appreciation of TV commercials. *Neuropsychol. Trends* 16, 23–29. doi: 10.7358/neur-2014-016-vecc

Vecchiato, G., Maglione, A. G., Cherubino, P., Wasikowska, B., Wawrzyniak, A., Latuszynska, A., et al. (2014b). Neurophysiological tools to investigate consumer's gender differences during the observation of TV commercials. *Comput. Math. Methods Med.* 2014:912981. doi: 10.1155/2014/912981

Vecchiato, G., Toppi, J., Astolfi, L., De Vico Fallani, F., Cincotti, F., Mattia, D., et al. (2011). Spectral EEG frontal asymmetries correlate with the experienced pleasantness of TV commercial advertisements. *Med. Biol. Eng. Comput.* 49, 579–583. doi: 10.1007/s11517-011-0747-x

Electroencephalography Amplitude Modulation Analysis for Automated Affective Tagging of Music Video Clips

Andrea Clerico, Abhishek Tiwari, Rishabh Gupta, Srinivasan Jayaraman and Tiago H. Falk*

Centre Energie, Materiaux, Telecommunications, Institut National de la Recherche Scientifique, University of Quebec, Montreal, QC, Canada

The quantity of music content is rapidly increasing and automated affective tagging of music video clips can enable the development of intelligent retrieval, music recommendation, automatic playlist generators, and music browsing interfaces tuned to the users' current desires, preferences, or affective states. To achieve this goal, the field of affective computing has emerged, in particular the development of so-called affective brain-computer interfaces, which measure the user's affective state directly from measured brain waves using non-invasive tools, such as electroencephalography (EEG). Typically, conventional features extracted from the EEG signal have been used, such as frequency subband powers and/or inter-hemispheric power asymmetry indices. More recently, the coupling between EEG and peripheral physiological signals, such as the galvanic skin response (GSR), have also been proposed. Here, we show the importance of EEG amplitude modulations and propose several new features that measure the amplitude-amplitude cross-frequency coupling per EEG electrode, as well as linear and non-linear connections between multiple electrode pairs. When tested on a publicly available dataset of music video clips tagged with subjective affective ratings, support vector classifiers trained on the proposed features were shown to outperform those trained on conventional benchmark EEG features by as much as 6, 20, 8, and 7% for arousal, valence, dominance and liking, respectively. Moreover, fusion of the proposed features with EEG-GSR coupling features showed to be particularly useful for arousal (feature-level fusion) and liking (decision-level fusion) prediction. Together, these findings show the importance of the proposed features to characterize human affective states during music clip watching.

1. INTRODUCTION

With the rise of music and video-on-demand, as well as personalized recommendation systems, the need for accurate and reliable automated video tagging has emerged. In particular, user-centric affective tagging has stood out, corresponding to the formation of user emotional tags elicited while watching video clips (Kierkels et al., 2009; Shan et al., 2009; Koelstra and Patras, 2013). Emotions

are usually conceived as physiological and physical responses, as part of natural communication between humans, and able to influence our intelligence, shape our thoughts and govern our interpersonal relationships (Marg, 1995; Loewenstein and Lerner, 2003; De Martino et al., 2006). Typically, machines were not required to have "emotion sensing" skills, but instead relied solely on interactivity. Recent findings from neuroscience, psychology and cognitive science, however, have modified this mentality and have pushed for such emotion sensing skills to be incorporated into machines. Such capability can allow machines to learn, in real-time, the user's preferences and emotions and adapt accordingly, thus taking the first steps toward the basic component of intelligence in human-human interaction (Preece et al., 1994).

Incorporating emotions into machines constitutes the burgeoning field of affective computing, which has as main purpose reduce the distance between the end-user and the machine by designing instruments that are able to accurately address human needs (Picard, 2000). To this end, the area of affective brain-computer interfaces (aBCIs) has recently emerged (Mühl et al., 2014). While BCIs have been mostly used to date for communication and rehabilitation applications (e.g., Li et al., 2006; Leeb et al., 2012; Sorensen and Kjaer, 2013), aBCIs (also known as passive BCIs) aim at measuring implicit information from the users, such as their moods and emotional states elicited by varying stimuli. Representative applications include neurogaming (Bos et al., 2010), neuromarketing (Lee et al., 2007), and "attention monitors" (Moore Jackson and Mappus, 2010), to name a few. As in Koelstra and Patras (2013), this paper concerns the measurement of emotions elicited on users by different music video clips, i.e., for automated multimedia tagging.

Within aBCIs, electroencephalography (EEG) has remained a popular modality due to its non-invasiveness, high temporal resolution (in the order of milliseconds), portability, and reasonable cost (Jenke et al., 2014). Typically, spectral features such as subband spectral powers have been used to measure emotional states elicited from music videos, pictures, and/or movie clips (e.g., Kierkels et al., 2009; Koelstra et al., 2012), as well as mental workload and stress (e.g., Heger et al., 2010; Kothe and Makeig, 2011). Moreover, an inter-hemispheric asymmetry in spectral power has been reported in the affective state literature (Davidson and Tomarken, 1989; Jenke et al., 2014), particularly in frontal brain regions (Coan and Allen, 2004).

Recent studies, however, have suggested that alternate EEG feature representations may exist that convey more discriminatory information over traditional spectral power and asymmetry indices (Jenke et al., 2014; Gupta and Falk, 2015). More specifically, statistical relations among temporal dynamics in different frequency bands (so-called "cross-frequency coupling") have been observed in several brain regions and are thought to reflect neural communication and information encoding to support different perceptual and cognitive processes (Cohen, 2008) and emotional states (Schutter and Knyazev, 2012). Typically, cross-frequency coupling can be measured in three ways, namely, phase-phase, phase-amplitude and amplitude-amplitude coupling. While the former two have

been widely studied and shown to be related to perception and memory (e.g., theta-gamma coupling Canolty et al., 2006), the latter has received lower attention. A few studies have shown amplitude-amplitude coupling effects on personality and motivation (Schutter and Knyazev, 2012) and recently, the authors proposed an inter-hemispheric cross-frequency amplitude coupling metric that correlated with affective states (Clerico et al., 2015). Notwithstanding, existing coupling metrics typically overlook temporal dynamics and are based on inter-hemispheric synchrony, thus overlook synchronization of other brain regions.

Moreover, in addition to EEG correlates, affective state information has been widely obtained from physiological signals measured from the peripheral autonomic nervous system (PANS) (Nasoz et al., 2003; Lisetti and Nasoz, 2004; Wu and Parsons, 2011), particularly the galvanic skin response (GSR), a measure of the amount of sweat (conductivity) in the skin (Picard and Healey, 1997; Bersak et al., 2001). More recently, the interaction between the PANS and central nervous systems (CNS) was measured via a phase-amplitude coupling (PAC) between GSR and EEG signals and promising emotion recognition results were found for highly arousing videos (Kroupi et al., 2014). As emphasized in Canolty et al. (2012), however, different ways of computing PAC may lead to complementary information. As such, in this paper we explore different PAC computation methods to gauge the advantages of one method over another.

In this paper, we build on the work of Clerico et al. (2015) and investigate the development of alternate features based on EEG amplitude modulation analysis for automated affective tagging of music video clips. In particular, we propose a number of innovations, namely: (1) extended the inter-hemispheric cross-frequency coupling measures of EEG amplitude modulations analysis to all possible electrode pairs, thus exploring connections beyond left-right pairs, (2) explored the use of a coherence based coupling metric, as opposed to mutual information, to explore linear relationships between inter-electrode coupling, (3) explored a total amplitude modulation energy measure to capture temporal dynamics, (4) proposed a normalization scheme based on normalization of the proposed features relative to a baseline period, thus facilitating cross-subject classification (as opposed to per-subject classification in Clerico et al., 2015), and (5) explored different ways of computing PAC between EEG and GSR in order to gauge the benefits of one computation method over another. Furthermore, we show the benefits of the proposed features relative to existing spectral power-based ones, and explore their complementarity via decision- and feature-level fusion. Experimental results show the proposed features outperforming conventional ones in recognizing arousal, valence, and dominance emotional primitives, as well as a "liking" subjective parameter.

The remainder of this paper is organized as follows: Section 2 provides the methodology used, including a description of the proposed and baseline features, as well as classification and fusion strategies used. Sections 3 and 4 describe the experimental results and discusses the findings, respectively. Lastly, section 5 presents the conclusions.

2. MATERIALS AND METHODS

In this section, the database, the proposed and benchmark feature sets, as well as the feature selection, classifier and classifier fusion schemes used are described.

2.1. Affective Music Clip Audio-Visual Database

In this paper, the publicly-available DEAP (Dataset for Emotion Analysis using EEG and Physiological signals) database was used (Koelstra et al., 2012). Thirty-two healthy subjects (gender-balanced, average age of 26.9 years) were recruited to watch 40 video music clips while their neurophysiological signals were recorded. The forty videos were carefully selected from a larger set (roughly 200 videos), corresponding to the ones eliciting the 10 highest ratings within each of the four quadrants of the valence-arousal plane (Russell, 1980). Participants were asked to rate their perceived valence, arousal, and dominance emotional primitives, as well as other subjective ratings such as liking and familiarity for each of the 40 music clips. The three emotional primitives were scored using the 9-point continuous self-assessment manikin scale (Bradley and Lang, 1994). The liking scale was introduced to determine the user's taste, and not their feelings, about the music clip; as such, 9-point scale with thumbs down/up symbols was adopted. Lastly, the familiarity rating was scored using a 5-point scale. For the purpose of this paper, the familiarity rating was not used.

Several neurophysiological signals were recorded during music clip watching, namely 32-channel EEG (Biosemi Active II, with 10–20 international electrode placement), skin temperature, GSR, respiration, and blood volume pulse. The raw signals were recorded at a 512 Hz sample rate and down sampled offline to 128 Hz. The EEG signals were further bandpass filtered from 4 to 45 Hz, pre-processed using principal component analysis to remove ocular artifacts, averaged to a common reference and made publicly available. The interested reader is referred to Koelstra et al. (2012) for more details about the database.

2.2. Feature Extraction

2.2.1. Spectral Features

Spectrum subband power features are the most traditional measures used in biomedical signal processing (Sörnmo and Laguna, 2005). Within the affective state recognition literature, spectral power in the theta (4–8 Hz), alpha (8–12 Hz), beta (12–30 Hz), and gamma (30–45 Hz) subbands are typically used (Jenke et al., 2014) across different brain regions (Schutter et al., 2001; Balconi and Lucchiari, 2008). In particular, alpha and gamma band inter-hemispheric asymmetry indices have been shown to be correlated with emotional ratings, particularly in frontal brain regions (Müller et al., 1999; Mantini et al., 2007; Arndt et al., 2013). Given their widespread usage and the fact that they were also used in Koelstra et al. (2012) for affect recognition from the DEAP database, spectral features ("SF") are used here as a benchmark to gauge the benefits of the proposed features. A total of 128 spectral power features (32 electrodes × 4 subbands) and 56 asymmetry indices (14 inter-hemispheric pairs × 4 subbands) were computed from the following electrode pairs: Fp1-Fp2,

AF3-AF4, F7-F8, F3-F4, FC5-FC6, FC1-FC2, T7-T8, C3-C4, CP5-CP6, CP1-CP2, P7-P8, P3-P4, PO3-PO4, and O1-O2 (see **Figure 1** for electrode labels and locations). Overall, a total of 184 "SF" features are used as benchmark.

2.2.2. Amplitude Modulation Features
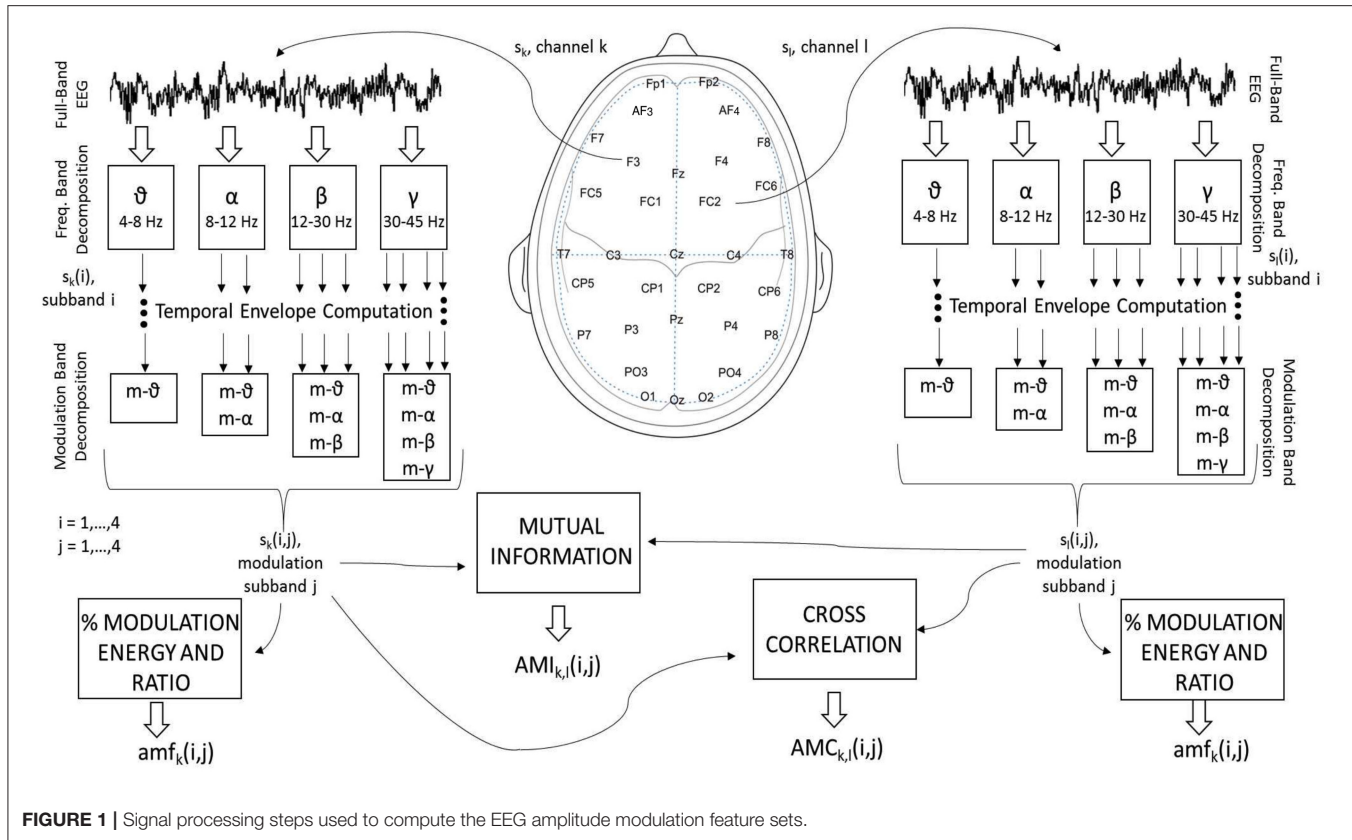
Cross-frequency amplitude-amplitude coupling in the EEG has been explored in the past as a measure of anxiety and motivation (e.g., Schutter and Knyazev, 2012), but has been under-explored within the affective state recognition community. Recently, beta-theta amplitude-amplitude coupling differences were observed between healthy elderly controls and age-matched Alzheimer's disease patients; such findings were linked to lack of interest and motivation within the patient population (Falk et al., 2012). To explore the benefits of cross-frequency amplitude-amplitude modulations for affective state recognition research, the authors recently showed that non-linear coupling patterns within inter-hemispheric electrode pairs was a reliable indicator of several affective dimensions, but particularly for the valence emotional primitive (Clerico et al., 2015). In this paper, we extend this work by extracting a number of other amplitude modulation features ("AMF") and show their advantages for affective state recognition.

More specifically, three new amplitude-amplitude coupling feature sets are extracted, namely the amplitude modulation energy (AME), amplitude modulation interaction (AMI), and the amplitude modulation coherence (AMC), as depicted by **Figure 1**. In order to compute these three feature sets, first the full-band EEG signal s_k for channel "k" (see left side of the figure) is decomposed into the four typical subbands (theta, alpha, beta and gamma) using zero-phase digital bandpass filters. Here, the time-domain index "n" is omitted for brevity, but without loss of generality. For the sake of notation, the decomposed time-domain signal is referred to as $s_k(i), i = 1, \ldots, 4$. The temporal envelope is then extracted from each of the four subband time series using the Hilbert transform (Le Van Quyen et al., 2001). **Figure 2** illustrates the extracted EEG subband time series in gray and their respective Hilbert amplitude envelopes in black. Here, the temporal envelopes $e_i(n)$ of each subband time series were computed as the magnitude of the complex analytic signal $\zeta(n) = s_k(i)^2 + j\mathcal{H}\{s_k(i)\}$, i.e.,
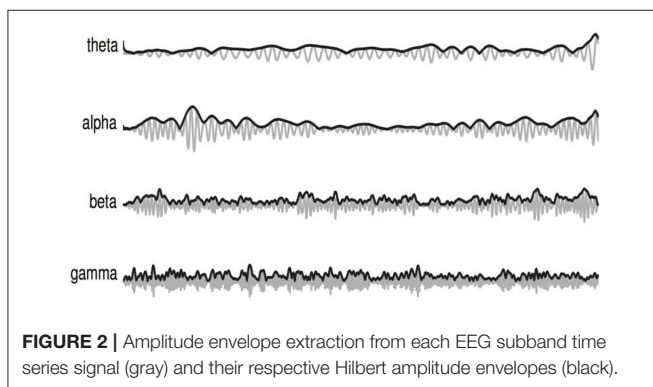
$$e_i(i) = \sqrt{s_k(i)^2 + \mathcal{H}\{s_k(i)\}^2}, \tag{1}$$

where, $\mathcal{H}\{\cdot\}$ corresponds to the Hilbert transform.

In order to measure cross-frequency amplitude-amplitude coupling, a second decomposition of the EEG amplitude envelopes is performed utilizing the same four subbands. To distinguish between modulation and frequency subbands, the former are referred to as m-θ (4–8 Hz), m-α (8–12 Hz), m-β (12–30 Hz) and m-γ (30–45 Hz). For notation, the amplitude-amplitude coupling pattern is termed $s_k(i, j), i, j = 1, \ldots, 4$, where "i" indexes spectral subbands and "j" the modulation spectral subbands. By using the Hilbert transform to extract the amplitude envelope, the types of cross-frequency interactions are limited by Bedrosian's theorem, which states that the envelope signals can only contain frequencies (i.e., modulated frequencies) up to the

FIGURE 1 | Signal processing steps used to compute the EEG amplitude modulation feature sets.

FIGURE 2 | Amplitude envelope extraction from each EEG subband time series signal (gray) and their respective Hilbert amplitude envelopes (black).

maximum frequency of its original signal (Boashash, 1991; Smith et al., 2002). As such, only the ten cross-frequency patterns shown in **Figure 1** are possible (per electrode), namely: θ_m-θ, α_m-θ, α_m-α, β_m-θ, β_m-α, β_m-β, γ_m-θ, γ_m-α, γ_m-β, and γ_m-γ. From these patterns, the three feature sets are computed, as detailed below:

2.2.2.1. Amplitude modulation energy (AME)

From the ten possible $s_k(i,j)$ patterns per electrode, two energy measures are computed. The first measures the ratio of energy in a given frequency–modulation-frequency pair ($\xi_k(i,j)$) over the total energy across all possible subbands

pair (i.e., $\sum_{i=1}^{4}\sum_{j=1}^{4}\xi_k(i,j)$), thus resulting in 320 features (32 electrodes × 10 cross-frequency coupling patterns; see possible combinations in **Figure 1**). The second measures the logarithm of the ratio of modulation energy during the 60-s music clip to the modulation energy during a 3-s baseline resting period, i.e., $10\log\left(\xi_k(i,j)^{video}/\xi_k(i,j)^{baseline}\right)$, thus resulting in an additional 320 features, for a total of 640 $\text{AME}_k(i,j)$ features, $k = 1,\ldots,32; i,j = 1,\ldots,4$.

2.2.2.2. Amplitude modulation interaction (AMI)

In order to incorporate inter-electrode amplitude modulation (non-linear) synchrony, the amplitude modulation interaction (AMI) features from Clerico et al. (2015) are also computed. Unlike the work described in Clerico et al. (2015), where interactions were only computed per symmetric inter-hemispheric pairs, here we measure interactions across all possible 496 electrode pair combinations (i.e., 2-by-2 combinations over all possible 32 channels) for each of the ten cross-frequency coupling patterns, thus resulting in 4960 features. The normalized mutual information (MI) is used to measure the interaction:

$$AMI_{k,l} = \frac{H(s_k) + H(s_l) - H(s_k, s_l)}{\sqrt{H(s_k)H(s_l)}}, \qquad (2)$$

where the $H(\cdot)$ operator represents marginal entropy and $H(\cdot, \times)$ the joint entropy, and s_k corresponds to $s_k(i,j)$ with the

frequency and modulation frequency indices omitted for brevity. Entropy was calculated using the histogram method with 50 discrete bins for each variable. Mutual information has been used widely in affective recognition research (e.g., Cohen et al., 2003; Khushaba et al., 2012; Hamm et al., 2014). Additionally a second measurement of logarithmic ratio between the 60-s clip and the 3-s baseline has been obtained, thus totalling 9920 AMI features.

2.2.2.3. Amplitude modulation coherence (AMC)

While the AMI features capture non-linear interactions between inter-electrode amplitude-amplitude coupling patterns, the Pearson correlation coefficient between the patterns can also be used to quantify the coherence, or linear interactions between the patterns. Spectral coherence measures have been widely used in EEG research and were recently shown to also be useful for affective state research (e.g., Kar et al., 2014; Xielifuguli et al., 2014). Hence, we explore the concept of amplitude modulation coherence, or AMC as a new feature for affective state recognition. The AMC features are computed as:

$$AMC_{k,l} = \frac{\sum_{n=1}^{N}(s_k(n) - \bar{s}_k)(s_l(n) - \bar{s}_l)}{\sqrt{\sum_{n=1}^{N}(s_k(n) - \bar{s}_k)^2 \sum_{n=1}^{N}(s_l(n) - \bar{s}_l)^2}}, \quad (3)$$

where $s_k(n)$ indicates the n-th sample of the $s_k(i,j)$ time-series (again, the frequency and modulation frequency indices were omitted for brevity), and $\bar{s}_k$ is the average over all samples of such time series. As previously, a total of 9920 AMC features are computed, including the logarithmic ratio with the 3-s baseline.

2.2.3. PANS-CNS Phase-Amplitude Coupling (PAC)

Electrophysiological signals reflect dynamical systems that interact with each other at different frequencies. Phase-Amplitude coupling represents one type of interaction and typically refers to modulation of the amplitude of high-frequency oscillators by the phase of low-frequency ones (Samiee et al.). Typically, such phase-amplitude coupling measures are computed from EEG signals alone (Schutter and Knyazev, 2012), but the concept of electrodermal activity phase coupled to EEG amplitude was recently introduced as a correlate of emotion, particularly for high arousing, very pleasant and very unpleasant stimuli (Kroupi et al., 2013, 2014). Here, we test three different GSR-phase and EEG-amplitude coupling measures. For the sake of notation, assume $u(n)$ is the rapid transient response called skin conductance response (SCR) with a narrowband of 0.5–1Hz (Kroupi et al., 2014), of the time-domain GSR signal. Using the Hilbert transform (Gabor, 1946), we can extract the signal's instantaneous phase $\phi_u(n)$ as in Kroupi et al. (2014):

$$\phi_u(n) = arctan\left(\frac{\mathcal{H}\{u(n)\}}{u(n)}\right). \quad (4)$$

For the amplitude envelope of the EEG signal $(A(s_k(n)))$, a shape-preserving piecewise cubic interpolation method of neighboring values is used, as in Kroupi et al. (2014). Given the GSR signal and phase, as well as the EEG amplitude envelope signals, the following coupling measures were computed.

2.2.3.1. Envelope-to-signal coupling (ESC)

The simplest coupling feature can be calculated via the Pearson correlation coefficient between the EEG amplitude envelope signal $A(s_k(n))$ and the raw GSR signal $u(n)$. The ESC feature can be computed using equation (3) with $A(s_k(n))$ and $u(n)$ in lieu of $s_k(i,j)$ and $s_l(i,j)$, respectively (Arnulfo et al., 2015). ESC has been shown to be particularly useful with noisy data (Onslow et al., 2011). A total of 32 ESC features were computed.

2.2.3.2. Cross-frequency coherence (CFC)

Cross-frequency coherence evaluates the magnitude square coherence between the filtered (0-1 Hz) GSR signal $u(n)$ and the filtered (4–45 Hz) envelope of the EEG signal $A(s_k(n))$, as in Onslow et al. (2011). The CFC feature is computed as:

$$CFC_k(f) = \frac{|P_{Au}(f)|^2}{P_{AA}(f)P_{uu}(f)}, \quad (5)$$

where $|P_{Au}(f)|^2$ is the cross power spectral density of the EEG amplitude $A(s_k(n))$ and GSR signal $u(n)$ at frequency f, and $P_{AA}(f)$ and $P_{uu}(f)$ are the spectral power densities of the two signals, respectively. The CFC feature ranges from 0 (no spectral coherence) to 1 (perfect spectral coherence) and has been used previously to quantify linear EEG synchrony in different frequency bands and its relationship with emotions (Daly et al., 2014). A total of 1344 CFC features were computed.

2.2.3.3. Modulation index (ModI)

PANS-CNS coupling measure tested is the so-called modulation index (ModI), which was recently shown to accurately characterize coupling intensity (Tort et al., 2010), particularly for emotion recognition (Kroupi et al., 2014). For calculation of the ModI feature, a composite times series is constructed as $[\phi_u(n), A(s_k(n))]$. The phases are then binned and the mean of $A(s_k(n))$ over each phase bin is calculated and denoted by $\langle A_s \rangle \phi_u(m)$, where m indexes phase bin; 18 bins were used in this experiment. Further, the mean amplitude distribution $P(m)$ is normalized by the sum over all bins, i.e.,:

$$P(m) = \frac{\langle A_s \rangle \phi_u(m)}{\sum_{m=1}^{18} \langle A_s \rangle \phi_u(m)}. \quad (6)$$

The normalized amplitude "distribution" $P(m)$ has similar properties as a probability density function. In fact, in the scenario in which no phase-amplitude coupling exists, $P(n)$ assumes a uniform distribution. Having this said, the ModI feature measures the deviation of $P(m)$ from a uniform distribution. This is achieved by means of a Kullback-Liebler (KL) divergence measure (Kullback and Leibler, 1951) between $P(m)$ and a uniform distribution $Q(m)$, given by:

$$D_{KL}(P, Q) = \sum_{m=1}^{18} U(m) log\left[\frac{P(m)}{Q(m)}\right], \quad (7)$$

The KL divergence $D_{KL}(P, Q)$ is always greater than zero, and equal to zero only when the two distributions are the same.

Finally, the ModI feature is defined as the ratio between the KL divergence and the log of the number of phase bins, i.e.,:

$$ModI = \frac{D_{KL}(P, Q)}{log(M)}. \tag{8}$$

where $M = 18$ is used in our experiments. A total of 32 ModI features were computed.

2.3. Feature Selection and Affective State Recognition

In this section, a description of the feature selection, classifiers, and classifier fusion strategies are discussed.

2.3.1. Feature Selection

As mentioned above, a large number of proposed and benchmark features were extracted. More specifically, a total of 184 SF, 20480 AMF, and 1408 PAC features were extracted. For classification purposes, these numbers are large and may lead to classifier overfitting. In such instances, feature ranking and/or feature selection algorithms are typically used. Recently, several feature selection algorithms were compared on an emotion recognition task (Jenke et al., 2014). The minimum redundancy maximum relevance (mRMR) algorithm (Peng et al., 2005) showed improved performance when paired with a support vector machine classifier (Wang et al., 2011). The mRMR is a mutual information based algorithm that optimizes two criteria simultaneously: the maximum-relevance criterion (i.e., maximizes the average mutual information between each feature and the target vector) and the minimum-redundancy criterion (i.e., minimizes the average mutual information between two chosen features). The algorithm finds near-optimal features using forward selection with the chosen features maximizing the combined max-min criteria.

Moreover, in an allied domain, multi-stage feature selection comprised of analysis of variance (ANOVA) between the features and target labels as a pre-screening, followed by mRMR, was shown to lead to improved results for SVM-based classifiers (Dastgheib et al., 2016). This multi-stage feature selection procedure is explored herein and during pre-screening, only features that attained *p*-values smaller than 0.1 were kept. Here, two tests are explored. With one, all top selected features for each feature class are used for classifier training. Given the different number of available features for each feature class, the input dimensionality of the attained classifiers will differ. For a more fair comparison, the second assumes that classifiers are trained on the same number of features for each feature class. To this end, the number of features used corresponds to the number of benchmark SF features that pass the ANOVA test.

In the available dataset, neurophysiological signals were recorded from 32 subjects while each watched a total of 40 music clips. Here, 25% of the available data (i.e., data from 10 music clips per subject, roughly half from the high and half from the low classes) was set aside for feature ranking. The remaining 75% was used for classifier training and testing in a leave-one-sample-out

(LOSO) cross-validation scheme, as described next. This hold-out scheme assures a more stringent setup, as feature selection and model training are not performed on the same data subset, which could lead to overly optimistic results. From the feature selection set, it was found that 35, 23, 19, and 21 SF features passed the ANOVA test for arousal, valence, dominance, and liking dimensions, respectively.

2.3.2. Classification
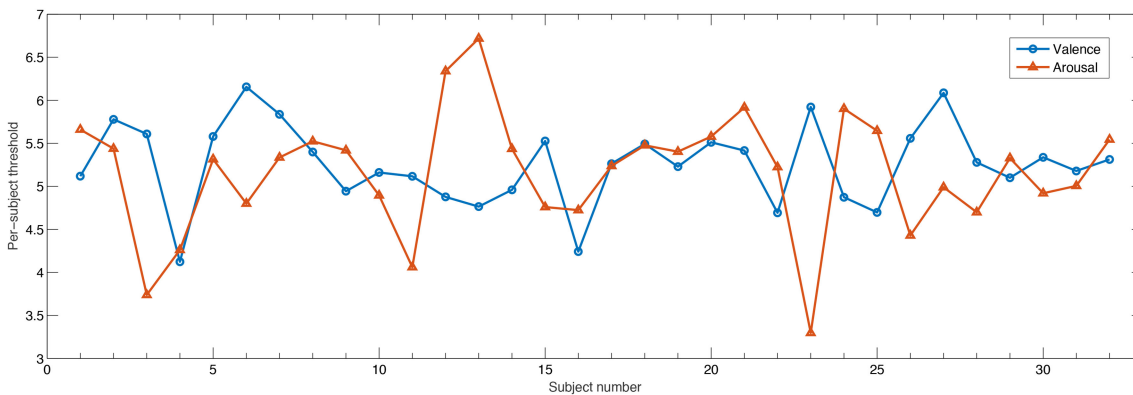
During pilot phase, support vector machine (SVM), relevance vector machine (RVM) and random forest classifiers were explored. Overall, SVMs resulted in improved performance. Indeed, they have been widely used in bioengineering and in affective state recognition (e.g., Wang et al., 2011). Given their widespread use, a description of the support vector machine approach is not included here and the interested reader is referred to Schölkopf and Smola (2002) and references therein for more details. Here, SVM classifiers are trained on four different binary classification problems, i.e., detecting low/high valence, low/high arousal, low/high dominance and low/high liking.

With the DEAP database, subjective ratings followed a 9-point scale. Typically, values greater or equal to 5 are assumed to correspond to high activation levels or low, otherwise. However, it is not guaranteed that all users objectively utilize the same scale for grading. In fact, by using a threshold of 5, a 60/40 ratio of high/low levels was obtained across all participants. In order to take into account individual biases during rating, here we utilize an individualized threshold corresponding to the value in which an almost balanced high/low ratio was achieved per participant. **Figure 3** depicts the threshold found for each participant for arousal and valence. As can be seen, on average a threshold of 5 was most often selected, though in a few cases, much higher or much lower values were found, thus exemplifying the need for such an individualized approach.

As mentioned previously, 75% of the available dataset was used for classifier training/testing using a leave-one-sample-out (LOSO) cross-validation scheme. For our experiments, a radial basis function (RBF) kernel was used and implemented with the Scikit-learn library in Python (Pedregosa et al., 2011). Since we are interested in gauging the benefits of the proposed features, and not of the classification schemes, we use the default SVM parameters throughout our experiments (i.e., $\lambda = 1$ and $\gamma_{RBF} = 0.01$). As such, it is expected that improved performance should be achieved once classifier optimization is performed, as in Gupta et al. (2016). Such analysis, however, is left for future study.

2.3.3. Fusion

In an attempt to improve classification performance, two fusion strategies are explored, namely, feature fusion and decision-level fusion. In feature fusion, we explore the combination of the three feature sets (SF, PAC, and AMF) and utilize the top selected features. With classifier decision-level fusion, on the other hand, the decisions of the three SVM classifiers trained on the top SF, PAC, and AMF sets were fused using a simple majority voting scheme with equal weights.

FIGURE 3 | Individualized threshold such that approximately 50/50 ratio was achieved for high/low class for valence and arousal dimensions.

2.4. Figure of Merit

Balanced accuracy (BACC) is used as a figure of merit and corresponds to the arithmetic mean of the classifier sensitivity and specificity, namely:

$$BACC = \frac{SENS + SPEC}{2}, \qquad (9)$$

where

$$SENS = \frac{TP}{P}; SPEC = \frac{TN}{N}, \qquad (10)$$

and $P = TP + FN$ and $N = FP + TN$, TP and FP correspond to true and false positives, respectively and TN and FN to true and false negatives, respectively. Balanced accuracy takes into account any remaining class unbalances and provides more accurate results than the conventional accuracy metric. To test the significance of the attained performances, an independent one-sample t-test against a random voting classifier was used ($p < 0.05$), as suggested in Koelstra et al. (2012).

3. RESULTS

Tables 1–4 show the top-selected features for the arousal, valence, dominance, and liking dimensions, respectively, following multi-stage feature selection and using the same number of features across sets. Feature names listed in the tables should be self explanatory. The "ratio" features correspond to the log-ratio ones between the video and baseline periods (see section 2.2.2). In the SF category, the "AI" features correspond to the asymmetry index between the indicated channels.

Table 5, in turn, reports the balanced accuracy results achieved with the individual features sets and the same dimensionality, as well as with the feature- and decision-level fusion strategies. All obtained results were significantly higher ($p < 0.05$) than those achieved with a random voting classifier (Koelstra et al., 2012). The column labeled "%" indicates the relative improvement in balanced accuracy, in percentage, relative to the SF baseline set. As can be seen, all proposed AMF features outperform the benchmark, by as much as 4.4,

5.6, 5.6, and 1.9% for valence, arousal, dominance, and liking, respectively. The PAC features also show advantages over the benchmark, particularly for the valence dimension, in which a 9.7% gain was observed. Feature fusion, in turn, showed to be useful mostly for arousal prediction, whereas decision-level fusion was useful for the liking dimension.

Moreover, for classifiers of varying dimensionality, maximum balanced accuracy values of 0.625 (AMI), 0.652 (AME), 0.659 (AMC) could be achieved for valence, dominance, liking, respectively, thus representing gains over the benchmark set of 8.1, 20.3, and 6.5%. For PAC features, gains could be seen only for the dominance dimension where a balanced accuracy of 0.592 could be seen, representing a gain over SF of 9.2%.

4. DISCUSSION

4.1. Feature Ranking

From **Tables 1–4**, it can be seen that with the exception of arousal, the number of SF features that passed the pre-screening test was roughly 20. For valence, roughly half those features corresponded to asymmetry index features, and across most emotional primitives, α, β and θ frequency bands showed to be the most relevant. These findings corroborate those widely reported in the literature (e.g., Davidson et al., 1979; Hagemann et al., 1999; Coan and Allen, 2004; Davidson, 2004).

Previous work on PAC, in turn, showed the coupling between EEG and GSR (computed via the ModI feature) to be relevant in emotion classification, particularly for arousal and valence (Kroupi et al., 2014). Interestingly, the CFC method of computing PANS-CNS phase-amplitude coupling was most often selected; for arousal 97% of the top features corresponded to CFC-type features. ModI features, in fact, were never selected as being a top candidate. PAC features showed to be particularly useful for valence estimation where 80% of the top features emanated from central brain regions (C3, CP1, FC1) and the attained balanced accuracy outperformed all other tested features. Such findings suggest that alternate PAC representations should be explored, especially within the scope of valence estimation.

TABLE 1 | Selected top-35 features for the arousal dimension.

Ranking	Arousal				
	AMI	**AMC**	**AME**	**PAC**	**SF**
1	γ_m-γ_FC5_CP2	α_m-α_T8_CP6	ratio_γ_m-γ_Fz	cfc_FC1_7_Hz	AI_β_FC1_FC2
2	β_m-α_FC5_CP5	θ_m-θ_Fp1_Pz	β_m-α_F7	cfc_CP5_7_Hz	AI_θ_FC1_FC2
3	γ_m-γ_FC5_Cz	γ_m-γ_FC5_FC1	ratio_γ_m-β_Pz	cfc_O1_19_Hz	γ_Fp1
4	γ_m-γ_FC5_AF4	γ_m-θ_CP5_F8	θ_m-θ_O1	cfc_FC5_15_Hz	θ_O2
5	γ_m-γ_AF4_CP2	θ_m-α_C3_O2	ratio_β_m-θ_CP5	cfc_FC1_44_Hz	α_O2
6	β_m-α_CP5_Pz	α_m-α_P7_C4	β_m-β_O2	cfc_O1_20_Hz	α_F7
7	γ_m-γ_FC5_PO4	α_m-θ_F7_T7	ratio_α_m-θ_O2	cfc_O1_27_Hz	θ_CP6
8	γ_m-α_PO3_F8	γ_m-γ_P7_F8	γ_m-β_F7	cfc_O1_28_Hz	α_Pz
9	γ_m-γ_FC5_C4	β_m-θ_C4_P4	ratio_α_m-α_T8	cfc_FC5_16_Hz	AI_β_AF3_AF4
10	γ_m-β_FC5_PO4	θ_m-θ_FC6_Cz	ratio_β_m-β_FC2	cfc_FC1_39_Hz	β_FC5
11	β_m-θ_FC2_P8	α_m-θ_T8_CP6	θ_m-θ_FC5	cfc_FC1_43_Hz	θ_AF4
12	γ_m-γ_FC5_Fp2	θ_m-θ_Fp1_P7	ratio_α_m-θ_Cz	cfc_FC1_42_Hz	θ_P4
13	γ_m-γ_FC5_Fz	γ_m-β_P7_F8	ratio_β_m-θ_Pz	cfc_O1_18_Hz	AI_β_P7_P8
14	γ_m-γ_AF4_Cz	α_m-α_FC2_P8	α_m-α_Cz	cfc_O1_26_Hz	θ_F8
15	β_m-β_AF3_CP5	α_m-θ_P7_C4	ratio_α_m-α_O2	cfc_P8_5_Hz	AI_β_FC5_FC6
16	β_m-β_FC5_CP5	β_m-α_C4_P4	ratio_α_m-θ_Fz	cfc_FC1_37_Hz	β_Fp2
17	α_m-α_FC1_T8	θ_m-θ_C3_O1	ratio_α_m-α_Cz	cfc_O1_29_Hz	θ_FC6
18	α_m-α_Oz_CP2	θ_m-θ_P3_P8	γ_m-α_F7	cfc_O1_23_Hz	θ_T8
19	γ_m-γ_FC5_FC6	α_m-θ_Fp1_Cz	α_m-θ_O2	cfc_O1_22_Hz	α_Fz
20	β_m-β_PO3_P8	γ_m-α_T7_FC2	ratio_β_m-θ_P3	cfc_FC1_8_Hz	α_PO3
21	γ_m-β_AF4_PO4	γ_m-β_FC5_FC1	α_m-θ_T8	cfc_FC5_18_Hz	γ_F4
22	γ_m-β_FC5_Fz	β_m-α_T7_T8	ratio_γ_m-γ_Oz	cfc_FC1_35_Hz	AI_θ_O1_O2
23	β_m-α_AF3_Pz	γ_m-α_FC5_FC1	θ_m-θ_P7	cfc_Fz_19_Hz	θ_P8
24	γ_m-γ_AF4_PO4	β_m-θ_Cz_PO4	ratio_γ_m-θ_CP1	esc_C4	AI_β_Fp1_Fp2
25	γ_m-β_FC5_Fp2	θ_m-θ_O1_CP6	α_m-θ_CP6	cfc_CP1_5_Hz	β_F3
26	γ_m-γ_Fp2_AF4	γ_m-γ_CP5_F8	α_m-α_T8	cfc_O1_25_Hz	β_FC1
27	α_m-θ_PO3_CP2	γ_m-γ_T7_FC2	β_m-α_C3	cfc_FC1_41_Hz	γ_P3
28	γ_m-γ_FC5_P3	β_m-β_F3_PO3	ratio_γ_m-γ_Pz	cfc_FC1_40_Hz	β_Fp1
29	γ_m-γ_FC5_FC1	γ_m-β_T7_FC2	ratio_γ_m-θ_Pz	cfc_FC1_38_Hz	α_PO4
30	β_m-β_AF3_O2	β_m-β_C4_P4	ratio_α_m-α_Fz	cfc_O1_30_Hz	θ_Fp2
31	α_m-θ_FC1_T8	α_m-θ_FC2_P8	ratio_γ_m-θ_P3	cfc_FC5_20_Hz	α_F4
32	α_m-θ_F3_Oz	γ_m-β_CP5_F8	α_m-θ_Cz	cfc_FC5_19_Hz	α_P7
33	γ_m-β_FC5_FC6	γ_m-β_P7_F8	ratio_θ_m-θ_O2	cfc_O1_21_Hz	AI_β_F7_F8
34	γ_m-γ_F3_Fp2	α_m-α_F7_T7	β_m-β_F7	cfc_FC5_17_Hz	β_AF3
35	γ_m-γ_FC1_AF4	α_m-α_Fp1_Cz	ratio_α_m-θ_AF4	cfc_O1_24_Hz	θ_CP2

Feature names listed should be self explanatory. The "ratio" features correspond to the log-ratio ones between the video and baseline periods; "AI" corresponds to the asymmetry index between the indicated channels.

Regarding the proposed AMF features, for arousal estimation, γ and β bands showed to be particularly useful, corresponding to roughly 86% of the top AMI features and 50% of the AMC and AME features. These findings are inline with results from Jenke et al. (2014). For valence, α interactions showed to be particularly useful, appearing in roughly 70% of the top AMI features. In particular α_m-θ interactions stood out, thus corroborating previous findings (Kensinger, 2004) which related these bands to states of internalized attention and positive emotional experience (Aftanas and Golocheikine, 2001). Such alpha/theta cross-frequency synchronization has also been previously related to memory usage (Chik, 2013). To corroborate this hypothesis, the correlation between the proposed features derived from the α_m-θ patterns and the subjective "familiarity" ratings reported by the participants was computed. The majority of the features showed to be significantly correlated (≥ 0.35, $p < 0.05$) with the familiarity rating, thus suggesting memory may have indeed played an effect on the elicited affective states.

Moreover, it was previously demonstrated that the power in the γ and β bands were also able to discriminate between liking and disliking judgements (Hadjidimitriou and Hadjileontiadis, 2012). By analyzing their amplitude modulation cross-frequency coupling via the proposed features, improved results were observed, thus showing the importance of EEG amplitude

TABLE 2 | Selected top-23 features for the valence dimension.

Ranking	Valence				
	AMI	AMC	AME	PAC	SF
1	α_m-α_O1_CP2	θ_m-θ_T7_F8	β_m-θ_PO4	cfc_T8_5_Hz	AI_α_PO3_PO4
2	α_m-α_O1_Oz	β_m-β_AF3_F4	ratio_γ_m-α_PO3	cfc_C3_26_Hz	α_P7
3	α_m-θ_F7_Pz	γ_m-γ_CP1_P7	ratio_β_m-β_Fp1	cfc_CP1_25_Hz	γ_Fz
4	α_m-α_F3_O1	γ_m-θ_AF3_Oz	ratio_α_m-θ_Oz	cfc_CP1_28_Hz	α_P3
5	α_m-α_O1_Fp2	β_m-α_F7_P8	ratio_γ_m-β_PO3	cfc_O2_15_Hz	AI_α_P3_P4
6	α_m-α_O1_O2	γ_m-β_F3_Oz	β_m-θ_Pz	cfc_C3_25_Hz	AI_γ_O1_O2
7	α_m-α_T7_O1	γ_m-γ_AF3_P7	ratio_γ_m-β_Fp1	cfc_C3_24_Hz	θ_Fz
8	β_m-β_CP6_CP2	γ_m-θ_AF3_P7	ratio_β_m-α_Fp1	esc_F3	α_PO3
9	α_m-θ_O1_CP2	γ_m-α_F3_Oz	γ_m-β_PO4	cfc_O2_14_Hz	AI_α_P7_P8
10	β_m-β_F4_CP2	θ_m-θ_Pz_PO4	ratio_β_m-θ_P8	cfc_FC1_42_Hz	θ_O1
11	β_m-θ_AF3_Oz	α_m-α_Fp1_Pz	β_m-β_P3	cfc_FC1_43_Hz	β_PO3
12	α_m-α_O1_PO4	θ_m-θ_F4_FC2	ratio_α_m-α_CP2	cfc_C3_27_Hz	AI_α_F7_F8
13	β_m-β_F4_F8	γ_m-γ_F3_Oz	γ_m-γ_PO4	cfc_CP1_23_Hz	AI_γ_C3_C4
14	γ_m-β_F7_Cz	γ_m-θ_F3_Oz	β_m-θ_T8	cfc_C3_23_Hz	AI_γ_FC1_FC2
15	α_m-θ_O1_O2	β_m-α_AF3_F4	β_m-α_P3	cfc_CP1_30_Hz	AI_β_PO3_PO4
16	α_m-θ_O1_Cz	γ_m-θ_Oz_O2	β_m-α_PO4	cfc_CP1_24_Hz	AI_β_FC5_FC6
17	α_m-α_CP1_PO4	β_m-α_F4_P8	β_m-β_T7	esc_F4	AI_α_O1_O2
18	γ_m-θ_F3_O1	γ_m-α_CP1_P7	β_m-θ_T7	cfc_FC1_45_Hz	AI_β_F7_F8
19	γ_m-β_P8_O2	γ_m-α_CP1_P7	ratio_β_m-α_PO3	cfc_CP1_26_Hz	AI_θ_AF3_AF4
20	α_m-θ_O1_Fz	β_m-β_CP5_T8	γ_m-θ_PO4	cfc_CP1_29_Hz	α_Fz
21	α_m-θ_F7_AF4	β_m-β_F7_P8	ratio_β_m-β_PO3	cfc_CP1_27_Hz	AI_β_P3_P4
22	α_m-α_O1_Cz	γ_m-β_AF3_P7	ratio_θ_m-θ_CP2	cfc_FC1_44_Hz	β_P3
23	α_m-θ_O1_Oz	θ_m-θ_O1_Cz	ratio_γ_m-α_Fp1	esc_AF3	θ_AF3

Feature names listed should be self explanatory. The "ratio" features correspond to the log-ratio ones between the video and baseline periods; "AI" corresponds to the asymmetry index between the indicated channels.

modulation coupling for affective state recognition. In fact, for the liking dimension 100% of the AMC features came from these two bands and this feature set resulted in the greatest improvement over the benchmark set (i.e., 1.9% increase). Moreover, β and α interactions were shown useful for dominance prediction in Liu and Sourina (2012). Here, 63% of the AMI features corresponded to those bands with several β_m-α features appearing at the top. Interestingly, for the AMC features, all top 19 features corresponded to β band interactions, with several coming from parietal regions, thus corroborating findings in Liu and Sourina (2012).

From the Tables, it can also be seen that the proposed normalization scheme over the baseline period was shown to be extremely important for the AME features, which unlike AMI and AMC, are energy-based features and not connectivity ones. For arousal, roughly 57% of the features corresponded to normalized features. For valence and liking they roughly corresponded to half of the top feature set. Normalization is important in order to remove participant-specific variability. Interestingly, only for the dominance dimension were normalized features seldom selected (20%) and it was for this emotional primitive that the AME features showed to be most useful. When analyzing the high/low threshold used per subject, it was observed that for the dominance dimension, the standard deviation of the optimal threshold

across participants was lower at 0.65. For comparison purposes, the standard deviation for arousal (shown in **Figure 3**) was of 0.71. As such, since there was lower inter-subject variability for the dominance dimension, normalization was not as important. Overall, for the entire AMF set, channels that involved the frontal region provided several relevant features, thus confirming the importance of the frontal region for affective state recognition (Mikutta et al., 2012).

4.2. Classification and Feature Fusion

As shown in **Table 5**, all tested features and feature combinations resulted in balanced accuracy results significantly greater than chance. When all classifiers relied on the same input dimensionality and default parameters, the superiority of the proposed amplitude modulation features could be seen, particularly for the arousal, dominance and liking dimensions. In the case of equal dimensionality, fusion of AMF features did not result in any improvements over the individual amplitude modulation features, both for feature- and decision-level fusion. Notwithstanding, some improvement was seen when more features were explored. PAC features, in turn, were shown to be particularly useful for valence estimation. When PAC features were fused with benchmark and proposed AMF features, (i) feature-level fusion was shown to be particularly useful for arousal estimation, achieving results significantly better than

TABLE 3 | Selected top-19 features for the dominance dimension.

Ranking	Dominance				
	AMI	AMC	AME	PAC	SF
1	θ_m-θ_CP1_T8	β_m-θ_P7_F8	γ_m-β_P7	esc_AF3	θ_FC2
2	α_m-α_P3_Oz	β_m-α_CP1_F8	β_m-β_P3	cfc_FC2_11_Hz	γ_F3
3	α_m-θ_AF3_T7	β_m-θ_T7_F8	α_m-α_Pz	cfc_FC2_8_Hz	α_PO3
4	γ_m-α_F7_CP6	β_m-α_CP5_AF4	γ_m-α_P7	cfc_CP6_7_Hz	θ_C3
5	θ_m-θ_P3_P8	β_m-β_CP1_Fz	γ_m-θ_PO4	cfc_CP6_8_Hz	θ_Pz
6	θ_m-θ_FC2_P8	β_m-α_P7_FC6	α_m-θ_Pz	cfc_F3_6_Hz	γ_P7
7	β_m-α_CP1_Pz	β_m-θ_PO3_P4	ratio_γ_m-β_P8	cfc_FC2_7_Hz	θ_FC6
8	α_m-α_F3_Fz	β_m-α_CP1_Fz	ratio_β_m-θ_P8	cfc_FC5_5_Hz	θ_P4
9	β_m-θ_P3_F4	β_m-θ_F8_P4	ratio_γ_m-γ_P8	cfc_F4_12_Hz	β_F3
10	β_m-α_CP1_P3	β_m-β_CP1_F8	θ_m-θ_Pz	cfc_FC2_9_Hz	α_P7
11	β_m-α_P3_Pz	β_m-α_PO3_PO4	γ_m-γ_PO4	cfc_FC5_11_Hz	β_C4
12	β_m-θ_P3_PO4	β_m-α_P7_F8	ratio_γ_m-γ_PO4	cfc_CP1_42_Hz	AI_β_CP5_CP6
13	α_m-α_AF3_Fz	β_m-β_CP5_Pz	β_m-α_F7	cfc_CP6_9_Hz	θ_PO3
14	β_m-β_FC5_Pz	β_m-α_CP5_Pz	γ_m-β_F7	cfc_P4_6_Hz	α_Pz
15	α_m-α_AF3_T7	β_m-β_CP5_AF4	γ_m-β_P3	cfc_F4_14_Hz	θ_P3
16	γ_m-α_F7_CP2	β_m-β_P7_F8	γ_m-γ_F7	cfc_AF4_5_Hz	θ_Fp2
17	θ_m-θ_CP1_CP2	β_m-β_PO3_PO4	γ_m-θ_Cz	cfc_F4_13_Hz	AI_β_PO3_PO4
18	θ_m-θ_T8_P8	β_m-θ_CP1_F8	β_m-β_Cz	cfc_FC2_12_Hz	θ_O1
19	β_m-β_FC5_P3	β_m-θ_CP1_Fz	β_m-β_F7	cfc_FC2_10_Hz	AI_γ_F7_F8

Feature names listed should be self explanatory. The "ratio" features correspond to the log-ratio ones between the video and baseline periods; "AI" corresponds to the asymmetry index between the indicated channels.

TABLE 4 | Selected top-21 features for the liking dimension.

Ranking	Liking				
	AMI	AMC	AME	PAC	SF
1	β_m-θ_AF4_CP6	γ_m-α_Pz_AF4	ratio_β_m-θ_FC6	cfc_P7_30_Hz	α_P3
2	β_m-α_PO3_P8	β_m-β_O1_T8	γ_m-β_P7	cfc_FC1_7_Hz	θ_C3
3	α_m-α_O1_Oz	β_m-β_Pz_FC2	ratio_γ_m-γ_P8	cfc_P7_29_Hz	β_P3
4	γ_m-γ_Fp1_T7	γ_m-β_Pz_AF4	γ_m-θ_P3	cfc_PO4_42_Hz	β_T8
5	α_m-α_Oz_FC2	β_m-β_CP5_AF4	α_m-α_AF4	esc_T8	β_O1
6	θ_m-θ_Fp1_AF4	γ_m-γ_Pz_AF4	ratio_γ_m-α_P8	cfc_P7_32_Hz	θ_P4
7	θ_m-θ_C3_P8	β_m-θ_FC1_O1	ratio_γ_m-θ_F3	cfc_P7_31_Hz	α_F8
8	θ_m-θ_CP5_AF4	γ_m-θ_Pz_AF4	α_m-α_CP1	cfc_PO4_39_Hz	β_PO3
9	β_m-θ_P3_AF4	γ_m-γ_AF3_Oz	ratio_β_m-θ_P8	cfc_PO4_45_Hz	AI_β_FC5_FC6
10	β_m-θ_F7_AF4	γ_m-β_CP1_AF4	γ_m-θ_F3	esc_F3	β_AF3
11	θ_m-θ_P7_AF4	β_m-α_O1_T8	ratio_β_m-β_C3	cfc_PO4_44_Hz	θ_CP1
12	β_m-β_PO3_P8	γ_m-α_Fp1_T7	ratio_β_m-α_C3	cfc_Fp1_8_Hz	α_CP5
13	θ_m-θ_PO3_Cz	β_m-α_CP5_P4	ratio_β_m-α_F3	cfc_P7_26_Hz	β_F3
14	β_m-θ_F3_AF4	γ_m-θ_CP1_AF4	ratio_α_m-θ_Fp1	esc_CP1	AI_α_P7_P8
15	θ_m-θ_CP1_AF4	γ_m-β_AF3_Oz	ratio_γ_m-γ_FC6	cfc_PO4_41_Hz	AI_β_F7_F8
16	α_m-θ_Oz_FC2	β_m-θ_FC5_PO3	ratio_β_m-α_Fp2	cfc_PO4_43_Hz	AI_β_PO3_PO4
17	α_m-θ_P7_P8	γ_m-γ_CP1_AF4	ratio_γ_m-β_P8	cfc_P7_27_Hz	θ_FC6
18	β_m-β_PO3_P4	γ_m-α_AF3_Oz	β_m-θ_P7	esc_P8	β_FC5
19	θ_m-θ_Pz_CP6	β_m-θ_F3_P8	ratio_θ_m-θ_P7	cfc_FC1_8_Hz	AI_θ_F7_F8
20	θ_m-θ_Pz_AF4	β_m-β_F3_P8	ratio_β_m-β_F3	cfc_FC6_10_Hz	θ_F4
21	β_m-θ_AF4_T8	γ_m-α_CP1_AF4	β_m-β_T7	cfc_P7_28_Hz	θ_Fz

Feature names listed should be self explanatory. The "ratio" features correspond to the log-ratio ones between the video and baseline periods; "AI" corresponds to the asymmetry index between the indicated channels.

TABLE 5 | Performance comparison of SVM classifiers for different feature sets and fusion strategies.

Feature class	Fusion type	Valence	%	Arousal	%	Dominance	%	Liking	%
AMI	–	0.604	4.4	0.583	5.6	0.564	4.1	0.626	1.1
AMC	–	0.594	2.7	0.563	1.9	0.569	5.0	0.630	1.9
AME	–	0.600	3.6	0.563	1.9	0.573	5.6	0.627	1.3
AMF	Feature-level	0.594	2.7	0.583	5.6	0.566	4.4	0.624	0.9
PAC	–	0.634	9.7	0.568	3.0	0.559	3.2	0.629	1.7
SF	–	0.578	–	0.552	–	0.542	–	0.619	–
AMF + SF + PAC	Feature-level	0.594	2.7	0.598	8.4	0.567	4.6	0.624	0.9
AMI + AMC + AME	Decision-level	0.594	2.8	0.563	1.9	0.567	4.6	0.625	1.0
AMF + PAC + SF	Decision-level	0.594	2.7	0.563	1.9	0.563	3.7	0.633	2.2

All reported results were significantly higher than chance achieved with a random voting classifier (p < 0.05). Column labeled "%" indicates relative improvement, in percentage, over the SF baseline set.

the benchmark ($p \leq 0.05$), and (ii) decision-level fusion was shown to be useful for liking prediction. Once varying input dimensionality was explored, the advantages of the proposed features over the benchmark became more evident, with gains as high as 8 and 20% being observed for the valence and dominance dimensions, respectively. Such results were significantly better than the benchmark ($p \leq 0.05$).

4.3. Study Limitations

This study has relied on the publicly available pre-processed DEAP database, which utilized a common average reference. Such referencing scheme could have introduced an artificial correspondence between nearby channels, thus potentially biasing the amplitude modulation and connectivity measures (Dezhong, 2001; Dezhong et al., 2005). By utilizing the multi-stage feature selection strategy, such biases were reduced, as feature redundancy was minimized and relevance was maximized. Moreover, from the relevant connections reported in the Tables, it can be seen that the majority of relevant connections are from electrodes that are sufficiently far apart, thus overcoming potential smearing contamination issues due to referencing. Moreover, as with many other machine learning problems, differences in data partitioning may lead to different top-selected features and, consequently, to varying performance results. This is particularly true for smaller datasets such as the one used herein. To test the sensitivity of data partitioning on feature selection, we randomly partitioned the 25% subset twice and explored the top selected features in each partition. For the AME features, for example, and the valence dimension, it was found that 13 of the top 23 features coincided for the two partitions. While this number is not very high, it is encouraging and future work should explore the use of boosting strategies and/or alternate data partitioning schemes to improve this.

5. CONCLUSIONS

In this work, experimental results with the publicly available DEAP database showed the EEG amplitude modulation

based feature sets such as amplitude-amplitude cross-frequency modulation coupling features, as well as linear and nonlinear connection between multiple electrode pairs outperformed benchmark measures based on spectral power by as much as maximum 20% for dominance. Moreover, phase-amplitude coupling of EEG and GSR signals outperformed the benchmark by over 9% and when fused with the proposed amplitude modulation features, further gains in arousal and liking prediction were observed. Such findings suggest the importance of the proposed features for affective state recognition and signal the importance of EEG amplitude modulation for affective tagging of music video clips and content.

ETHICS STATEMENT

This study relied on publicly available data collected by others. Details about the database can be found at: Koelstra et al. (2012).

AUTHOR CONTRIBUTIONS

AC performed data analysis and prepared the manuscript. RG assisted with data analysis and classification. SJ assisted with connectivity analysis and manuscript writing. TF contributed the study design, project supervision, and manuscript preparation. All authors read and approved the final manuscript.

FUNDING

ACKNOWLEDGMENTS

REFERENCES

Aftanas, L., and Golocheikine, S. (2001). Human anterior and frontal midline theta and lower alpha reflect emotionally positive state and internalized attention: high-resolution eeg investigation of meditation. *Neurosci. Lett.* 310, 57–60. doi: 10.1016/S0304-3940(01)02094-8

Arndt, S., Antons, J., Gupta, R., Schleicher, R., Moller, S., and Falket, T. H. (2013). "The effects of text-to-speech system quality on emotional states and frontal alpha band power," in *IEEE International Conference on Neural Engineering* (San Diego, CA), 489–492.

Arnulfo, G., Hirvonen, J., Nobili, L., Palva, S., and Palva, J. M. (2015). Phase and amplitude correlations in resting-state activity in human stereotactical EEG recordings. *NeuroImage* 112, 114–127. doi: 10.1016/j.neuroimage.2015.02.031

Balconi, M., and Lucchiari, C. (2008). Consciousness and arousal effects on emotional face processing as revealed by brain oscillations. A gamma band analysis. *Int. J. Psychophysiol.* 67, 41–46. doi: 10.1016/j.ijpsycho.2007.10.002

Bersak, D., McDarby, G., Augenblick, N., McDarby, P., McDonnell, D., McDonald, B., et al. (2001). "Intelligent biofeedback using an immersive competitive environment," in *Paper at the Designing Ubiquitous Computing Games Workshop at UbiComp* (Atlanta, GA).

Boashash, B. (1991). *Time-Frequency Signal Analysis*. Prentice Hall.

Bos, D. P.-O., Reuderink, B., van de Laar, B., Gurkok, H., Muhl, C., Poel, M., et al. (2010). "Human-computer interaction for BCI games: usability and user experience," in *Proceedings of the IEEE International Conference on Cyberworlds* (Singapore), 277–281. doi: 10.1109/CW.2010.22

Bradley, M., and Lang, P. (1994). Measuring emotion: the self-assessment manikin and the semantic differential. *Behav. Ther. Exp. Psychiatry* 25, 49–59. doi: 10.1016/0005-7916(94)90063-9

Canolty, R. T., Cadieu, C. F., Koepsell, K., Knight, R. T., and Carmena, J. M. (2012). Multivariate phase–amplitude cross-frequency coupling in neurophysiological signals. *IEEE Trans. Biomed. Eng.* 59, 8–11. doi: 10.1109/TBME.2011.2172439

Canolty, R. T., Edwards, E., Dalal, S. S., Soltani, M., Nagarajan, S. S., Kirsch, H. E., et al. (2006). High gamma power is phase-locked to theta oscillations in human neocortex. *Science* 313, 1626–1628. doi: 10.1126/science.1128115

Chik, D. (2013). Theta-alpha cross-frequency synchronization facilitates working memory control–a modeling study. *SpringerPlus* 2:14. doi: 10.1186/2193-1801-2-14

Clerico, A., Gupta, R., and Falk, T. (2015). "Mutual information between inter-hemispheric EEG spectro-temporal patterns: a new feature for automated affect recognition," in *IEEE Neural Engineering Conference* (Montpellier), 914–917.

Coan, J., and Allen, J. (2004). Frontal EEG asymmetry as a moderator and mediator of emotion. *Biol. Psychol.* 67, 7–50. doi: 10.1016/j.biopsycho.2004.03.002

Cohen, I., Sebe, N., Garg, A., Chen, L. S., and Huang, T. S. (2003). Facial expression recognition from video sequences: temporal and static modeling. *Comput. Vis. Image Understand.* 91, 160–187. doi: 10.1016/S1077-3142(03)00081-X

Cohen, M. X. (2008). Assessing transient cross-frequency coupling in eeg data. *J. Neurosci. Methods* 168, 494–499. doi: 10.1016/j.jneumeth.2007.10.012

Daly, I., Malik, A., Hwang, F., Roesch, E., Weaver, J., Kirke, A., et al. (2014). Neural correlates of emotional responses to music: an EEG study. *Neurosci. Lett.* 573, 52–57. doi: 10.1016/j.neulet.2014.05.003

Dastgheib, Z. A., Pouya, O. R., Lithgow, B., and Moussavi, Z. (2016). "Comparison of a new *ad-hoc* classification method with support vector machine and ensemble classifiers for the diagnosis of meniere's disease using evestg signals," in *IEEE Canadian Conference on Electrical and Computer Engineering* (Vancouver, BC).

Davidson, R., Schwartz, G., Saron, C., Bennett, J., and Goleman, D. J. (1979). Frontal versus parietal EEG asymmetry during positive and negative affect. *Psychophysiology* 16, 202–203.

Davidson, R. J. (2004). What does the prefrontal cortex "do" in affect: perspectives on frontal EEG asymmetry research. *Biol. Psychol.* 67, 219–234. doi: 10.1016/j.biopsycho.2004.03.008

Davidson, R. J., and Tomarken, A. J. (1989). Laterality and emotion: an electrophysiological approach. *Handb. Neuropsychol.* 3, 419–441.

De Martino, B., Kumaran, D., Seymour, B., and Dolan, R. J. (2006). Frames, biases, and rational decision-making in the human brain. *Science* 313, 684–687. doi: 10.1126/science.1128356

Dezhong, Y. (2001). A method to standardize a reference of scalp EEG recordings to a point at infinity. *Physiol. Meas.* 22, 693–711. doi: 10.1088/0967-3334/22/4/305

Dezhong, Y., Wang, L., Oostenveld, R., Nielsen, K. D., Arendt-Nielsen, L., and Chen, A. C.(2005). A comparative study of different references for EEG spectral mapping: the issue of the neutral reference and the use of the infinity reference. *Physiol. Meas.* 26, 173–184. doi: 10.1088/0967-3334/26/3/003

Falk, T. H., Fraga, F. J., Trambaiolli, L., and Anghinah, R. (2012). EEG amplitude modulation analysis for semi-automated diagnosis of alzheimer's disease. *EURASIP J. Adv. Signal Process.* 2012:192. doi: 10.1186/1687-6180-2012-192

Gabor, D. (1946). Theory of communication. part 1: the analysis of information. *J. IEE III* 93, 429–441. doi: 10.1049/ji-3-2.1946.0074

Gupta, R., and Falk, T. (2015). "Affective state characterization based on electroencephalography graph-theoretic features," in *IEEE Neural Engineering Conference* (Montpellier), 577–580.

Gupta, R., Laghari, U. R., and Falk, T. H., (2016). Relevance vector classifier decision fusion and EEG graph-theoretic features for automatic affective state characterization. *Neurocomputing* 174, 875–884. doi: 10.1016/j.neucom.2015.09.085

Hadjidimitriou, S. K., and Hadjileontiadis, L. J. (2012). Toward an EEG-based recognition of music liking using time-frequency analysis. *IEEE Trans. Biomed. Eng.* 59, 3498–3510. doi: 10.1109/TBME.2012.2217495

Hagemann, D., Naumann, E., Lürken, A., Becker, G., Maier, S., and Bartussek, D. (1999). EEG asymmetry, dispositional mood and personality. *Pers. Indiv. Diff.* 27, 541–568. doi: 10.1016/S0191-8869(98)00263-3

Hamm, J., Pinkham, A., Gur, R. C., Verma, R., and Kohler, C. G. (2014). Dimensional information-theoretic measurement of facial emotion expressions in schizophrenia. *Schizophr. Res. Treat.* 2014:243907. doi: 10.1155/2014/243907

Heger, D., Putze, F., and Schultz, T. (2010). "Online workload recognition from EEG data during cognitive tests and human-machine interaction," in *Advances in Artificial Intelligence: 33rd Annual German Conference on AI*, eds R. Dillmann, J. Beyerer, U. D. Hanebeck, and T. Schultz (Berlin; Heidelberg: Springer), 410–417.

Jenke, R., Peer, A., and Buss, M. (2014). Feature extraction and selection for emotion recognition from EEG. *IEEE Trans. Affect. Comput.* 5, 327–339. doi: 10.1109/TAFFC.2014.2339834

Kar, R., Konar, A., Chakraborty, A., and Nagar, A. K. (2014). "Detection of signaling pathways in human brain during arousal of specific emotion," in *2014 International Joint Conference on Neural Networks (IJCNN)* (Beijing: IEEE), 3950–3957.

Kensinger, E. A. (2004). Remembering emotional experiences: the contribution of valence and arousal. *Rev. Neurosci.* 15, 241–252. doi: 10.1515/REVNEURO.2004.15.4.241

Khushaba, R. N., Greenacre, L., Kodagoda, S., Louviere, J., Burke, S., and Dissanayake, G. (2012). Choice modeling and the brain: a study on the electroencephalogram (eeg) of preferences. *Exp. Syst. Appl.* 39, 12378–12388. doi: 10.1016/j.eswa.2012.04.084

Kierkels, J., Soleymani, M., and Pun, T. (2009). "Queries and tags in affect-based multimedia retrieval," in *IEEE International Conference on Multimedia and Expo* (New York, NY: IEEE), 1436–1439.

Koelstra, S., Mühl, C., Soleymani, M., and Patras, I. (2012). DEAP: a database for emotion analysis using physiological signals. *IEEE Trans. Affect. Comput.* 3, 18–31. doi: 10.1109/T-AFFC.2011.15

Koelstra, S., and Patras, I. (2013). Fusion of facial expressions and eeg for implicit affective tagging. *Image Vis. Comput.* 31, 164–174. doi: 10.1016/j.imavis.2012.10.002

Kothe, C. A., and Makeig, S. (2011). "Estimation of task workload from EEG data: new and current tools and perspectives," in *International Conference of the IEEE EMBS* (Boston, MA: IEEE), 6547–6551.

Kroupi, E., Vesin, J.-M., and Ebrahimi, T. (2013). "Phase-amplitude coupling between EEG and EDA while experiencing multimedia content," in *International Conference on Affective Computing and Intelligent Interaction* (Geneva: IEEE), 865–870.

Kroupi, E., Vesin, J.-M., and Ebrahimi, T. (2014). Implicit affective profiling of subjects based on physiological data coupling. *Brain Comput. Interf.* 1, 85–98. doi: 10.1080/2326263X.2014.912882

Kullback, S., and Leibler, R. A. (1951). On information and sufficiency. *Ann. Math. Stat.* 22, 79–86. doi: 10.1214/aoms/1177729694

Le Van Quyen, M., Foucher, J., Lachaux, J.-P., Rodriguez, E., Lutz, A., Martinerie, J., et al. (2001). Comparison of hilbert transform and wavelet methods for the analysis of neuronal synchrony. *J. Neurosci. Methods* 111, 83–98. doi: 10.1016/S0165-0270(01)00372-7

Lee, N., Broderick, A. J., and Chamberlain, L. (2007). What is "neuromarketing?" a discussion and agenda for future research. *Int. J. Psychophysiol.* 63, 199–204. doi: 10.1016/j.ijpsycho.2006.03.007

Leeb, R., Friedman, D., Slater, M., and Pfurtscheller, G. (2012). "A tetraplegic patient controls a wheelchair in virtual reality," in *BRAINPLAY 07 Brain-Computer Interfaces and Games Workshop at ACE (Advances in Computer Entertainment) 2007*, 37.

Li, H., Li, Y., and Guan, C. (2006). An effective bci speller based on semi-supervised learning. *Conf. Proc. IEEE Eng. Med. Biol. Soc.* 1, 1161–1164. doi: 10.1109/IEMBS.2006.260694

Lisetti, C. L., and Nasoz, F. (2004). Using noninvasive wearable computers to recognize human emotions from physiological signals. *EURASIP J. Appl. Signal Process.* 2004, 1672–1687. doi: 10.1155/S1110865704406192

Liu, Y., and Sourina, O. (2012). "EEG-based dominance level recognition for emotion-enabled interaction," in *IEEE International Conference on Multimedia and Expo* (Melbourne, VIC), 1039–1044.

Loewenstein, G., and Lerner, J. S. (2003). "The role of affect in decision making," in *Handbook of Affective Science*, eds R. Davidson, H. Goldsmith, and K. Scherer (Oxford: Oxford University Press), 619–642.

Mantini, D., Perrucci, M. G., Del Gratta, C., Romani, G. L., and Corbetta, M. (2007). Electrophysiological signatures of resting state networks in the human brain. *Proc. Natl. Acad. Sci. U.S.A.* 104, 13170–13175. doi: 10.1073/pnas.0700668104

Marg, E. (1995). Descartes'error: emotion, reason, and the human brain. *Optomet. Vis. Sci.* 72, 847–848.

Mikutta, C., Altorfer, A., Strik, W., and Koenig, T. (2012). Emotions, arousal, and frontal alpha rhythm asymmetry during beethoven's 5th symphony. *Brain Topogr.* 25, 423–430. doi: 10.1007/s10548-012-0227-0

Moore Jackson, M., and Mappus, R. (2010). "Applications for brain-computer interfaces," in *Brain-Computer Interfaces and Human-Computer Interaction Series*, eds D. Tan and A. Nijholt (London: Springer), 89–103.

Mühl, C., Allison, B., Nijholt, A., and Chanel, G. (2014). A survey of affective brain computer interfaces: principles, state-of-the-art, and challenges. *Brain Comput. Interf.* 1, 66–84. doi: 10.1080/2326263X.2014.912881

Müller, M. M., Keil, A., Gruber, T., and Elbert, T. (1999). Processing of affective pictures modulates right-hemispheric gamma band EEG activity. *Clin. Neurophysiol.* 110, 1913–1920. doi: 10.1016/S1388-2457(99)00151-0

Nasoz, F., Lisetti, C. L., Alvarez, K., and Finkelstein, N. (2003). "Emotion recognition from physiological signals for user modeling of affect," in *Proceedings of the 3rd Workshop on Affective and Attitude User Modelling* (Pittsburgh, PA).

Onslow, A. C., Bogacz, R., and Jones, M. W. (2011). Quantifying phase–amplitude coupling in neuronal network oscillations. *Prog. Biophys. Mol. Biol.* 105, 49–57. doi: 10.1016/j.pbiomolbio.2010.09.007

Pedregosa, F., Varoquaux, G., Gramfort, A., Michel, V., Thirion, B., Grisel, O., et al. (2011). Scikit-learn: Machine Learning in Python. *J. Mach. Learn. Res.* 12, 2825–2830.

Peng, H., Long, F., and Ding, C. (2005). Feature selection based on mutual information criteria of max-dependency, max-relevance, and min-redundancy. *IEEE Trans. Patt. Anal. Mach. Intell.* 27, 1226–1238. doi: 10.1109/TPAMI.2005.159

Picard, R. W. (2000). *Affective Computing*. Cambridge: MIT Press.

Picard, R. W., and Healey, J. (1997). Affective wearables. *Pers. Technol.* 1, 231–240. doi: 10.1007/BF01682026

Preece, J., Rogers, Y., Sharp, H., Benyon, D., Holland, S., and Carey, T. (1994). *Human-Computer Interaction*. Addison-Wesley Longman Ltd.

Russell, J. A. (1980). A circumplex model of affect. *J. Pers. Soc. Psychol.* 39:1161. doi: 10.1037/h0077714

Samiee, S., Donoghue, T., Tadel, F., and Baillet, S. *Phase-Amplitude Coupling*. Available online at: http://neuroimage.usc.edu/brainstorm/Tutorials/TutPac

Schölkopf, B., and Smola, A. J. (2002). *Learning with Kernels: Support Vector Machines, Regularization, Optimization, and Beyond*. Cambridge: MIT Press.

Schutter, D. J. L. G., and Knyazev, G. G. (2012). Cross-frequency coupling of brain oscillations in studying motivation and emotion. *Motiv. Emot.* 36, 46–54. doi: 10.1007/s11031-011-9237-6

Schutter, D. J. L. G., Putman, P., Hermans, E., and van Honk, J. (2001). Parietal electroencephalogram beta asymmetry and selective attention to angry facial expressions in healthy human subjects. *Neurosci. Lett.* 314, 13–16. doi: 10.1016/S0304-3940(01)02246-7

Shan, M.-K., Kuo, F.-F., Chiang, M.-F., and Lee, S.-Y. (2009). Emotion-based music recommendation by affinity discovery from film music. *Exp. Syst. Appl.* 36, 7666–7674. doi: 10.1016/j.eswa.2008.09.042

Smith, Z. M., Delgutte, B., and Oxenham, A. J. (2002). Chimaeric sounds reveal dichotomies in auditory perception. *Nature* 416, 87–90. doi: 10.1038/416087a

Sorensen, H., and Kjaer, T. (2013). A brain-computer interface to support functional recovery. *Clin. Recov. CNS Damage* 32, 95–100. doi: 10.1159/000346430

Sörnmo, L., and Laguna, P. (2005). *Bioelectrical Signal Processing in Cardiac and Neurological Applications*. San Diego, CA: Academic Press.

Tort, A. B., Komorowski, R., Eichenbaum, H., and Kopell, N. (2010). Measuring phase-amplitude coupling between neuronal oscillations of different frequencies. *J. Neurophysiol.* 104, 1195–1210. doi: 10.1152/jn.00106.2010

Wang, X.-W., Nie, D., and Lu, B.-L. (2011). "EEG-based emotion recognition using frequency domain features and support vector machines," in *Neural Information Processing* (Berlin: Springer), 734–743.

Wu, D., and Parsons, T. D. (2011). "Active class selection for arousal classification," in *Affective Computing and Intelligent Interaction* (Memphis, TN: Springer), 132–141.

Xielifuguli, K., Fujisawa, A., Kusumoto, Y., Matsumoto, K., and Kita, K. (2014). Pleasant/unpleasant filtering for affective image retrieval based on cross-correlation of EEG features. *Appl. Comput. Intell. Soft Comput.* 2014:415187. doi: 10.1155/2014/415187

frontiers
in Human Neuroscience

Positive Classification Advantage: Tracing the Time Course Based on Brain Oscillation

Tianyi Yan[1]*, Xiaonan Dong[1], Nan Mu[1], Tiantian Liu[1], Duanduan Chen[1], Li Deng[2], Changming Wang[3] and Lun Zhao[4]

[1]School of Life Science, Beijing Institute of Technology, Beijing, China, [2]Beijing Key Laboratory of Network System Architecture and Convergence, Beijing University of Posts and Telecommunications, Beijing, China, [3]Beijing Key Laboratory of Mental Disorders, Beijing Anding Hospital, Capital Medical University, Beijing, China, [4]Institute of Brain Research, Beijing Yiran Sunny Technology Co., Ltd., Beijing, China

The present study aimed to explore the modulation of frequency bands (alpha, beta, theta) underlying the positive facial expressions classification advantage within different post-stimulus time intervals (100–200 ms, 200–300 ms, 300–400 ms). For this purpose, we recorded electroencephalogram (EEG) activity during an emotion discrimination task for happy, sad and neutral faces. The correlation between the non-phase-locked power of frequency bands and reaction times (RTs) was assessed. The results revealed that beta played a major role in positive classification advantage (PCA) within the 100–200 and 300–400 ms intervals, whereas theta was important within the 200–300 ms interval. We propose that the beta band modulated the neutral and emotional face classification process, and that the theta band modulated for happy and sad face classification.

Keywords: positive classification, reaction times, brain oscillation, correlation, time intervals

INTRODUCTION

Facial expressions play an important role in social life. The information is valuable for interpreting how others feel and their behavioral tendencies. Ekman (1994) classified emotional facial expressions to six basic categories (happiness, sadness, anger, disgust, fear and surprise). So far, methods such as single cell recordings, functional brain imaging and event-related potentials (ERPs) have been used to investigate brain activity involving perception, emotion, behavior, etc. Thus, studies have shown the probable neural network of emotionally salient stimuli (Eimer and Holmes, 2007). As shown by previous studies, brain activities related to emotional events, including those in the higher order sensory cortex, amygdala, orbitofrontal cortex and ventral striatum, share complex interconnected structural network. However, much more research needed to understand the brain mechanisms underlying emotion.

The recognition speed of facial expressions of emotion is very easy to obtain. Abundant data from research has revealed that the recognition speed of happy faces is faster than sad faces (Crews and Harrison, 1994; Leppänen and Hietanen, 2004; Calvo and Beltrán, 2013; Liu et al., 2013), angry faces (Billings et al., 1993; Hugdahl et al., 1993; Calvo and Beltrán, 2013), disgusted faces (Stalans and Wedding, 1985) and neutral faces (Hugdahl et al., 1993; Leppänen and Hietanen, 2004; Calvo and Beltrán, 2013; Liu et al., 2013). However, behavioral experiments can only use simple measures such as performance accuracy and reaction times (RTs). In addition, the RTs of multiple expressions classification tasks are usually 1 s or above (e.g., Calder et al., 2000; Palermo and Coltheart, 2004; Calvo and Lundqvist, 2008), which, in terms of advance chronometry, are very large

time scales. For exploring more precise time processes, previous studies have explored the neural mechanism of facial expression classification using ERPs (e.g., Eimer and Holmes, 2007; Lynn and Salisbury, 2008). Some ERP research has revealed the phenomenon of positive classification advantage (PCA), which means that positive facial emotional expressions are recognized faster than negative ones (Leppänen and Hietanen, 2004). PCA is strongly linked to late perceptual processing, the differences between fearful and happy faces were shown over occipital regions as early as 80 ms post-stimuli, and those between happy and sad faces between 90 ms and 110 ms. Thus, our research focuses on this time course of PCA processing.

Many previous studies have revealed that ERP components are strongly linked to the categorization of facial emotion expression. Studies have shown that PCA is related to late components (Liu et al., 2013). However, information on the time course of facial emotion categorization has not been revealed. Brain oscillations, which could better track the activities of neurons, could be an efficient way to explore the time course of facial emotional categorizations. Oscillation activities could provide key physiologically information of brain dynamics. Furthermore, we can use neurofeedback to train different oscillation activities. Thus, we can discriminate between positive stimuli more quickly. Thus, the electroencephalogram (EEG) dynamics of face perception and facial expression have recently been analyzed through oscillation dynamics.

Event-related theta oscillations (4–7 Hz) have been reported to play an important role in cognitive processes such as memory, attention and cognition (Klimesch et al., 1997; Kahana et al., 2001; Khader et al., 2010; Sauseng et al., 2010). Balconi and Lucchiari (2006) reported enhanced frontal theta synchronization to emotional facial expressions as compared, with neutral expressions. Additionally, higher theta synchronization to fearful facial expressions than neutral expressions was observed. Similarly, Knyazev et al. (2009) reported that theta synchronization was higher in response to emotional faces (angry and happy faces) than neutral faces (Knyazev et al., 2009).

Alpha oscillations (8–15 Hz), which are pronounced due to their asymmetric effect, have been studied for many years (Davidson, 2003, 2004; Coan and Allen, 2004; Herrmann et al., 2004). Despite these obvious features on emotional processing, Güntekin and Basar (2007) found that in comparison with happy expressions, angry expressions elicited higher alpha responses at T5, P3 and O2 electrodes. Additionally, in an MEG experiment by Onoda et al., they found that event-related alpha power in the occipital region is higher in negative conditions than in other conditions (neutral and positive; Onoda et al., 2007). However, Balconi and Mazza (2009) reported that compared with neutral stimuli, positive and negative emotions trigger decreased alpha power responses. Furthermore, they also found that alpha oscillation was associated with an increase in left hemisphere activity (Balconi and Mazza, 2010). Thus, the modulation of alpha oscillations on emotional processes is still not clear.

Beta oscillations (16–30 Hz) have been thought to have a strong link with sensorimotor functions and could be reduced by voluntary movements and motor imagery (Neuper et al., 2009;

Engel and Fries, 2010). Some researchers have reported enhanced beta activities in response to affective stimuli compared with neutral stimuli (Woodruff et al., 2011). Güntekin and Başar (2010) also reported higher beta activity in response to negative images than positive images in frontal, central and parietal electrodes upon presentation of IAPS images (Güntekin and Başar, 2010). In addition, Schutter et al. (2001) conducted a spontaneous EEG study and found a significant relationship in response to angry facial stimuli between asymmetry in parietal beta power and the attentional response (Schutter et al., 2001). Güntekin and Basar (2007) also reported increased beta power in response to angry facial stimuli compared with happy stimuli at F3 and Cz (Güntekin and Basar, 2007). However, Zhang et al. (2013) found greater beta oscillation activity for positive facial expressions than for negative expressions. Emotion processing mechanisms are rather complicated to reveal; thus, more studies are needed to complete our knowledge on these related brain structures.

As mentioned above, the results on the brain oscillations produced upon the processing of emotional faces have been controversial. Thus, in the present study, we will trace the time course of PCA based on brain oscillations. Our goal is to find the modulation of PCA on frequency bands within different time intervals. In prior research, Liu et al. (2013) found the N170 (150–170 ms) component, posterior N2 (250–290 ms) component and P3 (350–450 ms) component using schematic face stimuli (Liu et al., 2013). Moreover, they found that neutral faces elicited a shorter N170 latency compared with happy and sad faces. Meanwhile, they found that happy faces elicited more negative N2 activity compared with neutral and sad faces. Additionally, happy and neutral faces elicited higher P3 amplitudes and shorter P3 latencies compared with sad faces. Based on these results, we assumed that when a subject makes a decision, he/she first classifies the neutral face (time window 1: 100–200 ms) and then discriminates between happy and sad expressions (time window 2: 200–300 ms and time window 3: 100–200 ms). Thus, the time course of PCA is time window 2 and 3. We will mainly focus on these two time windows.

To test our hypothesis, we used schematic face stimuli based on Liu et al. (2013). Schematic faces allow us to control physical features as carefully as possible, to minimize influence from additional information related to facial identity (e.g., gender, race) and to exclude the confounding effects of general arousal as well as valence, *per se* (Boucsein et al., 2001; Eger et al., 2003; Krombholz et al., 2007; Babiloni et al., 2010). Moreover, Sagiv and Bentin (2001) have proved that even schematic faces (only made from simple line fragments) could trigger face-sensitive N170, and that this effect was not attributable to an artifact arising from facilitated recognition of a single feature (Sagiv and Bentin, 2001; Leppänen and Hietanen, 2004). In addition, schematic face stimuli are reported to be able to provide emotional stimuli; significant increase of fMRI signal can be found in the amygdala, hippocampus and prefrontal cortex in response to emotional vs. neutral schematic faces (Wright et al., 2002), indicating the feasibility for applying the schematic faces to study PCA.

MATERIALS AND METHODS

Subjects

This study was carried out in accordance with the recommendations of "School of Life Science Ethics Committee, Beijing Institute of Technology" with written informed consent from all subjects. All subjects gave written informed consent in accordance with the Declaration of Helsinki. The protocol was approved by the "School of Life Science Ethics Committee, Beijing Institute of Technology". Eighteen young healthy individuals participated in our study (10 females; 20–25 years of age; mean: 22.6 years). All participants were right-handed, had normal or corrected-to-normal visual acuity and were free of a neurological or psychiatric history. They received payments for their participation and gave their written informed consent before the experiment (Liu et al., 2013); however, the study only examined PCA in the classic time-amplitude domain and no time-frequency analyses have been previously reported.

Stimuli and Procedure

To avoid the low-level processing of facial features, as well as boredom by the excessive repetition of one single model, each facial expression category consisted of 18 different schematic face models by manipulating the distance among facial features and by manipulating the shape of the facial features, particularly the mouths. **Figure 1** illustrates examples of schematic face expressions we used as stimuli. All stimuli were presented at the center of a cathode ray tube video monitor and were viewed from a distance of 100 cm at a visual angle of approximately $7.27° \times 6.06°$.
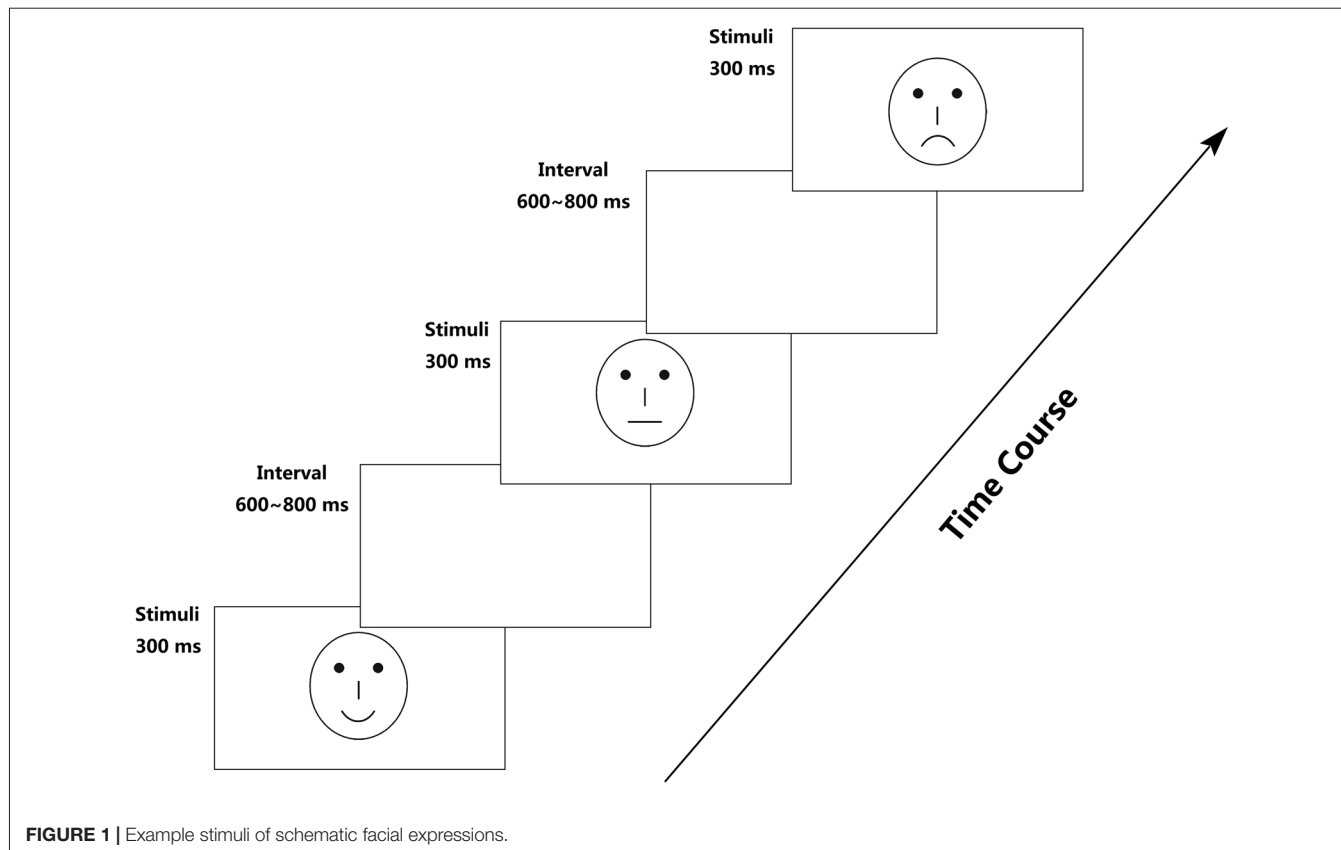
Following electrode application, the participants were seated in a dimly lit and sound-attenuated cabin. They were instructed to classify each face by the expression it represented (happy, neutral, or sad) and to respond by pressing correspondingly labeled buttons on the keyboard with the left index finger (Z key), right index finger (N key), or right middle finger (M key). Speed and accuracy were equally emphasized (Liu et al., 2013). All of the 324 stimuli (3 facial expressions × 108 faces) were randomly presented in a mixed design, with three blocks, each of which possess 108 stimuli and a short break in between. To offset the difference between the fingers, the labels of the response buttons (happy–neutral–sad/sad–happy–neutral/neutral–sad–happy) counterbalanced across the participants. Each face was presented for 300 ms with an inter-trial interval ranging randomly between 600 ms and 800 ms, starting after response.

The participants completed one practice sequence of 18 stimuli (six from each type, equally representing the three facial expressions). These stimuli were not used in the main experiment, which lasted approximately 15 min.

EEG Recording

An EEG was recorded continuously using an electrode cap with 64 sintered Ag/AgCI electrodes mounted according to the


FIGURE 1 | Example stimuli of schematic facial expressions.

extended international 10–20 system and referenced to the tip of the nose. An electrooculogram (EOG) was recorded via two pairs of additional electrodes, with one placed above and below the left eye and the other placed to the external canthi of both eyes. The EEG and EOG were amplified and digitized by the NeuroLab Amplifier (Yiran Sunny Technology Co. Ltd., Beijing, China) with a bandpass of 0.05–100 Hz and a sampling rate of 500 Hz. Electrode impedance was kept below 5 kΩ throughout the experiment.

Data Analysis

Data analysis was performed using MATLAB R2013a (Mathworks Inc., Natick, MA, USA) with the open source toolboxes EEGLAB (Swartz Center for Computational Neuroscience, La Jolla, CA, USA)[1]. The artifacts (e.g., eye artifacts, muscle artifacts and electrocardiographic activity) of all channels were removed by independent component analysis (ICA). After the artifact correction of EEF data, epochs (600 ms pre- to 900 ms post-stimulus onset) were sorted according to stimulus condition to create a plot of time-frequency representations (TFRs). Total frequency band responses were analyzed via a Morlet wavelet using the MATLAB wavelet toolbox (MathWorks). Morlet c was set to 7, and the final power was μV^2. The TFRs of the theta band power of each participant were calculated; these ranged from 4 Hz to 7 Hz, whereas the alpha band ranged from 8 Hz to 15 Hz, and the beta band from 16 Hz to 30 Hz. We calculated the synchrony among the medial, right, and left electrodes and subtracted the frequency-specific baseline (−300 to 0 ms pre-stimulus). Wavelet activity was individually returned by wavelet decomposition for each trail. Changes in the amplitude of activity were measured every 100 ms from 100 ms to 400 ms post-stimuli (e.g., 100–200 ms post-stimuli, 200–300 ms post-stimuli, 300–400 ms post-stimuli . . .) to cover a whole cycle of the high frequencies.

Accuracy rates and RTs (from the stimulus onset) were recorded and analyzed using a one-way ANOVA design, with expression (happy, neutral and sad) as the within- subjects factor. Based on previous studies, for each EEG frequency band the measurements were analyzed using a repeated-measures ANOVA treating facial expressions (happy, neutral and sad), hemisphere (left, right), and site (P7/8, PO7/8, P9/10) as within-subject factors. For factors with more than two levels, the degrees of freedom were corrected using the Greenhouse-Geisser procedure (for simplicity, the uncorrected degrees of freedom are presented). *Post hoc* comparisons were performed with the Bonferroni procedure.

RESULTS

Performance

A one-way ANOVA analysis was conducted for the percentage of correct responses. The main effect of expression was significant, $F_{(2,34)} = 7.95$, $p = 0.003$, partial $\eta^2 = 0.319$. *Post hoc* comparisons showed that neutral faces were identified more correctly (97.4%)

[1]http://sccn.ucsd.edu/eeglab/

than either happy faces (93.7%, $p = 0.002$) or sad faces (94.2%, $p = 0.007$), with no differences between the latter conditions ($p > 0.9$). For each participant, incorrect responses or responses with RTs more than ± 2 SDs from the mean in each condition were excluded for RT analysis. On average, 8.7% of the responses were removed. The RTs were analyzed by using the same statistical model as that for percentages of correct responses. There was a significant main effect of expression, $F_{(2,34)} = 95.2$, $p < 0.001$, partial $\eta^2 = 0.849$, showing that neutral face categorization was faster (551 ms) than happy face categorization (602 ms, $p < 0.001$), which was quicker than classifying sad faces (656 ms, $p < 0.001$). To investigate the possible source of the PCA, a Pearson correlation analysis was conducted. This comparison showed that there was an overall significant positive correlation between the RT to negative face stimuli and the size of the PCA, $r = 0.66$, $p < 0.005$ (two tailed), but not between the RTs to positive face stimuli and the PCA, $r = 0.17$, $p > 0.05$.
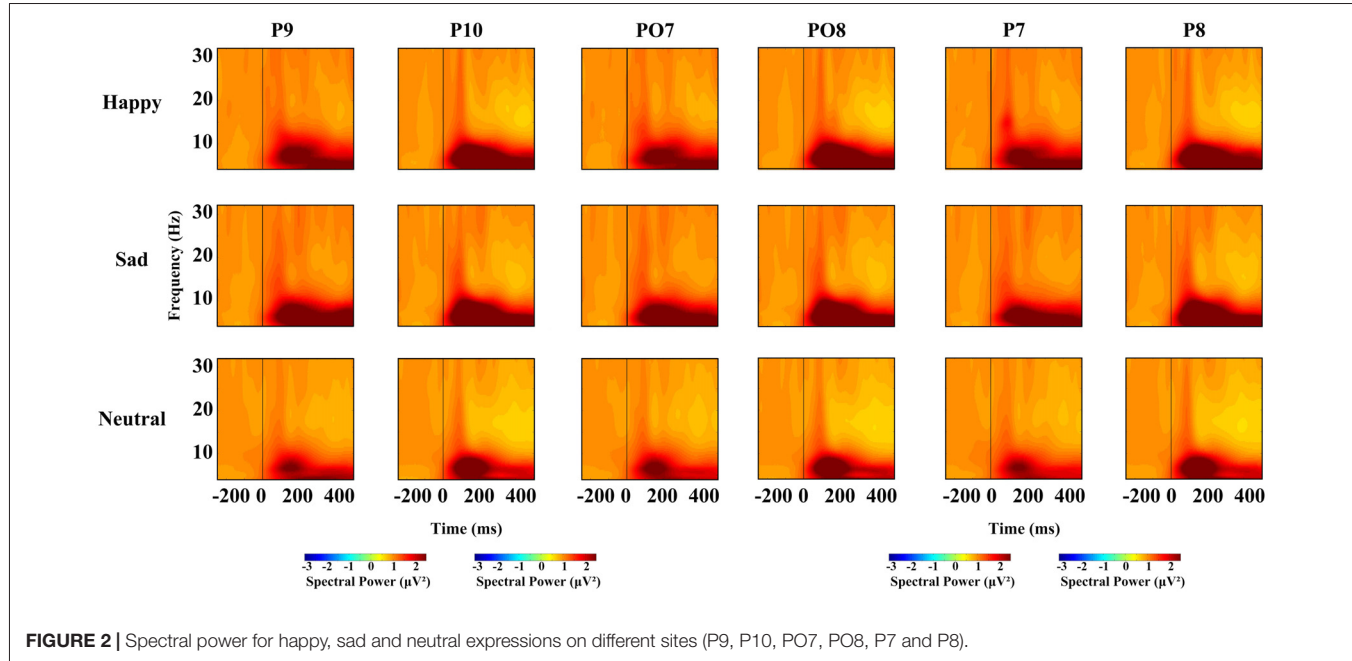
Time-Frequency Analysis

For each time window and each frequency, a repeated-measures ANOVA with facial expression (happy, neutral and sad), and hemisphere (left, right) was used to examine the overall effects for different oscillation (theta, alpha, beta), respectively. We conducted four ANOVAs, one for each time interval. Based on previous research, we conducted a repeated-measures ANOVA with within-subject factors as facial expression (happy, neutral and sad), hemisphere (left, right) and site (P7/8, PO7/8 and P9/10), and different frequency bands, were used at lateral posterior sites (left, P7, PO7 and P9; right, P8, PO8 and P10). For all the ANOVAs, the degrees of freedom were Greenhouse-Geisser corrected where appropriate. **Figure 2** shows the spectral power for happy, sad and neutral expressions on P9, P10, PO7, PO8, P7, P8, respectively.
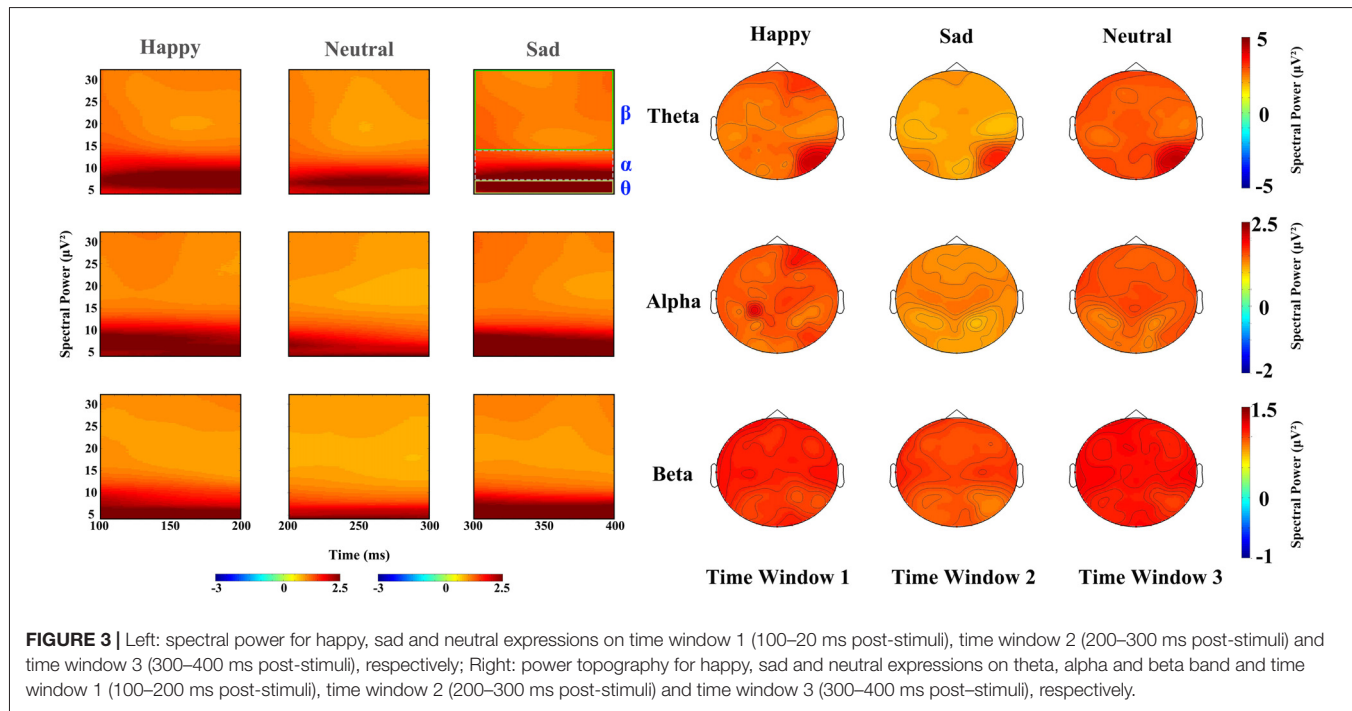
Oscillation Activities

In the 100–200 ms time window, the main effects for expressions on theta band revealed that sad faces (2.757 μV^2) elicited lower power than happy (3.126 μV^2, $p < 0.01$) and neutral faces (3.148 μV^2, $p < 0.02$), with no difference between latter two conditions, and that the power elicited by sad expressions was lower than happy ($p < 0.01$) and neutral expressions ($p < 0.001$) on alpha band ($F_{(2,34)} = 11.294$, $p < 0.001$, partial $\eta^2 = 0.399$) and beta band ($F_{(2,34)} = 14.699$, $p < 0.001$, partial $\eta^2 = 0.464$) with no difference between the latter two conditions. The main effect of hemisphere was also significant on theta ($F_{(1,17)} = 10.643$, $p < 0.01$, partial $\eta^2 = 0.385$) and beta band ($F_{(1,17)} = 8.056$, $p < 0.02$, partial $\eta^2 = 0.322$), revealing a right hemisphere dominance (3.634 μV^2 and 2.587 μV^2 for left and right hemisphere, respectively) on the theta band, while power at left occipital sites (1.029 μV^2) were larger than at right occipital sites (0.97 μV^2) on beta band. **Figure 3** shows the power for happy, sad and neutral expressions on difference time windows and different frequencies. There was no significant two-way interaction between factors (expression, hemisphere, site) on difference time windows and different frequencies (please refer to Supplementary Table S1).
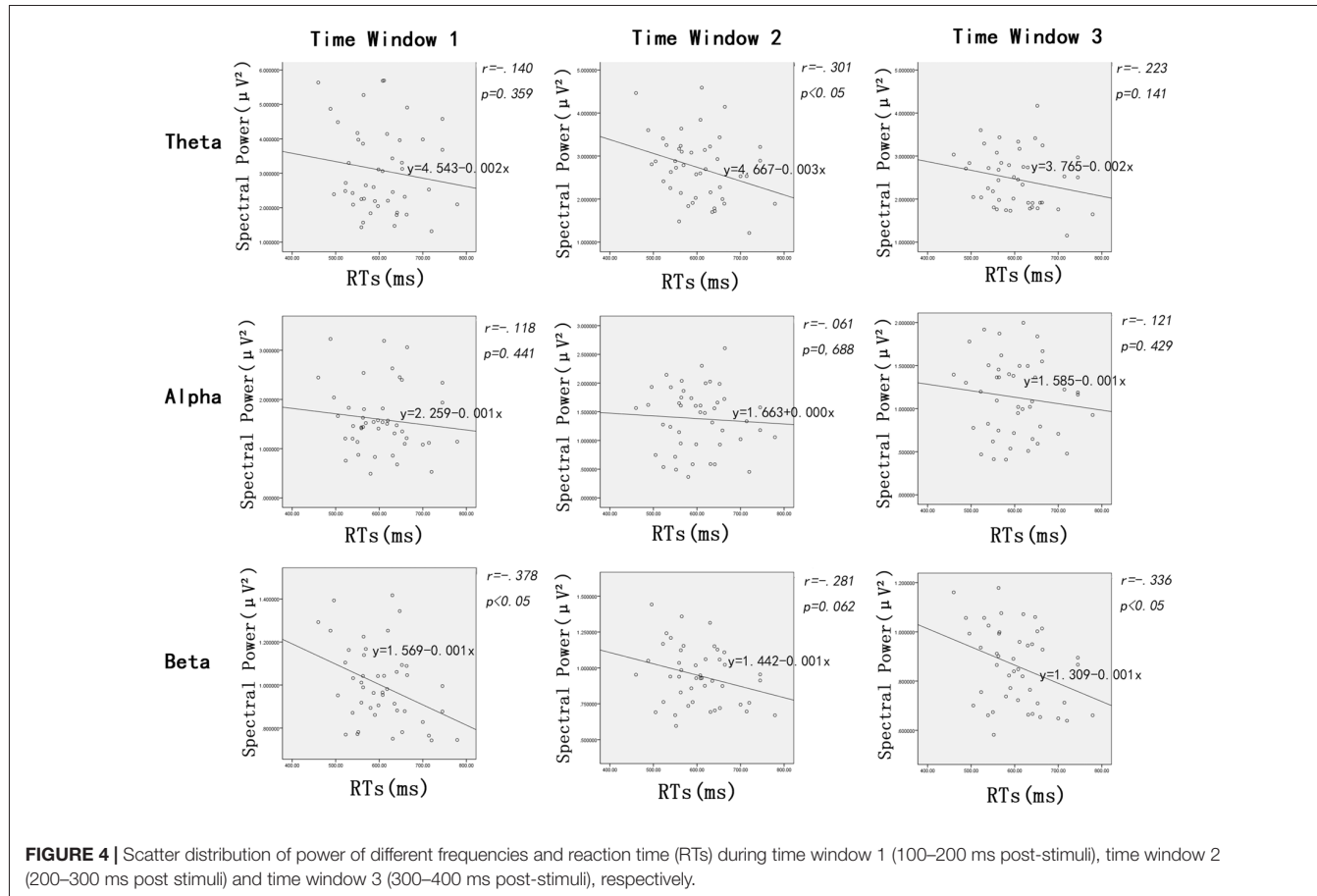
FIGURE 2 | Spectral power for happy, sad and neutral expressions on different sites (P9, P10, PO7, PO8, P7 and P8).

FIGURE 3 | Left: spectral power for happy, sad and neutral expressions on time window 1 (100–20 ms post-stimuli), time window 2 (200–300 ms post-stimuli) and time window 3 (300–400 ms post-stimuli), respectively; Right: power topography for happy, sad and neutral expressions on theta, alpha and beta band and time window 1 (100–200 ms post-stimuli), time window 2 (200–300 ms post-stimuli) and time window 3 (300–400 ms post–stimuli), respectively.

For the time window from 200 ms to 300 ms, theta band showed a significant difference in facial expressions ($F_{(2,34)} = 37.96$, $P < 0.001$, partial $\eta^2 = 0.691$), revealing a higher power for happy faces ($3.102\ \mu V^2$) than neutral faces ($2.86\ \mu V^2$, $p < 0.05$) and sad faces ($2.231\ \mu V^2$, $p < 0.01$). The effect of hemisphere for theta band also showed a significant difference ($F_{(1,17)} = 8.473$, $P < 0.01$, partial $\eta^2 = 0.322$), with the hemisphere being more prominent ($2.965\ \mu V^2$) than the left ($2.497\ \mu V^2$). Alpha oscillations also showed a significant difference in facial

expressions ($F_{(2,34)} = 9.681$, $P < 0.001$, partial $\eta^2 = 0.363$), revealing that sad faces elicited lower activity ($1.171\ \mu V^2$) than the happy ($1.509\ \mu V^2$, $p < 0.01$) and neutral faces ($1.458\ \mu V^2$, $p < 0.01$), but that there were no differences between the latter two types of faces ($p = 0.948$). There was a significant main effect of expression on beta band ($F_{(2,34)} = 14.324$, $P < 0.001$, partial $\eta^2 = 0.457$), showing less sad activity ($0.876\ \mu V^2$) than neutral activity ($0.999\ \mu V^2$, $p < 0.001$) and happy activity ($0.965\ \mu V^2$, $p < 0.01$), and no difference between the latter two conditions.

FIGURE 4 | Scatter distribution of power of different frequencies and reaction time (RTs) during time window 1 (100–200 ms post-stimuli), time window 2 (200–300 ms post stimuli) and time window 3 (300–400 ms post-stimuli), respectively.

Hemisphere also showed a significant difference in beta band ($F_{(1,17)} = 5.977$, $P < 0.05$, partial $\eta^2 = 0.26$), revealing a higher power at the left hemisphere ($0.987\ \mu V^2$) than that at the right ($0.907\ \mu V^2$).

The time window from 300 ms to 400 ms showed significant main differences in facial expression for theta ($F_{(2,34)} = 49.263$, $p < 0.001$, partial $\eta^2 = 0.743$), alpha ($F_{(2,34)} = 20.695$, $p < 0.001$, partial $\eta^2 = 0.495$), beta ($F_{(2,34)} = 48.283$, $p < 0.001$, partial $\eta^2 = 0.74$), revealing that neutral and happy expressions elicited higher power than sad expressions ($p < 0.001$), while there was no difference between neutral and happy expressions. A significant main effect of hemisphere also found on alpha ($F_{(1,17)} = 7.936$, $p < 0.02$, partial $\eta^2 = 0.318$) and beta band ($F_{(1,17)} = 15.907$, $p < 0.001$, partial $\eta^2 = 0.483$), showing a left hemisphere dominance ($1.204\ \mu V^2$ and $1.064\ \mu V^2$ for the left and right hemisphere on alpha band, $0.911\ \mu V^2$ and $0.817\ \mu V^2$ on beta band, respectively) on both alpha and beta bands.

Pearson Correlations

In addition to the ANOVAs, because we want to explore how the oscillation activities reflect modulations of the stimulus evaluation and decision processes, Pearson correlations between the RTs and power of all frequency bands (theta, alpha and beta, respectively) were conducted. **Figure 4** shows scatterplot diagrams and linear fitting of the scatter-plots.

The Pearson correlations between RTs and the power of frequency bands showed significant negative correlations between RTs and beta power during the time window of 100–200 ms ($r = -0.378$, $p < 0.02$) and 300–400 ms ($r = 0.336$, $p < 0.03$); that is, the longer the RTs, the lower the beta power within time window 1 and 3. Interestingly, power on theta band was also negatively linked to RTs, but the time window was 200–300 ms ($r = -0.301$, $p < 0.05$). Furthermore, there were no significant correlations between the RTs and power of other oscillation bands (i.e., alpha) modulated by facial expressions ($ps > 0.06$).

DISCUSSION

Below is a summary of the results of the present research. Through facial expression classification experiments, we will discuss the phenomenon of happy face classification advantage using oscillation characteristics as well as time course. In line with previous studies, we found that face expression classification is quicker for happy expressions than for sad expressions (e.g., Crews and Harrison, 1994; Leppänen and Hietanen, 2004), and faster for neutral faces than happy faces. Moreover, happy faces elicited a higher spectral power than sad face. In accordance with other studies (Balconi and Mazza, 2009), the results showed a left hemisphere dominance, revealing

the lateralization effect of positive expression classification. Although facial expressions elicited different activity on theta, alpha and beta frequencies, only beta and theta showed significant negative correlation with RT. Moreover, beta was strongly correlated with PCA in time window 1 and 3, whereas theta was correlated with time window 2. Additionally, the greater spectral power was linked to a shorter RT in all the three time windows and three frequency bands. Thus, quick responses require more brain activity, which was not obvious in the alpha bands.

In the present task, the theta oscillations showed that happy faces elicit higher power than sad faces, but the power elicited by neutral faces was higher than emotional faces (happy and sad faces). Previous studies with IAPS affective pictures as stimuli showed that emotional stimuli always elicited higher power than neutral stimuli (Balconi and Lucchiari, 2006; Zhang et al., 2013), which is in contrast with our results, but the stimuli in these experiments are not facial expressions. Studies using emotional video clips showed that power elicited by positive stimuli is higher than that by negative stimuli in the post-occipital area (Aftanas et al., 1998), which is similar to our results. Moreover, previous study using real emotional expressions suggested that happy expressions has faster results and higher accuracy than neutral expressions in discriminating tasks (Dasilva et al., 2016), which indicated the PCA.

As previously shown, alpha power showed an increase with positive stimuli in comparison with neutral stimuli after 100 ms post-stimuli, and although this difference is not significant, it is in line with previous studies that emotional stimuli elicits higher power than neutral stimuli. However, we found that in comparison with happy and neutral stimuli, power elicited by sad stimuli was the lowest. Interestingly, a study by Baumgartner et al. (2006) found that, when presenting IAPS pictures of fear, happiness and sadness, there were no differences in alpha power, but decreased alpha power was found when stimuli were emotional pictures accompanied with emotional music. For studies that found that negative stimuli elicits higher alpha responses, because negative stimuli in these studies were always angry pictures or affective pictures, the decreased alpha oscillations may be attributed to the facial classification mechanisms; however, whether real facial expressions would have same results as schematic facial expressions requires further study.

Previous studies on application of IAPS images found that negative images elicit greater beta responses compared with positive images in frontal, central and parietal electrodes (Güntekin and Başar, 2010); however, the stimuli they used were not facial expression pictures but affective pictures. A study by Zhang et al. (2013) with Chinese affective pictures as stimuli indicated that adolescents at the age of 12 exhibit more beta event-related synchronization (ERS) for positive vs. neutral stimuli. Other studies also verified that higher beta responses elicited both positive and negative stimuli than neutral stimuli (Miskovic and Schmidt, 2010; Cohen et al., 2013).

The ERP results have shown components (i.e., P1, N1, N170, P2, N2, P3) that have a strong relationship with facial emotion classification tasks. First, enhanced N170 (a negative

ERP component during 140–180 ms post-stimuli at occipito-temporal electrodes), which is thought to be an indicator of inverted-face recognition, shows significant differences to fearful faces than neural faces at 160 ms post-stimuli (Holmes et al., 2005). Compared with time window 1, we concluded that face categorization was pre-attended during this time window. For posterior N2, a negativity peaking between 200 ms and 300 ms may be modulated by factors influencing visual stimuli categorization such as mutual information level, determined by gross similarity between the fragment and image in an image patch (Harel et al., 2007). In addition, as a generic name for relatively late positive component with a distribution at centro-parietal or centro-frontal midline area, P3 is considered in conjunction with facial emotion categorization (Polich, 2007). It has shown higher amplitudes and shorter latencies in response to both happy and neutral stimuli than sad stimuli, while RT displayed a significant correlation with amplitude and latency of the P3. During time windows 2 and 3, which are linked to the N2 and P3 components, emotion categorization is completed. Thus, the time-division can help us to better analyze the process of emotion categorization.

Though there were significant differences in theta, alpha and beta oscillations for different emotional stimuli (happy, neutral and sad), only theta and beta band significantly were correlated with RTs. However, the correlation between beta oscillation and RTs was as early as 100 ms after stimuli onset. That is, beta oscillation may modulate the categorization of neutral faces. In our results, the beta band had a major impact upon face discrimination. Also, the categorization occurred as early as 100 ms after stimulus onset, which has important effects for our social life. Furthermore, researchers have revealed that beta oscillation contributed to classification of known faces and unknown faces within 100–200 ms (Ozgören et al., 2005). Based on these results, we propose that in time window 1, subjects can discriminate between neutral and emotional faces, and that beta band is related to the process. This suggests that neutral face may be classified the fastest; and is modulated by beta band.

As for time windows 2 and 3, previous studies revealed that theta power was related to the P3 component (see a review Polich, 2007) and that P3 was related to PCA (Liu et al., 2013). That is, theta (time window 2) and beta (time window 3) oscillations modulate the PCA. These results are consistent with other research that focused on negative stimuli (Cohen et al., 2013). This research demonstrated that the theta band contributed to early emotion selection (200–300 ms) and that the beta band was a late response (400–600 ms). Thus, our hypothesis was verified, meaning that the theta band and beta band had a major impact on PCA.

In conclusion, our research used schematic emotional faces and focused on the time course of the recognition advantage of happy faces. The results demonstrate that the categorization process was mainly associated with beta oscillations from the beginning, while theta oscillations participated during the later period. Thus, we could detect PCA as early as 200 ms post-stimuli through theta oscillations, earlier than the other findings on time domain (usually 300 ms). Moreover, we can train theta bands

in time window 2 and beta bands in time window 3, so that people can discriminate happy faces more quickly. This may have good implications for depressed patients. Therefore, advanced research on facial emotional processing is clearly needed.

AUTHOR CONTRIBUTIONS

TY contributed to the conception of the study. TL and XD performed the data analyses and wrote the manuscript. NM and DC contributed significantly to analysis and manuscript preparation. DC and LZ helped perform the analysis with constructive discussions. LD and CW provided data processing ideas and creative methods.

REFERENCES

Aftanas, L. I., Lotova, N. V., Koshkarov, V. I., Makhnev, V. P., Mordvintsev, Y. N., and Popov, S. A. (1998). Non-linear dynamic complexity of the human EEG during evoked emotions. *Int. J. Psychophysiol.* 28, 63–76. doi: 10.1016/s0167-8760(97)00067-6

Babiloni, C., Vecchio, F., Buffo, P., Buttiglione, M., Cibelli, G., and Rossini, P. M. (2010). Cortical responses to consciousness of schematic emotional facial expressions: a high-resolution EEG study. *Hum. Brain Mapp.* 31, 1556–1569. doi: 10.1002/hbm.20958

Balconi, M., and Lucchiari, C. (2006). EEG correlates (event-related desynchronization) of emotional face elaboration: a temporal analysis. *Neurosci. Lett.* 392, 118–123. doi: 10.1016/j.neulet.2005.09.004

Balconi, M., and Mazza, G. (2009). Brain oscillations and BIS/BAS (behavioral inhibition/activation system) effects on processing masked emotional cues. ERS/ERD and coherence measures of alpha band. *Int. J. Psychophysiol.* 74, 158–165. doi: 10.1016/j.ijpsycho.2009.08.006

Balconi, M., and Mazza, G. (2010). Lateralisation effect in comprehension of emotional facial expression: a comparison between EEG alpha band power and behavioural inhibition (BIS) and activation (BAS) systems. *Laterality* 15, 361–384. doi: 10.1080/13576500902886056

Baumgartner, T., Esslen, M., and Jäncke, L. (2006). From emotion perception to emotion experience: emotions evoked by pictures and classical music. *Int. J. Psychophysiol.* 60:34. doi: 10.1016/j.ijpsycho.2005.04.007

Billings, L. S., Harrison, D. W., and Alden, J. D. (1993). Age differences among women in the functional asymmetry for bias in facial affect perception. *Bull. Psychon. Soc.* 31, 317–320. doi: 10.3758/bf03334940

Boucsein, W., Schaefer, F., Sokolov, E. N., Schröder, C., and Furedy, J. J. (2001). The color-vision approach to emotional space: cortical evoked potential data. *Integr. Physiol. Behav. Sci.* 36, 137–153. doi: 10.1007/bf02734047

Calder, A. J., Young, A. W., Keane, J., and Dean, M. (2000). Configural information in facial expression perception. *J. Exp. Psychol. Hum. Percept. Perform.* 26, 527–551. doi: 10.1037/0096-1523.26.2.527

Calvo, M. G., and Beltrán, D. (2013). Recognition advantage of happy faces: tracing the neurocognitive processes. *Neuropsychologia* 51, 2051–2061. doi: 10.1016/j.neuropsychologia.2013.07.010

Calvo, M. G., and Lundqvist, D. (2008). Facial expressions of emotion (KDEF): identification under different display-duration conditions. *Behav. Res. Methods* 40, 109–115. doi: 10.3758/brm.40.1.109

Coan, J. A., and Allen, J. J. B. (2004). Frontal EEG asymmetry as a moderator and mediator of emotion. *Biol. Psychol.* 67, 7–50. doi: 10.1016/j.biopsycho.2004.03.002

Cohen, J. E., Shalev, H., Admon, R., Hefetz, S., Gasho, C. J., Shachar, L. J., et al. (2013). Emotional brain rhythms and their impairment in post-traumatic patients. *Hum Brain Mapp.* 34, 1344–1356. doi: 10.1002/hbm.21516

Crews, C. W. Jr., and Harrison, D. W. (1994). Cerebral asymmetry in facial affect perception by women: neuropsychological effects of depressed mood. *Percept. Mot. Skills* 79, 1667–1679. doi: 10.2466/pms.1994.79.3f.1667

ACKNOWLEDGMENTS

SUPPLEMENTARY MATERIAL

The Supplementary Material for this article can be found online at: https://www.frontiersin.org/articles/10.3389/fnhum.2017.006 59/full#supplementary-material

Dasilva, E. B., Crager, K., and Puce, A. (2016). On dissociating the neural time course of the processing of positive emotions. *Neuropsychologia* 83, 123–137. doi: 10.1016/j.neuropsychologia.2015.12.001

Davidson, R. J. (2003). Affective neuroscience and psychophysiology: toward a synthesis. *Psychophysiology* 40, 655–665. doi: 10.1111/1469-8986.00067

Davidson, R. J. (2004). What does the prefrontal cortex "do" in affect: perspectives on frontal EEG asymmetry research. *Biol. Psychol.* 67, 219–234. doi: 10.1016/j.biopsycho.2004.03.008

Eger, E., Jedynak, A., Iwaki, T., and Skrandies, W. (2003). Rapid extraction of emotional expression: evidence from evoked potential fields during brief presentation of face stimuli. *Neuropsychologia* 41, 808–817. doi: 10.1016/s0028-3932(02)00287-7

Eimer, M., and Holmes, A. (2007). Event-related brain potential correlates of emotional face processing. *Neuropsychologia* 45, 15–31. doi: 10.1016/j.neuropsychologia.2006.04.022

Ekman, P. (1994). Strong evidence for universals in facial expressions: a reply to Russell's mistaken critique. *Psychol. Bull.* 115, 268–287. doi: 10.1037//0033-2909.115.2.268

Engel, A. K., and Fries, P. (2010). Beta-band oscillations—signalling the status quo? *Curr. Opin. Neurobiol.* 20, 156–165. doi: 10.1016/j.conb.2010.02.015

Güntekin, B., and Basar, E. (2007). Emotional face expressions are differentiated with brain oscillations. *Int. J. Psychophysiol.* 64, 91–100. doi: 10.1016/j.ijpsycho.2006.07.003

Güntekin, B., and Başar, E. (2010). Event-related beta oscillations are affected by emotional eliciting stimuli. *Neurosci. Lett.* 483, 173–178. doi: 10.1016/j.neulet.2010.08.002

Harel, A., Ullman, S., Epshtein, B., and Bentin, S. (2007). Mutual information of image fragments predicts categorization in humans: electrophysiological and behavioral evidence. *Vision Res.* 47, 2010–2020. doi: 10.1016/j.visres.2007.04.004

Herrmann, C. S., Munk, M. H. J., and Engel, K. A. (2004). Cognitive functions of gamma-band activity: memory match and utilization. *Trends Cogn. Sci.* 8, 347–355. doi: 10.1016/j.tics.2004.06.006

Holmes, A., Winston, J. S., and Eimer, M. (2005). The role of spatial frequency information for ERP components sensitive to faces and emotional facial expression. *Cogn. Brain Res.* 25, 508–520. doi: 10.1016/j.cogbrainres.2005.08.003

Hugdahl, K., Iversen, P. M., and Johnsen, B. H. (1993). Laterality for facial expressions: does the sex of the subject interact with the sex of the stimulus face? *Cortex* 29, 325–331. doi: 10.1016/s0010-9452(13)80185-2

Kahana, M. J., Seelig, D., and Madsen, J. R. (2001). Theta returns. *Curr. Opin. Neurobiol.* 11, 739–744. doi: 10.1016/S0959-4388(01)00278-1

Khader, P. H., Jost, K., Ranganath, C., and Rösler, F. (2010). Theta and Alpha oscillations during working-memory maintenance predict successful long-term memory encoding. *Neurosci. Lett.* 468, 339–343. doi: 10.1016/j.neulet.2009.11.028

Klimesch, W., Doppelmayr, M., Schimke, H., and Ripper, B. (1997). Theta synchronization and alpha desynchronization in a memory task. *Psychophysiology* 34, 169–176. doi: 10.1111/j.1469-8986.1997.tb0 2128.x

Knyazev, G. G., Slobodskoj-Plusnin, J. Y., and Bocharov, A. V. (2009). Event-related delta and theta synchronization during explicit and implicit emotion processing. *Neuroscience* 164, 1588–1600. doi: 10.1016/j.neuroscience. 2009.09.057

Krombholz, A., Schaefer, F., and Boucsein, W. (2007). Modification of N170 by different emotional expression of schematic faces. *Biol. Psychol.* 76, 156–162. doi: 10.1016/j.biopsycho.2007.07.004

Leppänen, J. M., and Hietanen, J. K. (2004). Positive facial expressions are recognized faster than negative facial expressions, but why? *Psychol. Res.* 69, 22–29. doi: 10.1007/s00426-003-0157-2

Liu, X., Liao, Y., Zhou, L., Sun, G., Li, M., and Zhao, L. (2013). Mapping the time course of the positive classification advantage: an ERP study. *Cogn. Affect. Behav. Neurosci.* 13, 491–500. doi: 10.3758/s13415-013-0158-6

Lynn, S. K., and Salisbury, D. F. (2008). Attenuated modulation of the N170 ERP by facial expressions in schizophrenia. *Clin. EEG Neurosci.* 39, 108–111. doi: 10.1177/155005940803900218

Miskovic, V., and Schmidt, L. A. (2010). Cross-regional cortical synchronization during affective image viewing. *Brain Res.* 1362, 102–111. doi: 10.1016/j. brainres.2010.09.102

Neuper, C., Scherer, R., Wriessnegger, S., and Pfurtscheller, G. (2009). Motor imagery and action observation: modulation of sensorimotor brain rhythms during mental control of a brain-computer interface. *Clin. Neurophysiol.* 120, 239–247. doi: 10.1016/j.clinph.2008.11.015

Onoda, K., Okamoto, Y., Shishida, K., Hashizume, A., Ueda, K., Yamashita, H., et al. (2007). Anticipation of affective images and event-related desynchronization (ERD) of alpha activity: an MEG study. *Brain Res.* 1151, 134–141. doi: 10.1016/j.brainres.2007.03.026

Ozgören, M., Başar-Eroğlu, C., and Başar, E. (2005). Beta oscillations in face recognition. *Int. J. Psychophysiol.* 55, 51–59. doi: 10.1016/j.ijpsycho.2004. 06.005

Palermo, R., and Coltheart, M. (2004). Photographs of facial expression: accuracy, response times, and ratings of intensity. *Behav. Res. Methods Instrum. Comput.* 36, 634–638. doi: 10.3758/bf03206544

Polich, J. (2007). Updating P300: an integrative theory of P3a and P3b. *Clin. Neurophysiol.* 118, 2128–2148. doi: 10.1016/j.clinph.2007.04.019

Sagiv, N., and Bentin, S. (2001). Structural encoding of human and schematic faces: holistic and part-based processes. *J. Cogn. Neurosci.* 13, 937–951. doi: 10.1162/089892901753165854

Sauseng, P., Griesmayr, B., Freunberger, R., and Klimesch, W. (2010). Control mechanisms in working memory: a possible function of EEG theta oscillations. *Neurosci. Biobehav. Rev.* 34, 1015–1022. doi: 10.1016/j.neubiorev.2009.12.006

Schutter, D. J., Putman, P., Hermans, E., and van Honk, J. (2001). Parietal electroencephalogram beta asymmetry and selective attention to angry facial expressions in healthy human subjects. *Neurosci. Lett.* 314, 13–16. doi: 10.1016/s0304-3940(01)02246-7

Stalans, L., and Wedding, D. (1985). Superiority of the left hemisphere in the recognition of emotional faces. *Int. J. Neurosci.* 25, 219–223. doi: 10.3109/00207458508985373

Woodruff, C. C., Daut, R., Brower, M., and Bragg, A. (2011). Electroencephalographic α-band β-band correlates of perspective-taking and personal distress. *Neuroreport* 22, 744–748. doi: 10.1097/WNR.0b013e32834 ab439

Wright, C. I., Martis, B., Shin, L. M., Fischer, H., and Rauch, S. L. (2002). Enhanced amygdala responses to emotional versus neutral schematic facial expressions. *Neuroreport* 13, 785–790. doi: 10.1097/00001756-200205070-00010

Zhang, W., Lu, J., Liu, X., Fang, H., Li, H., Wang, D., et al. (2013). Event-related synchronization of delta and beta oscillations reflects developmental changes in the processing of affective pictures during adolescence. *Int. J. Psychophysiol.* 90, 334–340. doi: 10.1016/j.ijpsycho.2013.10.005

Exploring EEG Features in Cross-Subject Emotion Recognition

Xiang Li[1], Dawei Song[2,3]*, Peng Zhang[1]*, Yazhou Zhang[1], Yuexian Hou[1] and Bin Hu[4]*

[1] Tianjin Key Laboratory of Cognitive Computing and Application, Tianjin University, Tianjin, China, [2] School of Computer Science and Technology, Beijing Institute of Technology, Beijing, China, [3] School of Computing and Communications, The Open University, Milton Keynes, United Kingdom, [4] School of Information Science and Engineering, Lanzhou University, Lanzhou, China

Recognizing cross-subject emotions based on brain imaging data, e.g., EEG, has always been difficult due to the poor generalizability of features across subjects. Thus, systematically exploring the ability of different EEG features to identify emotional information across subjects is crucial. Prior related work has explored this question based only on one or two kinds of features, and different findings and conclusions have been presented. In this work, we aim at a more comprehensive investigation on this question with a wider range of feature types, including 18 kinds of linear and non-linear EEG features. The effectiveness of these features was examined on two publicly accessible datasets, namely, the dataset for emotion analysis using physiological signals (DEAP) and the SJTU emotion EEG dataset (SEED). We adopted the support vector machine (SVM) approach and the "leave-one-subject-out" verification strategy to evaluate recognition performance. Using automatic feature selection methods, the highest mean recognition accuracy of 59.06% (AUC = 0.605) on the DEAP dataset and of 83.33% (AUC = 0.904) on the SEED dataset were reached. Furthermore, using manually operated feature selection on the SEED dataset, we explored the importance of different EEG features in cross-subject emotion recognition from multiple perspectives, including different channels, brain regions, rhythms, and feature types. For example, we found that the Hjorth parameter of mobility in the beta rhythm achieved the best mean recognition accuracy compared to the other features. Through a pilot correlation analysis, we further examined the highly correlated features, for a better understanding of the implications hidden in those features that allow for differentiating cross-subject emotions. Various remarkable observations have been made. The results of this paper validate the possibility of exploring robust EEG features in cross-subject emotion recognition.

Keywords: EEG, emotion recognition, feature engineering, DEAP dataset, SEED dataset

1. INTRODUCTION

Emotion recognition as an emerging research direction has attracted increasing attention from different fields and is promising for many application domains. For example, in human-computer interaction (HCI), recognized user emotion can be utilized as a kind of feedback to provide better content to enhance the user experiences in e-learning, computer games, and information retrieval (Mao and Li, 2009; Chanel et al., 2011; Moshfeghi, 2012). Moreover, psychologists have verified the important roles that emotion plays in human health. Difficulties in the regulation of negative

emotions may cause various mood disorders, such as stress and depression (Gross and Muñoz, 1995), which may influence people's health (O'Leary, 1990). Hence, emotion recognition techniques also contribute to developing e-services for mental health monitoring. In particular, cross-subject emotion recognition (i.e., depression prediction based on a person's physiological data, with a classifier learnt from the training data from a group of patients who have been diagnosed as depression or not) has been considered an important task for its generality and wider applicability, compared with the intra-subject emotion recognition.

Electroencephalogram (EEG) measurements reflect the neural oscillations of the central nervous system (CNS) and are directly related to various higher-level cognitive processes (Ward, 2003), including emotion (Coan and Allen, 2004). EEG-based emotion recognition has shown a greater potential compared with the facial expression- and speech-based approaches, as the internal neural fluctuations cannot be deliberately concealed or controlled. However, a main issue confronted in this research area is how to improve the cross-subject recognition performance. The performances of current recognition systems are largely limited by the poor generalizability of the EEG features in reflecting emotional information across subjects. For example, Kim (2007) studied the bimodal data fusion method and utilized LDA to classify emotions. Using this method, the best obtained recognition accuracy on all three subjects' data was 55%, which was far lower than the best result of 92% obtained on a single subject's data. Zhu et al. (2015) adopted differential entropy as the emotion-related feature and the linear SVM as the classifier. The authors verified the recognition performance on intra-subject and cross-subject experimental settings respectively. The average recognition accuracy was 64.82% for cross-subject recognition tasks, which was also far lower than the results of 90.97% obtained in the intra-subject settings.

In the literature, there has been some related work that attempted to tackle this problem and to identify robust EEG features in cross-subject emotion recognition. For example, Li and Lu (2009) examined the recognition performance using ERD/ERS features extracted from different frequency bands and found that 43.5–94.5 Hz, the higher gamma band, was the optimal frequency band related to happiness and sadness. Lin et al. (2010) extracted DASM features and summarized the top 30 subject-independent features by measuring the ratio of between- and within-class variance, and found that the frontal and parietal electrode pairs were the most informative on emotional states. However, no significant difference between different frequency bands was observed in this work. Soleymani et al. (2012) performed cross-subject emotion recognition tasks on EEG and eye gaze data. The power spectral density (PSD) for EEGs was extracted. The most discriminative features for arousal were in the alpha band of the occipital electrodes, while those for valence were in the beta and gamma bands of the temporal electrodes. Kortelainen and Seppänen (2013) extracted the PSD from different frequency bands, and the best cross-subject classification rate for valence and arousal was obtained on the feature subset in the 1–32 Hz band. Zheng et al. (2016) focused on finding stable neural EEG patterns across subjects and

sessions for emotion recognition. The authors found that EEGs in lateral temporal areas were activated more for positive emotions than negative emotions in the beta and gamma bands and that subject-independent EEG features stemmed mostly from those brain areas and frequency bands.
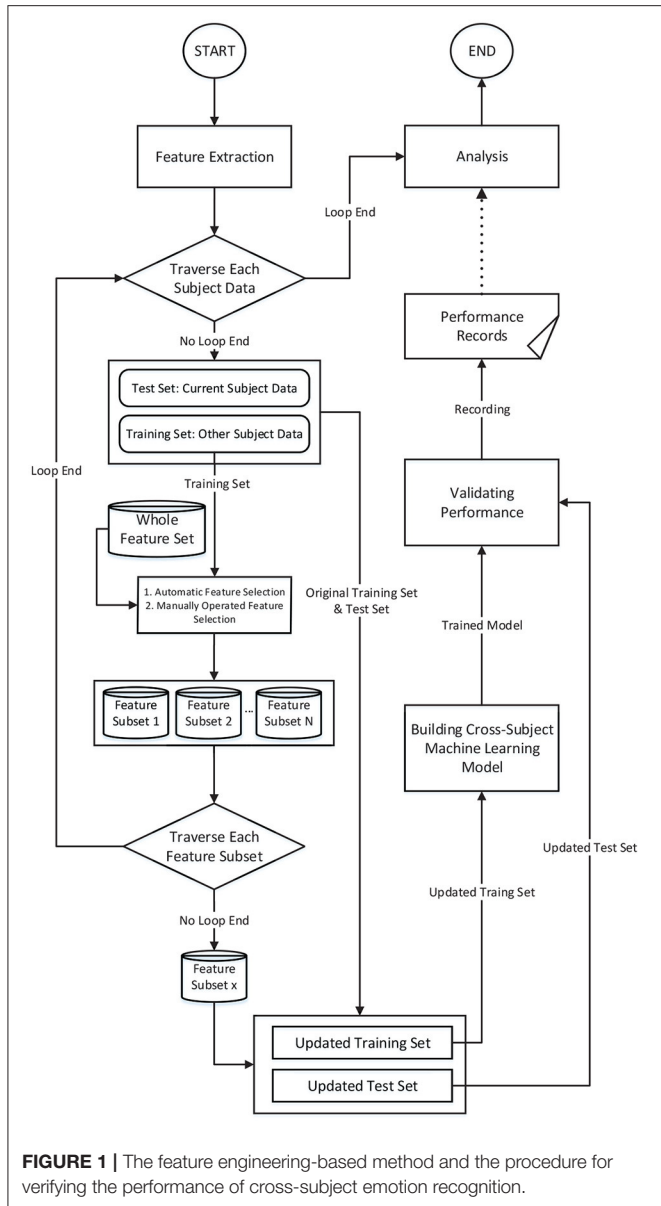
In the aforementioned existing work, however, only few kinds of features were examined and why those robust features contribute to cross-subject emotion recognition was not studied. Hence, in this work, we aim at a more comprehensive and systematic exploration of a wider range of EEG features. Specifically, we extracted nine kinds of time-frequency domain features and nine kinds of dynamical system features from EEG measurements. Through automatic feature selection, e.g., recursive feature elimination (RFE), we verified the effectiveness and performance upper bounds of those features in cross-subject emotion recognition. Furthermore, through manual selection of features from different aspects, e.g., different EEG channels, we studied the importance of different aspects in cross-subject emotion recognition. We further conducted a correlation analysis to better understand the implications of those features for differentiating cross-subject emotions. The support vector machine (SVM), a state of the art classifier, was used in all the experiments.

2. MATERIALS AND METHODS

The procedure of the proposed methodology is illustrated in **Figure 1**. We adopted a "leave-one-subject-out" verification strategy. Each time we left one subject's data out as the test set and adopted the other subjects' data as the training set. The feature selection was conducted on the training set, and then, the performance was evaluated on the test set. This procedure was iterated until each subject's data had been tested. This strategy can eliminate the risk of "overfitting."

2.1. Experimental Data
We conducted our analysis using two publicly accessible datasets, namely, DEAP (dataset for emotion analysis using physiological signals) (Koelstra et al., 2012) and SEED (SJTU emotion EEG dataset) (Zheng et al., 2016). DEAP includes 32-channel EEG data collected from 32 subjects (17 male, 27.2 ± 4.4 years). The subjects' emotions were induced through one-minute-long music video clips. After each stimulus, the subjects rated their emotional experience on a two-dimensional emotional scale proposed by Russell (1980). The two dimensions are arousal (ranging from relaxed to aroused) and valence (ranging from unpleasant to pleasant). The higher a specific rating is, the more intense the emotion is in a specific dimension. The SEED dataset contains 62-channel EEG data collected from 15 subjects (7 male, 23.27 ± 2.37 years), and each subject participated in the experiment three times. The subjects' emotions are induced through 15 film clips, and each film clip lasts for approximately 4 min. Three classes of emotions (positive, neutral, negative) are evaluated, and each class has five corresponding film clips. In this study, we utilized only the trials of positive and negative emotions to evaluate the features' ability to differentiate between these two emotions. For

FIGURE 1 | The feature engineering-based method and the procedure for verifying the performance of cross-subject emotion recognition.

FIGURE 2 | (A) The data normalization method for one subject's multi-channel signals. (B) The sliding window-based feature extraction method for one EEG signal (taking one 12-s signal as an example). The mean of the calculated values in all sliding windows was adopted as the feature.

consistency with the DEAP dataset, we used the one-minute-long data extracted from the middle part of each trial in SEED.

2.2. Data Preprocessing

2.2.1. EEG Preprocessing

As a kind of neurophysiological signal, EEG data are high dimensional and contain redundant and noisy information. In this work, after data acquisition, the raw data was firstly preprocessed, such as by removing the electrooculogram (EOG) and electromyogram (EMG) artifacts and downsampling the raw data to reduce the computational overhead in feature extraction. Two additional preprocessing procedures were needed before feature extraction, namely, rhythm extraction and data normalization. The multi-channel EEG is typically regarded as a reflection of brain rhythms. We first filtered out the four target rhythms, namely, the theta rhythm (4–7 Hz), alpha rhythm (8–15 Hz),

beta rhythm (16–31 Hz), and gamma rhythm (>32 Hz). We attempted to investigate the importance of these different rhythms in reflecting subjects' emotions. We excluded the delta rhythm (<4 Hz), as this rhythm is traditionally regarded as being correlated only with sleep. The four target rhythms were extracted through a custom finite impulse response (FIR) bandpass filter with a Hanning window. Secondly, we conducted data normalization as shown in **Figure 2A**. The extracted rhythm data for each subject were normalized channel by channel across all the trials. This procedure helped to remove subject bias and to generate more comparable features between subjects while allowing the variability of different channels to be preserved.

2.2.2. Label Preprocessing

For DEAP, we divided the subject trials into two classes according to their corresponding ratings on the valence dimension. A rating higher than 5 indicated a positive class, whereas a rating lower than 5 indicated a negative class. Hence, for valence, the two classes were high valence (positive) and low valence (negative). For SEED, the trials have already been categorized into three emotional classes (positive, neutral, negative); hence, we do not need to perform label preprocessing. For consistency, we studied only the positive and negative samples in SEED. The emotion recognition capability was evaluated using binary classification tasks.

2.3. Feature Extraction

In this work, we explored the robustness of a wider range of EEG features in cross-subject emotion recognition. Specifically, we extracted nine kinds of time-frequency domain features and nine kinds of dynamical system features from EEG measurements, as listed in **Table 1**. Extracting features based on some domain knowledge can provide a concise representation of the original data and materials. In this work, after preprocessing the data, we calculated the features for each of the four rhythms with a 4-s sliding window and a 2-s overlap, and then, the mean of the

TABLE 1 | This table lists the two main categories of EEG features that we extracted.

Feature type	Extracted features
Time-frequency domain features	1. Peak-Peak Mean. 2. Mean Square Value. 3. Variance. 4. Hjorth Parameter: Activity. 5. Hjorth Parameter: Mobility. 6. Hjorth Parameter: Complexity. 7. Maximum Power Spectral Frequency. 8. Maximum Power Spectral Density. 9. Power Sum.
Non-linear dynamical system features	10. Approximate Entropy. 11. C0 Complexity. 12. Correlation Dimension. 13. Kolmogorov Entropy. 14. Lyapunov Exponent. 15. Permutation Entropy. 16. Singular Entropy. 17. Shannon Entropy. 18. Spectral Entropy.

The features were extracted for four rhythms. For the DEAP dataset, the total number of features extracted for one trial is 2304. For the SEED dataset, the total number of features extracted for one trial is 4464.

feature values extracted from those sliding windows was adopted as the trial's feature. The sliding window-based feature extraction methods are illustrated in **Figure 2B**. For DEAP, the number of features extracted for one trial is: $((9 + 9) \times 32) \times 4 = 2304$. For SEED, the number of features extracted for one trial is: $((9 + 9) \times 62) \times 4 = 4464$. All features were normalized before further analysis.

The details and reasons for selecting these candidate features are elaborated below:

2.3.1. Time-Frequency Domain Features

Nine kinds of features in the time and frequency domains of each signal were considered. The *peak-to-peak mean* is the arithmetic mean of the vertical length from the very top to the very bottom of the time series. The *mean squared value* is the arithmetic mean of the squares of the time series. *Variance* measures the degree of dispersion of the time series. After transforming the time series into the frequency domain through Fourier transform, we calculated the sum of the power spectral, and we further extracted the maximum power spectral density along with its corresponding frequency value. Three *Hjorth parameters* that can reflect characteristics of activity, mobility, and complexity were also extracted according to the work by Hjorth (1970): the *activity* parameter reflects the information of the signal power, the *mobility* parameter is an estimation of the mean frequency, and the *complexity* reflects the bandwidth and the change in frequency. The Hjorth parameters are considered suitable for analyzing non-stationary EEG signals.

2.3.2. Non-linear Dynamical System Features

We also extracted nine kinds of features that can reflect the characteristics of non-linear dynamical systems. Researchers have found that human brain manifests many characteristics specifically belonging to non-linear and chaotic dynamical systems; thus, the EEG signal is inherently complex, non-linear, non-stationary, and random in nature (Stam, 2005; Sanei and Chambers, 2013). *Approximate entropy (ApEn)* is a non-linear measure of the regularity of a signal; the more regular a signal is, the smaller the ApEn will be (Pincus et al., 1991). *C0 Complexity*

is adopted to measure the amount of the stochastic components, which assumes that a signal consists of a regular part and a stochastic part (Lu et al., 2008). *Correlation dimension* determines the number of dimensions (independent variables) that can describe the dynamics of the system and reflects the complexity of the process and the distribution of system states in the phase space (Khalili and Moradi, 2009). The *Lyapunov exponent* is used to measure the aperiodic dynamics of a chaotic system. This feature can capture the separation and evolution of the system's initial states in the phase space. The positive Lyapunov exponent indicates the chaos in the system (Übeyli, 2010). The *Kolmogorov entropy* is also a metric of the degree of chaos and measures the rate at which information is produced by the system as well as the rate at which information is lost by the system (Aftanas et al., 1997). Note that ApEn is closely related to Komolgorov entropy. The calculation of Komolgorov entropy is greatly influenced by the noise and dimensionality of the data. The complexity of neural activity can also be measured using the symbolic dynamic theory, in which a time series can be mapped to a symbolic sequence, from which the *permutation entropy (PE)* can be derived. The largest value of PE is 1, which indicates that the time series is completely random, while the smallest value of PE is 0, which indicates that the time series is completely regular (Li et al., 2007). *Singular spectrum entropy* is calculated by a singular value decomposition (SVD) of the trajectory, which is obtained by reconstructing the one-dimensional time series into a multi-dimensional phase space. This feature reflects the uncertainty and complexity of the energy distribution and is an indicator of event-related desynchronization (ERD) and event-related synchronization (ERS) (Zhang et al., 2009). *Shannon entropy* is a classical quantification of uncertainty and is frequently used to measure the degree of chaos in the EEG signal. *Power spectral entropy* is based on the Shannon entropy and measures the spectral complexity of the system. After the Fourier transform is performed, the signal is transformed into a power spectrum, and the information entropy of the power spectrum is called the power spectral entropy (Zhang et al., 2008).

2.4. Automatic Feature Selection

In this work, we first try to determine the upper bound of the performance of the proposed features. Hence, we choose to utilize some automatic feature selection techniques. Five different automatic feature selection methods were used to extract the most informative EEG features from the whole candidate set. Specifically, the whole features are re-ranked according to a pre-defined ranking criteria, e.g., based on the degree of correlation between the feature and the target class or based on the value of the feature weight, and then, the features above a pre-defined threshold are selected (Huang et al., 2006; Maldonado and Weber, 2008).

Two typical automatic feature selection techniques are the filter-based strategy and the wrapper-based strategy (Guyon and Elisseeff, 2003). The former is independent of any pattern recognition algorithm and filters out a specific number of features according to some statistical properties of the features. The classical filter-based strategy includes the chi-squared (χ^2), mutual information, and *F*-test methods. The wrapper-based strategy, on the other hand, cooperates with a specific pattern

recognition algorithm. A widely adopted wrapper-based strategy is the recursive feature elimination (RFE) method. We also considered a more efficient L1-norm penalty-based feature selection method, which has been widely used in recent years.

The details of these feature selection methods are elaborated as follows:

2.4.1. Chi-Squared-Based Feature Selection (χ^2)

The Chi-squared test is a classical statistical hypothesis test method for testing the independence of two variables or to investigate whether the distribution of one variable differs from that of another. This work is concerned with the former, formulated as below:

$$\chi^2 = \sum_{i=1}^{r} \sum_{j=1}^{c} \frac{(O_{i,j} - E_{i,j})^2}{E_{i,j}}, \tag{1}$$

where r and c are the number of categories in the two random variables, $O_{i,j}$ is the number of observations of type i,j, and the $E_{i,j}$ is the expected frequency of type i,j. In our work, a higher χ^2 value indicates a higher correlation between a feature variable and the target classes.

2.4.2. Mutual Information-Based Feature Selection (MI)

The mutual information metric is derived from probability theory and information theory. This metric is adopted to measure the mutual dependence (shared information) between the feature variables and the target classes. It is closely linked to the concept of entropy, which defines how much information is contained in a variable. Mutual information can be expressed as follows:

$$
\begin{aligned}
I(X; Y) &= H(X) + H(Y) - H(X, Y) \\
&= \sum_x P(x) \log \frac{1}{P(x)} + \sum_y P(y) \log \frac{1}{P(y)} \\
&\quad - \sum_{x,y} P(x, y) \log \frac{1}{P(x, y)} \\
&= \sum_{x,y} P(x, y) \log \frac{p(x, y)}{P(x)p(y)},
\end{aligned} \tag{2}
$$

where $H(X)$ and $H(Y)$ are the marginal entropy of X and Y respectively, and $H(X, Y)$ is the joint entropy of X and Y.

2.4.3. ANOVA F-Value-Based Feature Selection (AF)

F-test is a representative version of the analysis of variance (ANOVA). It is typically used to test whether the means of multiple populations are significantly different. In feature selection, ANOVA can measure the "F-ratio" of the between-class variance (as in Equation 4) over within-class variance (as in Equation 5). The "F-ratio" indicates the degree of class separation, as formulated in Equation (3). The higher a feature variable's F-ratio is, the better this feature is in differentiating different classes.

$$F_{ratio} = \frac{\sigma^2_{between}}{\sigma^2_{within}} \tag{3}$$

where the between-class variance and within-class variance are:

$$\sigma^2_{between} = \frac{\sum_{j=1}^{J} (\bar{x}_j - \bar{x})^2 N_j}{J - 1} \tag{4}$$

and

$$\sigma^2_{within} = \frac{(\sum_{j=1}^{J} \sum_{i=1}^{N_j} (x_{i,j} - \bar{x})^2) - (\sum_{j=1}^{J} (\bar{x}_j - \bar{x})^2 N_j)}{N - J}, \tag{5}$$

respectively. J is the number of classes, N_j is the number of measurements in the jth class, $\bar{x}_j$ is the mean of the jth class, $\bar{x}$ is the overall mean, and $x_{i,j}$ is the ith measurement of the jth class.

2.4.4. Recursive Feature Elimination (RFE)

As first introduced in Guyon et al. (2002) for gene selection, RFE is a wrapper-based method that judges the importance of features using an external machine learning algorithm. It adopts a sequential backward elimination strategy. First, the algorithm is trained on the initial whole set of features and assigns weight to each of the features. Then, a pre-defined number of features with the lowest-ranking absolute weights are pruned from the current feature set. This procedure recursively repeats for several steps until the desired number of selected features is reached. The pseudo code of the RFE is illustrated below in Algorithm 1. In this work, we used SVM with a linear kernel as the ranking method, in which the RFE utilized $\|w\|$ as the ranking criteria for the importance of the features.

Algorithm 1: Pseudo Code for Recursive Feature Elimination (RFE) Algorithm

---

Input:
Training set: T
Feature set: $F = \{f_1, f_2, ..., f_p\}$
Ranking method: $M(T, F)$
Desired feature number: q
Number of feature to eliminate in each step: k
Output:
Final ranking feature set: $R = \{f_{r1}, f_{r2}, ..., f_{rp}\}$
Final selected feature set: $F = \{f_1, f_2, ..., f_q\}$
1 **Initialization**;
2 Steps: S = (p-q)/k;
3 **for** $i = 1 \rightarrow S$ **do**
4 $\quad$ Rank set F according to $M(T, F)$;
5 $\quad$ $L_k \longleftarrow$ Last ranked k features in F;
6 $\quad$ $R[p - i*k + 1 : p - (i - 1)*k] \longleftarrow L_k$;
7 $\quad$ $F \longleftarrow F - L_k$;
8 **end**

2.4.5. L1-Norm Penalty-Based Feature Selection (L1)

This method introduces a L1-norm regularization term into the objective function to induce the sparsity by shrinking the weights toward zero. Regularization is usually adopted in case that the size of the training set is smaller relative to the dimensionality of the features. This process favors small parameters of the model to prevent overfitting (Ng, 2004). It is natural in feature selection settings for features with weights of zero to be eliminated from

the candidate set. Some researchers have indicated that the L1-norm-based method is better than the L2-norm-based method, especially when there are redundant noise features (Zhu et al., 2004). In this work, we adopted an SVM with an L1-norm penalty to select the important features. The formulation of the objective function is as follows:

$$\min_{\omega_0, \omega} \sum_{i=1}^{n} [1 - y_i(\omega_0 + \sum_{j=1}^{q} \omega_j x_{i,j})] + C\|\omega\|_1 \qquad (6)$$

$\|\omega\|_1$ is the L1-norm term, in which the ω represents the model weights. The parameter "C" controls the trade-off between the loss and penalty.

2.5. Manually Operated Feature Selection

The upper bound of the performance of the proposed features can be verified using the previous automatic feature selection methods. We chose to further evaluate the performance and the importance of the features from different aspects, including different electrodes, locations, rhythms, and feature types. Haufe et al. (2014) indicated that the interpretation of the parameters in backward methods (multivariate classifiers) may lead to the wrong conclusions in neuroimaging data modeling. Hence, in this work, we did not conduct analyses based on the selected features or the corresponding feature weights of the automatic feature selection methods. However, we adopted a simple "searchlight" approach in which we manually selected features from different aspects and evaluated the performances independently.

The performances of automatic and manually operated feature selection were verified by applying a linear SVM. The codes for the data preprocessing, feature extraction, and cross-subject verification processes with different feature selection methods, as well as the extracted features, can be accessed at the following web page: https://github.com/muzixiang/EEG_Emotion_Feature_Engineering.

3. RESULTS

3.1. Overall Evaluation

We first determined the upper bound of the performance of the proposed features using all of the mentioned automatic feature selection methods. In the experiment, considering the computational overhead of different methods as well as the adequacy of the experiments, we employed different settings for different methods. For filter- and RFE-based methods, we set the step size for the number of selected features to 10. Hence, the number of steps for DEAP and SEED are 230 and 446, respectively. For the L1-norm penalty-based method, we set 100 different values for penalty parameter "C" ranging from 0.01 to 1 with a step size of 0.01. We adopted a "leave-one-subject-out" verification strategy, and the performance was evaluated by the mean recognition accuracy metric. **Figures 3A–C**, **4A–C** illustrate the performance of the automatic feature selection methods with different settings on the DEAP and SEED dataset, respectively.

For DEAP, when no feature selection method was utilized, the recognition performance was 0.5531 (std:0.0839). The best result of 0.5906 (std: 0.0868) was obtained with the L1-norm penalty-based method when the value of "C" is 0.08. For SEED, when no feature selection method was utilized, the recognition performance was 0.7844 (std:0.1119). The best result of 0.8333 (std: 0.1016) was obtained with the RFE-based method when the number of selected features is 130. **Table 2** shows the p-values calculated through one-way ANOVA test between the method with best performance and other methods. For a better comparison between those methods, as shown in **Figures 3D**, **4D**, we also produced ROC curves. Different feature selection methods were compared by analyzing their ROC curves and the Areas under the ROC curves (AUC). The results showed that the L1-norm penalty-based method outperformed other methods on both DEAP (AUC = 0.605) and SEED (AUC = 0.904). Moreover, the L1-norm penalty-based method incurred a lower computational cost than the other methods. Hence, considering both effectiveness and efficiency, the L1-norm penalty-based feature selection method is recommended to verify the upper bound of the recognition performance when a large amount of features are provided.
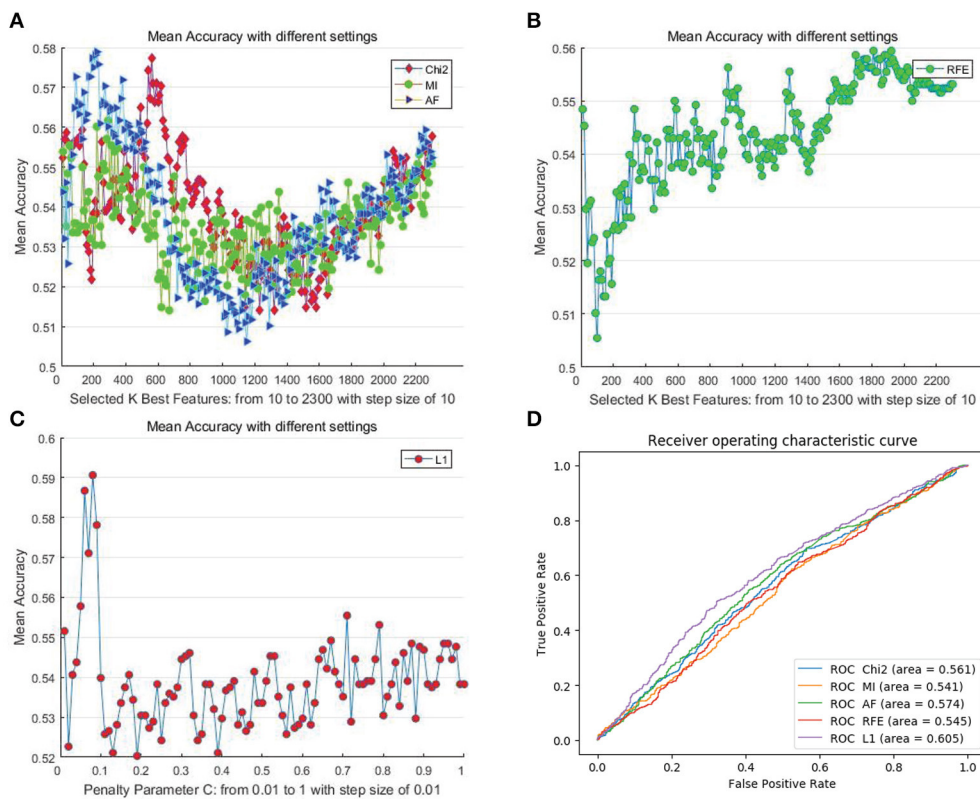
The results demonstrate the effectiveness of our proposed EEG features in cross-subject emotion recognition, especially on the SEED dataset. The performance on DEAP is significantly inferior to that on SEED. This is possibly due to the relatively low quality of the data and the emotional ratings of trials in the DEAP dataset. Hence, we chose to conduct further evaluation only on the SEED dataset.

3.2. Evaluation From Different Perspectives

We also explored the importance of different EEG features in cross-subject recognition from multiple perspectives, including different channels, brain regions, rhythms, and feature types.

Figure 5A illustrates the performance of each individual channel. We ranked the performance of these channels and labeled the top one-sixth of the channels on the diagram of the 10–20 international system of electrode placement. The channels on the bilateral temporal regions achieved higher mean accuracies for cross-subject emotion recognition. As shown in **Figure 5B**, we also evaluated the performance of different regions, including the left-right anterior regions, left-right posterior regions, left-right hemispheres, and anterior-posterior hemispheres. The partition of the regions is illustrated in the figure, and the channels in the cross regions were eliminated when evaluating the performance of the sub-regions. We found that the left anterior region achieved better performance compared to the right anterior region, left posterior region, and the right posterior region, especially when the information in the beta band was utilized. The left hemisphere performed better than the right hemisphere in each band except for the gamma band. Furthermore, the information from the anterior hemisphere enhanced recognition performance in each band more than that from the posterior hemisphere.

Validating the performance of different EEG rhythms was also of interest to us. As we can see in **Figure 5C**, the individual beta rhythm achieved the best performance, and the higher-frequency

FIGURE 3 | Mean cross-subject recognition performance with different methods and settings on DEAP. **(A)** The filter-based methods. **(B)** The RFE-based method. **(C)** The L1-based method. **(D)** The ROC curves of different methods with their best settings.

beta rhythm and gamma rhythm bands performed better than the lower-frequency theta rhythm and alpha rhythm bands. When the data on all four rhythms were concatenated, the performance was greatly promoted.
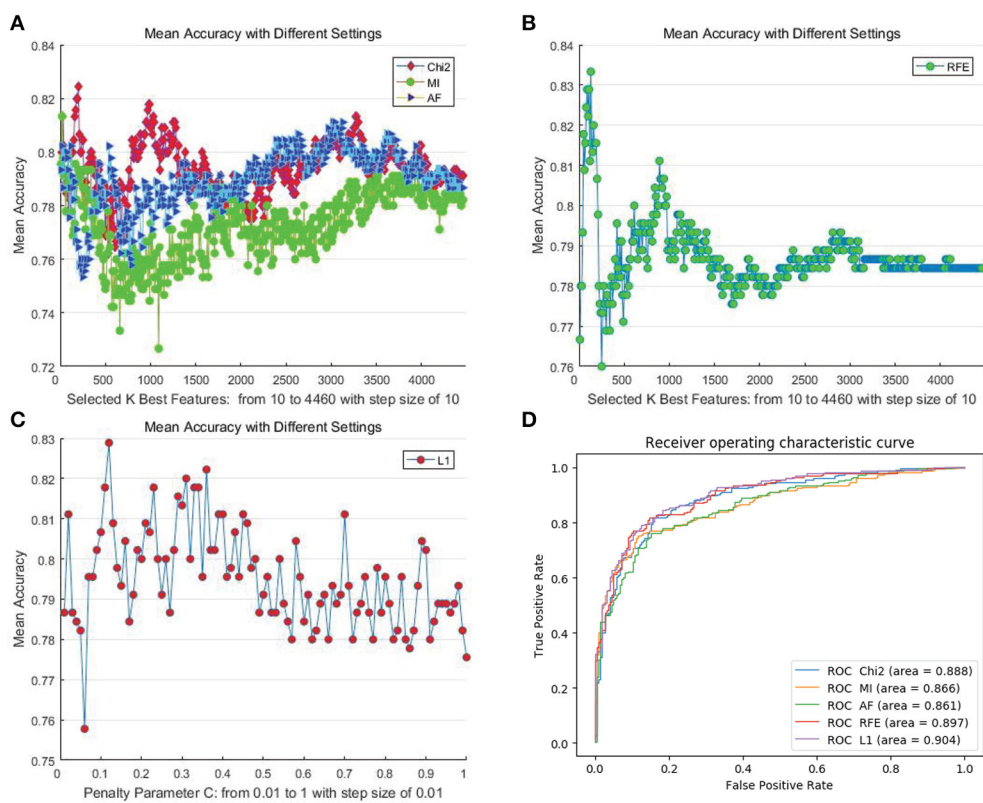
The main research objective of this paper is to verify the effectiveness of the proposed features. Thus, we also evaluated the performances of each kind of feature. As shown in **Figure 5D**, the information on linear features No. 5 (Hjorth parameter: mobility), No. 6 (Hjorth parameter: complexity), and No. 7 (maximum power spectral frequency) in the beta rhythm led to the best mean recognition accuracy. Only the non-linear features No. 12 (correlation dimension), No. 13 (Kolmogorov entropy), and No. 17 (Shannon entropy) can lead to a mean accuracy over 60%. **Figure 5E** presents the performance comparison between the linear and non-linear features in different frequency bands. The results show that using linear features outperformed the use of non-linear features in each frequency band when linear SVM and random forest (RF) classifiers were applied. Hence, considering the high computational overhead of extracting the non-linear features, solely adopting linear features seems an effective choice for constructing a real-time emotion recognition system. Nevertheless, we should also clarify that the values of the non-linear features calculated in this work may be not optimal. The performance of the non-linear features are influenced by many factors, e.g., the parameter settings and the data volume

limitations for the search space. The optimal values of those non-linear features are worth further exploration.

3.3. Correlation Analysis

As we can see in **Figure 5D**, the performances of some feature type (e.g., features No. 2, No. 3, No. 4, and No. 9) are seemingly identical. This result likely indicates that some features can be highly correlated in identifying a certain emotion class. Hence, for examining those highly correlated features, we calculated the Pearson correlation coefficients for those 18 different feature types. For example, as presented in **Figure 6**, the linear features No. 2, No. 3, No. 4, and No. 9 are absolutely positively correlated in each rhythm, which explains why the performances of these features are approximately identical. Linear features No. 1 and No. 8 are highly positively correlated with all other linear features except for the Hjorth parameters. For the Hjorth parameters, feature No. 5 is highly positively correlated with feature No. 7 in each rhythm, and is highly negatively correlated with feature No. 6 in the beta rhythm. For the non-linear features, we can see that feature No. 12 is highly and positively correlated with feature No. 13 and No. 17 in the higher-frequency bands, and that feature No. 16 is highly and negatively correlated with feature No. 18 in each rhythm.

Moreover, through analyzing the correlation of the channels based on those features, we attempted to investigate the

FIGURE 4 | Mean cross-subject recognition performance with different methods and settings on the SEED dataset. **(A)** The filter-based methods. **(B)** The RFE-based method. **(C)** The L1-based method. **(D)** The ROC curves of different methods with their best settings.

TABLE 2 | The performance upper bound of the proposed features using different automatic feature selection methods.

DEAP	χ^2	MI	AF	RFE
	Step No.: 56	Step No.: 29	Step No.: 22	Step No.: 181
	Mean: 0.5773	Mean: 0.5617	Mean: 0.5789	Mean: 0.5594
	St.Dev.: 0.0841	St.Dev.: 0.0914	St.Dev.: 0.1004	St.Dev.: 0.0818
L1				
Step No.: 8	$p = 0.5364$	$p = 0.1992$	$p = 0.6192$	$p = 0.1432$
Mean: **0.5906**				
St.Dev.: 0.0868				
SEED	χ^2	MI	AF	L1
	Step No.: 20	Step No.: 2	Step No.: 2	Step No.: 13
	Mean: 0.8244	Mean: 0.8133	Mean: 0.8111	Mean: 0.8289
	St.Dev.: 0.1151	St.Dev.: 0.1227	St.Dev.: 0.1389	St.Dev.: 0.0899
RFE				
Step No.: 12	$p = 0.8242$	$p = 0.6305$	$p = 0.4895$	$p = 0.8999$
Mean: **0.8333**				
St.Dev.: 0.1016				
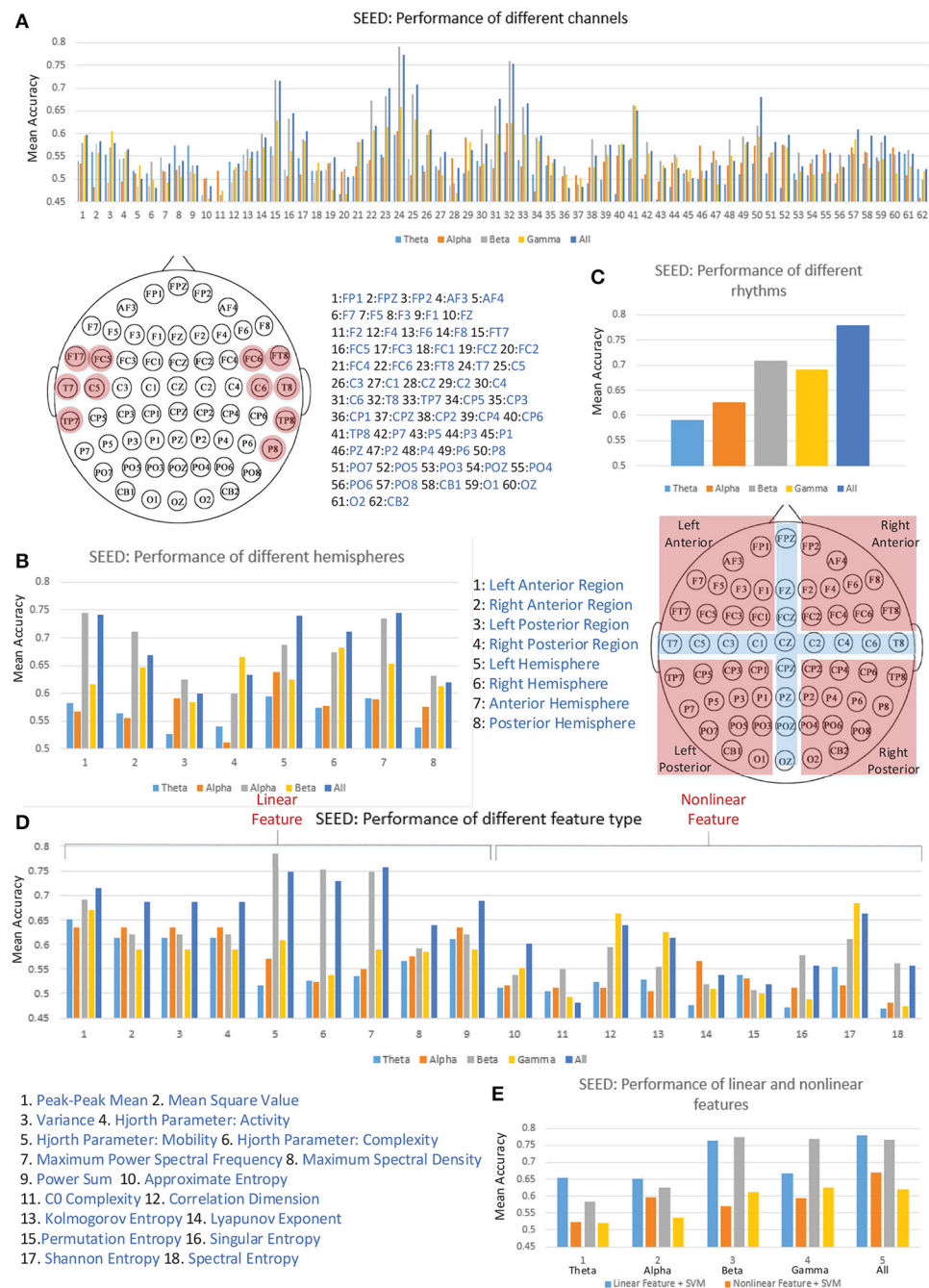
Meanwhile, the p-values calculated through one-way ANOVA between the method with best performance and other methods are also exhibited. The highest mean recognition accuracy is shown in bold type.

underlying mechanisms of those features that allow for differentiating cross-subject emotions. Specifically, for each subject and for each specific feature, we constructed correlation

matrices of the 62 channels for subjects' negative trials and positive trials. After all of the correlation matrices had been constructed, we averaged the correlation matrices in the negative group and positive group. The mean correlation matrices for specific features are presented in **Figure 7**. We also conducted statistical analyses to compare the differences in channel correlations between the negative group and the positive group. The t test results are illustrated in **Figure 8**. The results in both **Figures 7**, **8** indicate that for almost every feature, the mean correlations in the negative group are higher than those in the positive group.

The connection network of the 62 channels is represented in the form of a binary matrix, which was constructed based on the obtained correlation matrices. We first needed to determine the threshold of the correlation coefficients, based on which the connection between two channels could be established. To be more specific, the value in the binary matrix was set to 1 when the corresponding value in the correlation matrix was greater than the threshold. Otherwise, the value in the binary matrix was set to 0. The value of 1 in the binary matrix indicates that there is a connection between the two corresponding nodes. Based on the obtained binary matrix, the connection network of the channel nodes was constructed.
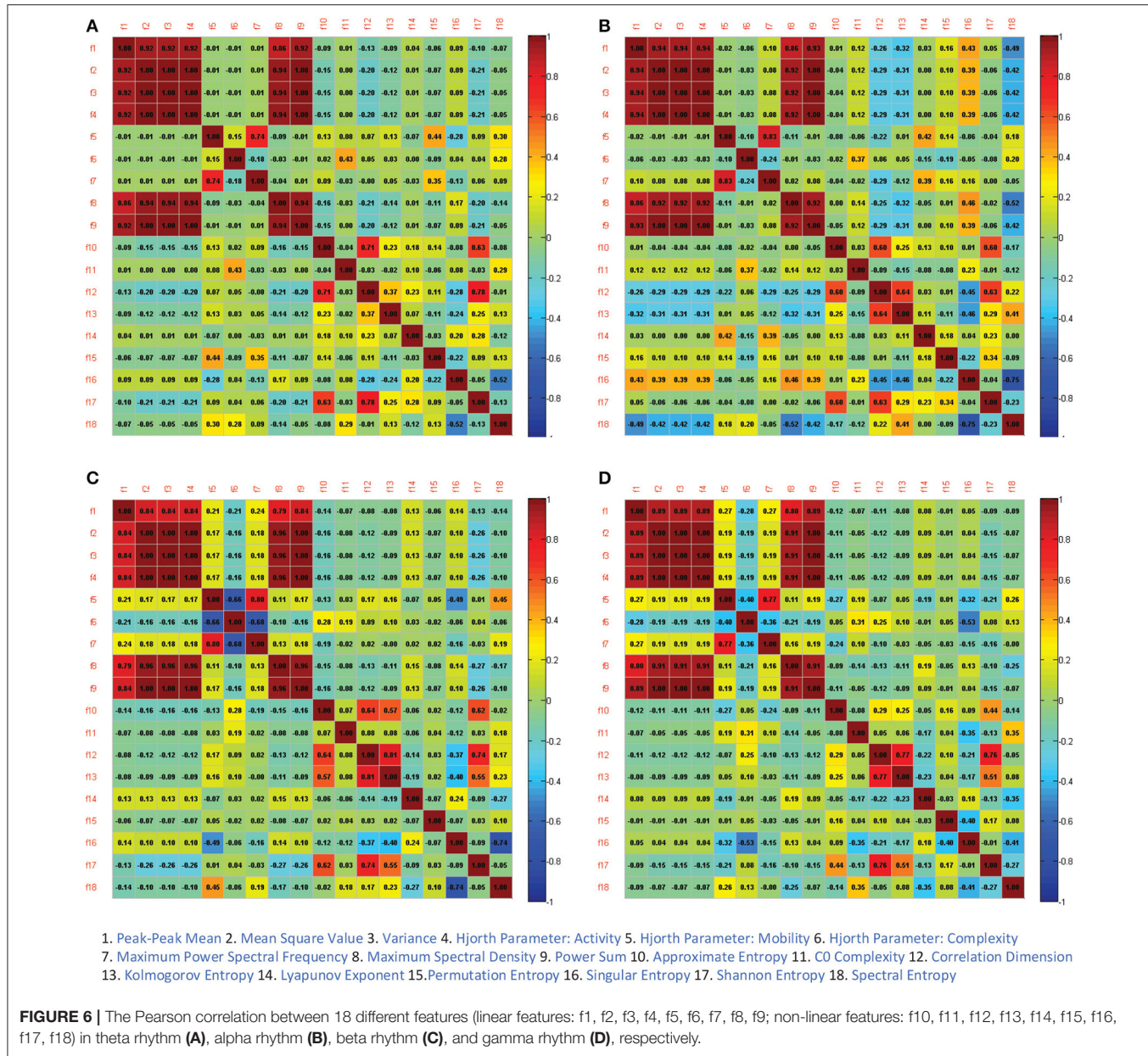
For measuring the coherence of different channel locations in different emotional states, we calculated the clustering coefficients of each node in the connection network. The clustering coefficient was a reflection of the degree of aggregation
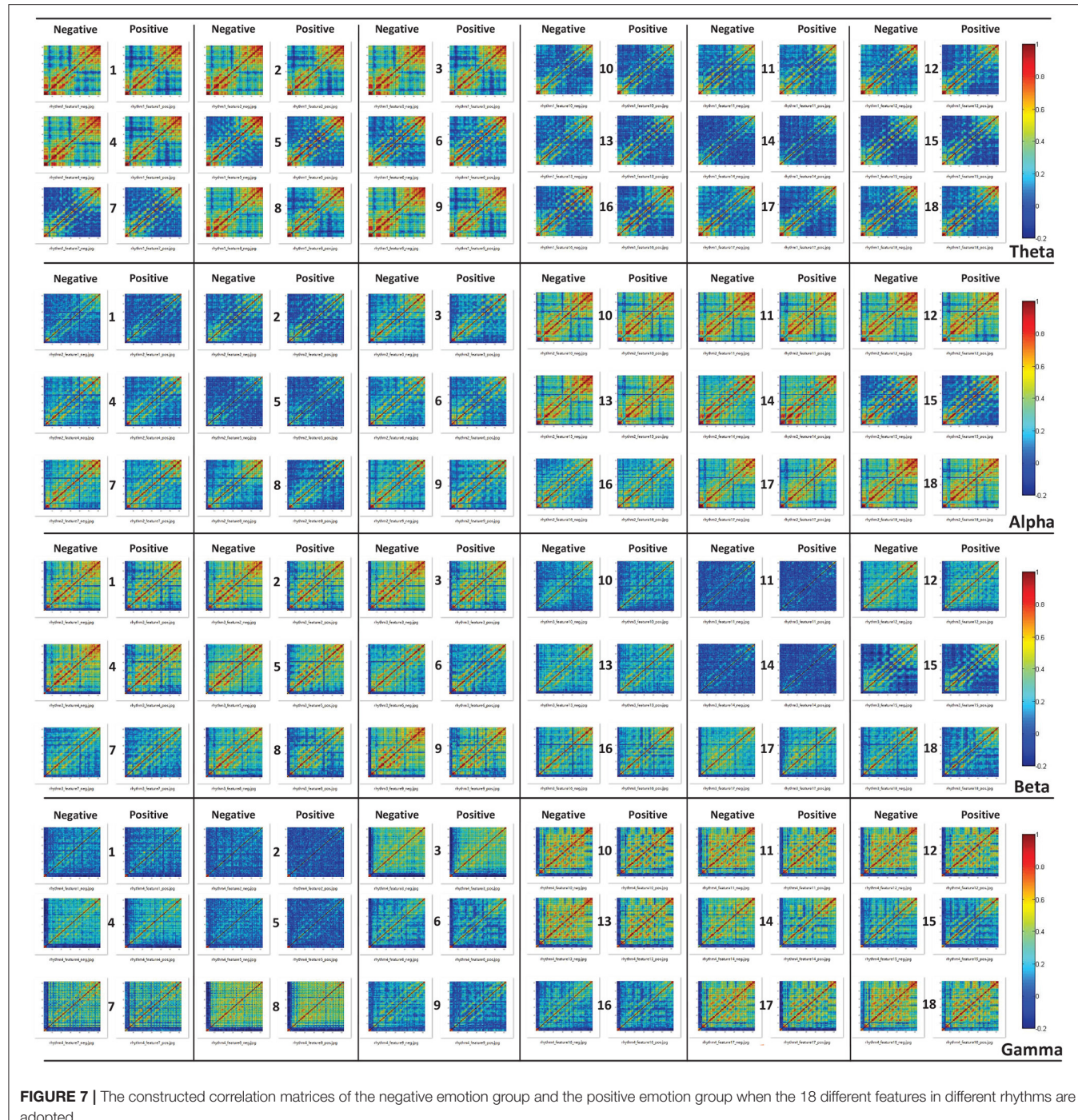
FIGURE 5 | The cross-subject recognition performance based on features from different channels **(A)**, different regions **(B)**, different rhythms **(C)**, different features **(D)**, and different feature types **(E)**.

of different channel locations. The thresholds at which the global clustering coefficients were significantly different between the positive group and negative group are illustrated in **Table 3**. As mentioned above in **Figure 5D**, feature No. 5 (Hjorth parameter: mobility) in beta rhythm achieved the best recognition performance. Thus, in this paper, we use this feature as an example to illustrate the topographic plot of the clustering

coefficients of the groups with negative and positive emotions. As shown in **Figure 9A**, at each threshold, the clustering coefficients in the left anterior regions of the negative groups are consistently higher than those of the positive groups. This dynamic may account for the results obtained in **Figure 5B** indicating that the left anterior regions yields the best recognition performance when beta rhythm information is utilized. Nevertheless, different

FIGURE 6 | The Pearson correlation between 18 different features (linear features: f1, f2, f3, f4, f5, f6, f7, f8, f9; non-linear features: f10, f11, f12, f13, f14, f15, f16, f17, f18) in theta rhythm **(A)**, alpha rhythm **(B)**, beta rhythm **(C)**, and gamma rhythm **(D)**, respectively.

features and thresholds could have different topographic plots in which the clustering coefficients may be quite different from those of feature No. 5 in the beta rhythm. For example, in addition to feature No. 5 in beta rhythm, feature No. 6 in beta rhythm also led to a high performance. We have also presented the clustering coefficients in **Figure 9B**. However, the topographic plot was different from that in **Figure 9A**, and the left anterior region was no longer significantly different between the two groups. Hence, the important locations for emotion recognition cannot be determined simply by analyzing only one or two features.

As described above, we should point out that such correlation analysis may not be adequate to fully interpret the mechanism of the features. Moreover, for example, as shown in **Figure 8**, the feature No. 1 in the gamma rhythm cannot significantly

differentiate the correlation coefficients of the two groups. However, as shown in **Figure 5D**, this feature can still lead to a better performance than most of the non-linear features.

4. DISCUSSIONS

In this work, we verified the effectiveness of 18 kinds of EEG features in cross-subject emotion recognition, including 9 kinds of time-frequency domain features and 9 kinds of dynamical system features. We adopted a "leave-one-subject-out" method to verify the performance of the proposed features. After automatic feature selection, the highest mean recognition accuracies of 59.06% (AUC = 0.605) on the DEAP dataset and 83.33% (AUC = 0.904) on the SEED dataset were reached.

FIGURE 7 | The constructed correlation matrices of the negative emotion group and the positive emotion group when the 18 different features in different rhythms are adopted.

The performance on DEAP was not as good as that on SEED, which could be due to the low quality of the data in the emotional ratings of the trials. The noise in the emotional ratings degraded the ability of the model to differentiate between different classes. Through drawing the ROC curves, we found that the L1-norm penalty-based feature selection method exhibited robust performance on both two datasets. Considering its lower computational overhead, this method is the

best strategy to adopt when analyzing large numbers of candidate features.

We also evaluated the cross-subject recognition performance from different perspectives, including different EEG channels, different regions, different rhythms, different features, and different feature types. We chose to conduct analyses on the SEED dataset because of its better performance. Specifically, through evaluation over individual channels, we found that

FIGURE 8 | The comparison of the mean global correlation between the groups of negative emotion and positive emotion when the 18 different features in theta rhythm **(A)**, alpha rhythm **(B)**, beta rhythm **(C)**, and gamma rhythm **(D)** are adopted. (***$p<0.001$, **$p<0.01$, *$p<0.05$)

the channels with the best performances were mainly located in the bilateral temporal regions, which was consistent with the finding in Soleymani et al. (2012), Zheng et al. (2016). We partitioned the channels into different groups according to the different regions and evaluated the performances of the different groups. We found that the left anterior region achieved a better performance compared to the other sub-regions, especially when the information in the beta band was utilized. The left hemisphere performed better than the right hemisphere except for in the gamma band. Furthermore, the anterior hemisphere exhibited an improved recognition performance compared to the posterior hemisphere, especially when data from all rhythms were utilized. The relationship between emotion recognition and frontal regions was illustrated in the studies of Schmidt and Trainor (2001), Lin et al. (2010). Schmidt and Trainor (2001) found the relatively higher left frontal EEG activity under exposure to happy musical excerpts and relatively higher right frontal EEG activity under exposure to sad musical excerpts, and the overall frontal EEG activity could distinguish the intensity of the emotions. Lin et al. (2010) found that the frontal and parietal electrode pairs were the most informative on emotional states.

The evaluation of different rhythms indicated that the information in higher-frequency bands contributed more to cross-subject emotion recognition compared to lower-frequency bands. The effectiveness of the beta and gamma rhythms in promoting emotion recognition was also presented in

Lin et al. (2010), Soleymani et al. (2012), Zheng et al. (2016). Moreover, some neuroscience studies have found that emotion-related neural information mainly resides in higher-frequency bands (Müller et al., 1999; Kortelainen et al., 2015). By evaluating the performances of individual features, we found that linear features No. 5 (Hjorth parameter: mobility), No. 6 (Hjorth parameter: complexity), and No. 7 (maximum power spectral frequency) in the beta rhythm led to the best mean recognition accuracy. However, the Hjorth parameters have not been widely adopted in EEG-based emotion recognition. We also found that the combination of the linear features greatly outperformed the combination of non-linear features in each frequency band. Considering the high computational overhead in extracting the non-linear features, adopting linear features in designing real-time emotion recognition systems is recommended. Nevertheless, the non-linear features calculated here may be not the optimal ones, given that emotional information is very likely processed in a non-linear way. The optimal values of the non-linear features for reflecting emotional processes are certainly worth further exploration.

For a better understanding of the mechanisms of those features that allow for differentiating between emotions, we further conducted a correlation analysis for 62 channels for each feature. We calculated and constructed correlation matrices using different features. We found that for nearly every feature, the negative group has a higher mean correlation coefficient
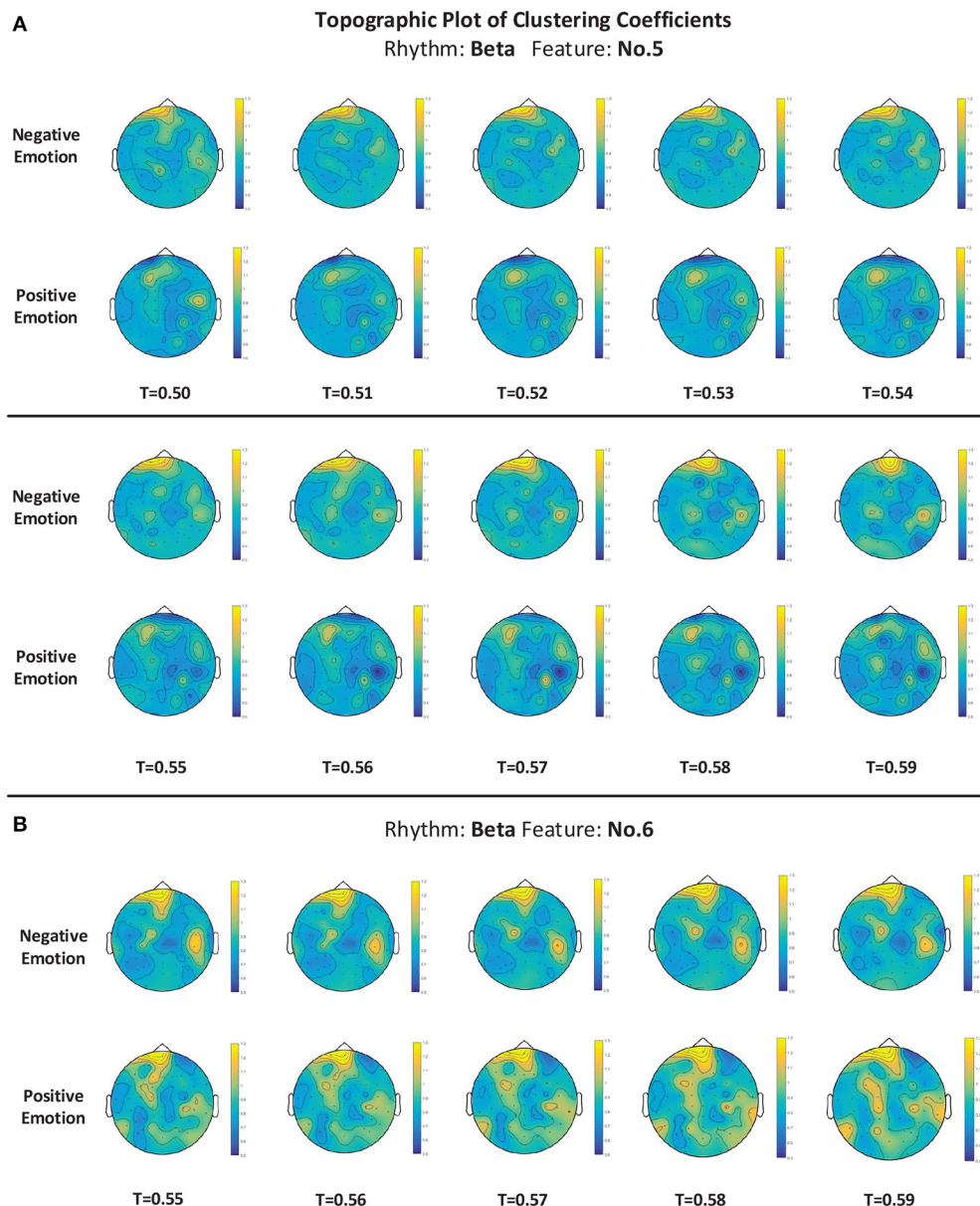
TABLE 3 | The threshold scope that can significantly differentiate the clustering coefficients in groups of positive emotion and negative emotion ($p < 0.05$).

Rhythm	Feature	Threshold scope	Feature	Threshold scope
Theta	No.1	0.34~0.65, 0.92~0.99	No.10	0.01~0.36, 0.62~0.63, 0.69~0.71, 0.89~0.92
Theta	No.2	0.01~0.66, 0.92~0.99	No.11	0.14~0.47, 0.71~0.74, 0.84~0.87, 0.97~0.98
Theta	No.3	0.01~0.66, 0.92~0.99	No.12	0.01~0.35, 0.59~0.62, 0.77~0.78, 0.94~0.96
Theta	No.4	0.01~0.66, 0.92~0.99	No.13	0.01~0.20, 0.49~0.50
Theta	No.5	0.01~0.39	No.14	0.21~0.31
Theta	No.6	0.01~0.24	No.15	0.07~0.32, 0.40~0.49, 0.70~0.72, 0.95~0.96
Theta	No.7	0.01~0.15	No.16	0.01~0.34, 0.54~0.58
Theta	No.8	0.01~0.65, 0.93~0.99	No.17	0.01~0.42
Theta	No.9	0.01~0.66, 0.93~0.99	No.18	0.49~0.50, 0.90~0.98
Alpha	No.1	0.01~0.58, 0.66~0.95	No.10	0.01~0.08, 0.53~0.56, 0.67~0.72, 0.96~0.99
Alpha	No.2	0.01~0.27, 0.49~0.60, 0.75~0.91	No.11	0.01~0.32, 0.64~0.76, 0.95~0.99
Alpha	No.3	0.01~0.41, 0.56~0.66, 0.83~0.95	No.12	0.01~0.08, 0.23~0.32, 0.67~0.76, 0.95~0.99
Alpha	No.4	0.01~0.40, 0.47~0.59, 0.90~0.93	No.13	0.01~0.05, 0.28~0.32, 0.67~0.78, 0.95~0.99
Alpha	No.5	0.01~0.29, 0.50~0.52	No.14	0.01~0.25
Alpha	No.6	0.01~0.25, 0.48~0.73	No.15	0.01~0.17, 0.24~0.28, 0.38~0.40, 0.89~0.92
Alpha	No.7	0.01~0.35, 0.46~0.48, 0.95~0.97	No.16	0.01~0.14, 0.36~0.39
Alpha	No.8	0.01~0.36, 0.49~0.70, 0.79~0.99	No.17	0.01~0.05, 0.64~0.66, 0.90~0.99
Alpha	No.9	0.01~0.35, 0.82~0.85, 0.95~0.98	No.18	0.01~0.06, 0.65~0.78, 0.95~0.99
Beta	No.1	0.01~0.44, 0.53~0.58, 0.90~0.92	No.10	0.01~0.13, 0.68~0.69
Beta	No.2	0.01~0.47	No.11	0.01~0.32, 0.42~0.43, 0.46~0.54, 0.67~0.80
Beta	No.3	0.01~0.49, 0.85~0.86	No.12	0.01~0.26, 0.91~0.98
Beta	No.4	0.01~0.49, 0.53~0.56, 0.85~0.86	No.13	0.01~0.34, 0.48~0.54, 0.87~0.92
Beta	No.5	0.01~0.16, 0.20~0.23, 0.48~0.61	No.14	0.01~0.26, 0.38~0.43, 0.62~0.74, 0.81~0.87
Beta	No.6	0.01~0.41, 0.55~0.64, 0.85~0.91	No.15	0.01~0.21
Beta	No.7	0.01~0.31, 0.67~0.71, 0.91~0.99	No.16	0.01~0.21, 0.57~0.62, 0.81~0.83, 0.86~0.88
Beta	No.8	0.01~0.40, 0.86~0.89, 0.96~0.99	No.17	0.01~0.12, 0.67~0.69, 0.86~0.88, 0.95~0.99
Beta	No.9	0.01~0.47	No.18	0.01~0.29, 0.39~0.46, 0.74~0.88
Gamma	No.1	0.14~0.27, 0.66~0.70, 0.76~0.81	No.10	0.15~0.33, 0.40~0.64, 0.83~0.88
Gamma	No.2	0.01~0.33, 0.85~0.98	No.11	0.17~0.22, 0.28~0.29
Gamma	No.3	0.01~0.17, 0.50~0.51	No.12	0.26~0.49
Gamma	No.4	0.01~0.47, 0.97~0.98	No.13	0.23~0.54
Gamma	No.5	0.01~0.31, 0.73~0.98	No.14	0.01~0.35, 0.97~0.99
Gamma	No.6	0.01~0.30, 0.80~0.99	No.15	0.01~0.22, 0.42~0.47, 0.72~0.74, 0.83~0.88
Gamma	No.7	0.01~0.35, 0.93~0.99	No.16	0.01~0.05, 0.81~0.84
Gamma	No.8	0.48~0.61, 0.98~0.99	No.17	0.01~0.49, 0.97~0.99
Gamma	No.9	0.01~0.32, 0.90~0.91, 0.95~0.99	No.18	0.01~0.17, 0.21~0.32, 0.40~0.42

than the positive group. Based on the constructed correlation matrices, we further calculated the clustering coefficients at different thresholds. We listed the thresholds at which the clustering coefficients were significantly different between the two groups, and we presented the clustering coefficients in detail with a topographic plot for features No. 5 and No. 6 in the beta rhythm. The preliminary analysis implied that the features' ability to reflect the channel correlation may contribute to the recognition of emotions. Nevertheless, considering the differences in the clustering coefficients of the different features, we should note that the correlation analysis is not sufficient to fully explain the mechanism of those features or to determine

the important locations. Additional analyses from different perspectives using different approaches are still needed in future work.

In the future, we should also further study the oscillatory and temporal process of emotion perception based on these features and verify the effectiveness of the proposed features on other datasets. In addition to correlation analysis, we need an in-depth study of the mechanisms of the features that allow for differentiating between positive and negative emotions. Another potential line of research is to further verify the ability of those features to identify emotion-related mental disorders, e.g., depression, as well as the

FIGURE 9 | (A,B) The topographic plot of the clustering coefficient of the groups of negative emotion and positive emotion when feature No. 5 (Hjorth parameter: mobility) and feature No. 6 (Hjorth parameter: complexity) in beta rhythm were utilized. Conditions with different thresholds (T) are illustrated.

effectiveness of those features in studying other cognitive processes.

AUTHOR CONTRIBUTIONS

XL proposed the idea, conducted the experiments, and wrote the manuscript. DS, PZ, YZ, and YH provided advice on the research approaches, guided the experiments, and checked and revised the manuscript. BH offered important help on EEG processing and analysis methods.

REFERENCES

Aftanas, L. I., Lotova, N. V., Koshkarov, V. I., Pokrovskaja, V. L., Popov, S. A., and Makhnev, V. P. (1997). Non-linear analysis of emotion EEG: calculation of Kolmogorov entropy and the principal Lyapunov exponent. *Neurosci. Lett.* 226, 13–16. doi: 10.1016/S0304-3940(97)00232-2

Chanel, G., Rebetez, C., Bétrancourt, M., and Pun, T. (2011). Emotion assessment from physiological signals for adaptation of game difficulty. *IEEE Trans. Syst. Man Cybern. Part A Syst. Hum.* 41, 1052–1063. doi: 10.1109/TSMCA.2011.2116000

Coan, J. A., and Allen, J. J. B. (2004). Frontal EEG asymmetry as a moderator and mediator of emotion. *Biol. Psychol.* 67, 7–50. doi: 10.1016/j.biopsycho.2004.03.002

Gross, J. J., and Muñoz, R. F. (1995). Emotion regulation and mental health. *Clin. Psychol. Sci. Pract.* 2, 151–164. doi: 10.1111/j.1468-2850.1995.tb00036.x

Guyon, I., and Elisseeff, A. (2003). An introduction to variable and feature selection. *J. Mach. Learn. Res.* 3, 1157–1182.

Guyon, I., Weston, J., Barnhill, S., and Vapnik, V. (2002). Gene selection for cancer classification using support vector machines. *Mach. Learn.* 46, 389–422. doi: 10.1023/A:1012487302797

Haufe, S., Meinecke, F., Görgen, K., Dähne, S., Haynes, J. D., Blankertz, B., et al. (2014). On the interpretation of weight vectors of linear models in multivariate neuroimaging. *Neuroimage* 87, 96–110. doi: 10.1016/j.neuroimage.2013.10.067

Hjorth, B. (1970). EEG analysis based on time domain properties. *Electroencephalogr. Clin. Neurophysiol.* 29, 306–310.

Huang, J., Cai, Y., and Xu, X. (2006). "A filter approach to feature selection based on mutual information," in *Proceedings of 5th IEEE International Conference on Cognitive Informatics*, Vol. 1 (New York, NY: IEEE Press), 84–89.

Khalili, Z., and Moradi, M. H. (2009). "Emotion recognition system using brain and peripheral signals: using correlation dimension to improve the results of EEG," in *Proceedings of the 2009 International Joint Conference on Neural Networks* (New York, NY: IEEE Press), 1571–1575.

Kim, J. (2007). "Chapter 15: Bimodal emotion recognition using speech and physiological changes," in *Robust Speech Recognition and Understanding*, eds M. Grimm and K. Kroschel (Rijeka: InTech Press), 265–280.

Koelstra, S., Muhl, C., Soleymani, M., Lee, J. S., Yazdani, A., Ebrahimi, T., et al. (2012). DEAP: A database for emotion analysis using physiological signals. *IEEE Trans. Affect. Comput.* 3, 18–31. doi: 10.1109/T-AFFC.2011.15

Kortelainen, J., and Seppänen, T. (2013). "EEG-based recognition of video-induced emotions: selecting subject-independent feature set," in *Proceedings of the 35th Annual International Conference of the IEEE Engineering in Medicine and Biology Society* (New York, NY: IEEE Press), 4287–4290.

Kortelainen, J., Väyrynen, E., and Seppänen, T. (2015). High-frequency electroencephalographic activity in left temporal area is associated with pleasant emotion induced by video clips. *Comput. Intellig. Neurosci.* 2015:31. doi: 10.1155/2015/762769

Li, M., and Lu, B.-L. (2009). "Emotion classification based on gamma-band EEG," in *Proceedings of the 31st Annual International Conference of the IEEE Engineering in Medicine and Biology Society* (New York, NY: IEEE Press), 1223–1226.

Li, X., Ouyang, G., and Richards, D. (2007). Predictability analysis of absence seizures with permutation entropy. *Epilepsy Res.* 77, 70–74. doi: 10.1016/j.eplepsyres.2007.08.002

Lin, Y. P., Wang, C. H., Jung, T. P., Wu, T. L., Jeng, S. K., Duann, J. R., et al. (2010). EEG-based emotion recognition in music listening. *IEEE Trans. Biomed. Eng.* 57, 1798–1806. doi: 10.1109/TBME.2010.2048568

Lu, Y., Jiang, D., Jia, X., Qiu, Y., Zhu, Y., Thakor, N., et al. (2008). "Predict the neurological recovery under hypothermia after cardiac arrest using C0 complexity measure of EEG signals," in *Proceedings of the 30th Annual International Conference of the IEEE Engineering in Medicine and Biology Society* (New York, NY: IEEE Press), 2133–2136.

Maldonado, S., and Weber, R. (2008). A wrapper method for feature selection using support vector machines. *Inform. Sci.* 179, 2208–2217. doi: 10.1016/j.ins.2009.02.014

Mao, X., and Li, Z. (2009). "Implementing emotion-based user-aware e-learning," in *Extended Abstracts Proceedings of the 2009 Conference on Human Factors in Computing Systems* (New York, NY: ACM Press), 3787–3792.

Moshfeghi, Y. (2012). *Role of Emotion in Information Retrieval*, PhD thesis, University of Glasgow, Glasgow.

Müller, M. M., Keil, A., Gruber, T., and Elbert, T. (1999). Processing of affective pictures modulates right-hemispheric gamma band EEG activity. *Clin. Neurophysiol.* 110, 1913–1920. doi: 10.1016/S1388-2457(99)00151-0

Ng, A. Y. (2004). "Feature selection, L1 vs. L2 regularization, and rotational invariance," in *Proceedings of the 21st International Conference on Machine Learning* (New York, NY: ACM Press) , 78–85.

O'Leary, A. (1990). Stress, emotion, and human immune function. *Psychol. Bull.* 108, 363–382.

Pincus, S. M., Gladstone, I. M., and Ehrenkranz, R. A. (1991). A regularity statistic for medical data analysis. *J. Clin. Monit. Comput.* 7, 335–345.

Russell, J. A. (1980). A circumplex model of affect. *J. Pers. Soc. Psychol.* 39, 1161–1178.

Sanei, S., and Chambers, J. A. (2013). *EEG Signal Processing.* Chichester: John Wiley & Sons Ltd.

Schmidt, L. A., and Trainor, L. J. (2001). Frontal brain electrical activity (EEG) distinguishes valence and intensity of musical emotions. *Cogn. Emot.* 15, 487–500. doi: 10.1080/02699930126048

Soleymani, M., Pantic, M., and Pun, T. (2012). Multimodal emotion recognition in response to videos. *IEEE Trans. Affect. Comput.* 3, 211–223. doi: 10.1109/T-AFFC.2011.37

Stam, C. J. (2005). Nonlinear dynamical analysis of EEG and MEG: review of an emerging field. *Clin. Neurophysiol.* 116, 2266–2301. doi: 10.1016/j.clinph.2005.06.011

Übeyli, E. D. (2010). Lyapunov exponents/probabilistic neural networks for analysis of EEG signals. *Expert Syst. Appl.* 37, 985–992. doi: 10.1016/j.eswa.2009.05.078

Ward, L. M. (2003). Synchronous neural oscillations and cognitive processes. *Trends Cogn. Sci.* 7, 553–559. doi: 10.1016/j.tics.2003.10.012

Zhang, A., Yang, B., and Huang, L. (2008). "Feature extraction of EEG signals using power spectral entropy," in *Proceedings of the 2008 International Conference on Biomedical Engineering and Informatics* (New York, NY: IEEE Press), 435–439.

Zhang, X. P., Fan, Y. L., and Yang, Y. (2009). On the classification of consciousness tasks based on the EEG singular spectrum entropy. *Comput. Eng. Sci.* 31, 117–120. doi: 10.3969/j.issn.1007-130X.2009.12.035

Zheng, W. L., Zhu, J. Y., and Lu, B. L. (2016). Identifying stable patterns over time for emotion recognition from EEG. *arXiv preprint arXiv:1601.02197.*

Zhu, J., Rosset, S., Tibshirani, R., and Hastie, T. J. (2004). "1-norm support vector machines," in *Proceedings of the 16th International Conference on Neural Information Processing Systems* (Cambridge: MIT Press), 49–56.

Zhu, J. Y., Zheng, W. L., and Lu, B. L. (2015). "Cross-subject and cross-gender emotion classification from EEG," in *Proceedings of the World Congress on Medical Physics and Biomedical Engineering* (Berlin: Springer Science and Business Media), 1188–1191.

The Early Facilitative and Late Contextual Specific Effect of the Color Red on Attentional Processing

Tao Xia[1†], Zhengyang Qi[1†], Jiaxin Shi[2], Mingming Zhang[1] and Wenbo Luo[1*]

[1] Research Center of Brain and Cognitive Neuroscience, Liaoning Normal University, Dalian, China, [2] Department of Psychology, The University of Hong Kong, Hong Kong, Hong Kong

Many studies have proved that color represents a variety of emotionally meaningful information. Researchers have proposed that context information endows colors with different associated meanings, and elicits corresponding behavior. Others have contended that the color red intensifies the stimulus' existing valence or motivation tendency in the early processing step. The present study attempts to incorporate these two effects of the color red to explore their differences in a dot probe task, using event-related potential (ERP). Our ERP results indicate that the color red intensifies the initial attention to emotion-congruent conditions, as indicated by the P1 component. However, the colors red and green lead to sustained attention to the expression of anger and happiness, respectively, but not fear, as shown by the late positive complex component (all results are available at: https://osf.io/k3b8c/). This study found the different processing stages of the effect of the color red during attentional processing in a discrete emotional context, using ERPs, and may refine the Color-in-Context theory.

Keywords: red-angry, green-happy, attention bias, Color-in-Context theory, ERPs

INTRODUCTION

As a basic dimension of human perception, color is ubiquitous in our surroundings, and plays a fundamental role in human perception and experience of the world (Valdez and Mehrabian, 1994; Müller et al., 2006; Bramão et al., 2011). Researchers have observed that the same color can convey inconsistent meanings under different conditions. For instance, the color red is not only associated with negative meanings but also linked to positive meanings in both natural and human societies. Specifically, in natural environments, the color red often plays an important role in warning the body of potential hazard from insects, birds, or reptiles (Stevens and Ruxton, 2012). On the other hand, the same color could also be an indication of ripe fruits which attract animals to consume them for living. In our daily life, the color red is often used to indicate dangerous situations which, if not avoided, will result in injury. Meanwhile, it is also a symbol of luck, festivities, and other positive themes in some cultures, such as in Chinese culture. The fact that the same color may convey contrary meanings in different situations is of scientific interest to investigators who wish to study its impact on the individual's psychological functioning.

Since the color red is associated with both negative and positive meanings, scholars have proposed the *Color-in-Context* theory, which states that the context in which the color red is perceived, influences people's interpretation of its associated meaning, and subsequently alters their behaviors accordingly (Elliot and Maier, 2012, 2014; Elliot, 2015). The *Color-in-Context* theory

hypothesizes that colors convey different meanings depending on the context (Elliot and Maier, 2012). Some studies have found that the color red, associated with danger and generally negative meanings in an achievement context, activates withdrawal responses, and influences cognition, emotion, and behavior (Moller et al., 2009; Kuhbandner and Pekrun, 2013; Pravossoudovitch et al., 2014; Shi et al., 2015). In contrast to achievement contexts, studies indicate that, in romantic contexts, the color red is associated with sexual attractiveness, and activates approach motivation, and impacts mating behavior in heterosexual individuals (Elliot and Niesta, 2008). However, recently, researchers have failed to replicate this attractive effect (Peperkoorn et al., 2016). In addition to being associated with danger or sexual desirability in different contexts, the color red is also an inherent feature of angry expressions in an emotional context. When angry, the faces of humans and other primates often turn red (Drummond, 1997; Changizi et al., 2006). The color red, in contrast to blue and gray, thus, facilitates the identification of angry, but not fearful, expressions which suggests a more specific association between the color red and anger (Young et al., 2013).

In addition to highlighting the important role of context information in color effect, researchers have recently suggested that attention may be involved in the context-dependency of the associations of the color red (Buechner et al., 2014, 2015; Buechner and Maier, 2016). An attentional-bias theory has been proposed, which hypothesizes that the color red could led to an automatic attentional bias toward stimuli that existing attentional priority caused by motivation tendency, making the target more prominent than others. Buechner et al. (2014) proposed that the color red intensifies the stimuli's existing valence or motivation tendency and impact on human behaviors in early processing steps. In a modified dot probe task, the reaction times show that the color red intensifies the perceiver's attentional engagement to angry and happy, but not neutral, expressions, in contrast to blue. Using a dot probe task with pictures of emotional scenes from International Affective Picture System (IAPS), studies of ERP components [early directing attention negativity (EDAN) and anterior directing attention negativity (ADAN)] have also revealed that the color red captures initial and later attention in both positive and negative conditions, but not in a neutral condition (Kuniecki et al., 2015). This result is consistent with Buechner's proposal that the color red intensifies the stimuli's existing motivation tendency (emotion effect). However, it is only involved in the valence of the stimuli, and does not influence more specific associations (e.g., anger) in attentional processing.

Taken together, previous studies have shown that the color red intensifies the stimulus' existing valence or motivation information in early processing steps. Context-specific effects may then emerge and influence human behavior (Buechner et al., 2014, 2015). It is important to investigate the relationship between attentional bias and context-specific information during visual processing in the presence of the color red, as it is useful to refine the theory of the influence of color on psychological functioning.

In this study, we attempted to integrate the two effects of the color red, and investigate its differential effects on attentional processing using ERPs, as it is an excellent tool to study the time course of mental processes. We hypothesized that the existing emotional attention aspects of red stimuli captures the perceiver's attentional resources in an early processing stage, while context information regarding discrete emotional association sustains the individual's attention to corresponding red targets in the late processing stage. A modified dot probe task, whose original version is often used to measure the attentional bias of emotional stimuli, has been used in this study, although we changed the target colors to red and green. Angry, fearful, and happy expressions were used as cues to create an emotional context. We selected the color green as a control color, as this condition has been used successfully in several previous studies (Elliot et al., 2007; Maier et al., 2009). Indeed, some researchers contend that green is a pleasant hue, and enhances the recognition of happy expressions. In fact, even in a cycling task, the color green makes individuals feel happy (Valdez and Mehrabian, 1994; Akers et al., 2012; Gil and Le Bigot, 2014). In previous studies, it has been shown that the P1 component of ERP is a good marker for capturing initial attention in the dot probe task (Brosch et al., 2008; Liu et al., 2013). The participants may also direct their attention to relevant stimuli and perform elaborate processing, as evidenced by a large late positive complex (LPC) in ERP (Jaworska et al., 2012; Gable and Adams, 2013; Zhang et al., 2014; Yi et al., 2015; Zhu et al., 2015). Therefore, we predicted that the color red may capture the initial attention to attended stimuli for all emotions (anger, fear, and happiness), as it leads to larger P1 responses. However, in the late processing stage, only angry facial expressions sustained the perceiver's attention to the red stimuli, as evidenced by a larger LPC.

MATERIALS AND METHODS

Participants

We did not run a power analysis to estimate our sample size before the study. And we decided the sample size based on our previous study (Liu et al., 2013; Zhang et al., 2014; Zhu et al., 2015). Seventy-two undergraduates were recruited from Chongqing University of arts and sciences in exchange for payment. They were randomly assigned: behavioral experiment ($n = 31$, 20 females, mean = 22, $SD = 1.67$) and ERP experiment ($n = 41$, 30 females, mean = 21.5, $SD = 1.96$). All participants were reported right-handed and having normal or corrected-to-normal vision without any color deficiencies. All subjects were provided informed written consent prior to the study. The study was approved by Chongqing University of Arts and Sciences Human Research Institutional Review Board in accordance with the Declaration of Helsinki (1991).

Stimuli

Sixty faces (10 angry, 10 happy, 10 fear, and 30 neutral faces) were chosen from the Chinese Facial Affective Picture System (Gong et al., 2011) depicting the emotion of people in black and white photograph, with an equal number of face pictures of males and females. We also assessed the valence and arousal on a 9-point scale with a sample of 45 Chinese subjects. We analyzed

the average score of all stimuli in our experiments which are reported in **Table 1**. The statistical results showed that angry and fearful faces were not significantly different in emotional valence [$F(3,44) = 203.09$, $p < 0.001$, $\eta^2 = 0.93$, 95% CI (0.88, 0.95); anger vs. fear: $p = 0.91$], while their valences were significantly different from happy faces ($ps < 0.001$) and neutral faces ($ps < 0.001$). The average arousal score between angry, fearful, and happy faces was not significantly different from each other [$F(3,44) = 53.54$, $p < 0.001$, $\eta^2 = 0.79$, 95% CI (0.64, 0.84); anger vs. fear vs. happiness: $ps > 0.10$], while they were significantly different from neutral faces ($ps < 0.01$). In addition, each facial expression had also been assessing the recognition rates and had been used successfully in previous studies.

Stimuli (260 pixels × 300 pixels) were presented on a liquid crystal display monitor (17-inch) at a viewing distance of 100 cm. The viewing angle was 3.9° × 4.5°, and the screen resolution was 72 pixels per inch.

Procedure

The experiment is within subject design and consisted of one practice block of 12 trials, followed by one experimental block of 960 trials. The participants had a rest period of 1 min every 160 trials. All trials were randomized. An example of the stimuli and the trial design of the experiment is illustrated in **Figure 1**. There were three factors in our experiment, including emotion (anger, fear, happy), congruency (congruent, incongruent), and color (red and green). A fixation cross appeared in the center of the screen for 300 to 600 ms, and was followed by a cue that consisted of two faces. There was an emotional (angry, fear, or happy)

and a neutral face on the left or right side of the screen. After a short interval (100 ms to 300 ms), a target appeared at either the same position as the emotional face (congruent) or at a different position (incongruent) for 150 ms. Congruent and incongruent trials appeared in random order with equal probability (50% each). To match the lightness we used the BabelColor Translator and Analyzer (CT&A) to transform the parameters of target colors from Adobe RGB (1998) color space (red = 255, green = 0, blue = 0; red = 0, green = 181, blue = 0) into CIE LCh color space (red: L = 61.4, C = 117, h = 40.0; green: L = 61.2, C = 128, h = 147). After the appearance of the target, the participants had to assess the position of the target as quickly and as accurately as possible. If the triangle was presented on the left, targets had to press "F" on the computer keyboard using their left index fingers. Otherwise, they were to press "J" using their right index fingers. The target was one of four types of triangle (red upper, red lower, green upper, and green lower). The participants were instructed to respond to only two types of triangles (red and green upper, or red and green lower, counterbalanced across subjects), but to ignore its color. Before the next trial started, the participants had a maximum of 1,000 ms to respond. Importantly, we used different percentages of response trials in our behavioral tasks (go trials, 50%; no-go trials, 50%) and electroencephalogram (EEG) studies (go trials, 10%; no-go trials, 90%) in order to study spatial orientation in the EEG task (Brosch et al., 2008; Liu et al., 2013). In addition, since we analyzed no-go, not go, trials in our ERP analysis, the ERPs (P1, LPC) may not be related to the behavioral response. The behavioral experiment is only for repeating the similar results of the previous study. Our main interests are focused on the ERPs results since we want to clarify the different stage of the color red and its effect on attentional processing.

EEG Recording and Analysis

Brain electrical activity was recorded at 64 scalp sites using tin electrodes mounted in an elastic cap with a sampling frequency of 500 Hz (Brain Products, Munich, Germany), according to the international 10–20 System. FCz was used as the reference, and ground electrode was on the medial frontal aspect. The horizontal EOG was recorded from the right orbital rim. All electrode impedance was <5 kΩ. The EEG and EOG were amplified using a 0.01–100 Hz bandpass.

TABLE 1 | Average ratings (mean ± SD) for valence and arousal of stimuli.

	Arousal	Valence
Anger	6.34 ± 1.20	2.82 ± 0.44
Fear	6.23 ± 1.68	2.81 ± 0.44
Happiness	5.97 ± 0.98	5.74 ± 0.89
Neutral	3.63 ± 0.54	4.12 ± 0.70

45 participants assessed the valence and arousal of sixty faces (10 angry, 10 happy, 10 fear, and 30 neutral faces) on a 9-point scale, and we analyzed the average scores of all stimuli per condition in our experiments.

FIGURE 1 | Schematic representation of experimental procedure. Each trial contained a cue (an angry/fear/happy face in one side of the screen and a neutral face in the other side) and a target stimulus (a red/green triangle that might be upper or lower). Congruent (the emotional face and the target appeared at the same position) and incongruent (the emotional face and the target appeared at different positions) trials were appeared in random order with equal probability (50% each). Participants were required to judge the target position by pressing "f" (left) or "j" (right), and they were instructed to respond only one kind of triangle (the upper or the lower, counterbalanced across subjects) but ignore its color. Importantly, we used a different percent of responding trials in our EEG (go trials, 10%, no-go trials, 90%) and behavioral tasks (go trials, 50%, no-go trials, 50%) to study the spatial orienting in EEG task.

EEG data were analyzed using BrainVision Analyzer (2.1) software (BrainProducts GmbH). Data were off-line mathematically re-referenced to the left and right mastoids, and filtered with band pass filter 0.1–30 Hz (24 dB). Filtered data were segmented beginning 100 ms prior to the onset of the target stimulus array and lasting for 950 ms. An ocular artifact reduction procedure (Semlitsch et al., 1986) based on right eye HEOG activity was used to remove blink artifacts. Baseline correction was performed using 100 ms prestimulus interval. EEG epochs in which the signal exceeded ± 100 μV were excluded. Artifact-free epochs were averaged separately for each electrode, condition, and individual. The average ERPs of the 41 subjects were computed based on no-go trials (80 * 90% = 72 trials precondition).

We analyzed the amplitudes of occipital P1 and LPC components across different set of electrodes in line with grand-mean ERP topographies and previous literatures (Yi et al., 2015), the mean amplitude of P1 was calculated at the electrode sites of PO3, PO4, PO7 and PO8 (time window = 100–150 ms). The mean amplitude of LPC was calculated at electrode sites C3, C4, Cz, CP3, CP4, CPz (time window = 340–460 ms). For each component, a four-way repeated-measures ANOVA was performed with the following variables as within-subject factors: "Color" (Red target vs. Green target), "Congruency" (Congruent vs. Incongruent), "Emotion" (Anger vs. Fear vs. Happy), and "Hemisphere" (P1: Left hemisphere vs. Right hemisphere; LPC: Left hemisphere vs. Medal region vs. Right hemisphere). P value was corrected using the Greenhouse–Geisser method.

RESULTS

Means and standard error (mean ± SE) of behavioral data at four experimental conditions are reported in **Table 2**, and more details are reported in **Table 3** with means and standard deviation (mean ± SD). Means and standard errors (mean ± SE) of electrophysiological data at different experimental conditions are reported in **Table 4**.

Behavioral Results

We only analyzed the reaction time in both EEG and behavioral experiment because there was a ceiling effect in accuracy as the task is too simple. In the behavioral experiment, the main effect of "Color" [$F(1,30) = 5.34$, $p = 0.03$, $\eta^2 = 0.15$, 95% CI (0,0.37)] was significant. Participants performed slower in red triangle (371 ± 15 ms) than green triangle (361 ± 15 ms). However, the main effects of "Emotion" and "Congruency" [$Fs < 0.45$,

TABLE 2 | Reaction time (mean ± SE) at four experimental conditions of Behavioral experiment ($N = 31$) and ERP experiment ($N = 41$).

	Behavioral experiment	ERP experiment
Congruent-Red (ms)	375 ± 16	308 ± 11
Congruent-Green (ms)	357 ± 15	292 ± 11
Incongruent-Red (ms)	366 ± 14	308 ± 10
Incongruent-Green (ms)	364 ± 15	295 ± 11

TABLE 3 | Reaction time (mean ± SD) at all experimental conditions.

	Anger				Fear				Happiness			
	Congruent		Incongruent		Congruent		Incongruent		Congruent		Incongruent	
	Red	Green	Red	Green	Red	Green	Red	Green	Red	Green	Red	Green
Behavioral exp. (ms)	375 ± 96	358 ± 92	367 ± 86	355 ± 76	374 ± 97	350 ± 79	367 ± 78	377 ± 96	375 ± 92	363 ± 100	365 ± 77	362 ± 96
ERP exp. (ms)	309 ± 80	293 ± 73	307 ± 64	290 ± 66	307 ± 70	295 ± 74	313 ± 75	299 ± 73	309 ± 70	288 ± 72	306 ± 72	295 ± 84

TABLE 4 | Amplitudes (mean ± SE) of P1 and LPC at all experimental conditions.

	Anger				Fear				Happiness			
	Congruent		Incongruent		Congruent		Incongruent		Congruent		Incongruent	
	Red	Green	Red	Green	Red	Green	Red	Green	Red	Green	Red	Green
P1 (μV)	0.83 ± 0.32	0.38 ± 0.27	0.72 ± 0.32	0.50 ± 0.27	0.86 ± 0.30	0.39 ± 0.31	0.50 ± 0.28	0.53 ± 0.27	0.93 ± 0.29	0.54 ± 0.29	0.72 ± 0.27	0.40 ± 0.33
LPc (μV)	7.96 ± 0.67	7.00 ± 0.61	7.63 ± 0.67	7.20 ± 0.58	7.07 ± 0.63	7.20 ± 0.64	7.24 ± 0.67	7.19 ± 0.53	6.77 ± 0.58	7.27 ± 0.57	6.84 ± 0.57	7.21 ± 0.60

ps > 0.63] were not significant. There was a significant interaction between "Congruency" and "Color" [$F(1,30)$ = 5.02, p = 0.03, η^2 = 0.14, 95% CI(0, 0.36)]. Simple effects analysis demonstrated that the reaction time of "Congruency" was significantly influenced by "Color". Participants performed slower to red triangle than green triangle in congruent condition (375 ± 16 ms vs. 357 ± 15 ms, $t(30)$ = 3.77, p < 0.001, d = 0.68, 95% CI (0.28, 1.06)); however, there was no difference between red triangle and green triangle in incongruent condition (366 ± 14 ms vs. 365 ± 15 ms, $t(30)$ = 0.26, p = 0.80). And there were no other significant interactions among "Color", "Emotion" and "Congruency" [Fs < 1.82, ps > 0.18].

In the EEG experiment, the main effect of "Color" [$F(1,40)$ = 31.89, p < 0.001, η^2 = 0.44, 95% CI(0.21, 0.60)] was significant. Participants performed slower to red triangle (308 ± 10 ms) than green triangle (293 ± 11 ms). While the main effect of "Emotion" and "Congruency" [Fs < 1.24, ps > 0.30], as well as all their interactions [Fs < 0.85, ps > 0.43] were not significant.

P1 Component
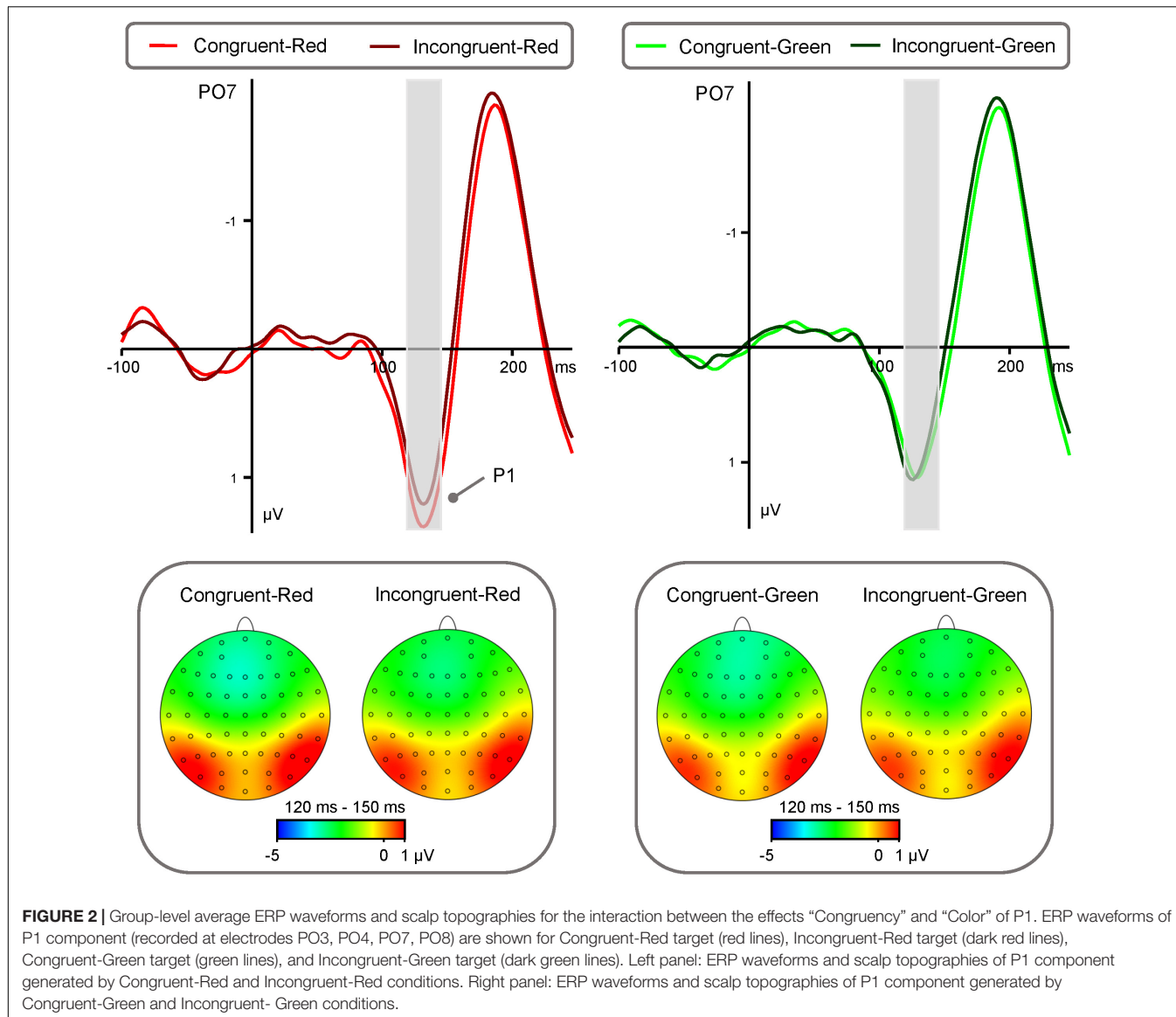
P1 amplitude (**Figure 2**) showed a significant main effect of "Color" [$F(1,40)$ = 17.25, p < 0.001, η2 = 0.30, 95 % CI (0.08, 0.49)]. Red triangle (0.76 ± 0.28 μV) elicited significantly larger P1 amplitude than green triangle (0.44 ± 0.27 μV). While the main effects of "Emotion", "Congruency" and "Hemisphere" were not significant [Fs < 1.77, ps > 0.19].

In addition, there was a significant interaction between the effects "Congruency" and "Color" [$F(1,40)$ = 7.15, p = 0.011, η^2 = 0.15, 95% CI (0.01, 0.35)]. Simple effects analysis indicated that the effect of "Color" significantly influenced the amplitudes of "Congruency". Simple effects analysis showed that congruent condition elicited significantly larger P1 amplitude than incongruent condition [0.87 ± 0.28 μV vs. 0.65 ± 0.28 μV, $t(40)$ = 3.01, p < 0.01, d = 0.47, 95% CI (0.15, 0.79)] in the red condition. While there was no difference between congruent condition and incongruent condition (0.44 ± 0.27 μV vs. 0.45 ± 0.27 μV, $t(40)$ = −0.15 p = 0.88) in the green condition.

LPC Component
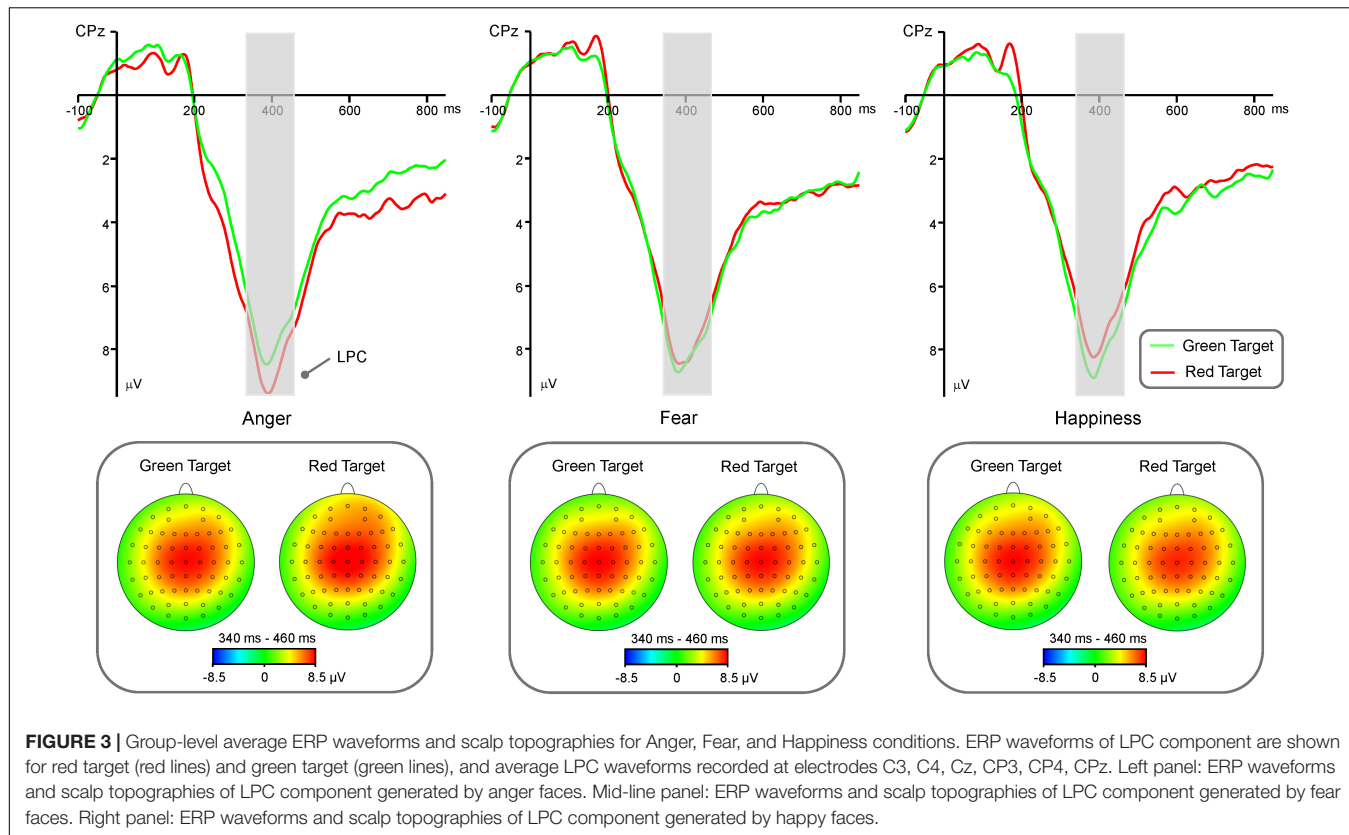
LPC amplitude (**Figure 3**) showed significant main effects of "Emotion" [$F(2,40)$ = 4.19, p = 0.02, η^2 = 0.17, 95% CI (0, 0.35)] and "Hemisphere" [$F(2,40)$ = 24.89, p < 0.001, η^2 = 0.55, 95% CI (0.31, 0.68)]. *Post hoc* pairwise comparisons showed that anger faces elicited significantly larger LPC amplitude than happy faces (7.44 ± 0.61 μV vs. 7.02 ± 0.59 μV, p = 0.01), while there was no difference between fearful faces and happy faces (7.17 ± 0.59 μV vs. 7.02 ± 0.59 μV, p = 0.24) or between fearful faces and angry faces (7.17 ± 0.59 μV vs. 7.44 ± 0.61 μV, p = 0.09). In addition, LPC amplitude was significantly larger in the mid-line region (8.27 ± 0.67 μV) than in the left hemisphere (6.65 ± 0.58 μV, p < 0.001) and right hemisphere (6.72 ± 0.58 μV, p < 0.001), while there was no difference between left hemisphere and right hemisphere (p = 0.80). The main effects of "Color" and "Congruency" were not significant [Fs < 0.36, ps > 0.55].

There was a significant interaction between the effects "Emotion" and "Color" [$F(1, 40)$ = 9.35, p < 0.001, η^2 = 0.19,

FIGURE 2 | Group-level average ERP waveforms and scalp topographies for the interaction between the effects "Congruency" and "Color" of P1. ERP waveforms of P1 component (recorded at electrodes PO3, PO4, PO7, PO8) are shown for Congruent-Red target (red lines), Incongruent-Red target (dark red lines), Congruent-Green target (green lines), and Incongruent-Green target (dark green lines). Left panel: ERP waveforms and scalp topographies of P1 component generated by Congruent-Red and Incongruent-Red conditions. Right panel: ERP waveforms and scalp topographies of P1 component generated by Congruent-Green and Incongruent- Green conditions.

95% CI (0.02, 0.38)]. Simple effects analysis showed that red triangle elicited significantly larger LPC amplitude than green triangle in angry condition [7.80 ± 0.66 µV vs. 7.09 ± 0.58 µV, $t(40) = 3.23$, $p = 0.002$, $d = 0.51$, 95% CI (0.18, 0.83)], while red triangle elicited significantly smaller than green triangle in happy condition [6.81 ± 0.56 µV vs. 7.24 ± 0.58 µV, $t(40) = -2.27$, $p = 0.029$, $d = -0.35$, 95% CI (−0.67, −0.04)], and there was no difference between red triangle and green triangle in fear condition (7.15 ± 0.64 µV vs. 7.20 ± 0.56 µV, $t(40) = -0.23$, $p = 0.82$). In addition, there was a significant interaction of "Emotion," "Color," and "Hemisphere" [$F(1,40) = 6.01$, $p < 0.001$, $\eta^2 = 0.13$, 95% CI(0,0.32)]. Simple effects analysis showed that red triangle under angry condition elicited significantly larger LPC amplitude than green triangle under angry condition in the left hemisphere [7.30 ± 0.62 µV vs. 6.46 ± 0.54 µV, $t(40) = 3.92$, $p < 0.001$, $d = 0.61$, 95% CI (0.27, 0.94)] and mid-line region [8.88 ± 0.76 µV vs. 8.06 ± 0.68 µV, $t(40) = 3.32$, $p = 0.02$,

$d = 0.52$, 95% CI(0.19, 0.84)], and red triangle under angry condition elicited marginally larger than green triangle under angry condition in the right hemisphere [7.21 ± 0.66 µV vs. 6.76 ± 0.59 µV, $t(40) = 1.96$, $p = 0.06$, $d = 0.31$, 95% CI (−0.01, 0.62)]. There was no difference between red triangle and green triangle under fearful condition in the left hemisphere (6.59 ± 0.59 µV vs. 6.62 ± 0.54 µV, $t(40) = -0.18$, $p = 0.86$), mid-line region (8.19 ± 0.74 µV vs. 6.46 ± 0.54 µV, $t(40) = -0.81$, $p = 0.42$), or right hemisphere (6.69 ± 0.62 µV vs. 6.60 ± 0.57 µV, $t(40) = 0.46$, $p = 0.65$). Green triangle under happy condition elicited significantly larger LPC amplitude than red triangle under happy condition in the left hemisphere [6.65 ± 0.54 µV vs. 6.26 ± 0.53 µV, $t(40) = -2.08$, $p = 0.044$, $d = -0.33$, 95% CI (−0.64, −0.01)] and mid-line region [8.36 ± 0.66 µV vs. 7.80 ± 0.65 µV, $t(40) = -2.52$, $p = 0.016$, $d = -0.39$, 95% CI (−0.71, −0.07)], while there was no difference between green triangle and red triangle under happy condition in the right

FIGURE 3 | Group-level average ERP waveforms and scalp topographies for Anger, Fear, and Happiness conditions. ERP waveforms of LPC component are shown for red target (red lines) and green target (green lines), and average LPC waveforms recorded at electrodes C3, C4, Cz, CP3, CP4, CPz. Left panel: ERP waveforms and scalp topographies of LPC component generated by anger faces. Mid-line panel: ERP waveforms and scalp topographies of LPC component generated by fear faces. Right panel: ERP waveforms and scalp topographies of LPC component generated by happy faces.

hemisphere (6.70 ± 0.59 μV vs. 6.37 ± 0.55 μV, $t(40) = -1.76$, $p = 0.09$).

DISCUSSION

In this study, we used behavioral measures and ERPs to assess the relationship between context information and attentional bias to the color red during visual processing. In a discrete emotional context, our behavioral results indicated that the reaction time for the color red was longer than that for color green. Moreover, the reaction time for the color red in the congruent condition was longer than that for the color green. The ERP results indicate that the color red captures initial attention in the congruent condition while the valence is ignored, as shown by the P1 component. We also found that the colors red and green led to sustained attention to angry and happy faces in the late processing stage in congruent and incongruent conditions, respectively, as determined using the LPC component. In addition, we reported the eta-squared, not partial eta-squared, and Cohen's d values and their 95% confidence interval in the current study. The eta-squared values range from 0.13 to 0.55 and the absolute d values range from 0.33 to 0.68 among the statistically significant results, which implies a moderate strength of association, representing effective experimental control, among experiment factors, reaction time, and ERPs (Pierce et al., 2004). Additionally, the effect size used in this study was similar to that used in previous related studies which indicated that the color red is a factor that influences

an individual's psychological functioning (Buechner et al., 2014; Kuniecki et al., 2015).

It is noteworthy that both in the behavioral and electroencephalography (EEG) experiments conducted previously, there were no main effects of congruency and the interaction of emotion and congruency. Indeed, a considerable number of previous studies have demonstrated that the dot probe task has poor internal and test-retest reliability for measuring the attentional bias to a threatening stimulus, based on reaction times evaluated in non-clinical populations, and have proposed that ERP would be a good indicator for performance in this task (Schmukle, 2005; Bar-Haim et al., 2007; Kappenman et al., 2014). However, we found a significant interaction between color and congruency. The difference in the result may be due to modification of the task, which may take into account the fact that the color red intensifies existing emotional attention priority. In addition, the reaction time for the color red was longer than that for the color green in both behavioral and ERP experiments. This may be because the color red captures the attention resources and interrupts the participants' task-related attention, resulting in a longer reaction time for red stimuli.

We used ERPs to investigate whether there is a difference between attentional bias and emotional context information during the visual processing of the color red. First, using facial expressions as cues, we found that the color red leads to a larger P1 component than green. This result suggests that red may capture the early attention as it belongs to the long-wave colors and is associated with higher arousal. In fact, previous studies

have found that even a simple red target circle elicits earlier latencies in the N2pc component than green targets (Fortier-Gauthier et al., 2013). In addition, a study has found that the color red increases blood pressure, skin electric potential, EEG alpha waves, and other physiological indicators (Ali, 1972; Jacobs and Hustmyer, 1974). Our results are in line with those of the aforementioned studies. Therefore, we propose that the color red captures initial attention, as indicated by the P1 amplitude in the dot probe task. Second, the interaction effect between color and congruency is significant. The color red, but not green, captured initial attention in the congruent condition with fearful, happy, and angry expressions, as shown by the P1 amplitude. The color red intensifies the attention during congruent conditions. This suggests that the attentional bias of the color red is influenced by the current tendency of the subjects. Indeed, behavioral studies have indicated that the color red intensifies attention to the stimuli that existing motivation tendency (Buechner et al., 2014, 2015). In our experiment, congruent conditional targets were considered the stimuli that existing attentional priority because emotional cues captured attention prior to the target presentation. Thus, red targets only intensify the emotional effect. Therefore, the red target modulates the P1 component, which takes into account the attentional bias toward red stimuli that is related to existing attentional priority.

The color red modulated the LPC, in addition to the P1 component, in response to angry, but not fearful and happy, facial expressions. Previous behavioral studies have found an association between the color red and anger conceptualization or experience in a discrete emotional context (Elliot and Aarts, 2011; Young et al., 2013). Our data suggest that differences in the amplitude of LPC between the red and green angry expression conditions may reflect the association between the color red and anger. The color red, thus, leads to higher arousal and attention priority, as shown by the LPC in the angry expression condition. It is noteworthy that there is no relationship between fearful expression and red based on the LPC amplitude. As mentioned above, the color red is often used to indicate dangerous situations. Elliot et al. (2007) has proposed that this association between the color red and danger often appears in the context of achievement, and undermines individuals' performances in intellectual tasks. However, in emotional contexts, the color red not only facilitates the processing of angry expressions, but also enhances the processing of the concept of anger, although it does not facilitate the expression or conceptualization of fear (Fetterman et al., 2011; Young et al., 2013). Our results are consistent with the

aforementioned findings, and rule out the idea that the color red has a generally negative emotional association. Thus, we provide additional evidence for a link between anger and the color red in a discrete emotional context. In addition to the association between the color red and anger, as shown by the LPC in our experiments, we found that, in the happy expression condition, the color green captured later attention, and led to a larger LPC than the color red. This result suggests that the green target, followed by the happy expression, sustains the perceiver's attention, and reflects an association between the color green and happiness. In fact, previous studies also indicate that the color green is a pleasant hue in different tasks (Valdez and Mehrabian, 1994; Gil and Le Bigot, 2014). In general, LPC modulates red and green targets in the angry and happy expression conditions, respectively, which reflects the context-specific effects of colors on discrete emotions.

Taken together, the reaction time and P1 amplitude results indicate an attentional bias to the red target, which is congruent with emotional (anger, fear, and happiness) cues. The LPC amplitude reflects the emotional context-specific effects of color. In a discrete emotional context, individuals focused their attention unconsciously on the red and green targets, which followed the angry and happy expression cues, respectively. In our study, the context was represented by discrete emotional facial expressions. Our results suggest that the color red captures the initial attention in any motivational context (approach or withdrawal), and sustains the attention to the color if associated with a corresponding emotion. Our results may reconcile the difference between attentional bias and the context-specific effects of the color red, and highlight the need for investigators to study the mechanisms underlying the effect of the color red.

AUTHOR CONTRIBUTIONS

TX developed the study concept and performed the testing and data collection. TX and ZQ performed the data analysis and interpretation under the supervision of WL. TX drafted the manuscript. JS and MZ provided critical revisions. All authors contributed to the study design and approved the final version of the manuscript for submission.

FUNDING

REFERENCES

Akers, A., Barton, J. L., Cossey, R., Gainsford, P., Griffin, M., and Micklewright, D. (2012). Visual color perception in green exercise: positive effects on mood and perceived exertion. *Environ. Sci. Technol.* 46, 8661–8666. doi: 10.1021/es301685g

Ali, M. R. (1972). Pattern of EEG recovery under photic stimulation by light of different colors. *Electroencephalogr. Clin. Neurophysiol.* 33, 332–335. doi: 10.1016/0013-4694(72)90162-9

Bar-Haim, Y., Lamy, D., Pergamin, L., Bakermans-Kranenburg, M. J., and Van Ijzendoorn, M. H. (2007). Threat-related attentional bias in anxious and

nonanxious individuals: a meta-analytic study. *Psychol. Bull.* 133, 1–24. doi: 10.1037/0033-2909.133.1.1

Bramão, I., Reis, A., Petersson, K. M., and Faísca, L. (2011). The role of color information on object recognition: a review and meta-analysis. *Acta Psychol.* 138, 244–253. doi: 10.1016/j.actpsy.2011.06.010

Brosch, T., Sander, D., Pourtois, G., and Scherer, K. R. (2008). Beyond fear: rapid spatial orienting toward positive emotional stimuli: research article. *Psychol. Sci.* 19, 362–370. doi: 10.1111/j.1467-9280.2008.02094.x

Buechner, V. L., and Maier, M. A. (2016). Not always a matter of context: direct effects of red on arousal but context-dependent moderations on valence. *PeerJ* 4:e2515. doi: 10.7717/peerj.2515

Buechner, V. L., Maier, M. A., Lichtenfeld, S., and Elliot, A. J. (2015). Emotion expression and color: their joint influence on perceived attractiveness and social position. *Curr. Psychol.* 34, 422–433. doi: 10.1007/s12144-014-9266-x

Buechner, V. L., Maier, M. A., Lichtenfeld, S., and Schwarz, S. (2014). Red-take a closer look. *PLoS One* 9:e108111. doi: 10.1371/journal.pone.0108111

Changizi, M. A., Zhang, Q., and Shimojo, S. (2006). Bare skin, blood and the evolution of primate color vision. *Biol. Lett.* 2, 217–221. doi: 10.1098/rsbl.2006.0440

Drummond, P. D. (1997). Correlates of facial flushing and pallor in anger-provoking situations. *Pers. Individ. Dif.* 23, 575–582. doi: 10.1016/S0191-8869(97)00077-9

Elliot, A., and Maier, M. A. (2012). Color-in-context theory. *Adv. Exp. Soc. Psychol.* 45, 61–125. doi: 10.1016/B978-0-12-394286-9.00002-0

Elliot, A. J. (2015). Color and psychological functioning: a review of theoretical and empirical work. *Front. Psychol.* 6:368. doi: 10.3389/fpsyg.2015.00368

Elliot, A. J., and Aarts, H. (2011). Perception of the color red enhances the force and velocity of motor output. *Emotion* 11, 445–449. doi: 10.1037/a0022599

Elliot, A. J., and Maier, M. A. (2014). Color psychology: Effects of perceiving color on psychological functioning in humans. *Annu. Rev. Psychol.* 65, 95–120. doi: 10.1146/annurev-psych-010213-115035

Elliot, A. J., Maier, M. A., Moller, A. C., Friedman, R., and Meinhardt, J. (2007). Color and psychological functioning: the effect of red on performance attainment. *J. Exp. Psychol. Gen.* 136, 154–168. doi: 10.1037/0096-3445.136.1.154

Elliot, A. J., and Niesta, D. (2008). Romantic red: red enhances men's attraction to women. *J. Pers. Soc. Psychol.* 95, 1150–1164. doi: 10.1037/0022-3514.95.5.1150

Fetterman, A. K., Robinson, M. D., Gordon, R. D., and Elliot, A. J. (2011). Anger as seeing red: perceptual sources of evidence. *Soc. Psychol. Pers. Sci.* 2, 311–316. doi: 10.1177/1948550610390051

Fortier-Gauthier, U., Dell'acqua, R., and JoliŒur, P. (2013). The "red-alert" effect in visual search: evidence from human electrophysiology. *Psychophysiology* 50, 671–679. doi: 10.1111/psyp.12050

Gable, P. A., and Adams, D. L. (2013). Nonaffective motivation modulates the sustained LPP (1,000-2,000ms). *Psychophysiology* 50, 1251–1254. doi: 10.1111/psyp.12135

Gil, S., and Le Bigot, L. (2014). Seeing life through positive-tinted glasses: color–meaning associations. *PLoS One* 9:e104291. doi: 10.1371/journal.pone.0104291

Gong, X., Huang, Y. X., Wang, Y., and Luo, Y.-J. (2011). Revision of the Chinese facial affective picture system. *Chin. Ment. Health* 25, 40–46.

Jacobs, K. W., and Hustmyer, F. E. Jr. (1974). Effects of four psychological primary colors on GSR, heart rate and respiration rate. *Percept. Mot. Skills* 38, 763–766. doi: 10.2466/pms.1974.38.3.763

Jaworska, N., Thompson, A., Shah, D., Fisher, D., Ilivitsky, V., and Knott, V. (2012). Acute tryptophan depletion effects on the vertex and late positive potentials to emotional faces in individuals with a family history of depression. *Neuropsychobiology* 65, 28–40. doi: 10.1159/000328992

Kappenman, E. S., Farrens, J. L., Luck, S. J., and Proudfit, G. H. (2014). Behavioral and ERP measures of attentional bias to threat in the dot-probe task: poor reliability and lack of correlation with anxiety. *Front. Psychol.* 5:1368. doi: 10.3389/fpsyg.2014.01368

Kuhbandner, C., and Pekrun, R. (2013). Joint effects of emotion and color on memory. *Emotion* 13, 375–379. doi: 10.1037/a0031821

Kuniecki, M., Pilarczyk, J., and Wichary, S. (2015). The color red attracts attention in an emotional context. An ERP study. *Front. Hum. Neurosci.* 9:212. doi: 10.3389/fnhum.2015.00212

Liu, Y., Zhang, D., and Luo, Y. (2013). How disgust facilitates avoidance: an ERP study on attention modulation by threats. *Soc. Cogn. Affect. Neurosci.* 10, 598–604. doi: 10.1093/scan/nsu094

Maier, M. A., Barchfeld, P., Elliot, A. J., and Pekrun, R. (2009). Context specificity of implicit preferences: the case of human preference for red. *Emotion* 9, 734–738. doi: 10.1037/a0016818

Moller, A. C., Elliot, A. J., and Maier, M. A. (2009). Basic hue-meaning associations. *Emotion* 9, 898–902. doi: 10.1037/a0017811

Müller, M. M., Andersen, S., Trujillo, N. J., Valdes-Sosa, P., Malinowski, P., and Hillyard, S. A. (2006). Feature-selective attention enhances color signals in early visual areas of the human brain. *Proc. Natl. Acad. Sci. U.S.A.* 103, 14250–14254. doi: 10.1073/pnas.0606668103

Peperkoorn, L. S., Roberts, S. C., and Pollet, T. V. (2016). Revisiting the red effect on attractiveness and sexual receptivity: no effect of the color red on human mate preferences. *Evol. Psychol.* 14, 1–13. doi: 10.1177/1474704916673841

Pierce, C. A., Block, R. A., and Aguinis, H. (2004). Cautionary note on reporting eta-squared values from multifactor anova designs. *Educ. Psychol. Meas.* 64, 916–924. doi: 10.1177/0013164404264848

Pravossoudovitch, K., Cury, F., Young, S. G., and Elliot, A. J. (2014). Is red the colour of danger? Testing an implicit red–danger association. *Ergonomics* 57, 503–510. doi: 10.1080/00140139.2014.889220

Schmukle, S. C. (2005). Unreliability of the dot probe task. *Eur. J. Pers.* 19, 595–605. doi: 10.1002/per.554

Semlitsch, H. V., Anderer, P., Schuster, P., and Presslich, O. (1986). A solution for reliable and valid reduction of ocular artifacts, applied to the P300 ERP. *Psychophysiology* 23, 695–703. doi: 10.1111/j.1469-8986.1986.tb00696.x

Shi, J., Zhang, C., and Jiang, F. (2015). Does red undermine individuals' intellectual performance? A test in China. *Int. J. Psychol.* 50, 81–84. doi: 10.1002/ijop.12076

Valdez, P., and Mehrabian, A. (1994). Effects of color on emotions. *J. Exp. Psychol. Gen.* 123, 394–409. doi: 10.1037/0096-3445.123.4.394

Yi, S., He, W., Zhan, L., Qi, Z., Zhu, C., Luo, W., et al. (2015). Emotional noun processing: an ERP study with rapid serial visual presentation. *PLoS One* 10:e0118924. doi: 10.1371/journal.pone.0118924

Young, S. G., Elliot, A. J., Feltman, R., and Ambady, N. (2013). Red enhances the processing of facial expressions of anger. *Emotion* 13, 380–384. doi: 10.1037/a0032471

Zhang, D., He, W., Wang, T., Luo, W., Zhu, X., Gu, R., et al. (2014). Three stages of emotional word processing: an ERP study with rapid serial visual presentation. *Soc. Cogn. Affect. Neurosci.* 9, 1897–1903. doi: 10.1093/scan/nst188

Zhu, C., He, W., Qi, Z., Wang, L., Song, D., Zhan, L., et al. (2015). The time course of emotional picture processing: an event-related potential study using a rapid serial visual presentation paradigm. *Front. Psychol.* 6:954. doi: 10.3389/fpsyg.2015.00954

Frontiers in
Behavioral Neuroscience

Explores the neural mechanisms underlying animal and human behavior

Part of the world's most cited neuroscience journal series, this journal highlights reseach in all species that advances our understanding of the neural mechanisms underlying behavioral outcomes.

Discover the latest Research Topics

See more →

frontiers | Research Topics